Ubiquinone binding sites of mitochondrial bc_1 complex

A thesis presented for the degree

of

Doctor of Philosophy

in the

University of London

by

Akinyemi Olutosin Akinsiku

Department of Biology,

University College London.

August 2001

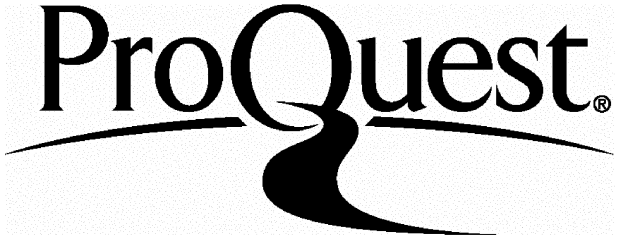

Abstract

The cytochrome bc_1 complex is a central component of the electron-transfer respiratory chain in mitochondria. It couples electron transfer to proton translocation across the membrane by a Q-cycle mechanism. It contains two ubiquinone-binding sites (Q_o, ubiquinol oxidation and Q_i, ubiquinone reduction) which are good targets for pesticides. Although the mechanism of the Q_o oxidation reaction has been much studied, the details remain controversial, in particular, the way in which electrons are bifurcated along two separate routes and whether the Q_o site has to bind one or two ubiquinones in order to be catalytically active. Resolving these issues is essential for understanding the chemistry of this unique reaction and useful in the development of pesticides.

This thesis describes studies of the occupancy state of the Q_o site, redox-linked changes in amino acids and protein conformation and characterisation of the binding site of new inhibitors using steady state kinetics, redox potentiometry, and optical, EPR and FTIR spectroscopy.

To address the question of the occupancy state of the Q_o site, steady state kinetics was used to characterise the binding mode of the Q_o site inhibitor MOA-stilbene in relation to the substrate decylubiquinol. This revealed a mixed type of inhibition, which shows that the previous conclusion of separate binding sites for MOA-stilbene and ubiquinone is questionable. A more direct method, EPR spectroscopy, which has proved to be highly sensitive to the degree and nature of the Q_o site occupants (Q/QH_2 or inhibitors), was also used. The results were consistent with a single occupancy model of the Q_o site. To complement these studies, molecular modelling studies with the available crystal structure and data from mutagenesis studies to identify residues conferring resistance to inhibitors were used. In addition, an

attempt was made to model two ubiquinone molecules into the Q_o site. Finally, competition between two classes of Q_o site inhibitors was also investigated. These studies were consistent with a single occupancy model of the Q_o site as suggested from kinetic and EPR studies.

FTIR difference spectroscopy in combination with selective photochemical reduction is a powerful technique for studying redox-linked changes in amino acids and protein conformation. The FTIR redox difference spectra of the components of bovine bc_1 complex in native and inhibitor bound states were resolved. Signal assignments were aided by comparison to FTIR redox difference spectra of soluble domains of individual redox centres and model compounds.

Inhibitors of the bc_1 complex have been an important tool in the elucidation of the mechanism of this multi-protein complex and are of great commercial interest as pesticides. Characterisation of new inhibitors revealed that eight were Q_o site inhibitors and the other two were Q_i site inhibitors.

Table of Contents

List of Figures

Chapter 1

List of Tables

Chapter 5

Chapter 6

Acknowledgements

This study was funded by The Engineering and Physical Sciences Research Council and Aventis Cropscience Ltd.

I would like to thank the Department of Biology at University College London and Aventis Cropscience Ltd for giving me the opportunity to perform this study. I am especially grateful to my supervisor Prof. P.R. Rich for his guidance, advice, support and encouragement throughout the course of this study. I would like to thank Dr S. Dunn, Dr J. Dancer and Prof. J. Pillmoor at Aventis Cropscience Ltd, for their support, advice and Dr. C. Earnshaw for help with molecular modelling.

I would like to thank Prof. P. Heathcote for his assistance in the acquisition of EPR data and its interpretation, and for many useful discussions. I would also like to thank Prof. U. Brandt, Prof. H. Schägger and members of their respective laboratories for their help and advice in the preparation of purified bc_1 complex and for welcoming me to their laboratories. For technical assistance I would like to thank Mr J. Ramsey.

I would like to thank current and former members of the Glynn Laboratory of Bioenergetics and the Photosynthesis group for their support, friendship and for many useful discussions. I would especially like to mention members of the GLOB laboratory, Dr N. Fisher, Dr S. Husain, Dr I.P. Muhiuddin, Dr S. Jünemann, Dr B. Meunier, Miss J. Jassal, Miss B. Stewart, and Mrs S. Jones whom have made my years at UCL an enjoyable and wonderful learning experience.

Finally I would like to extend my gratitude to my family and friends, in particular Ade Marcus, Bunmi Marcus, Folake Awe, Kehinde Fashina, Tayo Akinsiku, Banke Awe and Juwon Awe, whom have been very understanding and have given me great support and encouragement throughout my studies.

Dedicated to my family and friends, and to the memory of my beloved parents, (Mr & Mrs Akinsiku) and Dr A. A. Amure without whom none of this would have been possible.

Abbreviations

ADP/ATP	Adenosine diphosphate / adenosine triphosphate
AS	Ammonium sulphate
b_H/b_L	High/low potential cytochrome *b* haem
BAL	British anti-lewisite
BSA	Bovine serum albumin
CHAPS	3-[(3-Cholamidopropyl)dimethylammonio]-1-propane sulphonate
CD	Circular dichroism spectroscopy
CMC	Critical micelle concentration
DBMIB	2,5-dibromo-3-methyl-6-isopropyl-p-benzoquinone
DCMU or diuron	3-(3',4'-dichlorophenyl-1,1'-dimethylurea)
DMSO	Dimethylsulphoxide
DPA	Diphenylamine
DQ/DQH_2	Decylubiquinone/Decylubiquinol
EDTA	Ethylene diamine tetraacetylene
EPR	Electron paramagnetic resonance spectroscopy
E_m/ E_h	Redox midpoint potential at pH 7/actual potential
FTIR	Fourier transform infrared spectroscopy
FAD/$FADH_2$	Oxidised/reduced flavin adenine dinucleotide
FMN	Flavin mononucleotide
FP	Flavoprotein domain of complex I and II
g	Relative centrifugal force
g	Spectroscopic splitting factor
HEPES	4-(2-Hydroxyethyl)-1-piperazineethanesulphonic acid
HP	Hydrophobic domain of complex I
HXP	Hydroxylapatite
HQNO	2-*n*-nonyl-4-hydroxyquinoline-N-oxide
IR	Infrared
ISP	Iron-sulphur protein
I_{50}	Concentration for half inhibition of turnover
K_D	Dissociation constant
K_{ic} or K_{iu}	Inhibition constants

KHP	Keilin Hartree membrane particles
MES	2-[n-morpholino]ethanesulphonic acid
MOA	β-methoxyacrylate
MOPS	3-(n-morpholino)-propanesulfonic acid
NAD^+/NADH	Oxidised/reduced nicotinamide adenine dinucleotide
NQH_2	Nonylubiquinol
N	Negative side of the membrane (negative potential)
Δp	Protonmotive force
P	Positive side of the membrane (positive potential)
-PEWY-	Highly conserved span of cytochrome *b* with this sequence in single-letter amino acid code
PC	Personal computer
PMS	N-methyl-phenazine methosulphate
PMSF	Phenylmethylsulphonyl fluoride
Q_i or Q_N	Quinone reduction site of the bc_1 complex
Q_o or Q_p	Quinone oxidation site of the bc_1 complex
Q_{os}	A strongly bound prosthetic quinone species
Q_{ow}	A weakly bound exchangeable quinone species
Q/QH_2	Ubiquinone / Ubiquinol
$Q^{\bullet-}/QH^-$	Ubisemiquinone/partially deprotonated ubiquinol
Q-pool	Ubiquinone pool
Q-cycle	Mechanism by which complex III operates
QFR	Quinol:fumarate oxidoreductase
SCR	Succinate cytochrome *c* reductase
SDS	Sodium dodecyl sulphate
SHE	Standard hydrogen electrode
SNR	Signal to noise ratio
SQR or SDH	Succinate:quinone oxidoreductase
Tris	Tris (hydroxymethyl aminoethane
UHDBT	5-n-undecyl-6-hydroxy-4,7-dioxobenzothiazole
UHDBQ	5-n-undecyl-6-hydroxy-1,4-benzoquinone
UHNQ	3-un-decyl-2-hydroxy-1,4-naphthoquinone
UV	Ultraviolet

CHAPTER 1

Introduction

1.1 Background

Cytochrome bc_1 complex is a central component of the mitochondrial respiratory chain. This chapter introduces the redox components of the mammalian respiratory chain, with emphasis on the cytochrome bc_1 complex.

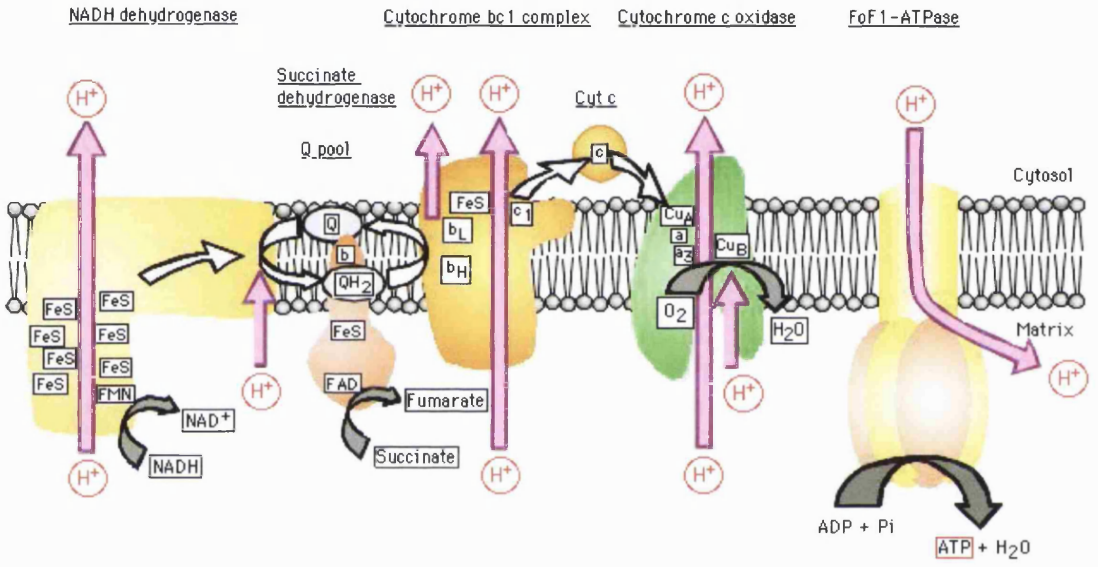

Fig. 1.1. The mitochondria respiratory chain and ATP synthase. Pink arrows indicate proton translocation. White arrows indicate electron transfer. Grey arrows indicate the conversion of substrate to products. Squares represent the redox groups of the respiratory chain. The figure was obtained from Prof. U. Brandt and adapted by Dr N. Fisher.

1.2 The respiratory chain

The respiratory chain (Fig. 1.1) oxidises substrates coming from a broad range of metabolic pathways, e.g. the citric acid cycle and the ß-oxidation pathway for fatty acids. Most of the chemical energy of the nutrient molecules is transformed into the group transfer potential of the hydrogen donors, NADH and $FADH_2$ [1]. The driving force of oxidative phosphorylation is the electron-transfer potential of these hydrogen

donors. The respiratory chain transfers electrons through a redox span of 1.1V, from the NAD^+ / NADH couple to the O_2 / $2H_2O$ couple (Fig. 1.2) [1].

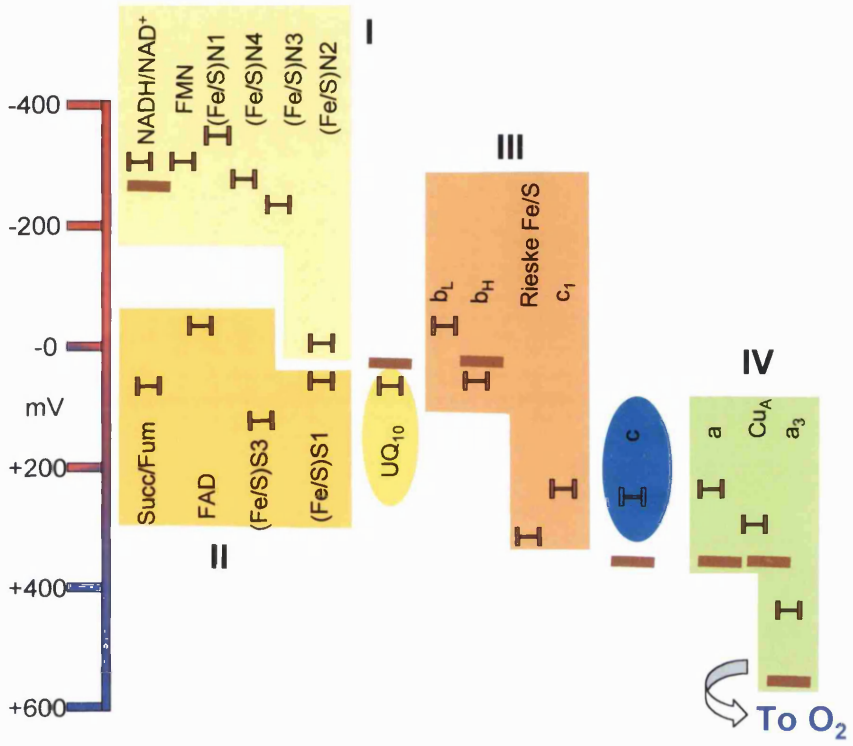

Fig 1.2. Midpoint potential (E_m) values for the components of the mitochondrial respiratory chain and actual potential (E_h) values for mitochondria respiring in state 4. Values are consensus values for mammalian mitochondria. (H) E_m values were obtained with de-energised mitochondria and (—) E_h values for mitochondria in state 4. The redox components fall into four equipotential groups, the gaps between which correspond to the regions where proton translocation occurs. The drop in E_h of the electrons across these gaps is conserved in protonmotive force (Δp). Succ, succinate; Fum, fumarate. The figure was reproduced from *Nicholls et al.* (1992) [1].

Oxidative phosphorylation supplies approximately 90% of the ATP synthesised in the cells of animals [2]. This process takes place at the inner mitochondrial membrane. The respiratory chain couples electron transfer to proton translocation across the inner mitochondrial membrane generating a protonmotive force (Δp), consisting of a pH gradient (ΔpH) and a membrane potential ($\Delta\psi$).

Subsequent diffusion of the protons back across the membrane via the F_1F_0 ATP synthase drives the synthesis of ATP within the mitochondrial matrix (Fig. 1.1). The protonmotive force is further used to drive the export of ATP into the cytosol. The respiratory chain of mammalian mitochondria is an assembly of more than 20 discrete carriers of electrons, which are grouped into four multi-subunit enzyme complexes. These enzymes are orientated in a side specific manner in the inner mitochondria membrane so that they can facilitate the establishment of a proton gradient.

Three of these enzymes, complexes I (NADH:ubiquinone oxidoreductase), III (ubiquinol:cytochrome *c* oxidoreductase) and IV (cytochrome *c* oxidase) act as redox driven proton pumps, in contrast to complex II (succinate:ubiquinone oxidoreductase). Essential for the completion of the electron transfer chain are two accessory redox components, the small lipophilic molecule ubiquinone or coenzyme Q and the relatively small hydrophilic protein cytochrome *c*. There are other complexes, not shown in Fig. 1.1, which allow entries of redox equivalents into the ubiquinone pool such as the electron transferring flavoproteins (ETF) and s,n-glycerophosphate dehydrogenase.

1.2.1 Redox carriers in the mammalian respiratory chain

The mammalian respiratory chain consists of many different redox carriers. Flavoproteins contain tightly bound FAD or FMN as prosthetic groups and undergo a ($2H^+ + 2e^-$) reduction. Cytochromes contain porphyrin prosthetic groups, which undergo a one electron reduction. Iron-sulphur (non-haem iron) proteins possess prosthetic groups, which also reduces in a one electron step. Ubiquinone (UQ) is a free lipid-soluble cofactor reduced by ($2H^+ + 2e^-$). Finally, the respiratory chain also consists of protein bound Cu, reducible from Cu^{2+} to Cu^+. The cytochromes are

classified according to the structure of their porphyrin prosthetic groups. The respiratory chain contains *a*-, *b*- and *c*- type cytochromes with haems A, B or C, respectively. In the case of haem C, it is covalently attached to the protein [1]. The redox carriers are arranged in such a way that there is a consecutive switching between proton and electron transfer carriers [2].

1.3 Quinone

Quinones are a central component of most photosynthetic and respiratory electron transfer chains. The three most commonly occurring quinones are ubiquinone, plastoquinone and menaquinone (Fig. 1.3). Ubiquinone is a component of mitochondrial and many bacterial respiratory chains, whereas plastoquinone is found in higher plant and algal photosynthetic chains. Menaquinone can be found in place of or in addition to ubiquinone in bacterial systems. All forms are extremely hydrophobic because of the long poly-isoprenyl side chain; n is generally between eight and 10 for ubiquinone and menaquinone, and nine for plastoquinone [3].

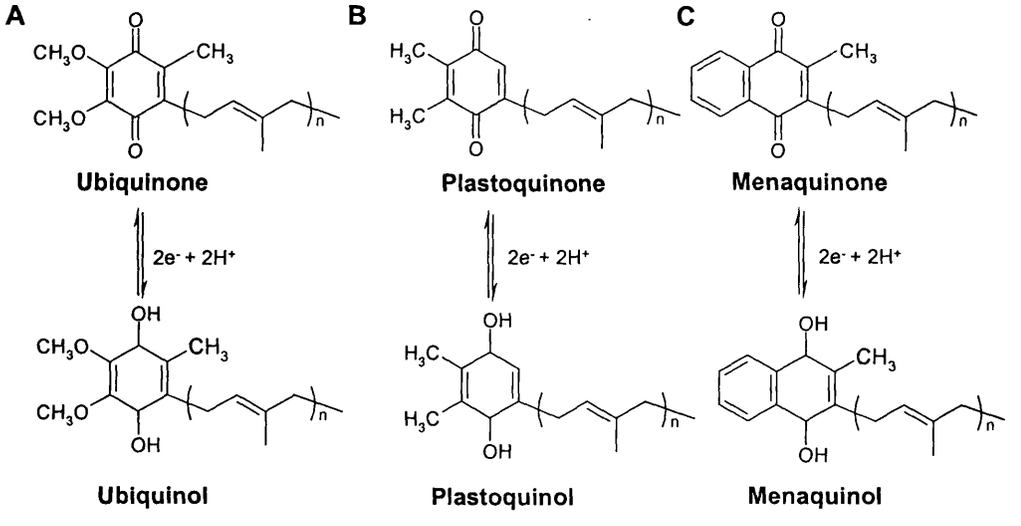

Fig. 1.3. Structures of naturally occurring quinone substrates and related redox carriers. n is generally between eight and 10 for ubiquinone and menaquinone, and nine for plastoquinone [3].

Ubiquinone (UQ) undergoes a $2H^+ + 2e^-$ reduction to form ubiquinol (UQH_2), although the partially-reduced free radical form ubisemiquinone, plays a role in cytochrome bc_1 complex. The half-protonated, fully reduced form UQH has a transient existence in both the photosynthetic reaction centre and the cytochrome bc_1 complex. Ubiquinone functions as a mobile redox carrier linking complexes I and II with complex III. In addition, it plays a more integral role as part of the 'Q-cycle' of electron transfer in complex III [1].

Quinones are often one of the essential elements of the energy coupling process. By using the mobility of quinones between quinone reactive sites (Q-sites) arranged on proteins across the membrane the coupling of electron transfer and proton translocation is achieved as part of the classical redox loop mechanism first described by Mitchell [4]. The proteins that reduce and oxidise these quinones have Q-sites that are good targets for pesticides. Many different Q-sites are known [3, 5].

1.4 Q-sites in membrane proteins as targets for inhibitors

A common feature of most biological respiratory and photosynthetic electron transfer chains is that at some stage they utilise the reduction and oxidation of quinones by redox proteins. These redox proteins all have Q-sites. The Q-sites are found in a number of enzymes in the mitochondria, such as complex I (NADH:ubiquinone oxidoreductase), complex II (succinate dehydrogenase, SDH) and the bc_1 complex (ubiquinol:cytochrome *c* oxidoreductase). In higher plant, yeast, fungi and green algal mitochondria, there are additional quinone binding enzymes such as ubiquinol oxidase and other types of NADH dehydrogenase ('externally facing' and NDH-2 types, Fig. 1.4). Bacterial systems, in addition to the enzymes already mentioned, contains a range of more specialised enzymes for the reduction or

oxidation of the quinone by diverse metabolic substrates.

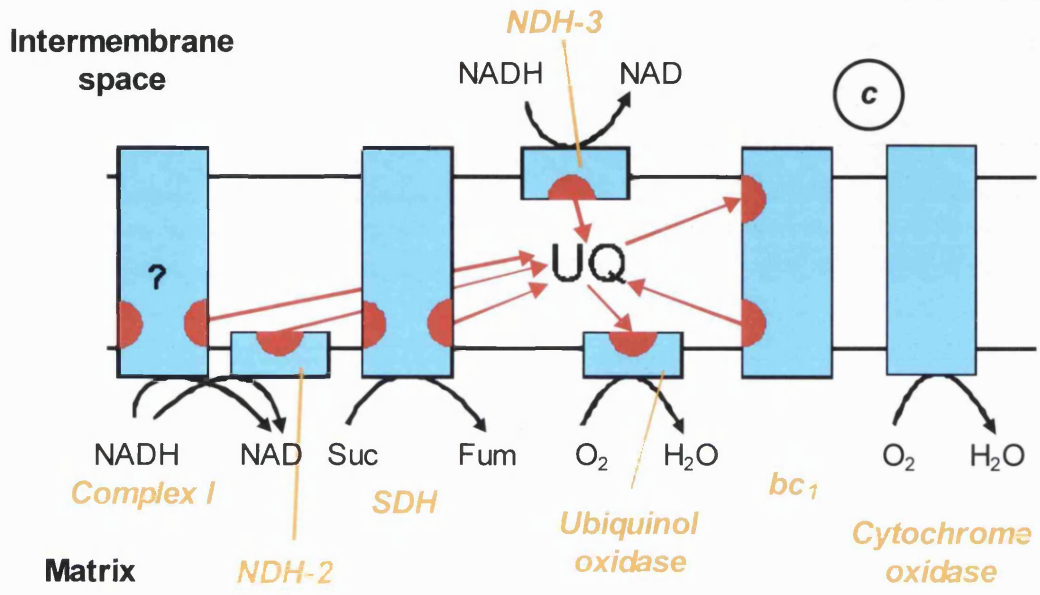

Fig. 1.4. Yeast, algal and higher plant mitochondria Q-sites as pesticide targets. Q-sites are indicated by red semicircles. Arrows indicate normal direction of electron flow. The question mark indicates uncertainty of the existence of the site. Components are not universally present in mitochondria from different species. UQ, ubiquinone, c, cytochrome *c*; Suc, succinate; Fum, fumarate. The figure was reproduced from *Rich* (1996) [3].

The Q-sites form a diverse class of target sites for specific inhibitors. Natural antagonists are known to target a number of these hydrophobic quinone-binding sites [3, 6, 7]. These antagonists are relatively hydrophobic and have considerable specificity for individual Q-sites [3]. Specificity for the enzyme in particular organism, e.g. for fungal or insect forms, remains a possibility. Differences in sensitivity of the same Q-site in different species are known, e.g. insensitivity of the bc_1 complex in fish to the classical inhibitor funiculosin [8]. Even a single amino acid change, which does not affect catalytic activity of the enzyme, can cause a dramatic change in inhibitor sensitivity. These properties make Q-sites good targets for pesticides [3, 9]. Commercial applications of some compounds that act on these Q-

sites have been described [10, 11].

1.4.1 Types of Q-sites

For many Q-sites, rapid movement of the quinone on and off the site occurs and the binding constant is relatively weak. This dynamic association is required if the quinone is to act to couple electron and proton transfer, and it provides the possibility of inhibition of the transiently unoccupied site by a quinone analogue or other molecule. Other Q-sites, such as the photosystem I A1-site, involve relatively immobile quinones and displacement by an antagonist is more difficult. In this case the quinone remains bound during its redox cycle and acts simply as a component of the intra-protein electron transfer chain [3].

1.4.2 Generic features of Q-sites

Some generic features of Q-sites may be defined. Typically, such sites are relatively hydrophobic and are accessed by the quinone from the membrane phase, as necessitated by the hydrophobic nature of the quinone substrate. The quinone/quinol group binds into the hydrophobic site primarily by interaction of appropriately placed hydrogen bonds with the carbonyl/hydroxyl moieties, and with the ring flanked by an aromatic and aliphatic residues [12]. Further interactions with the quinone hydrophobic side-chains occur and give steric limitations to possible antagonists [12]. For those sites (the majority) which interconvert the quinone, Q and the protonated quinol, QH_2, access of the sites to an aqueous phase is required so that associated protonation reactions can occur. Amino acid networks that might provide a proton-conducting hydrophilic channel through the protein structure can be identified in both the reaction centre and bc_1 structures. Lack of accessibility to protons radically

changes the properties of the bound quinone, such that it generally cycles only between the oxidised, Q, and ubisemiquinone, $Q^{\cdot-}$, forms [12]. Binding of the headgroup into the redox-competent Q-site may involve transient pre-binding steps within the approach channel [13].

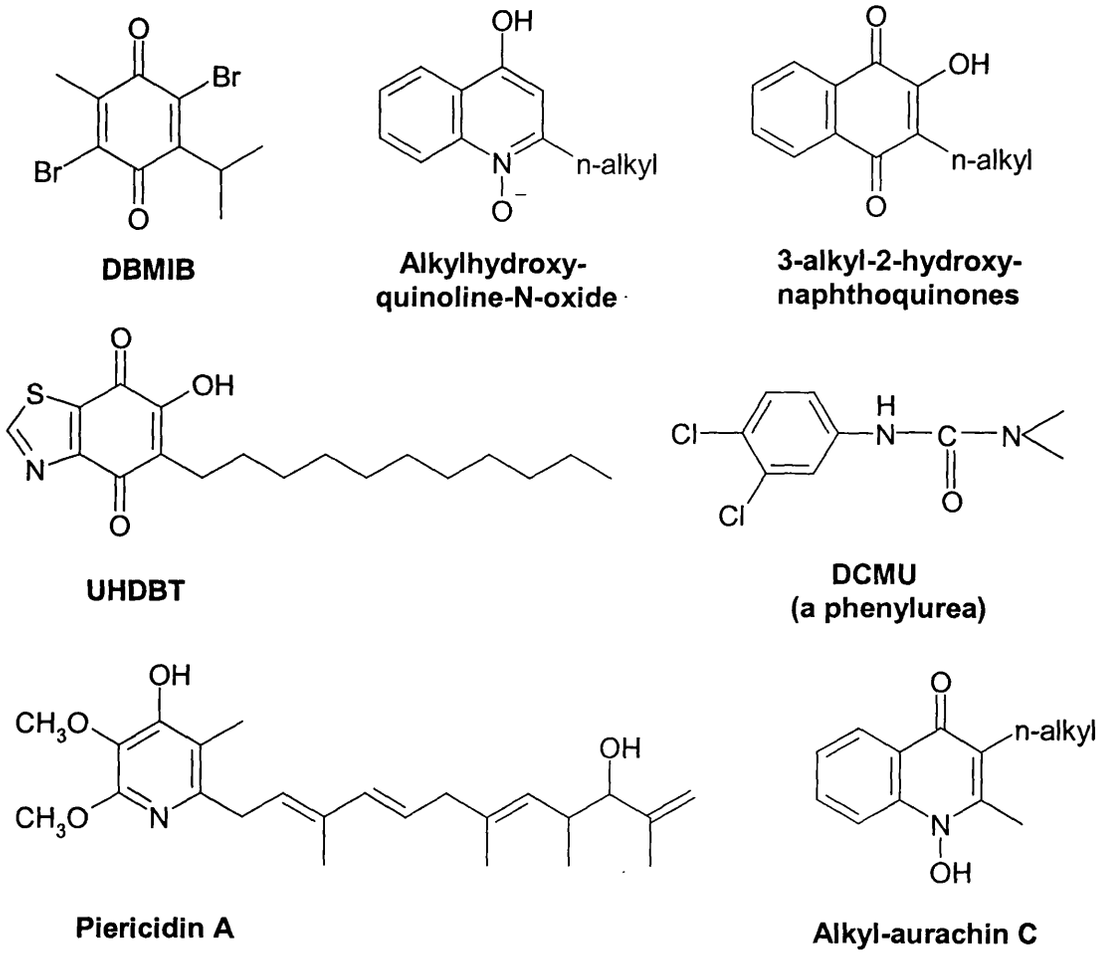

Fig. 1.5. Structures of quinone-like inhibitors of Q-sites. DBMIB, 2,5-dibromo-3-methyl-6-isopropyl-p-benzoquinone; UHDBT, 5-n-undecyl-6-hydroxy-4,7-dioxobenzothiazole; DCMU, 3-(3,4-dichlorophenyl-1,1-dimethylurea). The figure was reproduced from *Rich* (1996) [3].

1.4.3 Types of Q-site inhibitors

There is a large database of both synthetic and natural antagonists for a number of these Q-sites in photosynthesis and respiration. These inhibitors are extremely diverse. Many are relatively simple, with a clear resemblance to the structure of the natural quinones in terms of positions of hydrogen bonding groups and hydrophobic character. Indeed, some of these are quinones themselves or other redox active compounds (Fig. 1.5) [3, 6, 7]. They bind in place of the quinone in roughly the same manner. Some are redox inactive, at least in their mode of action (although unrelated electrochemical activity at extreme potentials is not uncommon). Such molecules have been discovered from natural sources, e.g. aurachins and piericidin A, but many synthetic compounds are also known e.g. triazines and DCMU (3-(3',4'-dichlorophenyl)-1,1'-dimethylurea).

Many synthetic quinones are known in this category (redox active inhibitors), e.g. various hydroxyl naphthoquinones and DBMIB (2,5-dibromo-3-methyl-6-isopropyl-p-benzoquinone). Although most presumably bind to the Q-site in the same manner as substrate quinone, their physical properties are such that catalytic turnover cannot be completed. In other instances redox active chemicals may not bind strongly to a Q-site at all, but show biological toxicity because they are biochemically reduced at the site and then autoxidise to produce toxic species such as superoxide anions.

Other Q-site inhibitors have a more complex structure (Fig. 1.6), and regions capable of binding in place of the substrate quinone are not so clear. These complex antagonists are likely to interact with the surrounding protein structure/approach channel so that the binding site only partly overlaps with that of the quinone, providing the possibility of specificity of inhibitors for individual Q-sites. Inhibition

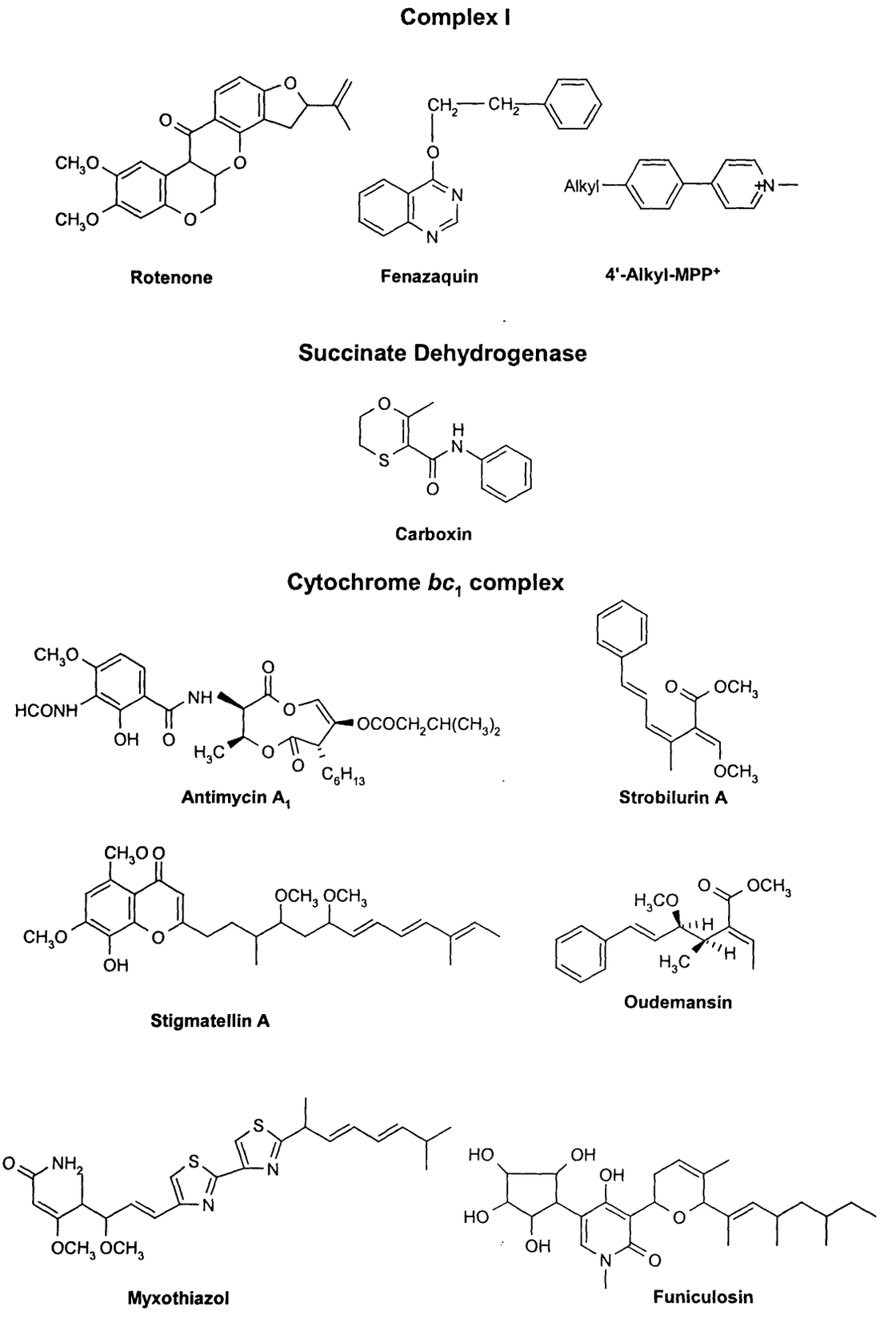

Fig. 1.6. Structures of some complex mitochondrial Q-site inhibitors. The figure was reproduced from *Rich* (1996) [3].

-again probably occurs by blocking the binding of the natural quinone, or possibly its access route to the site, although in some instances a more allosteric effect on the Q-site has been postulated. The more complex molecules were discovered initially from natural sources, e.g. antimycin A, stigmatellin, myxothiazol and rotenone (Fig. 1.6). For rotenone and (+)- antimycin A_1, the detailed molecular stereochemistry has been shown to be critical for activity. However, the full complexity of some natural compounds is not always essential. For example, in the case of stigmatellin the complicated tail can be replaced by a simple n-alkyl one of appropriate partition coefficient [3]. The crystal structure of a reaction centre-stigmatellin complex clearly shows that only the headgroup has specific interactions with the protein, to which it binds in a quinone-like manner [3]. Regardless of complexity of structure, some inhibitors are tight and immobile, staying attached to a single site for many seconds, whereas others are tight but rapidly mobile on a time scale between identical sites in the same membrane. The degree of inhibitor mobility is not directly correlated with quinone exchangeability in the site, and the factors which control the rate constants of inhibitor exchange are not understood [3]. The search for new inhibitors offers exciting prospects both for aiding the elucidation of the molecular properties of the enzymes and for providing new types of pesticides.

1.5 Complex I (NADH:ubiquinone oxidoreductase or NADH dehydrogenase)

Complex I is by far the most complex and largest multi-subunit complex of the respiratory chain. It is a major entrance for electrons into the respiratory chains of many purple bacteria and of mitochondria of most eukaryotes[14]. Complex I couples the transfer of two electrons from NADH to ubiquinone with the translocation of four

to five protons across the membrane of mitochondria and bacteria, conserving energy from the redox reactions in the form of protonmotive force (Δp). One molecule of FMN, up to nine iron-sulphur clusters and possibly two bound ubiquinone species participate in the reaction as redox groups. The exact sequence of operation of these groups and their coupling to proton translocation are not yet understood.

1.5.1 Subunit composition and redox centres

The bacterial complex consists of 14 different subunits, representing a minimal structural form of complex I. The *Neurospora crassa* complex contains 18 additional proteins that are unlikely to participate in electron transfer and proton translocation. Mammalian mitochondrial complex contains at least 29 additional proteins. The molecular mass of the bacterial complex is approximately 530kDa, the *N. crassa* complex is approximately 700kDa and that of the mitochondrial complex is approximately 1MDa respectively. The gross structure of complex I is known largely from image reconstruction pictures of electron microscopy patterns of two-dimensional crystals of *N. crassa* complex and *Escherichia coli*. Both have the same L-shaped overall structure with the peripheral arm protruding into the aqueous phase and a membrane arm extending into the membrane (Fig. 1.7). The similarity in structure of the two complexes shows that this unusual shape has been conserved in evolution and is essential for function.

N. crassa has been used as a eukaryotic model organism to study complex I structure. Such studies have revealed that its complex I is constructed of two distinct parts as described above. The peripheral arm contains some 15 nuclear-encoded subunits, seven of which are homologues of the seven in the bacterial complex. The arm corresponds to the bovine flavoprotein (FP) and iron-sulphur protein (ISP)

domains, and it contributes the NADH dehydrogenase function of the electron pathway with the NADH binding site, the FMN and at least four iron-sulphur clusters (N1a, N1b, N3 and N4). The membrane arm corresponds to the bovine hydrophobic (HP) domain and is composed of some 17 proteins among which are the seven most hydrophobic polypeptides that are homologues of the seven in the bacterial complex. They are encoded by the mitochondrial genome. The arm contributes the ubiquinone hydrogenase function of complex I with one iron-sulphur cluster (N2) and the ubiquinone binding site(s) [15].

1.5.2 Mechanism

The catalytic activity of complex I can be summarised by the following reaction (Eq. 1.1, m, matrix and c, cytosol):

$$NADH + Q + 5H^{+}_{m} \rightarrow NAD^{+} + QH_2 + 4H^{+}_{c} \qquad \textbf{(Eq. 1.1)}$$

NADH is oxidised at the flavin centre. Two electrons are transferred with release of $2H^+$ from the flavin centre through the multitude of iron-sulphur clusters within the peripheral arm to a ubiquinone-binding site whose location is still unknown. Proton translocation could occur by a ubiquinone cycle analogous to that discussed for the bc_1 complex [2]. The existence of multiple inhibitor binding sites has been taken as evidence for independent ubiquinone binding sites; two classes of complex I inhibitors are represented by rotenone and piericidin (Fig. 1.5-6) respectively. Whether the flavin participates in proton pumping is still a matter of discussion, this would require a long proton channel from the peripheral arm out in the matrix to the cytosol for which there is no precedent [2].

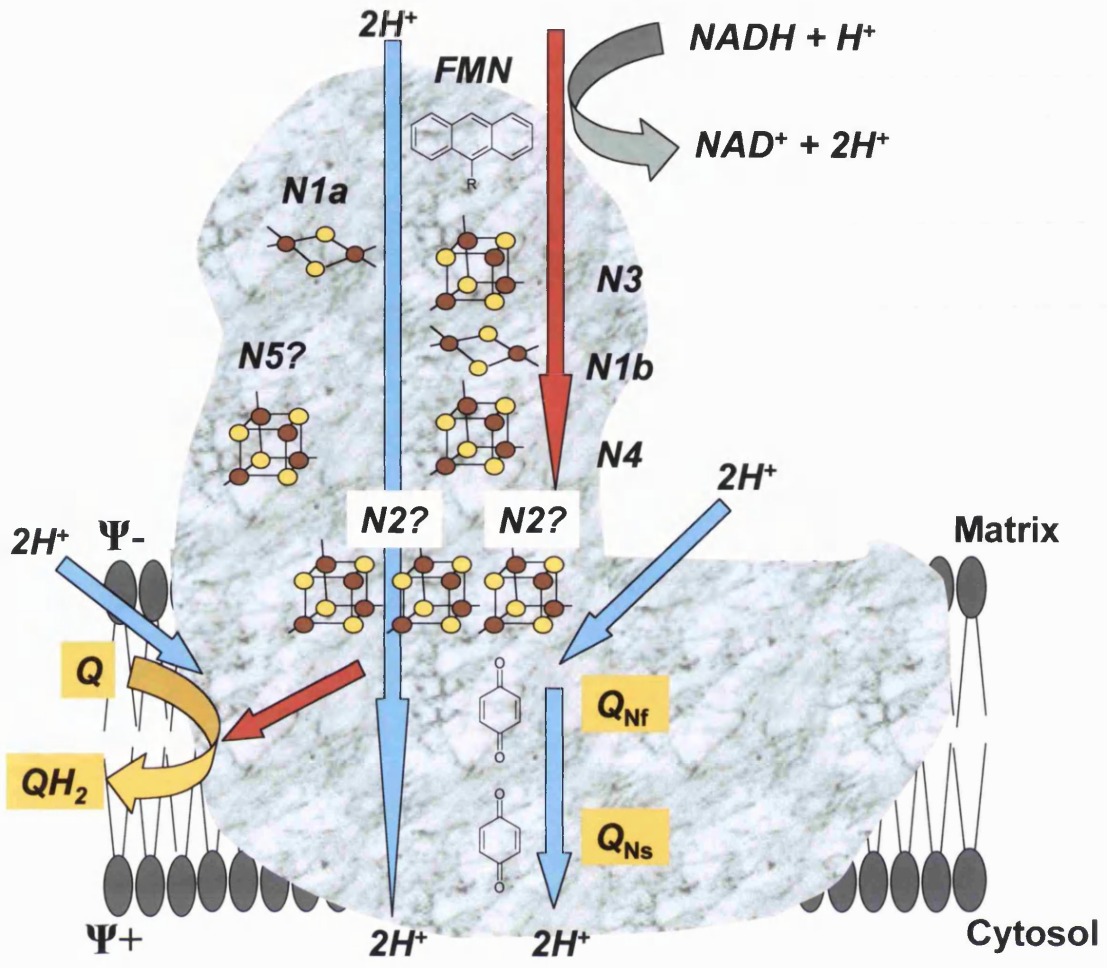

Fig. 1.7. A schematic outline of minimal Complex I (NADH:ubiquinone oxidoreductase). A summary of present knowledge on the proposed distribution of different redox centres, NADH and Q binding sites. The cluster N1c is not included in this figure because this cluster is not present in the bovine heart, *Paracoccus denitrificans* and *Rhodobacter capsulatus* Complex I. Blue arrows indicate proton translocation. Red arrows indicate electron transfer. Yellow and grey arrows indicate conversion of substrate to products. Ψ, membrane potential; Question marks indicate uncertainty of the location of redox centre, Q_{Nf} and Q_{Ns}. 'N' refer to the closeness of the ubiquinones to N2, and 's' and 'f' refer to the speed (slow or fast) of spin relaxation of the ubisemiquinones formed, reflecting their different strength of spin coupling with cluster N2 [16].

1.6. Complex II (Succinate:ubiquinone oxidoreductase, SQR)

Complex II of the aerobic respiratory chain oxidises succinate (a product of the citric acid cycle) to fumarate and via a series of electron carriers, reduces a ubiquinone to ubiquinol (in effect passing electrons into the ubiquinone pool) [17]. The details of the reactions and interactions of Complex II are not well understood. However, Complex II has extremely similar structural and catalytic properties to quinol:fumarate oxidoreductase (QFR), for which X-ray crystal structures have recently become available [17]. These offer new insights into the structure-function relationships of this class of flavoenzymes. QFR is found in anaerobic organisms that respire using fumarate as terminal electron acceptor instead of oxygen [18].

1.6.1 Subunit composition and redox centres

Complex II consists of only three or four subunits (Fig. 1.8). The mammalian enzyme has four subunits and has a hydrophilic domain exposed to the matrix in mitochondria, and a hydrophobic domain that spans the membrane and acts as a membrane anchor [18]. The hydrophilic domain which contains the dicarboxylate binding site is composed of FP (64-79kDa) subunit, with one covalently bound FAD molecule to a histidine ligand and ISP (27-31kDa) subunit containing three iron-sulphur clusters, a [2Fe2S] cluster denoted S1, a [4Fe4S] cluster denoted S2 and a [3Fe4S] cluster denoted S3. These catalyse electron transfer between the FAD and the ubiquinone pool in the membrane [18].

The hydrophobic domain anchors the FP and ISP subunits to the membrane and is required for ubiquinone reduction and oxidation. The anchor domains, although sharing a common origin, show the largest variation in composition and primary sequence. It consists of one larger or two smaller hydrophobic polypeptides and

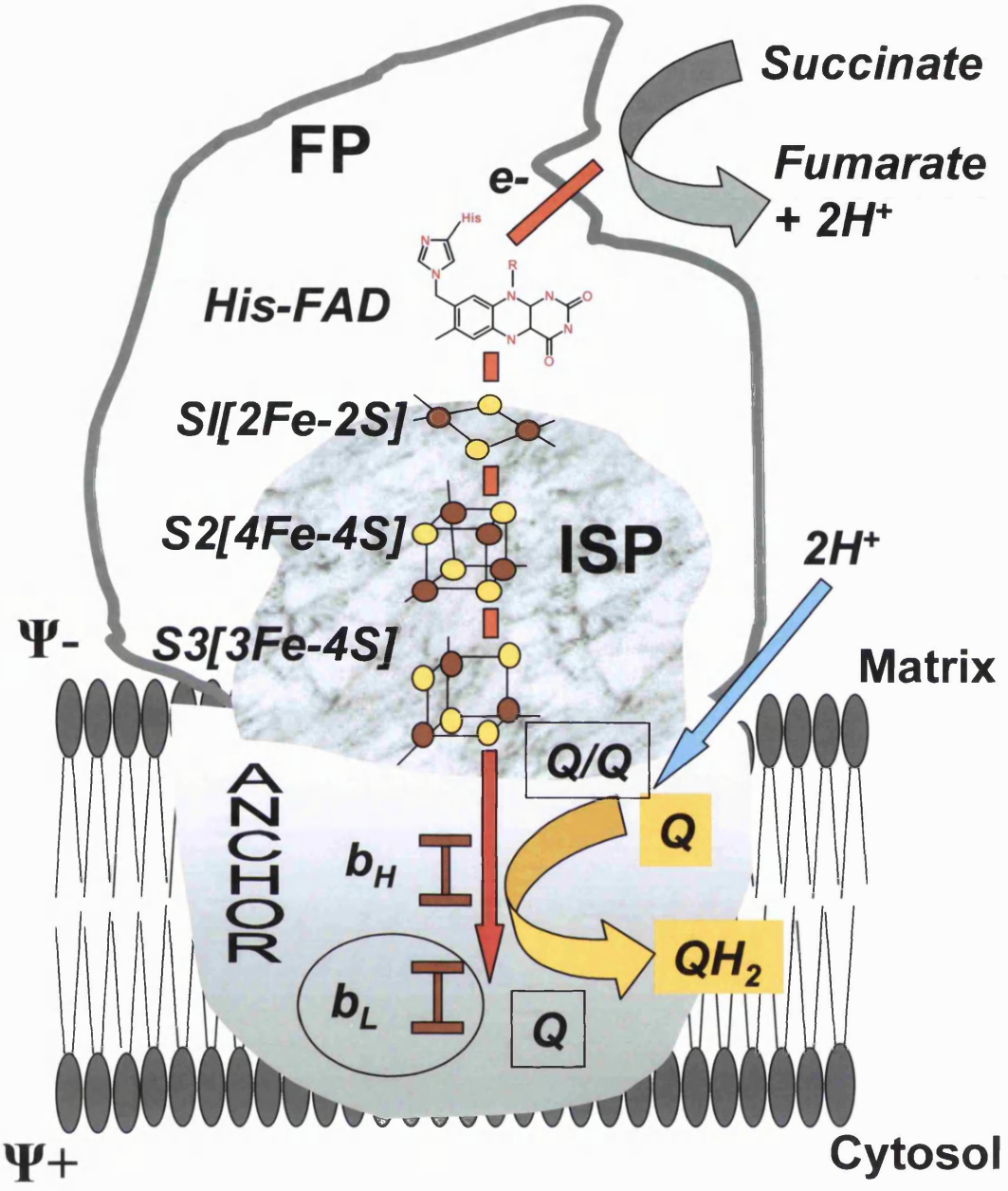

Fig. 1.8. A schematic of Complex II (succinate:ubiquinone oxidoreductase, SQR). The sequence of electron carriers is based largely on the X-ray crystal structures of quinone fumarate reductase (QFR) [17, 18]. Different numbers of quinone binding sites and haems are present in SQR/QFR. The mitochondrial Complex II consists of cytochrome b_H and one ubiquinone binding site, located between S3 and haem b_H. Red arrow indicates electron transfer. Blue arrow indicates proton uptake. Grey and yellow arrows indicate conversion of substrate to products. FP, flavoprotein; ISP, iron-sulphur protein; Ψ, positive or negative membrane potential.

-contains either one or two protohaem IX groups (b_H and b_L, indicating a high and low redox midpoint potential respectively), with hexa-coordinated iron, or no haem at all. The mitochondrial Complex II anchor consists of two small hydrophobic polypeptides (15kDa and 13kDa respectively) and only one protohaem IX group with hexa-coordinated iron. The ubiquinone and inhibitor binding site/s are located in the membrane anchor but the exact number and location are still uncertain. The ubiquinone binding site in mammalian SQR is likely to be close to the negative side of the membrane, bordering both ISP and the membrane anchor, in close contact with both iron-sulphur cluster S3 and haem b_H (Fig. 1.8) [18]. The exact detail of the ubiquinone chemistry is subject to much debate due to the different membrane anchor types and final ubiquinone acceptors found in SQR/QFR.

1.6.2 Mechanism

The catalytic activity of complex II can be summarised by the following reaction (Eq. 1.2):

$$\text{Succinate} + Q = \text{Fumarate} + QH_2 \qquad \textbf{(Eq. 1.2)}$$

This is composed of 'two half reactions' (Eq. 1.3-4):

$$\text{Succinate} = \text{Fumarate} + 2H^+ + 2e^- \ (E_m = +30\text{mV}) \qquad \textbf{(Eq. 1.3)}$$

$$\text{Quinone} + 2H^+ + 2e^- = \text{Quinol} \ (E_m = +70\text{mV}) \qquad \textbf{(Eq. 1.4)}$$

Electron transfer is not coupled to proton translocation across the membrane: $2H^+$ are released into the matrix space during oxidation of succinate and $2H^+$ are taken up from the matrix space during reduction of ubiquinone.

The redox centres of complex II shows a large disparity of potentials (Table 1.1). This makes a linear sequence of electron transfer with the interposition of S2 [4Fe4S] cluster between S1 [2Fe2S] and S3 [3Fe4S] difficult to envisage due to its characteristic low potential. However, progress in the field during the last few years culminating in the X-ray crystallographic structural information for the *E. coli* and *Wolinella succinogenes* QFR enzymes [17] do indeed support such a linear pathway (Fig. 1.8).

Table 1.1. The midpoint potential of the redox centres of *Bos taurus* complex II

Prosthetic groups	E_{m7} (mV)
FAD	-79
S1 [2Fe2S]	+0
S2 [4Fe4S]	-260
S3 [3Fe4S]	+60 / +120
Haem b_H	-185

The E_{m7} (mV) values were obtained from *Hägerhäll et al.* (1997) [18].

The first electron acceptor is FAD. However FAD is a two-electron carrier, in contrast to the other prosthetic groups, which are one-electron carriers. The FAD free radical state has a high stability constant, indicating that FAD performs the n = 2 to n = 1 conversion required to transfer electrons from succinate to the iron-sulphur cluster [18]. S1 [2Fe2S] is the next electron acceptor and it is in close proximity to FAD. Interestingly, in the crystal structures the next acceptor is the S2 [4Fe4S] cluster, dispelling past misgivings about a role for [4Fe4S] in linear electron transport because of its low potential. One possibility for the low observed E_m of S2 is anti-

cooperative electrostatic interactions, so that its operative potential is much higher than that measured by redox titration. The integrity of S3 [3Fe4S] is essential for binding of the ISP to the anchor domain and electron exchange with bound ubiquinone [17]. It thus acts as a gateway for electron transfer to haem b_H.

The role of haem in electron transfer remains enigmatic, especially since some forms of SQR/QFR have no haem group. It seems likely that the presence of haem is not obligatory for succinate oxidation *per se*. Kinetic evidence from isolated *W. succinogenes* QFR suggests the rate constants for reduction of the haem by succinate and oxidation by fumarate are at least as fast as the enzyme turnover. Therefore, in the case of this QFR, the haems may play a more essential role [18].

1.7 Cytochrome *c* oxidase (complex IV)

Cytochrome *c* oxidase is the terminal electron transfer complex of the respiratory chains of mitochondria and many aerobic bacteria. It catalyses the transfer of electrons from cytochrome *c* to molecular oxygen (reducing the latter to water) and couples this reaction to the pumping of protons across the inner membrane from the matrix to the cytoplasmic side. This is then used to drive the synthesis of ATP, transport solutes and perform other useful work. The reaction is inhibited by a range of small molecules such as cyanide [19].

Cytochrome *c* oxidases are members of the superfamily of haem-copper containing terminal oxidases, which also includes many ubiquinol oxidases, e.g. cytochrome bo_3 from *E. coli*. The crystal structures of a number of cytochrome *c* oxidases have been determined including the bacterial cytochrome *c* oxidase from the soil bacterium *Paracoccus denitrificans* and its mammalian counterpart from bovine heart mitochondria [20].

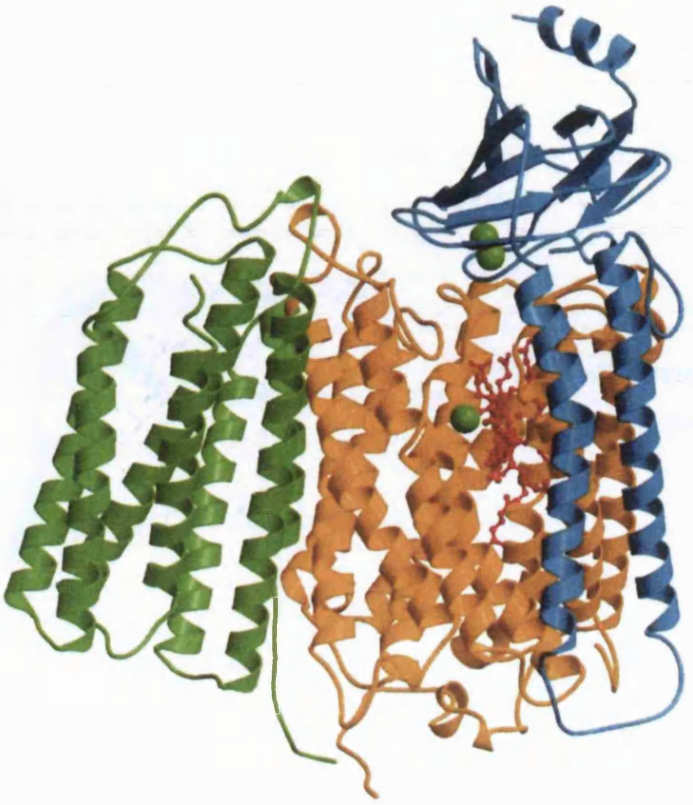

Fig. 1.9. Critical subunits of bovine cytochrome *c* oxidase. The core of cytochrome *c* oxidase has three subunits. Subunit I (yellow) has two haem groups, *a* and a_3 (red), and a copper ion, Cu_B (green sphere). Haem a_3 and Cu_B form the binuclear Fe-Cu centre. Subunit II (blue) contains two Cu ions (green spheres) complexed with the SH groups of two cysteine residues in a binuclear centre, Cu_A, that resembles the [2Fe2S] centres of iron-sulphur proteins. This binuclear centre and the cytochrome *c* binding site are located in a domain of subunit II that protrudes from the inner membrane into the intermembrane space. Subunit III (light green) is apparently essential for function but its role is not well understood. The figure was reproduced from *Lehninger et al.* (2000) [21].

1.7.1 Subunit composition and redox centres

Mammalian mitochondrial cytochrome *c* oxidase is composed of 13 polypeptides. Subunits I, II, and III (the three largest) are common to all eukaryotic cytochrome oxidases, and to many from prokaryotes, and form the catalytic core of the enzyme (Fig. 1.9). Only subunits I and II have redox-active catalytic sites. Subunit

I contain low spin haem *a* and the binuclear copper-iron centre consisting of a high spin haem a_3 and a Cu_B atom. Subunit II contains the EPR- and optically-visible mixed valence [Cu(1.5)-Cu(1.5)] binuclear copper complex, Cu_A centre [20]. The function of subunit III remains enigmatic, although it is present in nearly all cytochrome *c* oxidases. It does not contain redox active centres and appears not to be essential for catalytic activity. However, like the nuclear-encoded subunits, it may be important for the assembly and/or stability of the enzyme. It may also have a role in modulating the activity of the oxidase or form the entrance to a proposed oxygen channel leading to the active site [19, 20].

The number of additional subunits is variable between organisms and they have no known functions [19]. Subunit VI_b binds a zinc ion of unknown function in a tetrahedral co-ordination and subunit VI_a seems to be responsible for the dimerisation of the mitochondrial cytochrome *c* oxidase [20]. The rest might have a structural role, perhaps being required for correct assembly or for anchoring the enzyme in the membrane in some way. Furthermore, they might also have a regulatory role modulating the activity of the enzyme in response to the binding of allosteric effectors, e.g. nucleotides. The notion of subtle mechanistic influences is partly supported by the occurrence of enzyme isoforms [19].

Cytochrome *c* oxidase is dimeric *in situ* and is often dimeric when isolated. However, it appears that the monomeric reaction cycle is rapid and coupled to proton-translocation. Perhaps the most likely reason for the dimeric structure of many respiratory and photosynthetic complexes, including the terminal oxidases, is the enhanced opportunity to shield the biochemical reactions from unwanted side reactions by the binding together of the faces of the protein which are closest to the redox centres [19].

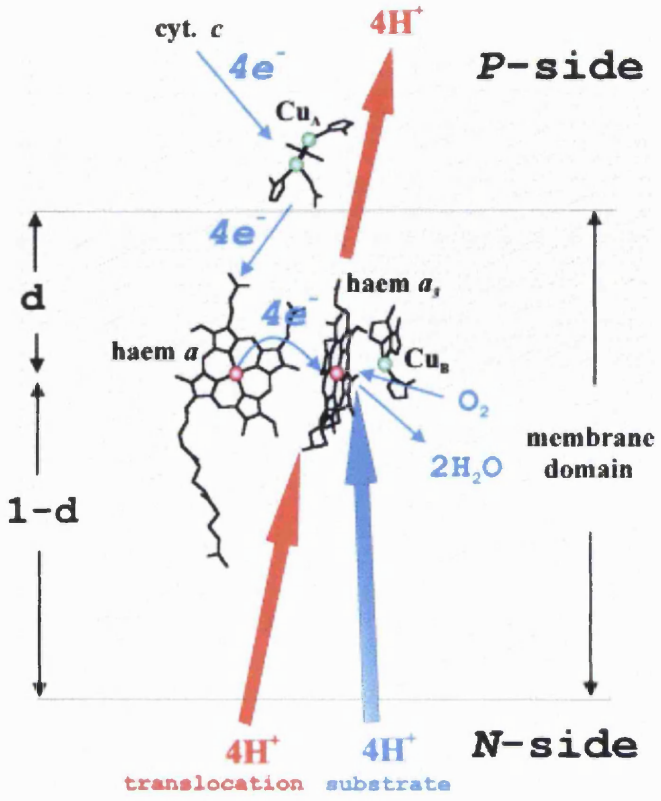

Fig. 1.10. Overall functioning of cytochrome *c* oxidase. d is the relative dielectric depth of the haem groups and Cu_B in the membrane domain of the protein. Thick red arrows indicate proton translocation. Thick blue arrow indicates the uptake of substrate protons to the binuclear centre. Thin blue arrows indicate electron transfer, oxygen uptake and water release. The figure was reproduced from *Wikström et al.* (2000) [22].

1.7.2 Mechanism

Cytochrome *c* oxidase reaction is deceptively simple (Eq. 1.5), the four-electron reduction of dioxygen to two water molecules. Four equivalents of cytochrome *c* provide the electrons and the four-substrate protons are taken up by the enzyme, finally forming the product H_2O (Fig. 1.10) [23].

$$4\ \text{cyt}\ c^{2+} + 4\ H^+ + O_2 \rightarrow 4\ \text{cyt}\ c^{3+} + 2\ H_2O \qquad \textbf{(Eq. 1.5)}$$

In addition, for every electron that is transferred from cytochrome *c* to cytochrome *c* oxidase, one proton is pumped through the protein giving four

translocated protons to add to the electrochemical gradient across the respiratory membrane (Eq. 1.6) [24].

$$8H^{+}_{in} + 4\,\text{cyt c}^{2-} + O_2 \Leftrightarrow 4\,\text{cyt c}^{3-} + 2H_2O + 4H^{+}_{out} \qquad \textbf{(Eq. 1.6)}$$

Hence for each turnover, a total of eight charges are moved across the membrane through the enzyme, eight protons are taken up from the mitochondrial matrix (or bacterial cytoplasm for the prokaryotic oxidase) and four protons are delivered to the mitochondrial intermembrane space (or bacterial periplasm for the prokaryotic oxidase) (Eq. 1.6) [23].

1.7.2.1 Electron transfer pathways

The electron source for cytochrome *c* oxidase is cytochrome *c*. This small water-soluble protein is located in the aqueous space between the outer and inner mitochondrial membranes. It contains one covalently linked haem C group in a protein structure, which has been well resolved and intensively studied as a model haem-containing protein. Cytochrome *c* is itself reduced by cytochrome c_1 of the cytochrome bc_1 complex and diffuses in its reduced form to cytochrome *c* oxidase where it is oxidised. It therefore acts as an electron shuttle between the last two protein complexes of the mitochondrial respiratory chain [19].

The primary electron acceptor from cytochrome *c* is generally accepted as being Cu_A. From Cu_A the electron is transferred to haem *a* and then onto haem a_3 of the binuclear haem a_3/Cu_B centre. Electron transfer between haem *a* and the binuclear centre is complicated by the fact that oxygen reduction chemistry takes place in four distinct steps [19, 20].

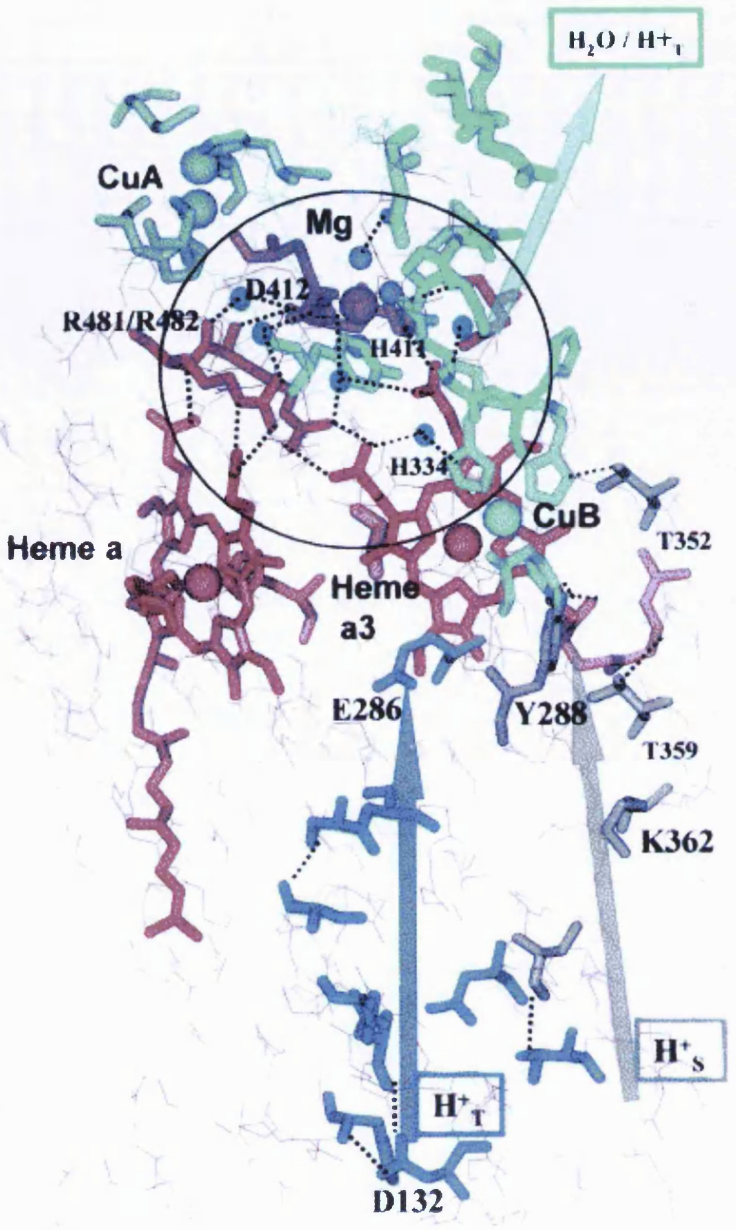

Fig. 1.11. Structure of the metal centres and key residues from the co-ordinates of the bovine heart cytochrome *c* oxidase, showing proposed proton pathways and the subunit I/II interface region above the haems. H^+_T translocated proton; H^+_S substrate protons; Cu_A^+ ligands (blue); Cu_B^+ ligands (green); Mg^+ ligands (purple); haems Fe^+ (red); K-channel residues (olive); D-channel residues (dark blue); H_2O (blue). Circle indicates hydrogen-bonded network surrounding Mg and involving the haem *a* and a_3 propionates with hydrogen bonds depicted as dotted lines. The figure was reproduced from *Mills et al.* (2000) [24].

1.7.2.2 Proton transfer pathways

Mutational studies and X-ray crystal structures have revealed at least two putative proton-conducting pathways that are common to bacterial and mammalian oxidases, designated the D- and K-channels due to an aspartate (D132, *Rb. sphaeroides* numbering) and a lysine (K362), which are key conserved residues in these proton channels (Fig. 1.11) [23, 24].

The K-channel leads from the mitochondrial matrix (bacterial cytoplasmic surface) to the region on the haem-copper centre (Fig. 1.11). The K-channel is necessary for the reduction of the haem-copper prior to the binding of oxygen [23]. The D-channel leads from an aspartic acid group (D132) near the surface of the enzyme facing the mitochondrial matrix (bacterial cytoplasm) to a buried glutamic acid (E286) in the middle of the protein. There are a number of internal water molecules within the protein that provide a reasonable pathway for proton diffusion between these two residues, separated by 25Å. Mutational studies indicate that proton translocation through the D-channel occurs during the steps in the catalytic cycle (Fig. 1.12) following the binding of dioxygen to the reduced haem-copper centre. The role of the D-channel, if any, in the steps prior to the binding of O_2 is still an open question. The fate of protons beyond E286 is not clear. It is possible that the E286 side chain swings between alternate positions to switch the direction of proton flux. In one position, E286 can direct substrate protons to the active site possibly using transient water molecules to provide connectivity. Similarly, in another position, E286 might direct pumped protons across the membrane via a transient connection with the propionate residues of haem a_3 [23].

Initially, the K-channel was originally designated as the "substrate" proton channel and the D-channel as the proton-pumping channel. However, mutational

studies offer conflicting evidence over the role of the two channels. It is generally accepted that the D-channel is required for proton pumping but the question remains whether protons from the D-channel are also required as substrate protons in the second half of the reaction cycle. An alternative explanation is that only when the K-channel is compromised are substrate protons supplied by the D-channel [24]. Regarding the K-channel, there are questions as to whether it is performing a simple static role as a pathway for transfer of substrate protons (or ligands generally) into the binuclear centre in the initial reductive half of the reaction cycle, or is a proton trap for the neutralisation of charge ("dielectric well") throughout the cycle [24, 25].

The entry channel for oxygen (if at all required) and the exit channels for pumped-protons and water remain unclear. However, several channels have been proposed. The proposed exit channel for water and pumped-protons centre around the charged residues (mainly arginines) and the Mg-binding site [20, 23-25].

1.7.2.3 The dioxygen cycle

The catalytic dioxygen cycle of cytochrome *c* oxidase with respect to the oxygen chemistry is summarised in Fig. 1.12. The catalytic cycle is traditionally viewed as consisting of two asymmetric halves. The first part includes the initial reduction of both haem a_3 and Cu_B in the binuclear centre, the initial binding of dioxygen, and its reduction to the intermediate compound P. The second part of the catalytic cycle includes two single electron transfer steps, first to convert compound P to compound F, and then converting compound F to the ferric form of haem a_3. The detailed mechanisms of the catalytic cycle are still uncertain.

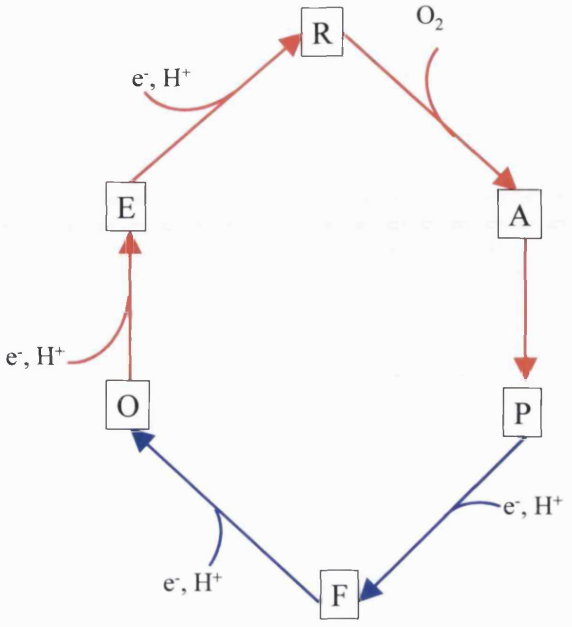

Fig. 1.12. The dioxygen cycle of cytochrome *c* oxidase. The cycle starts with the fully oxidised binuclear centre denoted O. When the first electron arrives at the active site, species E forms. This reaction is coupled to a proton uptake via the K-channel to maintain electroneutrality. Species E waits for the second electron to arrive at the binuclear centre to form species R, which is known to react rapidly with dioxygen to form compound A. After compound P formation, the catalytic cycle proceeds by two single electron steps of reduction of compounds P and F to return to the oxidised species O. The figure was adapted from *Zaslavsky et al.* (2000) [23].

1.7.2.4 The coupling of electron transfer and proton translocation

The mechanism by which electron transfer and proton translocations are coupled to each other at the molecular level remains unclear. A direct mechanism where the coupling is achieved by subtle changes occurring very close to the redox centres, e.g. through the involvement of metal ligands, is favoured.

Rich et al. 1998 [25] suggest a model (a "glutamate trap" mechanism) in which electron accumulation at the binuclear centre drives the uptake of protons (to maintain local electroneutrality) from the i-side, i.e. the bacterial cytoplasm. These

protons are stored in a proton trap close to the binuclear site but physically separated from the oxygen chemistry. Upon formation of the reactive oxygen species P and F, protons required for water formation are taken up from the i-side and through electrostatic repulsion, the trapped protons are expelled into the periplasm. Critical to such a scheme is the nature of the gating process that inhibits the access of the trapped protons to the i-side (preventing the trapped protons from being expelled back into the cytoplasm) and at the same time, allowing substrate protons to enter from the i-side. There are many proposals concerning the nature of the gating mechanism all involve protonation and ligand exchanges on haem a_3, between haem a_3 and Cu_B, and on Cu_B (the "histidine cycle") [20, 22, 26].

1.8 ATP synthase (complex V or F_1F_o ATPase)

ATP synthase is a ubiquitous enzyme that is located in the thylakoid membrane of chloroplasts, and the inner membranes of bacteria and mitochondria. The binding change mechanism proposed by Boyer (see below), allows ATP synthase to employ mechanical rotation to convert the protonmotive force generated by respiration or photosynthesis to drive the synthesis of ATP from ADP and inorganic phosphate (P_i) [15, 27].

1.8.1 Subunit composition

ATP synthase exhibits a tripartite structure consisting of an extrinsic membrane complex, an intrinsic membrane domain and the two connecting stalks, the central rotor and the stator stalks (Fig. 1.13). The enzyme resolves into two parts: F_1 (factor 1), a globular water soluble unit in the form of a sphere 9-10nm in diameter which contains the catalytic binding sites for the substrates ADP and inorganic

phosphate, and F_O (factor oligomycin), a detergent soluble unit which is embedded in the membrane. The two connecting stalks are composed of components of both F_1 and F_O [15]. The X-ray crystal structure of the F_1 catalytic domain has been completed and an electron density map of the F_1-c_{10} sub-complex has provided a glimpse of the motor in the membrane domain [28].

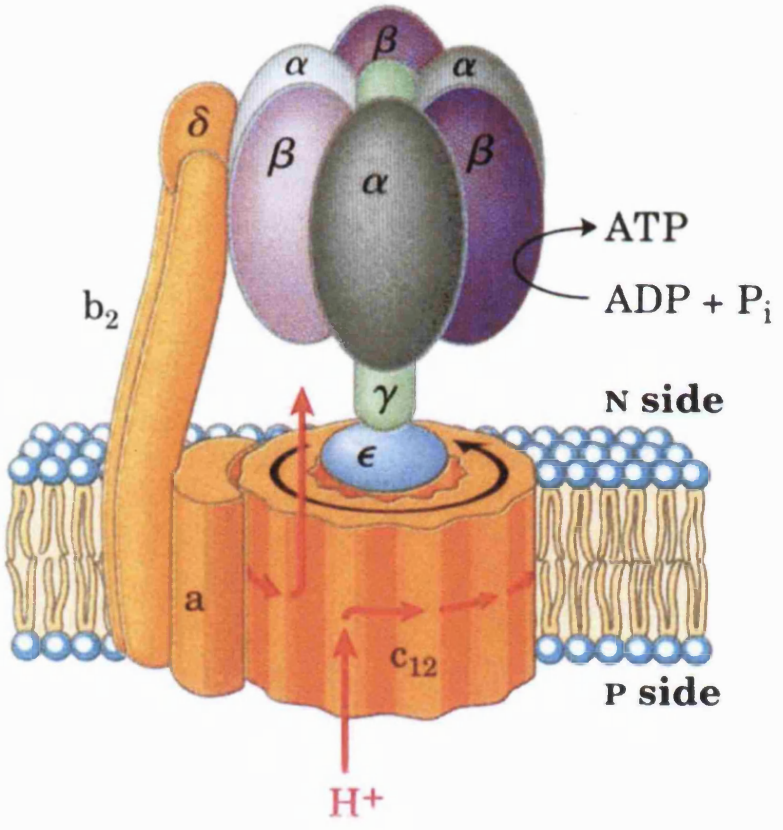

Fig. 1.13. Structure of ATP synthase deduced from biochemical and crystallographic studies. The two b subunits of F_O associate firmly with the α and β subunits of F_1, holding them fixed relative to the membrane. In F_O, the membrane-embedded cylinder of c subunits is attached to the shaft made up of F_1 subunits γ and ε. As protons flow through the membrane from the 'P' side to the 'N' side via F_O, the cylinder and shaft rotate, and the β subunits of F_1 change conformation as the γ subunit associates with each in turn. The structure largely resembles the eubacterial enzyme [28]. Proton transfer is mediated between subunit-a and c [29]. The figure was reproduced from *Lehninger* (2000) [21].

The F_1 complex is composed of five subunit types in an $\alpha_3\beta_3\gamma_1\delta_1\varepsilon_1$ stoichiometry, with a ring of α and β subunits alternating around a single γ subunit. The three catalytic sites of F_1 are located on the three β subunits at α/β subunit interfaces. They exist in three conformational states, designated 'loose', 'tight' and 'open' according to their binding affinities for different substrates. The F_O domain is formed from three subunits types in an ab_2c_{12} stoichiometry in bacterial systems. Up to 10 additional subunits are found in animal enzymes. The relationship of the eight subunits is shown in Fig. 1.13. The c subunits form an annular arrangement, with subunits a and b_2 on the periphery of the cylinder. The ring of c subunits makes contact with subunit a in F_O. The long helical b subunit dimer forms the stator stalk by linking subunit a of F_O with the δ subunit and one of the α subunits of F_1. Subunits γ and ε form the central stalk linking the $(\alpha\beta)_3$ sub-complex of F_1 to subunit c of F_O in eubacteria [28].

1.8.2 Mechanism

The reaction catalysed by ATP synthase is summarised in Eq. 1.7 (the intermembrane space is denoted 'out' and the matrix as 'in'):

$$ADP + Pi + nH^+_{out} \rightarrow ATP + H_2O + nH^+_{in} \qquad \textbf{(Eq. 1.7)}$$

ATP synthesis is dependent upon the rotation of F_1 relative to F_O and this movement is driven by protons passing between the c subunits. A model suggested by W. Junge is that the a-subunit provides a port for entry of protons from outside and also interacts with one of the twelve c subunits. This interaction deprotonates a conserved acidic amino acid residue on the c subunit. When a proton enters from the outside, it neutralises the conserved acidic residue in the c-subunit. Only in this neutral form can

the c-subunit now rotate away from association with the a-subunit. Rotation then brings the next neutral c-subunit to the exit port, allowing it to lose its proton (which migrates to the inside of the membrane, i.e. matrix) and associate with the a-subunit complex. Successive protonations allow the c-subunit complex to rotate. About nine to 12 protons are needed for a full rotation of ATP synthase. The number is dependent upon the number of c subunits in the complex. The continuous rotation in 30° steps of one c-subunit relative to the a-subunit generates the torque necessary for the 120° rotation of the γ-ε subunit of the central stalk. The b and δ-subunits acts as a stator, keeping the $\alpha_3\beta_3$-subunits stationary [29].

As described above, rotation drives synthesis of ATP at the three β subunits of F_1 (Fig. 1.14) [30]. The active site on the β subunit can exist in three states, loose, tight and open. Each β subunit on F_1 is in a different state. ATP production occurs as follows. One ADP and one inorganic phosphate bind to a β subunit in its loose state. A one-third clockwise rotation (120°) of the γ subunit in the core of F_1 domain changes the conformation of the β subunits. The subunit in the loose state now switches to tight, bringing the ADP and phosphate in close proximity. ADP and phosphate then react to form ATP. More protons passing through subunit c cause another rotation and the β subunit in the tight state now switches to the open state. In this state, the active site does not bind ATP well and the molecule diffuses into the cytoplasm. Another rotation changes the state back to loose and the β subunit is ready for another cycle. The cycle is continuous and for each full turn (360°) of the γ subunit, three molecules of ATP are produced.

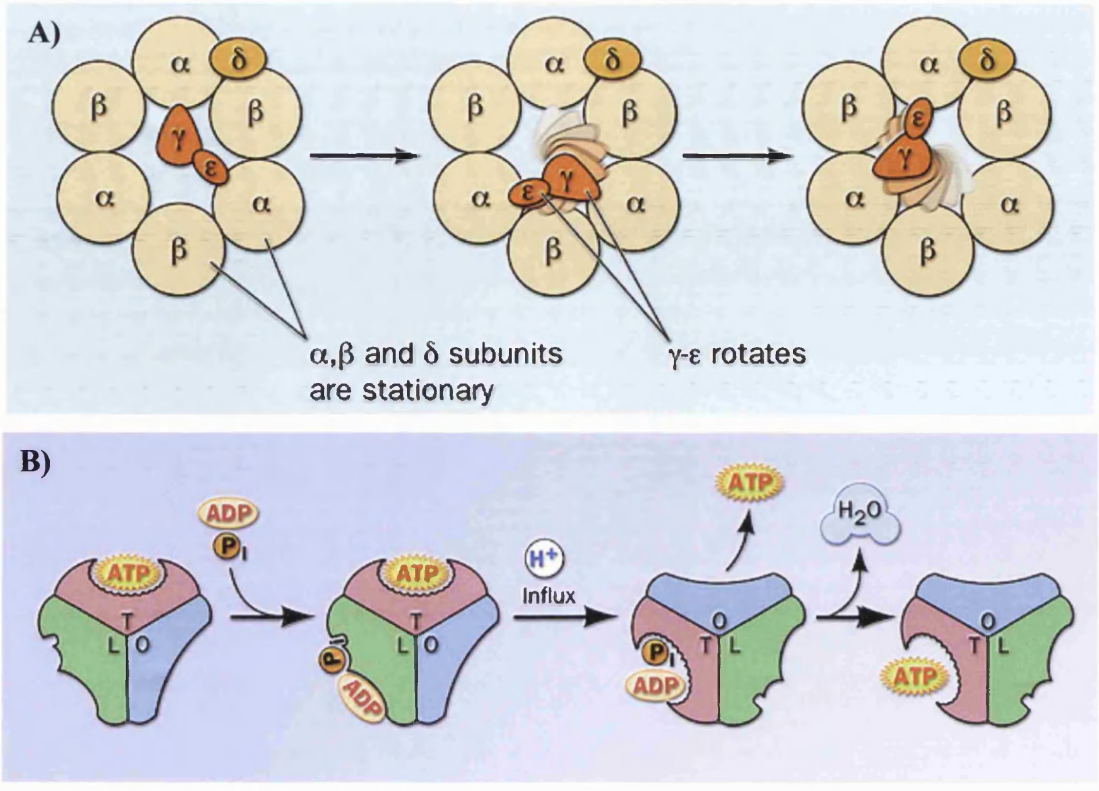

Fig. 1.14. Mechanism of the ATP synthase. (F_1 viewed from above the membrane) **A)** Rotation of the γ-ε subunit. The rotation is initiated by protonation of a carboxylate residue in the c-subunit via a-subunit. The rotation is transmitted to the γ-ε subunit and results in changes in the conformation of β subunits, which drives ATP synthesis. **B)** Boyer's binding change mechanism. β subunits sequentially cycle through three different conformational states, open (O), loose (L) and tight (T) during which ATP is synthesised. The figures were reproduced from *Lehninger* (2000) [21].

1.9 Cytochrome bc_1 complex (Complex III or ubiquinol:cytochrome *c* oxidoreductase)

The cytochrome bc_1 complex is a central component of the electron transfer respiratory chain in mitochondria and in many aerobic or photosynthetic bacteria. It is a member of the cytochrome *bc* superfamily, which also includes the thylakoid cytochrome b_6f complex. The cytochrome *bc* complexes catalyse electron transfer from a hydroquinone [ubiquinol, menaquinol, or plastoquinol (Fig. 1.3)] to a small soluble redox protein such as cytochrome *c* or plastocyanin. The mammalian

cytochrome bc_1 complex oxidises ubiquinol and transfers one electron via a bifurcated pathway to cytochrome *c*. The *bc* complexes couple electron transfer to proton translocation across the membranes of mitochondria, chloroplast and bacteria. Members of the cytochrome *bc* superfamily all have cytochrome *b* and 'Rieske' ISP with significant sequence homology [31].

1.9.1 Subunit composition

The complexity of the subunit composition has increased in the course of evolution. Some of the bc_1 complexes from *Parococcus*, *Rhodospirillum rubrum*, *Rb. capsulatus* and α-proteobacteria have been isolated in a fully functional state with only three subunits: cytochrome *b* (with two B-type haems), cytochrome c_1 and 'Rieske' ISP [31]. In contrast, eukaryotic bc_1 complexes have an additional seven or eight subunits lacking prosthetic groups. In summary, bacterial bc_1 complexes consist of only three or four subunits, chloroplast complexes of four or five subunits, yeast of 10 and mammals of 11 subunits [2].

1.9.2 Structure

Even before atomic structures were available, general features of structure and mechanism were anticipated from sequence analysis, structural prediction, and biochemical and biophysical studies. Furthermore, the positions of residue changes leading to inhibitor resistance [32-34] have provided a wealth of additional detail. Atomic models of several vertebrate mitochondrial complexes have become available [35-39]. In addition, that of the yeast complex has recently been published (Table 1.2). Aside from the different positions of the 'Rieske' ISP extrinsic domain, and

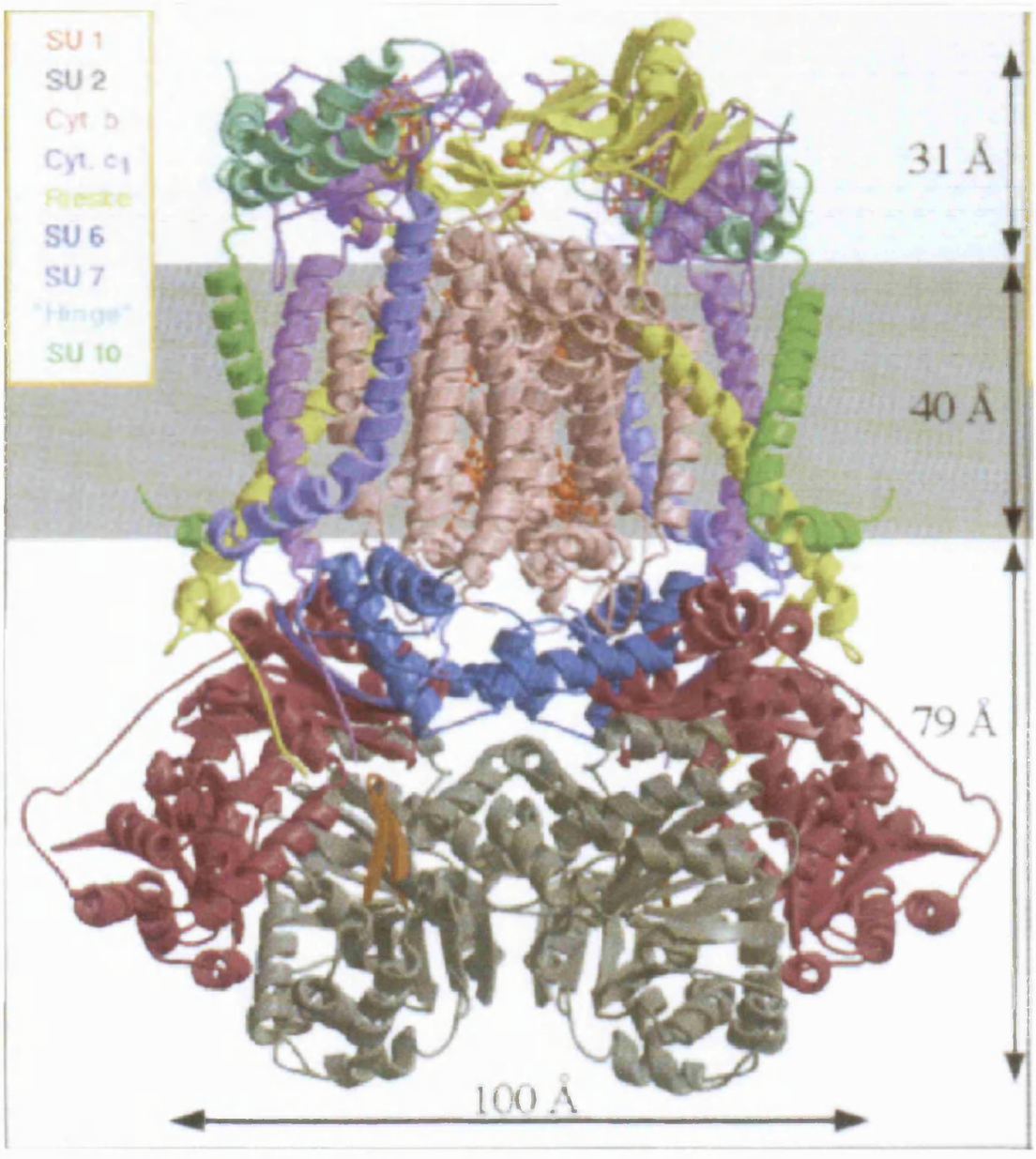

Fig. 1.15. Stereo-view ribbon diagrams of native chicken bc_1 complex dimer. The molecular two-fold axis runs vertically between the two monomers. The key for the colour coding of each subunit is given in the inset. Ubiquinones, phospholipids and detergent molecules are not shown for clarity. The presumed membrane bilayer is represented by a grey band. The molecule can be divided into three regions from top to bottom: intermembrane space region, membrane spanning region and matrix region. The dimensions of each region of the molecule and the colour code of each subunit are indicated. The figure was reproduced from *Zhang et al.* (1998) [35].

-excepting subunit 9, there were no major differences between the six vertebrate structures [31].

Table 1.2. Published cytochrome bc_1 complex crystal structures

Source	PDB code	Resolution (Å)	Authors	Additional information
Bovine	1QCR	2.7	*Xia et al.* [36]	α–Carbon atoms only
Chicken	1BCC	3.16	*Zhang et al.* [35]	Ubiquinone and phospholipid present
Chicken	3BCC	3.7	*Zhang et al.* [35]	Stigmatellin and antimycin A bound
Chicken	2BCC	3.5	*Crofts et al.* [40]	Stigmatellin bound
Bovine	1BE3	3.0	*Iwata et al.* [37]	
Bovine	1BGY	3.0	*Iwata et al.* [37]	
Yeast	1EZV	2.3	*Hunte et al.* [41]	Antiybody Fv-fragment present
Bovine	1RIE	1.50	*Iwata et al.* [42]	'Rieske' ISP only

PDB, Protein database; ISP, iron-sulphur protein.

The main features of the crystal structures of the bc_1 complexes from chicken [35] (Fig. 1.15) and bovine heart [38] are: the bc_1 complex is a dimer in its native state; the prosthetic groups required for full function are in subunits 3 (cytochrome *b*), 4 (cytochrome c_1) and 5 ('Rieske' ISP); the cytochrome b_L haems of the two monomers are 21Å apart in the dimer and are closest to the interface between the two monomers, while the cytochrome b_H haems are 33Å apart and the distance between the iron-sulphur cluster; cytochrome c_1 in both structures is about 31Å. However, these structures and others revealed that the iron-sulphur cluster could occupy two positions, the proximal position in which the cluster is close to the surface of cytochrome *b* and the distal or c_1 position, in which the cluster is close to the haem of

cytochrome c_1 and farther from cytochrome *b* [31]. In addition, further analysis of crystal structures suggests internal conformational changes of the 'Rieske' ISP [37, 43]. These differences, together with the fact that electron transfer between the iron-sulphur cluster and cytochrome c_1 is rapid (with $t_{1/2} < 10^{-6}$s) and the distance of 31Å would not permit this rate, suggests that the flexibility of the 'Rieske' ISP is mechanistically important in the electron transfer process [31,35-38,44]. Structures of bc_1 complexes have shown some surprising features associated with the Q_o site. Most dramatic has been the position of the extrinsic head of the 'Rieske' ISP, which has now been found in at least three different conformations in different crystals of the native enzyme. A second feature of interest has been the large volume of the Q_o site and the differential binding of inhibitors of different classes in the site. Most importantly, the native structures show no ubiquinone occupant, so conclusions about the binding of substrate, intermediate ubisemiquinone and product remains speculative [45].

1.9.3 Individual protein subunits

The subunit composition has been well characterised and all sequences have been determined for the mitochondrial complexes from three divergent branches of metazoans: bovine, potato and yeast [31]. Ten subunits show sequence similarity between all three complexes and constitute the entire complexes of yeast and potato. An eleventh subunit present only in bovine complex (subunit 9) turned out to be the leader sequence of the 'Rieske' ISP, which is retained within the mature complex [31]. Table 1.3 relates the subunit numbers in the different complexes.

Table 1.3. Correlation of the subunits of the bc_1 complex from bovine, potato and yeast

Subunit	Name	Bovine		Potato		Yeast	
		Subunit	MW (kDa)	Subunit	MW (kDa)	Subunit	MW (kDa)
1	Core I	1	53.603	1	56.222	1	48.729
2	Core II	2	46.524	2	51.744	2	38.705
3	Cytochrome *b*	3	42.734	3	44.283	3	43.663
4	Cytochrome c_1	4	27.287	4	27.106	4	27.771
5	'Rieske'	5	21.609	5	23.141	5	20.099
6	Quinone binding	6	13.477	6	14.471	7	10.975
7	Quinone binding	7	9.720	7	8.317	8	17.257
8	Hinge	8	9.175	9	8.048	6	14.565
9	Cytochrome c_1 associated	10	7.197	8	7.977	9	7.476
10	'Rieske' associated	11	6.520	10	6.874	10	8.593

The subunits are listed in order of decreasing molecular weight of the bovine protein. The molecular mass of a monomer of bovine cytochrome bc_1 complex, calculated from sequences and including the haems, iron-sulphur cluster and post-translationally modified residues, is 243kDa [31]. The table was reproduced from *Berry et al.* (2000) [31].

The peripheral core proteins (Fig. 1.15) are the two largest proteins and have sequence homology with a family of heterodimeric zinc proteases including insulinase and the general mitochondrial processing peptidase [46]. In fact, in some mitochondria the bc_1 core subunits serve as the matrix processing peptidase [31, 46].

The next largest three subunits are those with redox centres (Fig. 1.16). The cytochrome *b* has two B-type haems, which are quite different in spectral and redox properties. The two components are haems b_H and b_L, 'H' indicating the higher and 'L' the lower midpoint potential species. The haems are located on opposite sides of

the membrane, each ligated by two axial histidines. Cytochrome *b* is the only mitochondrially-encoded protein in the bc_1 complex. It also contains the ubiquinone (Q_i, reduction and Q_o, oxidation) and inhibitor binding sites [31].

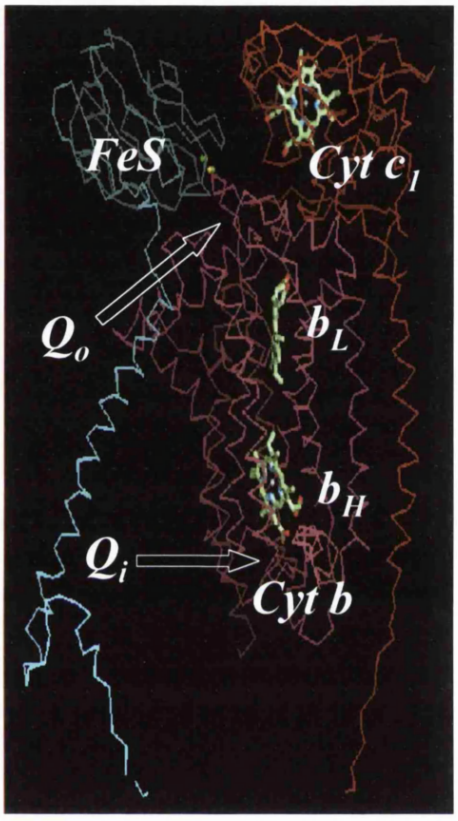

Fig. 1.16. Positions of the metal centres of the bc_1 complex. The arrows indicate the ubiquinol oxidation (Q_o) and reduction (Q_i) sites. The figure was produced using co-ordinates from *Zhang et al.* (1998) [35] datafile 3BCC in the molecular simulation software Quanta' 97 protein design (MSI, molecular simulations). Haems are shown in green as stick models. 'Rieske' [2Fe2S] cluster atoms are shown as small green and yellow spheres. Cytochrome *b*, magenta; Cytochrome c_1, red; 'Rieske' ISP, blue.

Cytochrome c_1 was the second mitochondrial protein (cytochrome *c* was the first) to have its sequence determined. Associated with it is subunit 8 (the hinge protein), which is required for interaction between cytochrome c_1 and cytochrome *c*. The bovine cytochrome consists of 241 residues, with a hydrophobic domain near the

C terminus acting as the hydrophobic anchor to the membrane. It is the only one of the seven transmembrane subunits that does not have its N-terminus on the matrix (N) side of the membrane. The X-ray crystal structure showed that the hydrophilic domain has a similar basic fold to that of cytochrome *c* and other class I *c*-type cytochromes [31]. It differs in having insertions and deletions in the various linker peptides between the core helices. It has a long N-terminal extension before the first helix. [31]. Subunit 8 is bound to the side of the extrinsic domain of cytochrome c_1, contacting mainly the N-terminal extension [31].

The 'Rieske' ISP was first described and isolated by *Rieske et al.* (1967) [47, 48] and was later identified as the 'oxidation factor' of the bc_1 complex [49-51]. Its presence in the bc_1 complex was recognised by its characteristic electron paramagnetic resonance (EPR) spectrum in the reduced form [52, 53] with a $g_y = 1.9$ EPR signal, the g_x band of which is sensitive to the occupant of the Q_o site. The iron-sulphur cluster has an unusually high redox midpoint potential. In contrast to the classical ferredoxin-type [2Fe2S] centres, where all the ligands are all cysteine residues (via the γ-sulphur), the 'Rieske' ISP centre has two cysteine and two histidine ligands (via the Nδ atoms) [31, 54]. A further two cysteines form disulphide bridges that are important for the stability of the cluster [31]. The mature 'Rieske' ISP has 196 residues with a membrane anchor of one transmembrane helix near the N terminus. The water-soluble global domain (incorporating the cluster) provided the first atomic-resolution structure of a part of the mitochondrial bc_1 complex [55]. The extrinsic domain crosses over and associates with cytochromes *b* and c_1 of the other monomer. Thus dimerisation is required to complete the high-potential chain. However, there are reports of active monomers of the complex [31, 56].

The terminology of smaller subunits in different bc_1 complexes varies (Table 1.3). For example, the hinge protein is subunit 8 in bovine complex, subunit 9 in the potato complex and subunit 6 in the yeast complex [31]. The small subunits, i.e. subunits 6-10, in the yeast enzyme are important for the assembly of the oligomeric complexes and for the integration of the redox centres into the larger "apo-redox peptides" [2].

Subunits 6 and 7 (bovine) have both been called quinone-binding proteins but from the structure it appears that neither has any role in either of the known ubiquinone binding sites [31]. Subunit 9 of the bovine complex is the presequence of the 'Rieske' ISP and has no homologue in the yeast or potato complexes. Subunits 10 and 11 (bovine) are small hydrophobic proteins making a single transmembrane helix each. Subunit 11 is the first protein to be dissociated when the complex is delipidated by binding to hydroxylapatite and washing with increasing Triton X-100 concentrations. Full activity can be restored to the subunit by adding phospholipid, so subunit 11 is not required for activity. Upon fractionation of bovine bc_1 complex the first two subunits to be removed are subunit 11 and the 'Rieske' ISP. Therefore, subunit 11 has become known as the 'Rieske' associated protein. Subunit 11 is not seen in all of the crystal structures, in contrast to subunit 10, which is always present.

1.9.4 The protonmotive Q-cycle

The bc_1 complex transfers electrons from ubiquinol to cytochrome *c* and couples this electron transfer to proton translocation across the inner mitochondrial or bacterial plasma membrane, establishing a protonmotive force (Δp) across the membrane by a Q-cycle mechanism first described by Peter Mitchell [4]. The Q-cycle as originally proposed adequately accounts for most of the experimental results.

However, recent structural data revealing a number of unexpected features have led to refinement of the model. Of particular interest is the mobility of the 'Rieske' iron-sulphur centre and the rather large possible domain in which ubiquinol might bind [31].

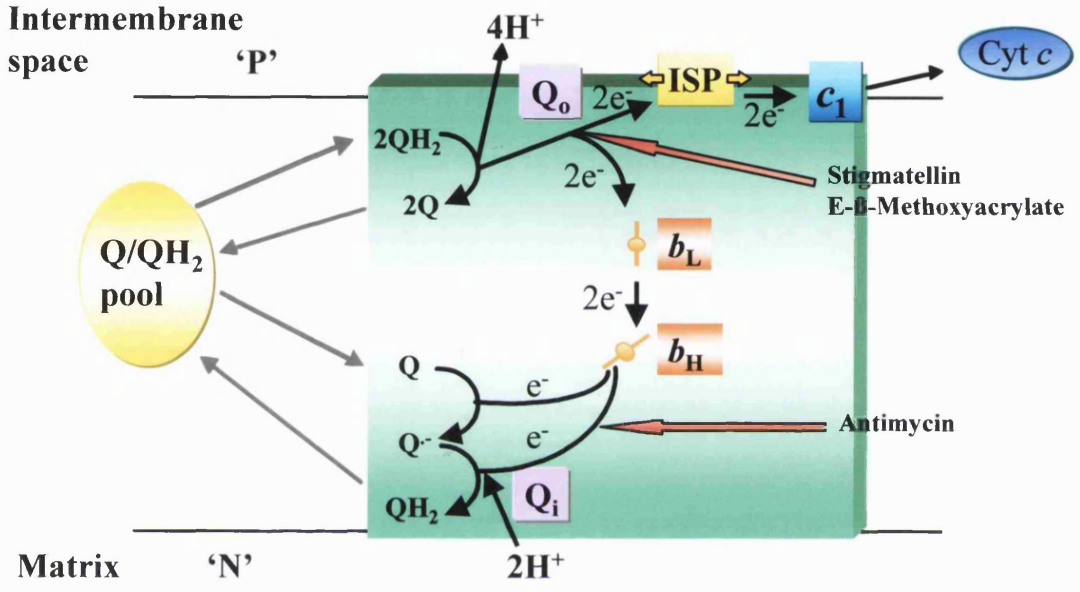

Fig. 1.17. The protonmotive Q-cycle. Solid arrows indicate the path of electron flow from ubiquinol (QH_2) to cytochrome *c* (Cyt *c*) through the redox prosthetic groups of the bc_1 complex. Grey arrows indicate exchange of ubiquinones (Q) with the Q-pool. Red arrows point to the sites of inhibition for the respective inhibitors. Yellow arrows indicate the mobility of the soluble head domain of the 'Rieske' iron-sulphur protein (ISP). P/N, positive and negative side of the membrane; haems b_L and b_H, low- and high-potential haems of cytochrome *b*; e^-, electron; c_1, cytochrome c_1; $Q^{\cdot-}$, ubisemiquinone.

The Q-cycle (Fig. 1.17) involves the oxidation of ubiquinol at the Q_o site. As a result, two protons are released on the 'P' side of the membrane (cytoplasmic side) and electron flow is bifurcated. One electron is transferred via the 'Rieske' ISP and cytochrome c_1 onto cytochrome *c* (a mobile electron carrier) to finally reduce cytochrome *c* oxidase. The second electron reduces the b_L haem, then passes across

the membrane to the b_H haem and finally onto the Q_i site where it reduces a ubiquinone to a relatively stable ubisemiquinone (the low-potential chain). A second oxidation of ubiquinol at the Q_o site completes the cycle with the ubisemiquinone at the Q_i site reduced to a ubiquinol with the uptake of two protons from the matrix ('N' side).

The QH_2 oxidation reaction is the limiting step and proceeds through a high activation barrier. It is generally proposed that an intermediate ubisemiquinone is generated at the Q_o site but this has not been detected. The overall reaction generates four protons in the intermembrane space (periplasmic space in bacteria), called the P-side for its positive potential, and the formation of ubiquinol uses up two protons from the mitochondrial matrix (or cytoplasmic side), called the N-side for its negative potential (Eq. 1.8):

$$QH_2 + 2cyt^{c3+} + 2H^+_N \Leftrightarrow Q + 2cyt^{c2+} + 4H^+_P \qquad \textbf{(Eq. 1.8)}$$

1.9.4.1 Inhibitors of the Q-cycle

There is large database of both synthetic and natural antagonists for the bc_1 complex Q-sites (Fig. 1.5-6). These specific and tight inhibitors are classified according to whether they affect the Q_o or Q_i sites. They have played a crucial role in defining cytochrome bc_1 complex function [57]. The Q_o site inhibitors prevent the reduction of the b_L haem and the 'Rieske' ISP. However, there are two modes of binding of these Q_o site inhibitors (Fig. 1.18). There are those such as stigmatellin (class I), which binds closer to the 'Rieske' ISP by H-bonding to the histidine ligand of the cluster [58-61]. This induces a change in its EPR line shape, locks the extrinsic domain in the proximal position (close to the surface of cytochrome *b*) such that oxidation by cytochrome c_1 is inhibited, and raises its redox potential. Other

compounds (class II), e.g. myxothiazol, bind closer to haem b_L, causing a red shift of its optical spectrum [9,58,60-62].

The Q_i site inhibitors (class III) such as antimycin A and funiculosin, inhibit b_H haem oxidation. The binding modes of the two inhibitors are similar but they induce a different shift in the optical spectrum of haem b_H [58, 63]. Some Q_i site inhibitors, e.g. funiculosin, HQNO (2-*n*-nonyl-4-hydroxyquinoline-N-oxide) and antimycin A, have been shown to stimulate H_2O_2 and $O_2^{\bullet-}$ generation in the bc_1 complex. This is proposed to occur as a result of the absence of the physiological electron acceptor haem b_L. Ubisemiquinone then accumulates at the Q_o site and can react with oxygen, yielding superoxide [64, 65]. This property increases the pesticide potency of the compounds.

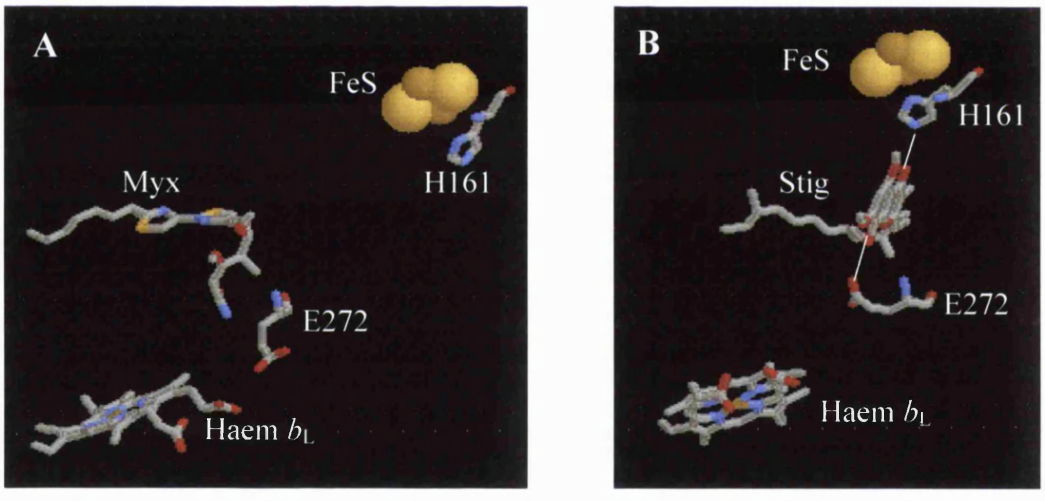

Fig. 1.18. Structures of the Q_o site with (A) myxothiazol or (B) stigmatellin bound. The figures were produced using co-ordinates from *Zhang et al.* (1998) [35] datafile 3BCC in the molecular simulation software RasMol (R. Sale). Selected residues, stigmatellin (stig), myxothiazol (myx) and haem b_L are shown as sticks. 'Rieske' [2Fe2S] cluster atoms (FeS) are shown as brown spheres.

The inhibitors of the bc_1 complex can be split into two functional domains, the "toxophore", which binds to cytochrome *b* in a specific manner and the "backbone", which provide hydrophobicity for the toxophore [66]. A common structural feature of

the classical Q_o-site inhibitors MOA-stilbene, myxothiazol, strobilurin (mucidin), and oudemansin A and B is that they all contain a conjugated carbonyl ethylene group (the β-methoxyacrylate) segment as part of their toxophore (Fig. 1.19), which resemble part of the structure of ubiquinone. They are collectively referred to as the methoxyacrylate (MOA) inhibitors [9, 63]. Myxothiazol, isolated from the myxobacterium *Myxococcus fulvus* is the most potent of the methoxyacrylate inhibitors [62].

The β-methoxyacrylate segment is essential for binding [9, 66]. Modification inevitably leads to an increase in dissociation constant (K_D), e.g. the K_D of demethylmyxothiazol (having a β-keto-propionate group instead of the β-methoxyacrylate) is 500-fold more than the K_D of the parent compound. The loss of activity resulting from changes in the volume of the toxophore and the oxygen atoms of the ester and methoxy groups for non-hydrogen bonding groups show that the dimensions of the binding site are a close fit for the toxophore and that these groups form hydrogen bonds that contribute significantly to the binding energy [9].

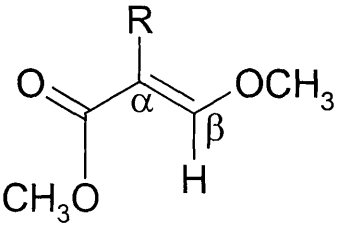

Fig. 1.19. The β-methoxyacrylate segment of the toxophore (headgroup) of inhibitors of the bc_1 complex.

The chromone inhibitor stigmatellin was isolated from *Stigmatella aurantiaca* [59-61, 63]. Its specific inhibition of the Q_o site was first demonstrated by *Thierbach et al.* (1981) [67]. Its affinity for this site is even higher than that of myxothiazol [60]. It binds four orders of magnitude more tightly to the reduced form of the 'Rieske' ISP

than to the oxidised form [59]. With the exception of stigmatellin, all of the inhibitors which are so far known to bind to the 'Rieske' ISP of the bc_1 complex, such as the hydroquinones, e.g. UHDBT (5-n-undecyl-6-hydroxy-4,7-dioxobenzothiazole) and UHNQ (3-un-decyl-2-hydroxy-1,4-naphthoquinone), have structure related to benzoquinone [59, 68].

Alteration of the side chain of stigmatellin by saturation of the C=C double bonds, shift of a methoxy group or loss of the methyl groups specifically affects the binding characteristics. Besides changing the red-shifted spectrum of reduced haem b_L and the EPR spectrum of the 'Rieske' ISP, the side chain alterations diminish the binding affinity and the extent of the midpoint potential shift of the 'Rieske' ISP. Thus, the side chain of the molecule makes an essential contribution to the binding energy and is not necessarily solely for partitioning the molecule into the hydrophobic phase [60]. Stigmatellin also affects photosystem II as well as the Q_o site of the cytochrome b_6f complex [61].

1.9.5 The bifurcation reaction at the Q_o site

The bifurcation reaction at the Q_o site is a unique functional characteristic of the bc_1 complex. The bifurcation of the two electrons from ubiquinol between high- and low-potential chain is crucial to the process through which the free-energy drop between the ubiquinol pool and oxidised acceptor is used to generate a proton gradient. The complex has evolved to maximise the efficiency of this process and achieves a remarkable partitioning in which the second electron is passed almost exclusively to the low-potential acceptor provided by haem b_L. This is despite the availability of a thermodynamically much more favourable pathway to the high-potential chain by 25-30kJ/mol [31, 54]. How this control is built into the chemistry

of the centre 'P' reaction is not addressed by the reaction scheme of the protonmotive Q-cycle [69].

Although there are several plausible mechanisms proposed for the bifurcation reaction, the details remains controversial for two principle reasons: firstly the presence/lack of an EPR-detectable ubisemiquinone at the Q_o site and secondly uncertainty as to whether the required occupancy state of the site is with one or two ubiquinones [31]. Resolving the latter will be a prerequisite to understanding the chemistry of this unique reaction.

Apart from elucidating the mechanism for ubiquinol oxidation at the Q_o site, the question of single or double occupancy of the Q_o binding site is important in the development of fungicides. If more than one compound can bind at the Q_o site, the simultaneous use of two compounds that can bind at the same time could limit the risk of generation of inhibitor resistant strains since it is very likely that fungus would develop resistance to both compounds.

1.9.5.1 Evidence in support of single or double occupancy

Although the question of the occupancy state of the Q_o reaction site remains largely unresolved, there are arguments in favour of either a double or single occupancy. However, no one model is fully consistent with the available data and further studies will be needed to resolve this question.

The main evidence in support of a double occupancy model of the Q_o site comes from solvent extraction and re-titration of quinone to a redox-poised iron-sulphur cluster of the bc_1 complex, resulting in changes in the EPR line shape of the reduced cluster [57, 70-74]. The results were interpreted in terms of binding of two ubiquinone molecules within two distinct binding domains, a strongly bound

prosthetic species (Q_{os}) located near the iron-sulphur cluster (distal domain) and a weakly bound exchangeable species (Q_{ow}) located near the b_L haem (proximal domain). On the basis of this, a plausible model for one turnover of the cytochrome bc_1 complex has been presented which only required exchange of ubiquinone in the Q_{ow} domain with the Q-pool. However, there are alternative interpretations of these results in terms of a single occupancy model of the Q_o site, as will be discussed in Chapter 4.

Similar conclusions to the EPR studies above were drawn by Brandt and co-workers [75-78] for MOA-stilbene inhibition of the bovine cytochrome bc_1 complex, as will be discussed in Chapter 3. They proposed that MOA-stilbene disrupted the enzyme activity in a non-competitive manner with respect to ubiquinone [75]. The same group has also provided evidence that two MOA-stilbene inhibitors can bind to the fully reduced enzyme Q_o site [78]. In addition, *Bartoschek et al.* (personal communication, 2001) from the same group, using high resolution magic-angle-spinning nuclear magnetic resonance spectroscopy has indicated that two out of three n-decyl-ubiquinones bind at the Q_o site, again supporting their view that the site has two distinct ubiquinone binding sites. This is the first time that two ubiquinone molecules have been indicated to bind at the Q_o site of the mammalian (bovine) bc_1 complex, confirming that this feature is not limited to the bacterial enzyme.

Evidence in support of single occupancy comes from studies of mutants, which have failed to identify ligands specific to either Q_{ow} or Q_{os}. In addition, inhibitor studies have showed two types of binding behaviour in the Q_o reaction site, i.e. stigmatellin and myxothiazol type binding as previously explained in Section 1.9.4.1. This is further supported by studies on removal of the 'Rieske' ISP, which cause an increase in the K_D for stigmatellin but not for myxothiazol [63, 68]. Co-

crystals with stigmatellin or myxothiazol bound have confirmed these observations (Fig. 1.18) [31, 35-38, 79]. The overlap between these sites is consistent with the finding that binding of the two classes of Q_o site inhibitors are mutually exclusive [58-60, 62, 63, 68, 75], i.e. class I (stigmatellin) inhibitors are competitive with respect to class II inhibitors (methoxyacrylate type).

1.9.5.2 EPR-detectable ubisemiquinone?

Antimycin A, by blocking the Q_i site, acts as an effective inhibitor of net electron transfer by the bc_1 complex. Under steady-state conditions in the presence of antimycin A, the low-potential chain becomes reduced, preventing haem b_L from accepting further electrons from ubiquinol. The high-potential chain remains oxidised, so that the Q_o site is poised with excess of substrate (ubiquinol and oxidised 'Rieske' ISP) so as to strongly favour formation of the ubisemiquinone product of the first electron transfer reaction. The antimycin A-induced effect is referred to as oxidant-induced reduction, since it leads to reduction of cytochrome *b* haems on addition of an oxidant for cytochrome c_1. Inhibition of the reaction is a paradox of the bifurcated reaction, since the high-potential chain is available to accept electrons, but no flux is observed.

De Vries et al. (1982) [80] showed that although no reduced 'Rieske' ISP could be detected by EPR, a weak ubisemiquinone signal that was insensitive to antimycin A but sensitive to British Anti-Lewisite (BAL), was present in mitochondrial preparations [31, 81, 82]. However, *Jünemann et al.* (1998) [83], using mitochondrial preparations and *Crofts and Wang et al.* (1989) [84], using *Rhodobacter capsulatus* chromatophores could detect no myxothiazol-sensitive ubisemiquinone under these conditions. The authors therefore concluded that the

equilibrium constant for formation of ubisemiquinone is very small, which means that the Gibbs (free) energy (ΔG) is large and positive, and might contribute a significant part of the activation barrier. However, *Link et al.* (1997) [54] have favoured an alternative interpretation that a relatively stable complex of reduced 'Rieske' ISP with ubisemiquinone is formed, but that both EPR signals are lost due to spin coupling. Other spectroscopic methods such as circular dichroism (CD) spectroscopy could be used to test this hypothesis. In addition, as noted by *Brandt et al.* (1996) [69, 85], the oxidant induced reduction conditions may bias the reaction against ubisemiquinone production. This would be the case if ferrohaem b_L exerted a local coulombic effect on the ubisemiquinone anion [31].

Since there is conflicting evidence in the literature regarding the presence of an EPR-detectable ubisemiquinone at the Q_o site, different investigators favour either a transient unstable ubisemiquinone(s) species or a stabilised deprotonated ubiquinol(s) species (Table. 1.4).

1.9.6 Proposed mechanisms of the bifurcation reaction at the Q_o site

There are several plausible mechanisms proposed for bifurcation of the electron transfer reaction in the Q_o site. The models (Table. 1.4) differ primarily in terms of the event determining the activation barrier, the number of ubiquinone occupants (Fig. 1.20) in the Q_o site (which governs the electron transfer distance to haem b_L) and the stabilisation of the ubisemiquinone intermediate.

These mechanisms include: a thermodynamic explanation [44]; formation of an unstable 'mobile' ubisemiquinone that diffuses within the Q_o site to facilitate bifurcated electron transfer by a catalytic switching movement [34, 45, 84, 86]; a

proton-gated affinity-change mechanism implicating a less unstable ubisemiquinone intermediate [54]; a proton-gated charge-transfer mechanism, where the activation barrier for the reaction is deprotonation of QH_2 [44, 69, 87, 88]; or a catalytic-switching mechanism that employs two conformational states of the Q_o site to explain the obligatory bifurcation of electron flow at the Q_o site [88, 89]. The recent structural demonstration that the 'Rieske' iron-sulphur cluster moves over a distance of 10Å between the Q_o site and cytochrome c_1 adds another factor for achieving efficient bifurcation of electron transfer [35, 36]. All of these mechanisms must explain the inhibition by antimycin A under conditions of oxidant-induced reduction of cytochrome *b* as well as the proton-pumping stoichiometry under normal turnover. These mechanisms will be considered briefly below.

Table. 1.4. Synopsis of mechanistic models for Q_o site bifurcation reaction

Model	Number of quinones	Initial arrangement of quinones	Nature of transition state	Semi-quinone stability	References
Crofts and Wang	1	Not defined	$Q^{\bullet-}$	Highly unstable	[34, 45, 84, 86]
Link	1	H-bond of QH^- to FeS-imidazole	QH^-	Stabilised by reduced FeS	[54]
Ding and co-workers	2	Preferably edge to edge; H-bonds to haem b_L and FeS imidazole	$Q^{\bullet-}$/ $Q^{\bullet-}$ or $Q^{\bullet-}$	Highly unstable	[70, 71]
Brandt	2	Stacked; H-bond of Q to FeS-imidazole	QH^-	Partially stabilised	[69, 85, 87, 88]

The table was reproduced from *Brandt et al.* (1998) [88]. $Q^{\bullet-}$, semiquinone; QH^-, deprotonated quinone; Q, quinone; FeS, iron-sulphur cluster.

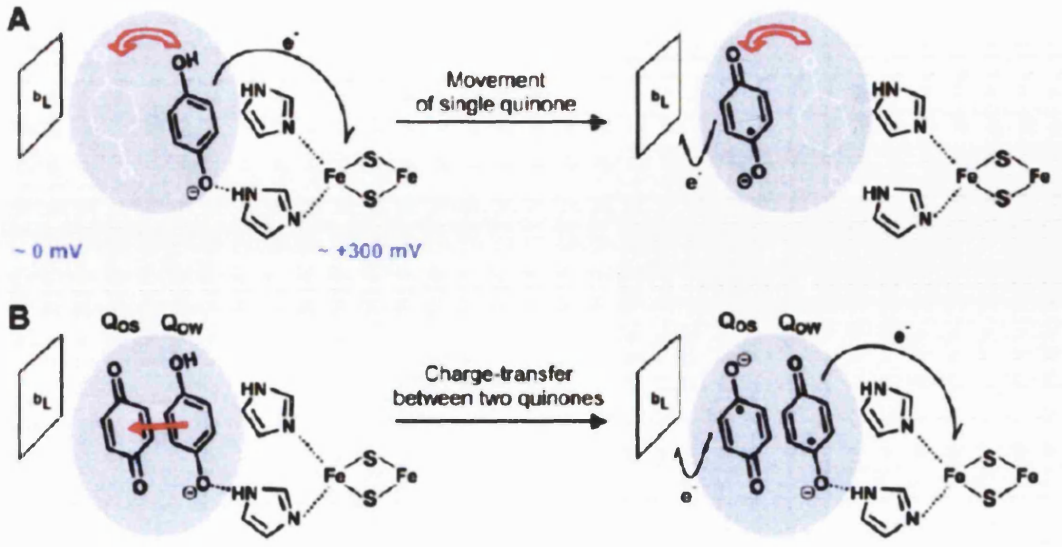

Fig. 1.20. Involvement of one or two ubiquinones in bifurcated electron flow at the ubiquinol oxidation site (Q_o site) of the cytochrome bc_1 complex. The chemistry of ubiquinol oxidation has to ensure divergent reduction of the high-potential 'Rieske' iron-sulphur cluster and the low-potential haem b_L. Curved black arrows indicate electron transfer. **(A)** Crofts model, involving one ubiquinol molecule and a mobile ubisemiquinone intermediate [45] with the unoccupied alternate binding site highlighted in white and a curved red arrow indicating the direction of the movement. **(B)** Ding-Brandt model involving a tightly bound ubiquinone (Q_{os}) and a weakly bound ubiquinol (Q_{ow}) that co-operate by charge-transfer (red arrow) during catalysis [69, 70]. The figure was reproduced from *Bartoschek et al.* (personal communication, 2001).

1.9.6.1 Thermodynamic explanation

In the thermodynamic explanation, no special mechanism is required to enforce the bifurcation. It is proposed that the instability of the ubisemiquinone, together with the fact that the 'Rieske' ISP can only accept one electron at a time, will prevent both electrons from going down the high-potential chain. The equilibrium constant for the oxidation of ubiquinol by the 'Rieske' ISP is so unfavourable that it only proceeds at a competent rate if the ubisemiquinone can immediately reduce cytochrome *b*. If the second electron cannot be transferred to cytochrome *b*, for

example because antimycin is present and cytochrome *b* is fully reduced, the reversal of the first electron would be so fast that the 'Rieske' ISP could never reduce cytochrome c_1. The necessity for domain movement of the 'Rieske' ISP to reduce cytochrome c_1 makes this argument stronger. Since the 'Rieske' ISP cannot be docked to both the Q_o site and cytochrome c_1 simultaneously, allowing the first electron to 'hop' over 'Rieske' ISP onto cytochrome c_1, leaving the 'Rieske' ISP immediately available to receive the second electron.

The ubiquinone is proposed to occupy the same position as bound stigmatellin (Fig. 1.18B) and to be hydrogen-bonded to the 'Rieske' ISP for reduction of both the 'Rieske' ISP and cytochrome *b*. The ubisemiquinone, is proposed not to move because of its short lifetime. The distance of some 10Å from the carbonyl oxygen on the first ring of stigmatellin to the methyl carbon of pyrrole ring A of the low-potential haem and 11Å to C_3 of the same ring for the transfer of the second electron to haem b_L is considered to be compatible with concerted or nearly concerted reduction of the iron-sulphur cluster and cytochrome *b* by ubiquinone in this position for a number of reasons. The application of Dutton and colleague's ruler [90] can be used to assess possible electron transfer rate over this distance from the highly unstable ubisemiquinone to haem b_L. Assuming negative ΔG is roughly equal to re-organisation energy, maximal tunnelling rate can be calculated to be (0.2 – 1.5) x $10^6 s^{-1}$ [44], which is well in excess of turnover rate of the enzyme. A highly conserved aromatic Y132 (chicken numbering) lies between stigmatellin and the haem, and might provide an additional intermediate electron transfer partner that could further enhance net rate. Hence, the estimated electron transfer rate is considerably faster than the turnover of the Q_o site following flash activation (around $2000 s^{-1}$ [84]) so that there is no theoretical reason why electron transfer could not occur with a single

substrate ubiquinol bound in a location modelled on the known position of stigmatellin [44].

Unfortunately, some additional *ad hoc* assumptions need to be introduced to account for inhibition by antimycin A, as can be seen from the following argument. If the ubisemiquinone is a strong-enough oxidant to immediately re-oxidise the 'Rieske' ISP when cytochrome *b* is reduced and it's close enough to the low-potential haem of cytochrome *b* to reduce it when cytochrome *b* is oxidised. Then what is to prevent the ubisemiquinone from oxidising cytochrome *b* under conditions of oxidant-induced reduction? Such a reaction has been proposed to account for initiation of the Q-cycle under highly reducing conditions. Then respiration could proceed at nearly the normal rate in the presence of antimycin A by alternating cycles of (i) an aberrant reaction in which ubiquinone reduces the 'Rieske' ISP and the resulting ubisemiquinone oxidises cytochrome *b*, and (ii) the normal Q-cycle mechanism, which is possible now that the low-potential haem of cytochrome *b* is oxidised [44]. The thermodynamic explanation is very similar to the "all or nothing reaction" mechanism proposed by *Rich et al.* (1999) [91].

1.9.6.2 Mobile ubisemiquinone intermediate

The second mechanism is based on the inference of two different binding modes for quinone species at Q_o site from the different binding positions of the two classes of Q_o-site inhibitor (Fig. 1.18) and consequences of mutation, showing critical roles for residues lining the proximal domain. One end of the pharmacophore of the MOA inhibitors is in van der Waals contact with the ring of Y132, which is nearly in contact with the low-potential haem. At the same time, these inhibitors do not approach the 'Rieske' ISP closely enough to form a hydrogen bond. Thus it has been

proposed that after the transfer of the first electron to the 'Rieske' ISP, the hydrogen bond between the ubiquinol and H161 breaks, and the ubisemiquinone flips into the position seen with MOA inhibitors, before reducing cytochrome *b*. This second binding site could be much more favourable for the ubisemiquinone so that, if cytochrome *b* cannot accept the electron, the ubisemiquinone rarely visits its first binding site and thus transfer of the second electron to the 'Rieske' ISP is slowed greatly. The conserved residue E271, which is found in different configuration in the co-crystals with stigmatellin or myxothiazol, is proposed to be essential in the 'flipping' of the ubisemiquinone and in proton translocation [34, 45]. The inhibition of electron transfer by mutations in the proximal domain then arises from need for movement of the ubisemiquinone into this domain. This movement would decrease the reaction distance from ~11 to 5.5Å and so increase the reaction rate for reduction of haem b_L [34].

This "mobile" ubisemiquinone model predicts high occupancy of a ubisemiquinone under conditions of oxidant-induced reduction and the failure to observe the radical by EPR spectroscopy under these conditions [83] needs to be explained [44, 45].

1.9.6.3 Proton-gated affinity change mechanism

The third mechanism is the proton-gated affinity-change mechanism. In this mechanism the ubisemiquinone formed upon transfer of the first electron to the 'Rieske' ISP, like stigmatellin, binds tightly to the 'Rieske' ISP (the "affinity-change") and raises its midpoint potential above that of cytochrome c_1. The 'Rieske' ISP is thus blocked, both physically and thermodynamically, from disposing of the first electron until after deprotonation and transfer of the second electron converts the

ubisemiquinone into the weakly binding species ubiquinone. The re-oxidation of the iron-sulphur cluster requires electron transfer to haem b_L [44, 54]. The affinity-change of the iron-sulphur cluster enables the obligatory bifurcation of electron flow since it prevents both types of wasteful side reactions, dissociation of ubisemiquinone as well as transfer of the second electron into the high-potential chain.

This model also predicts accumulation of the ubisemiquinone under conditions of oxidant-induced reduction, but failure to observe the ubisemiquinone can be explained by assuming that the radical is spin-coupled with the unpaired electron of the reduced 'Rieske' ISP. It also predicts that the 'Rieske' ISP is reduced under these conditions, which could not be detected by the EPR signal but which might be determined from visible CD spectra. Like the first model, it requires that the second electron is transferred from ubisemiquinone in the stigmatellin position to the low-potential haem of cytochrome *b*. As discussed above this seems feasible.

1.9.6.4 Proton-gated charge transfer mechanism

The fourth mechanism is the proton-gated charge transfer mechanism. The primary difference to other proposed mechanisms is that the reaction is controlled by the concentration of QH^- (deprotonated ubiquinol) rather than $Q^{\bullet-}$ (highly unstable ubisemiquinone). In this model, the Q_o site is occupied by the ubiquinone/ubiquinol pair bound at the Q_{os} and Q_{ow} domains in a stacked configuration (a quinhydrone-like charge transfer complex). The second ubiquinone overcomes difficulties arising from too-long electron transfer distance and may be more efficient. The bifurcation is performed by symproportionation of a charge transfer complex allowing for rapid reduction of the two redox centres, thereby completing substrate oxidation [85, 88]. The oxidised 'Rieske' ISP acting as a Lewis acid drives the symproportionation.

In contrast to the proton-gated affinity change mechanism, no accumulation of ubisemiquinone is predicted by the proton-gated charge transfer mechanism, which postulates an exergonic first electron transfer and a moderate thermodynamic stabilisation of the double-ubisemiquinone intermediate. The key difference is that in this model the first electron transfer is limited by the deprotonation of ubiquinol and for electrostatic reasons occurs rapidly only if the acceptor of the second electron, haem b_L, is oxidised. This means that ubisemiquinone is only formed if it can be oxidised immediately. Thus, for kinetic reasons this model predicts a very low occupancy of the ubisemiquinone state under all conditions [44, 69, 88].

1.9.6.5 Catalytic-switch mechanism

The fifth model involves a "catalytic switch" mechanism to prevent inappropriate reduction of the 'Rieske' ISP by a ubisemiquinone at the Q_o site [77, 89]. A conformational change was suggested largely from observations of specific redox-dependent affinity changes for different inhibitors of the Q_o site [76, 77]. Arrival of the second electron on the high-potential cytochrome b_H haem or on ubiquinone at the Q_i site could be the trigger gating the Q_o site to the 'Rieske' ISP for the next turnover. Although the mechanism was proposed before any X-ray crystal structure was available, the movement of the 'Rieske' ISP could obviously be involved in the gating as proposed [76, 88, 89]. If the oxidised 'Rieske' ISP is not allowed to approach the Q_o site until the second electron has gone to haem b_H, the bifurcated reaction will be ensured. Although this is still an attractive hypothesis, there is no evidence to date from the structures for a significant conformational change of the transmembrane helices linked to antimycin A binding or redox state and the flexibility of the 'neck' region of the 'Rieske' ISP makes it hard to imagine any

way of transmitting a conformational change to the 'Rieske' ISP to control the movement of its head [44].

A combination of a chemical control of ubiquinol oxidation (proton-gated charge-transfer mechanism) and a catalytic switch (as presented here) of the 'Rieske' ISP between two positions is proposed by the author of both mechanisms to explain the obligatory bifurcation of electron flow at the Q_o site [88].

1.10 Cytochrome b_6f complex (plastoquinol:plastocyanin oxidoreductase)

The cytochrome b_6f complex functions in the electron transport chains of oxygen-evolving photosynthesis in chloroplasts and cyanobacteria. In some cyanobacteria and algal chloroplasts, cytochrome c_6 is an alternative electron acceptor. It accepts electrons from plastoquinol (reduced by photosystem II) and transfers them to plastocyanin which reduces photosystem I. This electron transfer is coupled to proton translocation across the thylakoid membrane by a Q-cycle mechanism (Fig. 1.17). Thus, the cytochrome b_6f complex contributes to the formation of protonmotive force that is used to synthesise ATP. It is a member of the cytochrome *bc* superfamily, closely related to its mitochondrial homologue the cytochrome bc_1 complex. The X-ray crystal structure of cytochrome b_6f complex remains unsolved. However, the structure of the soluble domain of spinach 'Rieske' ISP [92, 93] and of turnip cytochrome *f* [94] has been resolved.

The b_6f and bc_1 complexes share not only the same function of electron transfer and proton translocation by a Q-cycle mechanism (Fig. 1.17) but also a number of structural homologies: the four main prosthetic groups (contained in the three catalytic subunits) are the same in both types of complex, and there is strong

homology between cytochrome b_6, subunit IV and the 'Rieske' ISP of the b_6f complex, and the N- and C terminal parts of cytochrome *b*, and the 'Rieske' ISP of the bc_1 complex respectively. Cytochrome c_1 (of the bc_1 complex) and cytochrome *f* (of the b_6f complex), on the other hand, are both *c*-type cytochromes but do not share any sequence homology although they have the same function within the complexes. The same type of movement of the 'Rieske' ISP observed in bc_1 complex was also seen in the b_6f complex upon the binding of stigmatelliin [95]. Spectroscopic, EPR and redox properties of the haems and of the iron-sulphur cluster are similar. Some inhibitors affect both complexes equally, especially the inhibitors of the Q_o site e.g. stigmatellin. The cytochrome b_6f complex has another three or four small subunits (eight in total) and two additional prosthetic groups, a chlorophyll *a* molecule and a β-carotene. The function of these pigment molecules is unknown [95].

1.11 Project objectives

One of the major aims of this project was to try and resolve the controversy concerning whether the Q_o site has to bind one or two ubiquinones to be catalytically active. Resolving these issues is essential for understanding the chemistry of this unique reaction and useful in the development of pesticides. A further aim was to resolve the related questions, with the aid of MOA-derivatives as to whether two inhibitors can be accommodated within the Q_o site at one time, and whether a MOA compound and a ubiquinone can bind at the same time within the site. The information was combined with molecular modelling studies to assess whether rational design of new pesticides to have radically altered activity at the site might be feasible.

To address the question of whether a MOA compound and a ubiquinone can bind at the same within the Q_o site, an indirect method, the steady state kinetics of the bc_1 complex was used to characterise the binding mode of the Q_o site inhibitor MOA-stilbene in relation to the substrate ubiquinol analogue decylubiquinol (Chapter 3).

To complement this study, further studies were carried out using more direct methods (Chapter 4). To address the question of whether two inhibitors can be accommodated within the Q_o site, competition between two classes of Q_o site inhibitors was investigated. In addition, computer modelling studies with the available crystal structure co-ordinates and data from mutagenesis studies to identify residues conferring resistance to inhibitors was also used to address this question. The question of whether two ubiquinone molecules can bind in the site at one time was assessed by trying to model their binding into the Q_o site. Finally, EPR spectroscopy, which has proved to be highly sensitive to the degree and nature of the Q_o site occupants (Q/QH_2 or inhibitors) [70-74], was used to investigate whether the Q_o site can bind one or two compounds at the same time.

The second aim was to use Fourier transform infrared (FTIR) difference spectroscopy to study changes in protein and prosthetic group conformations upon photochemical reduction. Chapter 6 describes its application to the bovine cytochrome bc_1 complex to determine redox-induced infrared (IR) difference spectra of each redox component in native and inhibitor-bound states. For comparative purposes, FTIR redox difference spectra of horse heart cytochrome *c*, turnip cytochrome *f*, and cytochrome *f* and 'Rieske' ISP of lettuce cytochrome b_6f complex were also determined.

The third aim was to characterise the binding modes of a range of new inhibitors of the bc_1 complex (Chapter 5) using a combination of spectroscopic

methods: inhibitor titrations of the steady state kinetics of bovine and yeast bc_1 complexes; absorbtion spectra (binding spectra); oxidant-induced reduction of cytochrome *b*; redox potentiometry; EPR line shape of the 'Rieske' ISP. These compounds were supplied by Aventis Cropscience Ltd and were initially screened in a photometric assay, based on a crude preparation from rat liver mitochondria.

CHAPTER 2

General materials and methods: Isolation of cytochrome bc_1 complex, cytochrome c_1 sub-complex and 'Rieske' iron-sulphur protein using Cholate or Triton X-100

2.1 Preparation of succinate cytochrome *c* reductase (SCR) using Cholate

The isolation of succinate cytochrome *c* reductase (SCR) was adapted from the method of *Yu et al.* (1974) [96] and is schematically depicted in Fig. 2.1. SCR is mostly cytochrome bc_1 complex with a small fraction of succinate dehydrogenase (Complex II).

2.1.1 Keilin Hartree particle (KHP) preparation (Day 1)

Fresh lean bovine heart 480g was cut up into 1-2cm^3 and washed thoroughly with ice-cold distilled water (squeezing with three changes of water). The meat was then placed into Waring blender and 1.45l of 50mM sodium bicine pH 8.0 and about 15ml of 2M sodium bicine pH 9.0 were added. The mixture was blended for 1min on low, 1min on medium and 1min on high, after which the pH was adjusted to pH 8.0 with 2M bicine pH 9.0 (50-100 ml). The solution was then centrifuged at about 3,000*g* for 30min at 4°C. The supernatant was decanted through two layers of butter muslin into a 2l beaker and the pellet discarded. The supernatant was then centrifuged at 20 000*g* for 1hr at 4°C. The pellets were resuspended in six times the original volume of 0.1M sodium borate (orthoborate, BO_3^{3-})/0.1M sodium phosphate buffer pH 8.5 and then spun as before to re-recover the pellets, which were largely free of haemoglobin/myoglobin. The pellets were further resuspended in 80-100ml 0.1M sodium borate (orthoborate, BO_3^{3-})/0.1M sodium phosphate buffer pH 8.5. The protein concentration of Keilin Hartree particle (KHP) was determined by the Biuret method (Section 2.1.1.1) [97]. The sample was frozen overnight.

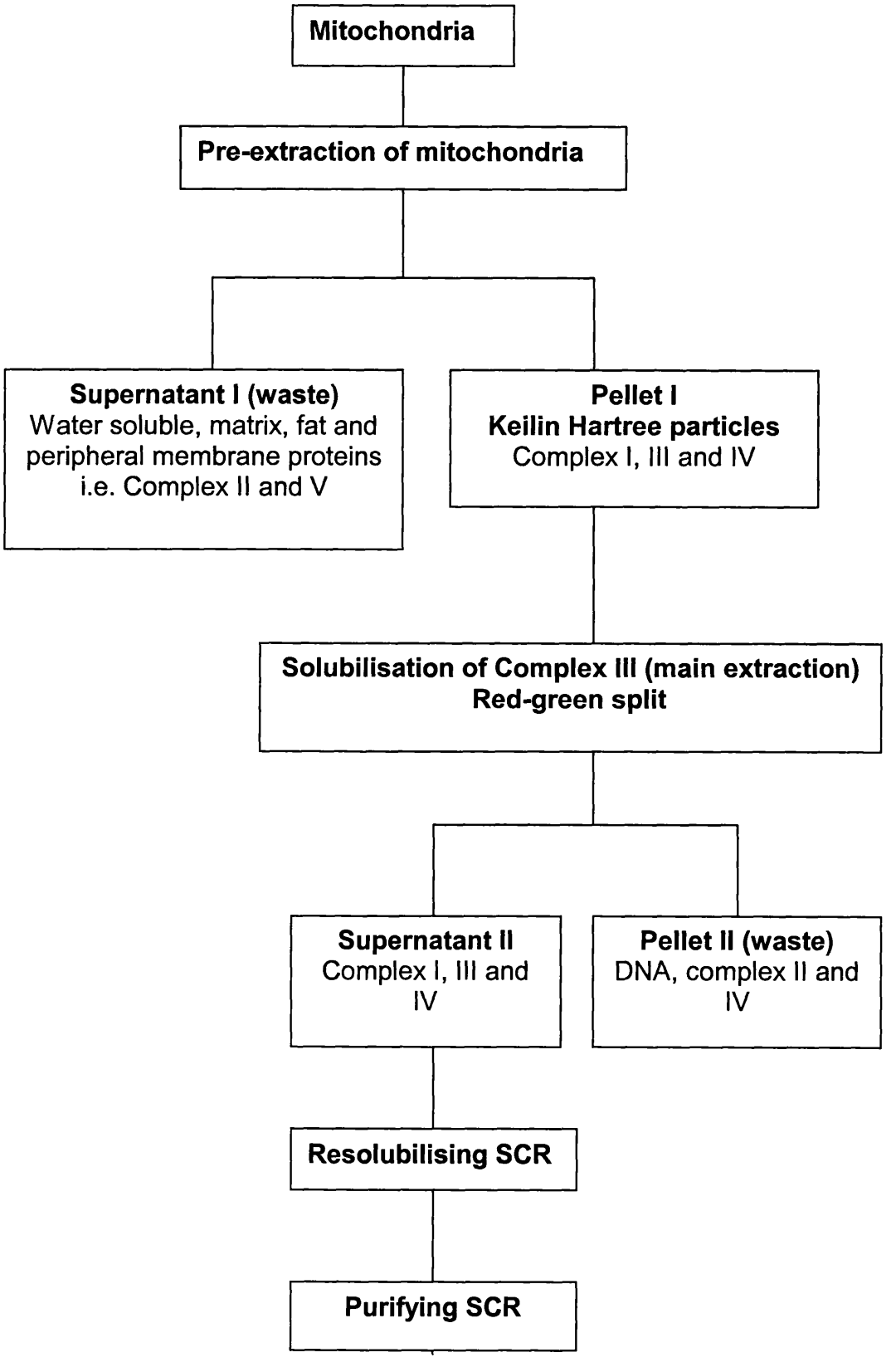

Fig. 2.1. Scheme for the preparation of succinate cytochrome *c* reductase (SCR) from bovine heart using Cholate.

2.1.1.1 Estimation of the protein concentration by Biuret method

1. Biuret reagent:

A well mixed solution containing 40ml of 30% w/v NaOH, (0.6g) of $CuSO_4 \bullet 5H_2O$ and 2.4g of potassium sodium tartrate was diluted to 200ml with double distilled water and then stored at room temperature in a polythene bottle.

2. Bovine serum albumin (BSA) standard

Fatty-acid free bovine serum albumin (BSA, Sigma) was dissolved in water to form a 10mg/ml standard. This was frozen at -20°C until required.

3. Sample preparation

Duplicates of the following were prepared (Table 2.1):

Table 2.1. Estimation of the protein concentration in KHP by Biuret method

Tube	20% w/v Cholate (µl)	30% w/v H_2O_2 (µl)	KHP (µl)	BSA stock (µl)	H_2O (ml)
S10	25	25	10	-	0.44
S20	25	25	20	-	0.43
S40	25	25	40	-	0.41
St	25	25	-	100	0.35
B	25	25	-	-	0.45

B, reagent blank. St, Standard.

To each tube 2ml of Biuret reagent was added and mixed thoroughly. They were then left to incubate for 30min at room temperature and the A_{550} was then read against the reagent blank (B). The A_{550} of St tube (containing 1mg albumin) was about 0.1A. The absorbance shows a correlation with BSA concentration up to at least 2.5mg albumin. This correlation was lost when KHP preparations exceeded A_{550} of about 0.15A.

2.1.2 The red-green split (Day 2)

KHP were thawed, homogenised and diluted to a protein concentration of 20mg/ml of protein with 0.1M sodium borate/phosphate buffer pH 8.5. The concentrations of bc_1 complex and cytochrome oxidase in the diluted KHP were determined as follows:

i) A dithionite-reduced *minus* oxidised difference spectrum of the diluted KHP before Cholate addition (waiting 5-10min after dithionite addition to make sure that all haems are reduced) was recorded. A rough estimate of total haem *b* from peak-trough at 562-575nm (ε = 28.5mM^{-1} cm^{-1}) and total cytochrome oxidase from peak-trough at 606-629nm (ε = 25.6mM^{-1} cm^{-1}) was made.

After the analyses, the KHP were stirred at 4°C and 47µl of a 20% (w/v) stock solution of sodium Cholate (Sigma C-1254) was added per ml of diluted KHP. This gave a final Cholate concentration of 0.90% w/v. The mixture was then stirred gently for 10min at 4°C. A test sample (0.5ml) was withdrawn and 0.33ml of saturated $(NH_4)SO_4$, pH 8.5 was added, to give 40% saturation. This was subsequently centrifuged at 13 000*g* for 4min in a microfuge. The spectra of the supernatant from the test sample were obtained as described in (i). From these, the yield of haem *b* and cytochrome oxidase were calculated. The amount of cytochrome oxidase in the

supernatant had a marked effect on the haem *b* yield. If there was little or no cytochrome oxidase in the supernatant the concentration of Cholate in the bulk solution was increased by 4µl/ml in order to increase the haem *b* yield. The test was then repeated. However, if there was a lot of oxidase in the supernatant, then the bulk solution was diluted slightly with buffer and another test sample withdrawn. The ideal ratio depended on whether bc_1 complex, cytochrome oxidase, or both are to be produced. The ideal ratio for the production of bc_1 complex was obtained after the addition of 60µl/ml Cholate to the bulk solution (Table 2.2).

Table 2.2. Ideal ratio for the production of bc_1 complex

Fraction Test samples content	bc_1 complex yield (%)	Cytochrome oxidase (%)
Diluted test sample	100%	100%
47µl/ml Cholate AS cut 1, supernatant	37%	2.3%
51µl/ml Cholate AS cut 2, supernatant	46%	2.2%
55µl/ml Cholate AS cut 3, supernatant	49%	2.2%
60µl/ml Cholate AS cut 4, supernatant	67%	4%

AS, ammonium sulphate.

After the tests, solid $(NH_4)_2SO_4$ was added to the bulk solution to give 40% w/v saturation, keeping the pH to 8.5 with NH_4OH. The mixture was stirred gently for 1hr at 4°C and then centrifuged at 35 000*g* for 20min at 4°C. The supernatant contained mostly bc_1 complex and was left to stand overnight at 4 °C.

2.1.3 Resolubilising the SCR (Day 3)

The supernatant of the red-green split was spun at 35 000*g* for 1hr at 4°C. Pulverised $(NH_4)_2SO_4$ was added to give 55% saturation, adding 5µl NH_4OH per g $(NH_4)_2SO_4$. The mixture was left to stand for 20min and then centrifuged at 35 000*g* for 20min at 4°C. The supernatant was discarded and the pellet was resuspended in a solution of 0.1M sodium phosphate containing 0.5% sodium Cholate pH 7.4 to 37ml. The solution was left overnight at 4°C.

Table 2.3. Ammonium sulphate fractionation

Cut number (Precipitates)	Volume of 100% $(NH_4)_2SO_4$ (ml)	% $(NH_4)_2SO_4$	Total volume (ml)
1	8.5	20	45
2	3	26	48
3	2	30	50
4	2	34	50
5	1.5	37	51.5
6	1.5	40	53
7	1.5	43	54.5
8	2.5	48	56

2.1.4 Purifying SCR (Day 4)

The solution was centrifuged at 35 000*g* for 1hr at 4°C. The pellet was discarded and the clear red supernatant was retained for $(NH_4)_2SO_4$ fractionation with saturated ammonium sulphate pH 8.5. The first precipitate occurred at 20%

$(NH_4)_2SO_4$ saturation and fractionation from there were carried out in 3-7% steps up to 50% (Table 2.3). The formula for calculating volume of saturated and solid $(NH_4)_2SO_4$ to add and for calculating saturation of $(NH_4)_2SO_4$ after addition of 100% solution are given below. The pellets of each fraction was resuspended in a small volume of 0.1M sodium phosphate pH 8.0 and a dithionite-reduced *minus* ferricyanide-oxidised spectrum was recorded to assess the bc_1 complex content (Table 2.4). There was no detectable bc_1 complex or cytochrome oxidase left in the supernatant after fractionating up to 48% ammonium sulphate (fraction 8).

Table 2.4. The enzyme content of ammonium sulphate fractionation

Fraction No	Volume (ml)	bc_1 complex (μM)	(nmol)	Cytochrome oxidase (μM)
1	-	-	-	-
2	1	53	53	10
3	0.95	155	147	18
4	1	230	230	0.296
5	1.3	207	269	None
6	0.9	197	177	None
7	0.63	104	66	2.9
8	0.48	51	25	13

The best fractions 4, 5 and 6 were pooled, which gave a total volume of 3-4ml and contained 741nmol of haem *b*. The solution was dialysed overnight against 300ml 0.1M sodium phosphate pH 8.0 (with two changes of medium). Fraction 7 was also dialysed overnight with two changes of medium. If after dialysis some of the SCR

precipitated, the mixture was spun and only the soluble fraction used. Alternatively, it was re-dissolved by adjusting the pH, or adding more Cholate or, preferentially, dodecyl maltoside. The samples were either frozen in liquid nitrogen as SCR or taken to the next stage. The yield of haem *b* at various stages is given in Table 2.5.

Table 2.5. Yield of haem *b* at various stages of SCR preparation

Step	Protein (mg)	Haem *b* (nmol)	Yield (%)
KHP (Day 1)	6800	5565	100
Red-Green Split (Day 2)	4556	3729	67
Fractionation (Day 4)	1156	967	17
Purified SCR (Day 4)	884	741	13

Formula for calculating volume of saturated $(NH_4)_2SO_4$ to add

$e=d\times((c-a) / (b-c))$

where

a = current saturation of Ammonium sulphate (A.S)

b = saturation of A.S. being added (i.e. 100 %)

c = saturation of A.S. required

d = the volume that is being added to

e = volume of A.S. that is to be added

and for calculating saturation of $(NH_4)_2SO_4$ after addition of 100% solution:

$c = (eb + ad) / (d + e)$

Formula for calculating weight of solid $(NH_4)_2SO_4$ to add

$x = 533 (S_2 - S_1) / (1 - 0.3 S_2)$

where x = g of solid $(NH_4)_2SO_4$ to be added to 1000ml to bring the saturation from S_1 to S_2

S_1 = initial fractional saturation of $(NH_4)_2SO_4$

S_2 = final fractional saturation of $(NH_4)_2SO_4$

2.2 Isolation of bc_1 complex from bovine heart using Triton X-100

The isolation of bc_1 complex from bovine heart was prepared according to the method described in *Schägger et al.* (1994) [98] and depicted in Fig. 2.2. All steps were performed at 4°C for optimal protein stability.

2.2.1 Isolation of mitochondria

Between three to four bovine hearts were placed in 6 x 4l buffer containing 250mM sucrose, 10mM Tris and 0.5mM EDTA at pH 7.4. Excess fat and tissue were removed and the lean hearts were cut into cubes. The mince meat cubes were placed into a mixer and 5ml of 2M Tris (the pH was not adjusted) was added. The mixture was blended for 5sec at low and 60sec at high. The pH was controlled with Tris to pH 7.4. Suspensions were centrifuged at 356g for 20min. The supernatant was passed through 4-8 layers of muslin and centrifuged at 7000g for 30min. The supernatant was discarded and the pellet resuspended in a total volume of 2.4l buffer. The solution was centrifuged at 17600g for 30min. The pellet was resuspended in minimum amount of buffer, homogenised and then centrifuged at g for 20min. The protein concentration was determined by the Biuret method (Section 2.1.1.1). The pellet was frozen in liquid N_2.

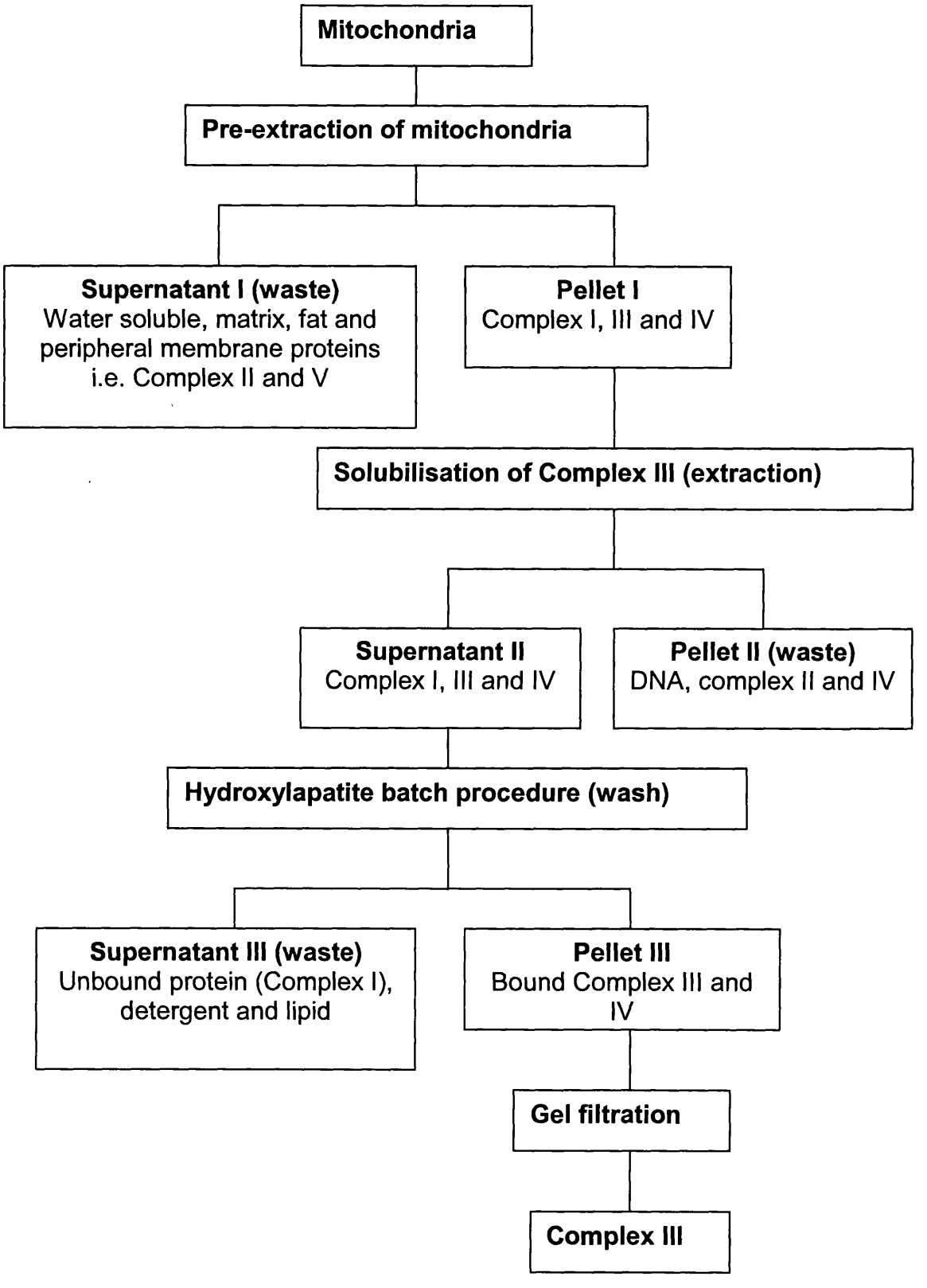

Fig. 2.2. Scheme for preparation of purified Complex III (cytochrome bc_1 complex) from bovine heart and wild type yeast.

2.2.2 Engel's pre-extraction of mitochondria

Bovine heart mitochondria (5-6μmol haem *b)* was resuspended in buffer A (Table 2.6). The solution was diluted to 17.5μM cytochrome *b* with buffer A. Solutions of 20% w/v Triton X-100 (11.6% of initial volume) and 4M NaCl (20% of initial volume) were added slowly to the suspension. The mixture was then ultracentrifuged at 107100g for 70min.

Table 2.6. Buffers for the preparation of the bovine heart bc_1 complex*

	A	B	C	D	E	F	G
	Dilution		Extract -ion	HXP Equil.	HXP Wash	HXP Elution	CL6B
Triton X100 (w/v)	-	-	4%	0.5%	0.05%	0.3%	0.05%
K^+/MOPS	20mM	20mM	20mM	-	-	-	20mM
Sucrose	-	300mM	300mM	-	-	-	-
NaCl	-	-	1.2M	250mM	250mM	-	100mM
NaH_2PO_4 x H_2O	-	-	-	50mM	90mM	-	-
KH_2PO_4	-	-	-	-	-	250mM	-
Quan. (l)	0.5	0.5	1	1	2	1	5

*All buffers were adjusted to pH 7.2. Quan, quantity. Equil, equilibration.

2.2.3 Solubilisation of Complex III

The pellets were resuspended in minimum volume of buffer B and then homogenised. A spectrum was recorded and the concentration set to 28μM haem *b*

(diluting with buffer B if necessary). An equal volume of buffer C was added and mixed thoroughly before ultracentrifuging at 107100g for 70min. The pellet was discarded and the supernatant was retained for the hydroxylapatite batch procedure (Section 2.2.6)

2.2.4 Preparation of hydroxylapatite (HXP)

Four tubes from a multichannel peristaltic pump for the delivery of $CaCl_2$ and Na_2HPO_4 were affixed separately to the lid of a 20l saucepan. 1l of 1M NaCl solution was added to the 20l saucepan continuously stirred and heated to 70°C on a cooker. Solutions of 0.5M $CaCl_2$ (2 x 4l) and 0.5M Na_2HPO_4 (2 x 4l) were fed at an initial flow rate of 100ml/hr for each of the tubings into the stirred NaCl solution, with the temperature kept at 70°C. The flow rate was increased twice, firstly after 500ml to 250ml/hr and then after 1.5l to 400ml/hr. The cooker was switched off but the stirrer was left on to prevent caking of the precipitate.

The Brushite crystals were allowed to settle and the supernatant removed by suction. The sediment was then washed through with 10l of deionised water and kept overnight at room temperature. In the morning, 10l of water was added to loosen the Brushite crystals from the walls and 900ml of 17.7% w/v NaOH was subsequently added while stirring the solution. The stirred suspension was heated to 90°C within 45-60min. After which, the intensity of the heating plate was reduced and the temperature maintained at 95°C for 60min. The heating plate was then turned off and after 10min (when the temperature was 85°C) the stirrer was turned off. The HXP was allowed to completely settle before the hot alkaline supernatant was removed. HXP was resuspended in stirred 10l of deionised water and allowed to settle for 5min. The supernatant together with "fine" were removed. In the next step, 10l of deionised

water and 200ml of 0.5M NaH_2PO_4 were added to HXP, and the suspension was heated to 80°C while stirring. The HXP was allowed to settle completely before the supernatant was removed. This step was repeated twice but 200ml of 0.5M sodium phosphate buffer adjusted to pH 6.8 was added second time round. The HXP was finally suspended in 10mM sodium phosphate buffer and stored at 4°C.

2.2.5 Hydroxylapatite batch procedure

Triton X-100 to 1% w/v final concentration, sodium phosphate pH 7.2 to 50mM final concentration and about 200ml HXP (equilibrated with buffer D) were added to the supernatant (Section 2.2.4). The mixture was spun at low speed stopping when 439g was reached. The spectrum of the supernatant was recorded before it was discarded to ensure there was no bc_1 complex left. The HXP mixture was washed in a total volume of 500ml buffer E and then spun at low speeds. Again the spectrum of the supernatant was recorded before it was discarded. A minimum amount of buffer E was added to the HXP and mixed gently. The mixture was then poured onto a column setting without air bubbles, washed with one column volume of buffer E and eluted with buffer F. The fractions with high haem *b* content were pooled. If the pooled volume was greater than 25-35ml, it was concentrated by pressure filtration through an Amicon YM100 membrane.

2.2.6 Gel filtration

The pooled fractions were loaded onto a 700ml sepharose CL-6B column (equilibrated with buffer G) and eluted overnight with buffer G. The fractions were pooled, concentrated and glycerol added. The protein was then frozen quickly in

liquid N_2 and store at -80°C. The yield of haem *b* at various stages is given in Table 2.7.

Table 2.7. Yield of haem *b* at various stages

Step	Haem *b* (nmol)	Yield (%)
Mitochondria	3828	100
Pre-extract	2695	70
Extraction	1587	42
Hydroxylapatite	936	25
Gel filtration	642	17

Cytochrome bc_1 complex concentration was 13.2 mg/ml (198mg of protein in a total volume of 15ml).

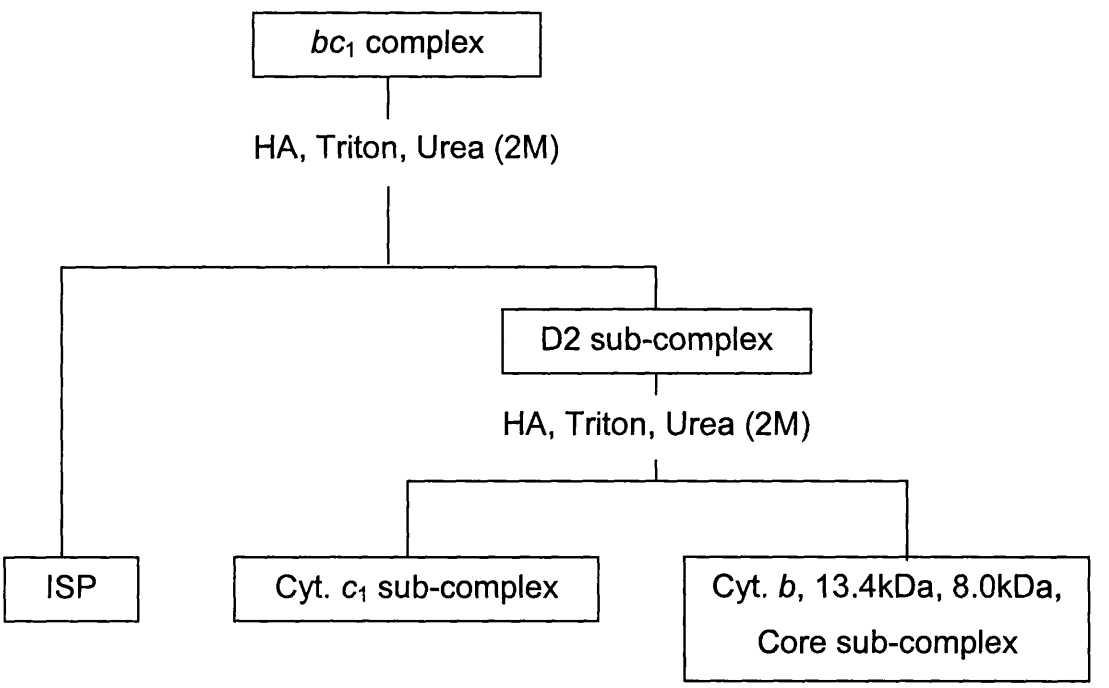

Fig. 2.3. Scheme for preparation of cytochrome c_1 sub-complex and the 'Rieske' iron-sulphur protein subunits of Complex III (cytochrome bc_1 complex) from bovine heart mitochondria. HA, hydroxylapatite; D2 sub-complex, complex III missing the 6.4kDa protein and 'Rieske' iron-sulphur protein (ISP); Triton, Triton X-100. Cyt, cytochrome.

2.3 Isolation of cytochrome c_1 sub-complex and the 'Rieske' ISP using Triton X-100

The isolation of cytochrome c_1 sub-complex and the ISP from bovine heart bc_1 complex were prepared according to the method described in *Schägger et al.* (1986) [99] and depicted in Fig. 2.3. All steps were performed at 4°C for optimal protein stability.

Table 2.8. Buffers for the preparation of protein subunits of the bc_1 complex*

	1	2	3	5	6	7
Triton X100 (%)	0.05	1.0	0.05	0.5	0.5	0.5
NaCl (M)	0.05	0.4	0.4	0.2	0.25	-
Sodium Phosphate (M)	0.035	0.025	0.05	0.025	0.085	0.35
Guanidine	-	-	-	1.5	-	-
Sodium dithionite (M)	-	0.002	-	-	-	-
PMSF (M)	-	0.0002	-	-	-	-
Urea (M)	-	2.0	2.0	-	-	-
Antimycin (nmol)	-	-	2000	-	-	-
Quantity (ml)	500	50	50	100	200	500

*All buffers were adjusted to pH 7.2. PMSF, phenylmethylsulphonyl fluoride.

2.3.1 Step I. Cleavage of bc_1 complex into three fractions: The 6.4 kDa protein, the 'Rieske' ISP and D2 sub-complex

Freshly prepared bc_1 complex (676nmol) in 1mM NaCl, 10mM MOPS, 0.05% w/v Triton X-100 and 200µl of 10mM antimycin A in excess were applied onto a 100ml HXP column after addition of sodium phosphate buffer, pH 7.2, to a final concentration of 35mM. The HXP column was pre-equilibrated with buffer 1 (Table 2.8). The HXP-bound bc_1 complex was washed with 50ml of buffer 1. The application of 30ml of buffer 2 to HXP column, resulted in the separation of the 6.4kDa protein and the 'Rieske' ISP. The addition of 50ml of buffer 3 and 50ml of buffer 1 resulted in the 6.4kDa protein eluting first, followed by the 'Rieske' ISP. The protein was then dialysed against 500ml dialysis buffer pH 7.2 containing 20mM MOPS and 100mM NaCl.

2.3.2 Step II. Cleavage of the D2 sub-complex into a fraction comprising 6 proteins and a cytochrome c_1 sub-complex composed of three proteins

The D2 sub-complex (Complex III missing the 6.4kDa protein and 'Rieske' ISP) still bound to the HXP column was cleaved further by the application of one column volume of buffer 5 (100ml) and this lead to the elution of 6 proteins. The cytochrome c_1 sub-complex remained bound to the column and was washed with buffer 6. The column was brought to room temperature and then the cytochrome c_1 sub-complex was eluted with buffer 7. The protein was dialysed against 500ml dialysis buffer pH 7.2 containing 20mM MOPS and 100mM NaCl. The protein content of the various fractions were verified using SDS-polyarylamide gel

electrophoresis (results not shown). The method used was essentially the same as those described in *Schägger et al.* (1994) [100]. The concentration of cytochrome c_1 sub-complex was estimated from the reduced *minus* oxidised difference spectrum using extinction coefficient ($\varepsilon = 18.8 mM^{-1} cm^{-1}$) at 554-540nm [101].

2.4 Isolation of bc_1 complex from yeast preparation using Triton X-100

The isolation of bc_1 complex from wild type yeast was also prepared according to the method described in *Schägger et al.* (1994) [98] and depicted in Fig. 2.2. All steps were performed at 4°C for optimal protein stability.

Table 2.9. Buffers for preparation of the yeast bc_1 complex*

	1 2 Dilution	3 HXP Equil	4 HXP Wash	5 HXP Elution	6 CL6B
Triton X100 (w/v)	- -	0.5%	0.05%	0.25%	0.05%
K^+/MOPS	- -	-	-	-	20mM
EDTA	5mM 5mM	-	-	-	-
NaCl	200mM 600mM	250mM	250mM	-	100mM
KH_2PO_4	10mM 10mM	-	-	250mM	-
$NaH_2PO_4 \bullet H_2O$	- -	100mM	100mM	-	-
Quantity (l)	1.0 0.5	0.5	0.5	0.5	2.0

*All buffers are adjusted to pH 7.2.

2.4.1 Pre-extraction of wild type yeast mitochondria

Wild type yeast membranes were prepared according to the methods described in *Clejan et al.* (1986) [102]. The membranes were thawed, resuspended in minimum amount of buffer 1 (Table 2.9) and homogenised. The reduced *minus* oxidised spectrum of the membrane suspension was recorded, from which the concentration of haem *b* was determined. Triton X-100 was added to the membrane suspension to a final concentration of 1.1% w/v. The final concentration of haem *b* (with Triton X-100 present) was adjusted to 4μM (if necessary diluting with buffer 1). A solution of 500mM PMSF (Phenylmethylsulphonyl fluoride) was added to the membrane suspension to a final concentration of 1mM and ultracentrifuged at 107100g for 70min. Before discarding the supernatant its spectrum was recorded.

2.4.2 Solubilisation of complex III

The pellet was resuspended in minimum amount of buffer 2. Triton X-100 was added to a final concentration of 2.2% w/v. After which, the concentration of haem *b* was adjusted to 10μM (if necessary diluting with buffer 2). PMSF was added to the mixture to a final concentration of 1mM. This was then spun at 107100g for 2hrs.

2.4.3 Hydroxylapatite batch procedure

The pellet was discarded and sodium phosphate 100mM final concentration was added to the supernatant. Spectrum of the supernatant was recorded. About 100ml HXP (pre-equilibrated with buffer 3 for at least 10hrs) was added to the supernatant. The mixture was spun at low speed, stopping when 439g was reached. The spectrum of the supernatant was recorded before it was discarded to ensure that there was no bc_1 complex left in the supernatant. Approximately the same volume of

buffer 3 was added to the HXP mixture and the centrifugation repeated. Spectrum of the supernatant was again recorded before it was discarded. A small amount of buffer 4 was added to the HXP, mixed gently and poured into a column setting without air bubbles. The column was washed with buffer 4 until the elute was no longer green. The column was then eluted with buffer 5. Fractions with high haem *b* concentration were pooled, their spectrum recorded and PMSF added. If the pooled fractions were more than 15ml, it was concentrated by pressure filtration through an Amicon YM100 membrane.

2.4.4 Gel Filtration

The protein was loaded (15ml) onto a 300ml CL-6B sephorose column (pre-equilibrated with buffer 6) and eluted overnight with buffer 6. The fractions were pooled and concentrated. For long time storage 1.1% glycerol and 1mM PMSF were added. The sample was frozen quickly in liquid N_2 and stored at -80°C.

2.5 Materials

All chemicals used in this thesis were obtained from Sigma (Poole, Dorset, UK) except where stated in the text, and were the highest analytical grade possible.

CHAPTER 3

Characterisation of steady state kinetics of the *bc*$_1$ complex to determine the binding mode of the Q_o site inhibitor MOA-stilbene in relation to ubiquinone

3.1 Background

To address the question of whether a MOA compound and a ubiquinone can bind at one time to the Q_o site, an indirect method, the steady state kinetics of the bc_1 complex were used to characterise the binding mode of the Q_o site inhibitor MOA-stilbene in relation to the substrate ubiquinol analogue decylubiquinol. Reaction rates, rate constants, turnover numbers, and the effects on turnover numbers of substrate concentrations, pH, ionic strength and detergents were determined using Cholate-prepared SCR and the ubiquinol analogues duroquinol and decylubiquinol as substrates (Fig. 3.1). The optimum condition was then used to characterise the binding mode of MOA-stilbene. For comparative purposes, the optimum condition was also used to perform kinetic analyses of bc_1 complex in KHP, and Triton-prepared purified bovine and yeast bc_1 complexes.

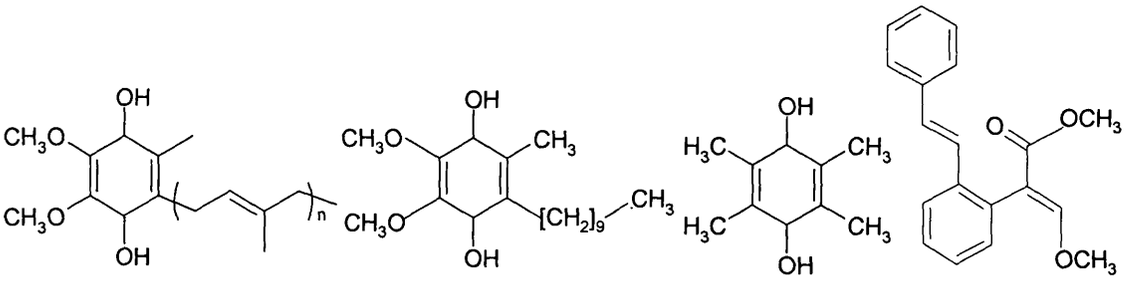

Ubiquinol **Decylubiquinol** **Duroquinol** **MOA-stilbene**

Fig. 3.1. Structure of ubiquinone, its analogue decylubiquinol and duroquinol, and the Q_o site inhibitor MOA-stilbene. n is generally 8 for ubiquinol.

3.1.1 Steady state kinetics

The Michaelis-Menten equation (Eq. 3.1) is the fundamental equation of enzyme kinetics. The equation accounts for the simple model presented in (Eq. 3.2) and the kinetic data given in (Fig. 3.2). At very low substrate concentration, when [S] is much less than K_M, $V = [S] V_{max}/K_M$; that is, the rate is proportional to the

substrate concentration. At high substrate concentration, when [S] is much greater than K_M, V = V_{max}; that is, the rate is maximal, independent of substrate concentration. K_M is equal to the substrate concentration at which the reaction rate is half of its maximal value [103]. The value of the Michaelis constant K_M and the maximal rate V_{max} can be determined using a variety of straight line plots (Table 3.1).

$$V = V_{max} \frac{[s]_o}{[s]_o + K_M} \qquad \textbf{(Eq. 3.1)}$$

$$E + S \underset{k_2}{\overset{k_1}{\rightleftharpoons}} ES \xrightarrow{k_3} E + P \qquad \textbf{(Eq. 3.2)}$$

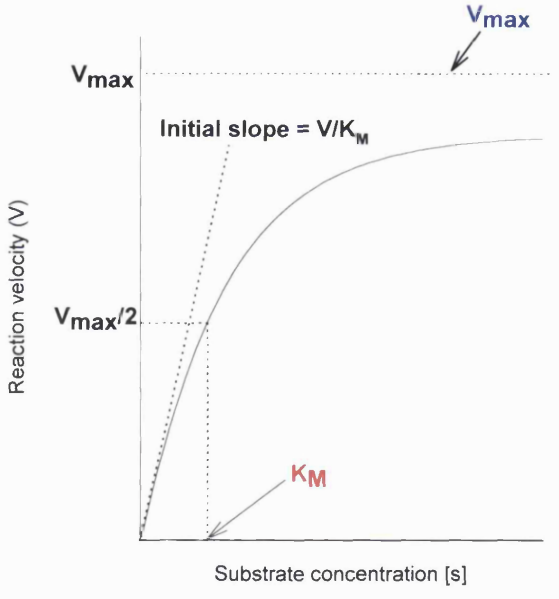

Fig. 3.2. Dependence of initial rate (V) on the substrate concentration (S) for a reaction obeying the Michaelis-Menten equation. The curve represents a rectangular hyperbola. For many enzymes, the rate of catalysis, V, varies with the substrate concentration, [S], in a manner shown. V is defined as the number of moles of product formed per second. At a fixed concentration of enzyme, V is almost linearly proportional to [S] when [S] is small. At high [S], V is nearly independent of [S]. See text for definition of kinetic constants.

Table 3.1 Graphs of the Michaelis-Menten equation

Plot	Graph	Intercept	Gradient
Lineweaver-Burk	1/V against 1/[S]	$1/V_{max}$	K_M/V_{max}
Eadie-Hofstee plot	V against V/[S]	V_{max}/K_M	$-K_M$
Hanes plot	[S]/V against [S]	K_M/V_{max}	$1/V_{max}$

3.1.2 Specificity constant

The most useful index for enzyme effectiveness and specificity is not the 'old' idea of K_M but rather the 'specificity constant' (Eq. 3.3) [103], which describes how effective an enzyme converts substrate into products rather than how strongly the enzyme binds the substrate.

$$\text{Specificity constant} = \frac{k_{cat}}{k_M} \qquad \textbf{(Eq. 3.3)}$$

The specificity constant is an apparent second order rate constant for the reaction (Eq. 3.4-5) at low substrate concentration. The ultimate limit on the value of the specificity constant is set by k_1, the rate of formation of the ES complex (Eq. 3.2). In turn this rate is governed by the diffusion-controlled encounter of an enzyme and its substrate [103]. The catalytic rate constant k_{cat} (Eq. 3.6), also known as turnover number, which derives from the fact that it is a reciprocal time, and defines the number of catalytic cycles ("or turnovers") the enzyme can undergo in unit time.

$$[E] + [S] \longrightarrow [E] + [P] \qquad \textbf{(Eq. 3.4)}$$

$$V = \frac{k_3}{k_M}[E_T][S] \qquad \text{(Eq. 3.5)}$$

$$V_{max} = k_3[E_T] \qquad \text{(Eq. 3.6)}$$

3.1.3 Reversible and irreversible inhibition

Inhibition can arise in a wide variety of ways and there are many different classes of inhibitors. Furthermore, inhibition can be a source of insight into the mechanism of enzyme action: residues critical for catalysis can often be identified using specific inhibitors e.g. poisoning by mercury (II) compounds has often being used to implicate sulphydryl groups in the catalytic activity of enzymes. Enzyme inhibition can either be reversible or irreversible. Irreversible inhibitors are unable to dissociate from the enzyme on the time scale of catalytic turnover. Reversible inhibitors are characterised by rapid dissociation of the enzyme-inhibitor complex. There are three types of reversible inhibition, competitive, mixed and uncompetitive inhibition [104].

3.1.3.1 Competitive inhibition

The commonest type, is so-called competitive inhibition because the substrate and the inhibitor compete for the same active site. The mechanism may be represented in the simplest terms shown in Eq. 3.7, in which [EI] is a dead end complex, as the only reaction it can undergo is reformation of [E] + [I]. However, in many of the more complex types of competitive inhibition, including most types of product inhibition,

the inhibition constant is not a true equilibrium constant because the enzyme-inhibitor complex is not a dead end complex [104].

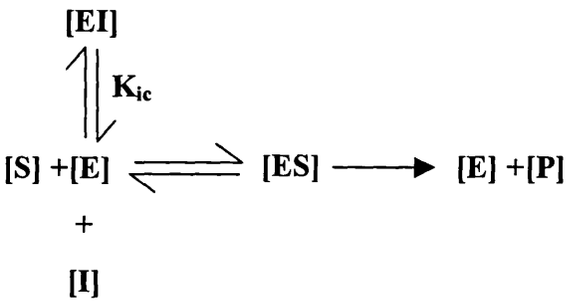

(Eq. 3.7)

The inhibition constant (K_{ic}) is defined as (Eq. 3.8):

$$K_{ic} = [E][I]/[EI] \qquad \textbf{(Eq. 3.8)}$$

The defining equation for linear competitive inhibition, which applies to all competitive inhibition mechanisms, is shown in Eq. 3.9:

$$V = \frac{V_{max}[S]}{K_M(1 + i/K_{ic}) + [S]} \qquad \textbf{(Eq. 3.9)}$$

in which i is the free inhibitor concentration and V_{max} and K_M have their usual meaning. The equation is of the form of Michaelis-Menten equation. It can be written as (Eq. 3.10):

$$V = \frac{V^{app}[S]}{K_M^{app} + [S]} \qquad \textbf{(Eq. 3.10)}$$

where V^{app} and K_M^{app} are the apparent values of V_{max} and K_M and are given by:

$$V^{app} = V_{max} \qquad \textbf{(Eq. 3.11)}$$

$$K_M^{app} = K_M(1 + i/K_{ic}) \qquad \textbf{(Eq. 3.12)}$$

$$V^{app}/K_M^{app} = \frac{V_{max}/K_M}{1 + i/K_{ic}} \qquad \textbf{(Eq. 3.13)}$$

Hence the effect of a competitive inhibitor is to decrease the apparent value of V_{max}/K_M by the factor $(1 + i / K_{ic})$ while leaving that of V_{max} unchanged [104].

3.1.3.2 Mixed inhibition

Linear mixed inhibition is the type of inhibition in which both specific and catalytic effects are present, i.e. both V^{app}/K_M^{app} and V^{app} vary with the inhibitor concentration according to the following equations:

$$V^{app} = \frac{V_{max}}{1 + i/K_{iu}} \qquad \textbf{(Eq. 3.14)}$$

$$K_M^{app} = \frac{K_M(1 + i/K_{ic})}{1 + i/K_{iu}} \qquad \textbf{(Eq. 3.15)}$$

$$V^{app}/K_M^{app} = \frac{V_{max}/K_M}{1 + i/K_{iu}} \qquad \textbf{(Eq. 3.16)}$$

The simplest formal mechanism for this behaviour is one in which the inhibitor can bind both to the free enzyme to give a complex [EI] with dissociation constant K_{ic} and also to the enzyme-substrate complex to give a complex [ESI] with dissociation constant K_{iu}, as shown in Eq. 3.17. In this scheme both inhibitor-binding reactions are shown as dead end reactions and are therefore at equilibrium, but as [EI] and [ESI] both exist there is no obvious mechanistic reason why [S] should not bind directly to [EI] to give [ESI] [104].

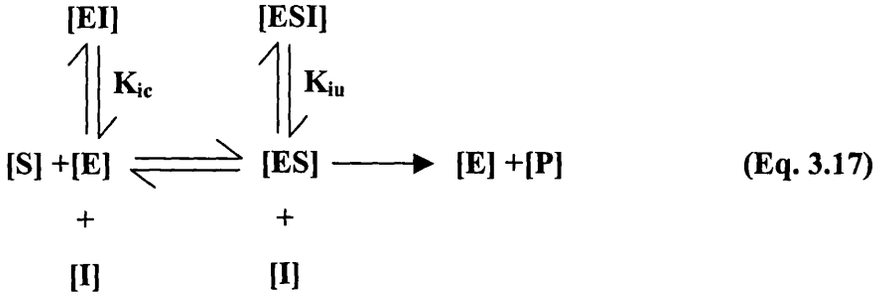

(Eq. 3.17)

Non-competitive inhibition is a special case of mixed inhibition in which the apparent value of V_{max} is decreased with no corresponding effect on that of K_M. In other words the inhibitor interferes with the catalytic properties of the enzyme without affecting the binding of the substrate. Such an effect is an obvious alternative to competitive inhibition and was termed "non-competitive inhibition". The inhibition constants K_{ic} and K_{iu} are equal (Eq. 3.17) [104].

3.1.3.3 Uncompetitive (catalytic) inhibition

Uncompetitive inhibition is at the other extreme from competitive inhibition; it is the case where the inhibitor decreases the apparent value of V_{max} with no effect on that of V_{max}/K_M:

$$V^{app} = \frac{V_{max}}{1 + i / K_{iu}} \qquad \textbf{(Eq. 3.18)}$$

$$K_M^{app} = \frac{K_M}{1 + i / K_{iu}} \qquad \textbf{(Eq. 3.19)}$$

$$V^{app} / K_M^{app} = V_{max} / K_M \qquad \textbf{(Eq. 3.20)}$$

$$[S] + [E] \rightleftharpoons \begin{matrix} [ESI] \\ \Big\uparrow\Big\downarrow K_{iu} \\ [ES] \\ + \\ [I] \end{matrix} \longrightarrow [E] + [P] \qquad \textbf{(Eq. 3.21)}$$

Comparisons of (Eq. 3.14-16) with (Eq.3.18-20) shows that uncompetitive inhibition is a limiting case of mixed inhibition in which K_{ic} approaches infinity i.e. i / K_{ic} is negligible at all values of i and hence disappears from (Eq. 3.14-16); it is thus the converse of competitive inhibition, which is the other limiting case of mixed inhibition in which K_{iu} approaches infinity. Uncompetitive inhibition is also, at least in principle, the mechanistic converse of competitive inhibitor because it is predicted for mechanisms in which the inhibitor binds only to the enzyme-substrate complex and not to the free enzyme (Eq. 3.21). Such mechanisms are not particularly common, and uncompetitive inhibition occurs mainly as a type of product inhibition that is common in reactions with several substrates and products [104].

Table 3.2. Characteristics of linear inhibitors

Type of inhibition	V^{app}	V^{app}/K_M^{app}	K_M^{app}
Competitive	V_{max}	$\frac{V_{max}/K_M}{1+i/K_{ic}}$	$K_M(1+i/K_{ic})$
Mixed	$\frac{V_{max}}{1+i/K_{iu}}$	$\frac{V_{max}/K_M}{1+i/K_{ic}}$	$\frac{K_M(1+i/K_{ic})}{1+i/K_{iu}}$
Non-competitive	$\frac{V_{max}}{1+i/K_{iu}}$	$\frac{V_{max}/K_M}{1+i/K_{ic}}$	K_M
Uncompetitive	$\frac{V_{max}}{1+i/K_{iu}}$	V_{max}/K_M	$\frac{K_M}{1+i/K_{iu}}$

The table was reproduced from *Cornish-Bowden* (1995) [104]. See text for definition of kinetic constants.

3.1.3.4 Summary and determination of linear inhibition types

The properties of the various types of linear inhibition are summarised in (Table 3.2). They are easy to memorise as long as the following points are noted:

1. The two limiting cases are competitive and uncompetitive inhibition; non-competitive inhibition is simply a special case of mixed inhibition in which two inhibition constants K_{ic} and K_{iu} are equal.
2. The effects of inhibitors on V^{app}/K_M^{app} and V^{app} are simple and regular; if they are decreased at all by the inhibitor they are decreased by factors of $(1 + i/K_{ic})$ and $(1 + i/K_{iu})$ respectively.
3. The effects of inhibitors on K_M^{app} are confusing; they are most easily remembered by thinking of K_M^{app} as $V^{app}/(V^{app}/K_M^{app})$ and not as a parameter in its own right [104].

Any of the plots summarised in Table 3.1 can be used to diagnose the type of inhibition, as they all provide estimates of the apparent values of the kinetic parameters. For example, if plots of V against V/[S] (Eadie-Hofstee plot) are made at several values of *i* (inhibitor concentration), the slope ($-K_M^{app}$) and the intercept on the abscissa (V^{app}/K_M^{app}) varies with *i*, if there is a specific component in the inhibition i.e. competitive inhibition. Indeed the plot obtained is characteristics of the type of inhibition (Fig. 3.3). Other plots are needed for determining the actual values of the inhibition constants. The simplest approach is to estimate the apparent kinetic constants at several values of *i*, by the methods of Table 3.1, and to plot K_M^{app}/V^{app} and $1/V^{app}$ against *i*. In each case the result should be a straight line, with intercept $-K_{ic}$ on the *i* axis if K_M^{app}/V^{app} is plotted and intercept $-K_{iu}$ on the *i* axis if $1/V^{app}$ is plotted [104]. An alternative method of estimating K_{ic} was introduced by Dixon and one for K_{iu} by Cornish-Bowden (Fig. 3.4).

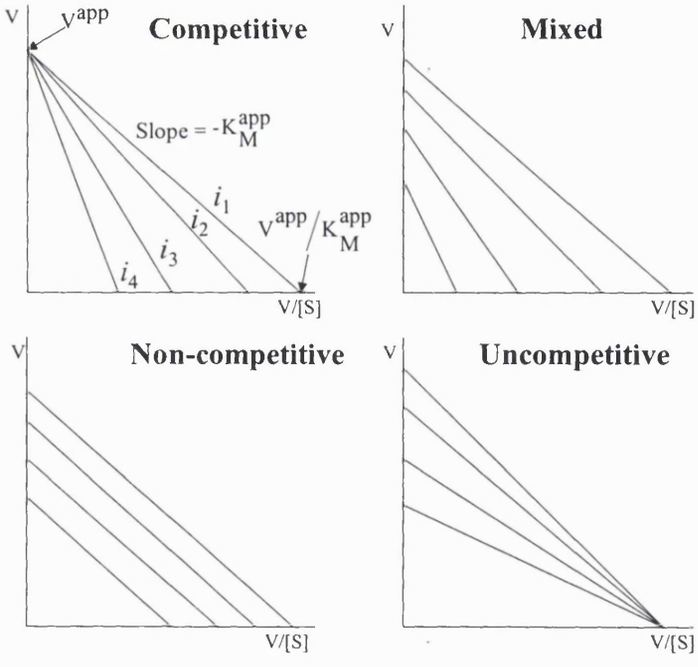

Fig. 3.3. Effects of various types of inhibition on the Eadie-Hofstee plot. See text for details (Section 3.1.3.4).

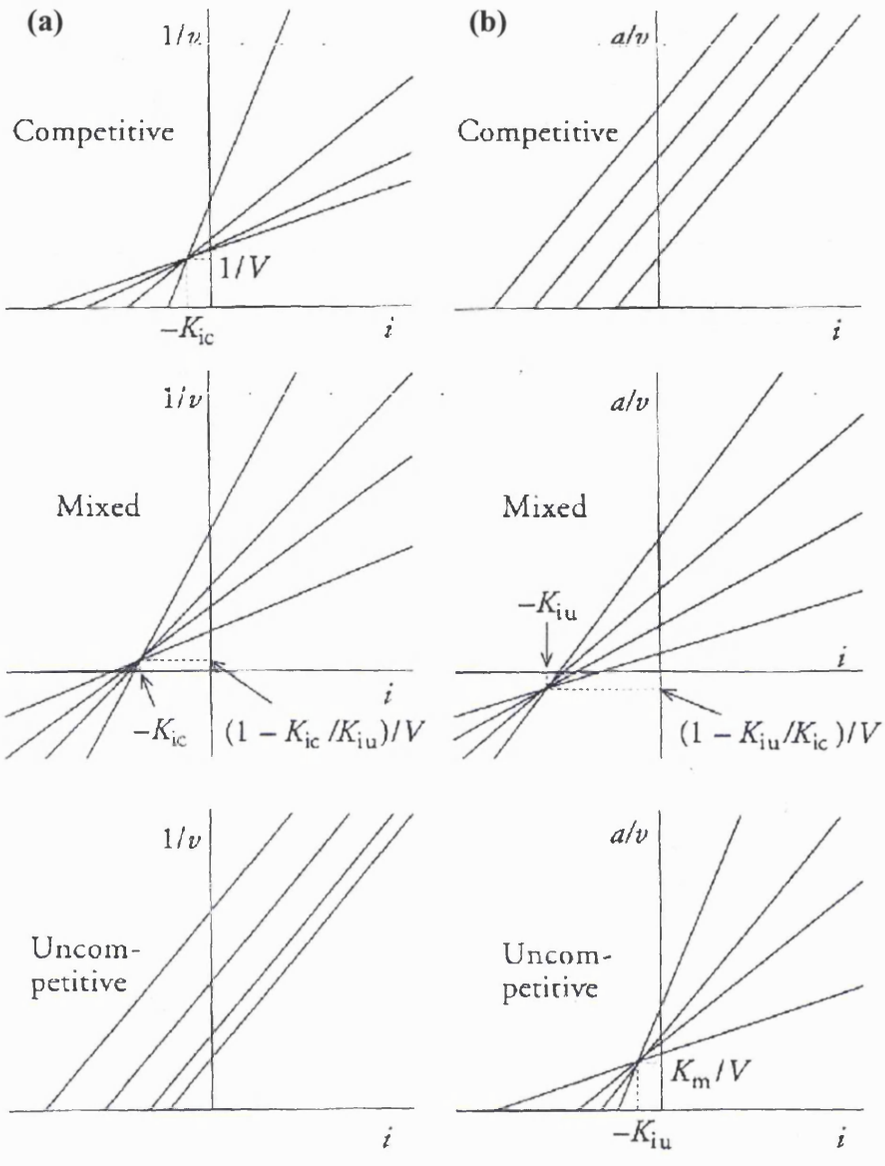

Fig. 3.4. Determination of competitive and uncompetitive inhibition constants. (a) K_{ic} is given by plots of 1/V against *i* at various [S] values (Dixon). **(b)** K_{iu} is given by plots of [S]/V against *i* at various [S] values (Cornish-Bowden). In the case of mixed inhibition the point of intersection can be above the axis in the first plot and below in the second, or vice versa, or it can be on the axis in both plots if $K_{ic} = K_{iu}$. In the idealised case (without experimental error), all lines intersect at a unique point whose co-ordinates yields the values of K_{ic} and K_{iu} that fit the data. More realistically, experimental error causes the unique point to degenerate into a family of points, each of which yields an estimate $*K_{ic}$ of K_{ic} and $*K_{iu}$ of K_{iu}, and the best estimates can be taken as the medians (middle value) of the two series [104]. The figure was reproduced from *Cornish-Bowden* (1995) [104].

3.2 Methods

3.2.1 Preparation of duroquinol and decylubiquinol from their oxidised forms

Duroquinol was prepared as follows. Duroquinone (0.25g) was dissolved in 100ml of diethyl ether in a 500ml separating funnel. A solution containing 1g of sodium dithionite dissolved in 100ml of 50mM sodium phosphate buffer pH 8 was prepared as the reducing agent. 50ml was added to the yellow diethyl ether solution containing duroquinone. This was shaken in the separating funnel, taking care to release the pressure built up by vapour until the diethyl ether solution became colourless and then the water phase discarded. This step was repeated to ensure the complete reduction of the duroquinone to the duroquinol. The diethyl ether solution was shaken with 100ml of 10mM HCl saturated with NaCl and the water phase was discarded. This was repeated a total of three times. The solution was then dried by passing it through anhydrous sodium sulphate in a sintered Buchner funnel. The dried solution was evaporated to dryness using a rotary evaporator under reduced pressure at 30-35°C. The white solid duroquinol was stored anhydrously at -20°C to prevent auto-oxidation to duroquinone.

Decylubiquinol was prepared as follows. 20µl of decylubiquinone dissolved in 50ml of diethyl ether in a 100ml separating funnel. This was then treated as for duroquinone. To prevent auto-oxidation of the newly formed decylubiquinol to decylubiquinone, all solutions and air spaces were kept free of oxygen by bubbling through with nitrogen or argon gas. Droplets of decylubiquinol were dissolved in a

small amount of acidic (10mM HCl) ethanol and stored in liquid nitrogen or at -20°C under nitrogen gas.

Duroquinol and decylubiquinol were quality-controlled by recording their respective UV spectra. Using a matched pair of quartz cuvettes for the assay, a final concentration of 25μM of duroquinol dissolved in acidified ethanol (10mM HCl) was prepared in the sample cuvette. The standard quartz cuvette contained 2.5ml acidified ethanol (10mM HCl). The spectrum was taken from 220-360nm at intervals of 5nm using a LKB. Biochrom ultrospec 2 spectrophotometer. For reference, spectra of duroquinone and duroquinol after treatment with KBH_4 were taken. The molar extinction coefficient of duroquinol is $2.2mM^{-1}$ cm^{-1} at 285-320nm and duroquinone is $18.2mM^{-1}$ cm^{-1} at 265-320nm [105-107]. The spectrum of decylubiquinol was taken from 200-400nm using a Unicam UV/VIS spectrophotometer UV2. The molar extinction coefficient of decylubiquinol is $4.14mM^{-1}$ cm^{-1} at 288-320nm and decylubiquinone is $14mM^{-1}$ cm^{-1} at 279-320nm [105-107]

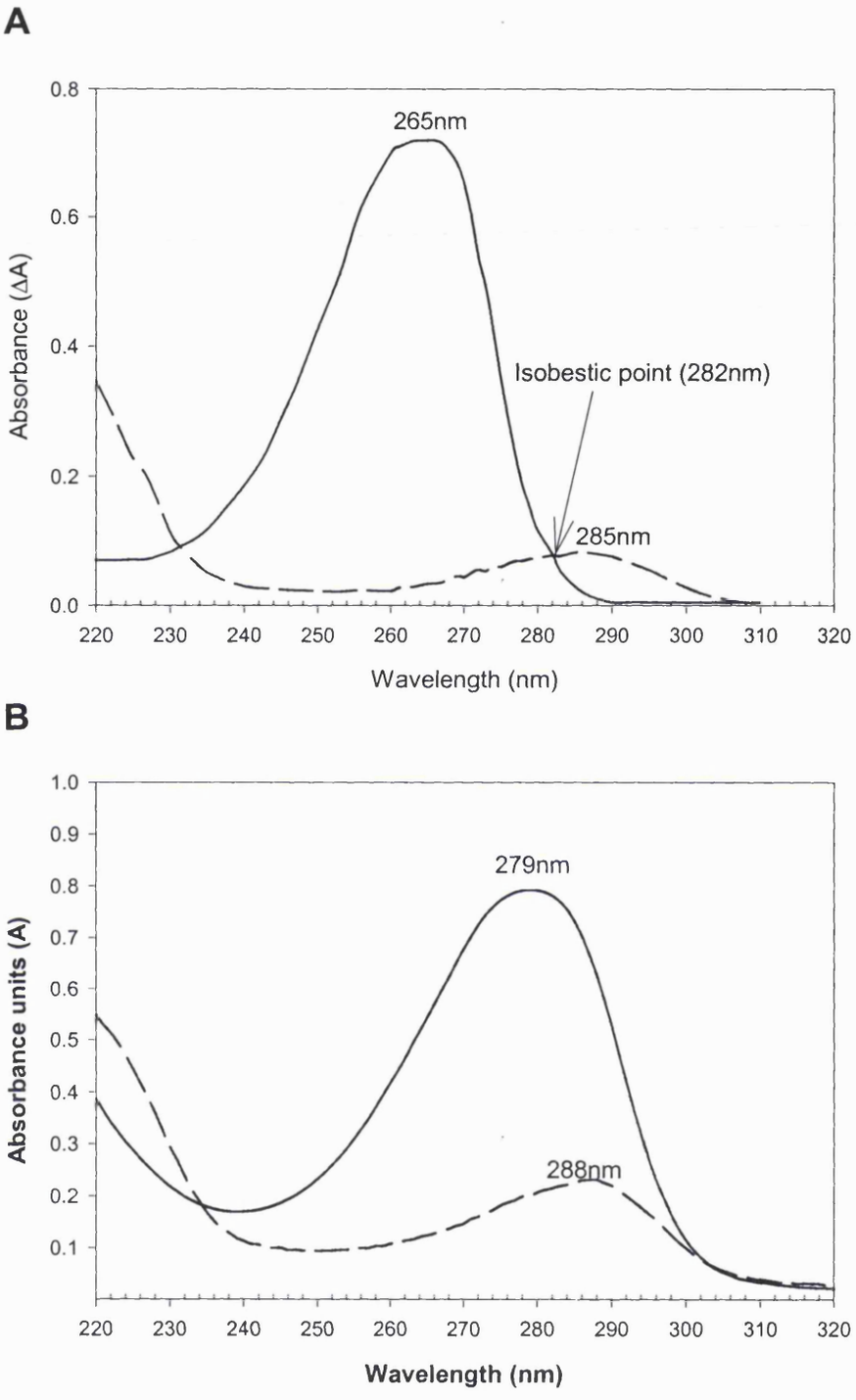

Fig. 3.5. UV absorbance spectra of (A) duroquinone (—) and duroquinol (----) (B) decylubiquinone (—) and decylubiquinol (----). Experimental conditions as described in Section 3.2.1. The concentration of duroquinone and duroquinol were 40μM, and those of decylubiquinone and decylubiquinol were 56μM in acidified ethanol (10mM HCl). Duroquinone and decylubiquinone were reduced with KBH_4.

3.2.2 Decylubiquinol cytochrome *c* oxidoreductase assay

The steady state kinetics of the bc_1 complex were recorded as the rate of cytochrome *c* reduction at 550-542nm in a computer linked Sigma-ZWSII dual-wavelength spectrophotometer (bc_1 complex assay). The reaction buffer was 50mM potassium phosphate, 2mM EDTA at pH 7.0 and 25°C (2.5ml final volume). The order of addition of components was (final concentration): i) 1mM KCN; ii) 12nM SCR isolated from bovine heart tissue or 12nM bc_1 complex KHP or 33nM purified yeast bc_1 complex or 24nM purified bovine bc_1 complex; iii) 30μM horse heart cytochrome *c* (Sigma). The reaction was started by the addition of 6μM decylubiquinol or 78μM duroquinol unless specified otherwise. The concentration of the bc_1 complex was determined by the reduced *minus* oxidised haem *b* spectrum at 562-575nm ($\varepsilon = 28.5 mM^{-1} cm^{-1}$). The same batch of enzyme was used throughout the studies. Non-enzymatic rates of duroquinol reduction of cytochrome *c* were subtracted from the measured rate to give the enzymatic rates [108]. Cuvettes, Hamilton syringes and glass vessels containing inhibitor solutions were washed with ethanol before and after use to avoid adsorption of inhibitor onto glass surfaces.

3.2.2.1 Inhibitor titrations

The bc_1 complex was pre-incubated with MOA-stilbene for at least 1min before the reaction was started. The reaction buffer was at pH 8 (2.5ml final volume). The order of addition of components was (final concentration): i) 0.01% w/v dodecyl maltoside; ii) 1mM KCN; iii) 10-150nM MOA-stilbene; iv) 12nM SCR; v) 30μM horse heart cytochrome *c* (Sigma). The reaction was started by the addition of 6-70μM decylubiquinol [75, 108].

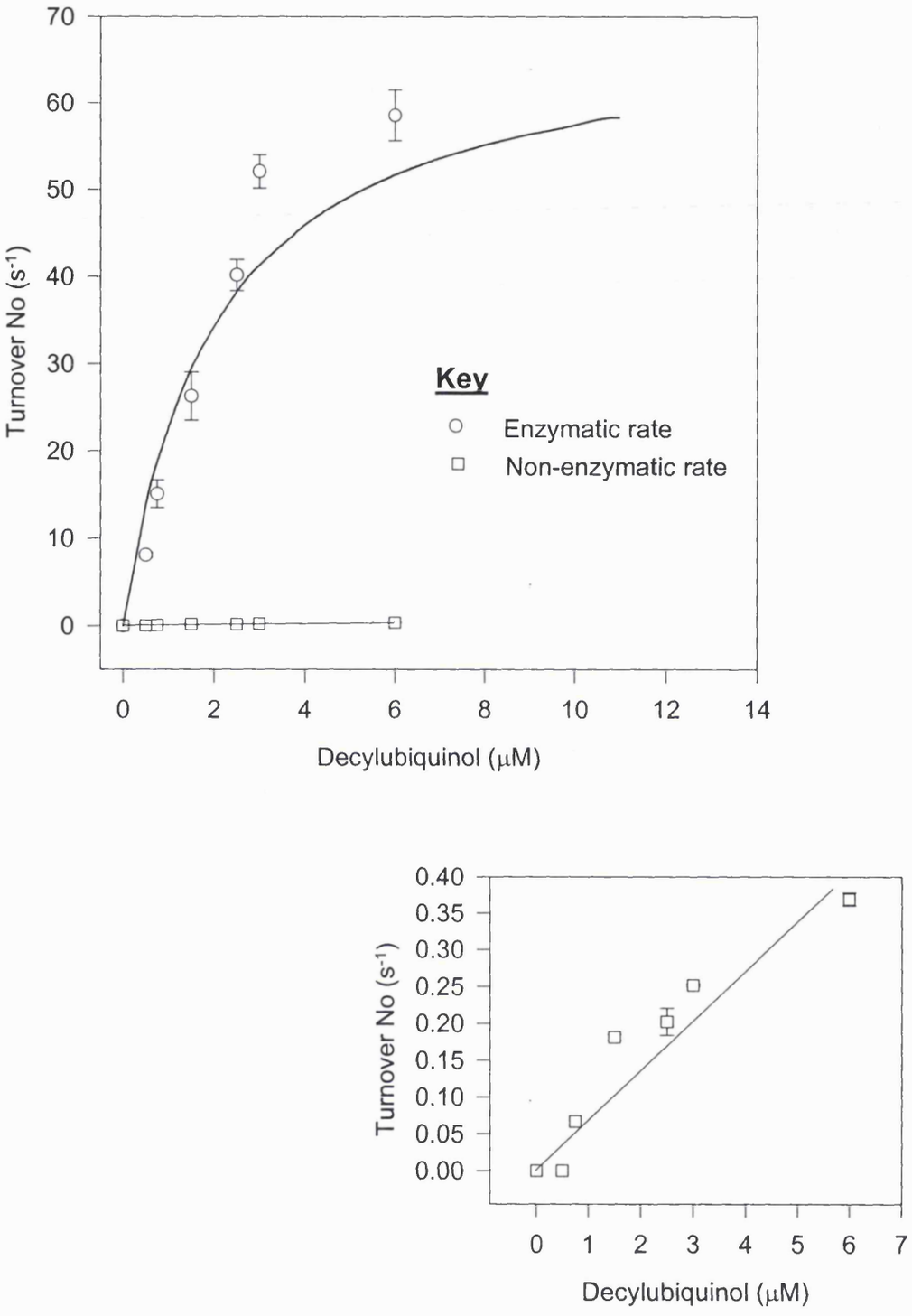

Fig. 3.6. The effect of decylubiquinol on the steady state kinetics of the bc_1 complex in 50mM potassium phosphate buffer. Experimental conditions as described in Section 3.2.2. The concentration of decylubiquinol was varied accordingly. Inset shows the non-enzymatic reaction rate.

3.3 Results and discussion

3.3.1 Optimisation of the bc_1 complex assay using SCR

3.3.1.1 Duroquinol Vs decylubiquinol

The reduction of cytochrome *c* by duroquinol gave a lower turnover number and a higher non-enzymatic rate in comparison to decylubiquinol (results not shown). This is explained by the fact that duroquinol is the more hydrophilic substrate with no hydrophobic sidechain (Fig. 3.1). Its random chemical reaction with soluble cytochrome *c* and other hydrophilic reactants would be expected to be faster, whereas its enzymatic reaction would be expected to be slower due to the hydrophobicity of the Q_o site than the more hydrophobic decylubiquinol with a C_{10} tail. Indeed it follows that the more hydrophobic the substrate to a limit, the greater the enzymatic rate and the slower the non-enzymatic reaction rate. Duroquinol is on the boundary of hydrophilicity, i.e. slightly more hydrophilic and the enzymatic reaction will be abolished. On the other hand, decylubiquinone is on the boundary of hydrophobicity; any more hydrophobic and it will form micelles. The natural substrate ubiquinol is so hydrophobic due largely to its C_{50} isoprene tail that it is very difficult to add with accuracy to the assay and will also form micelles in solution. *In vivo*, it is solubilised in the membrane, where the enzymatic reaction is fast and the non-enzymatic reaction is non-existent. As a result, decylubiquinol was chosen as the substrate for the steady state kinetics characterisation of the binding mode of MOA-stilbene to the Q_o site.

The k_{cat} for decylubiquinol at a fixed (saturating) concentration of 30μM cytochrome *c* is $71\pm9s^{-1}$, the apparent V_{max} is $0.9\pm0.1\mu Ms^{-1}$ and the apparent K_M is

2±1μM under the condition specified (Section 3.2.2). The specificity constant is 36±13 x $10^6 M^{-1}s^{-1}$. The non-enzymatic rate was less than the standard deviation of the enzymatic rate and therefore was not significant as shown in Fig. 3.6.

3.3.1.2 Ionic strength effects

An increase in ionic strength resulted in a decrease in rate of cytochrome *c* reduction (Fig. 3.7). Therefore the same buffer was used for the rest of the experiments. The ions are likely to be affecting the reaction between the bc_1 complex and cytochrome *c* by weakening inter-protein salt bridge formation and screening of surface charges.

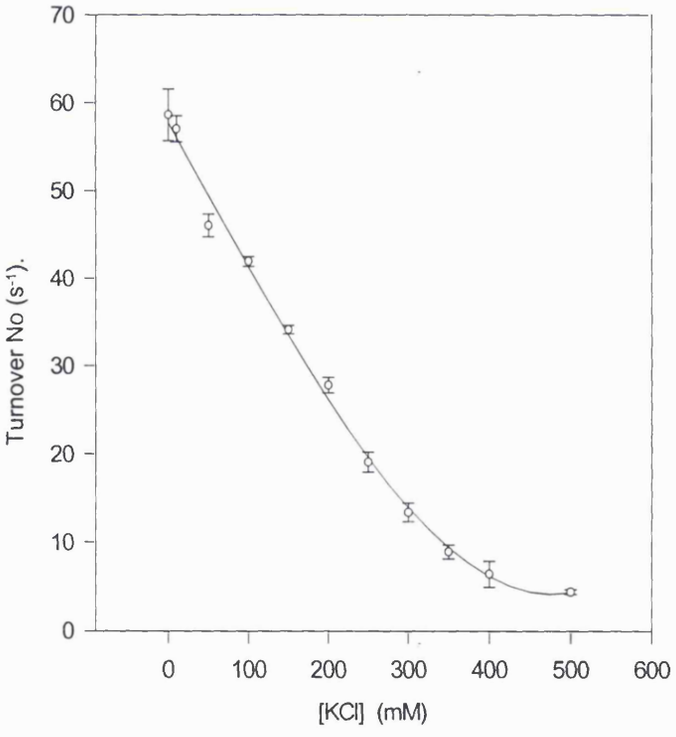

Fig. 3.7. The effect of ionic strength on the steady state kinetics of the bc_1 complex. Experimental conditions as described in Section 3.2.2. The ionic strength was adjusted by the addition of a solution of KCl to the reaction buffer.

3.3.1.3 pH effects

A characteristic bell shaped curve was obtained for the effect of pH on the activity of the bc_1 complex with an optimum of pH 8 (Fig. 3.8). The decrease in rate with decreasing pH is either due to the protonation/deprotonation of active site residues or an artefact of the denaturing of the enzyme. To distinguish between these alternatives the enzyme was incubated at various pH and the readings repeated for reversibility (results not shown). The reaction was not reversible below pH 6.5, which suggest denaturing of the enzyme occurring. At low pH, Cholate that was used to solubilised the enzyme precipitates out, so this may explain the non-reversibility of the reaction. The non-enzymatic rate increased with increasing pH due to the deprotonation of decylubiquinol to form the more reactive anionic form (Fig. 3.8).

3.3.1.4 The effects of different detergents

Ten detergents were screened for their effects on the steady state kinetics (Fig. 3.9A). The addition of detergent in the majority of cases, resulted in an initial increase in turnover before decreasing as the concentration of detergent increased. The concentration at which the best turnover was obtained for the detergents (Fig. 3.9B) was then used to determine an apparent K_M for decylubiquinol, and k_{cat} and apparent V_{max} (Fig. 3.10). The results are summarised in Table 3.3.

The classification of detergents is based on the nature of their hydrophilic head group, i.e. ionic, non-ionic and zwitterionic detergents [109]. The detergents used in this assay fall into the two latter categories. Ionic detergents are limited to alkaline pH range and are more effective in dissociation of protein-protein interactions, and so may acts as protein denaturants.

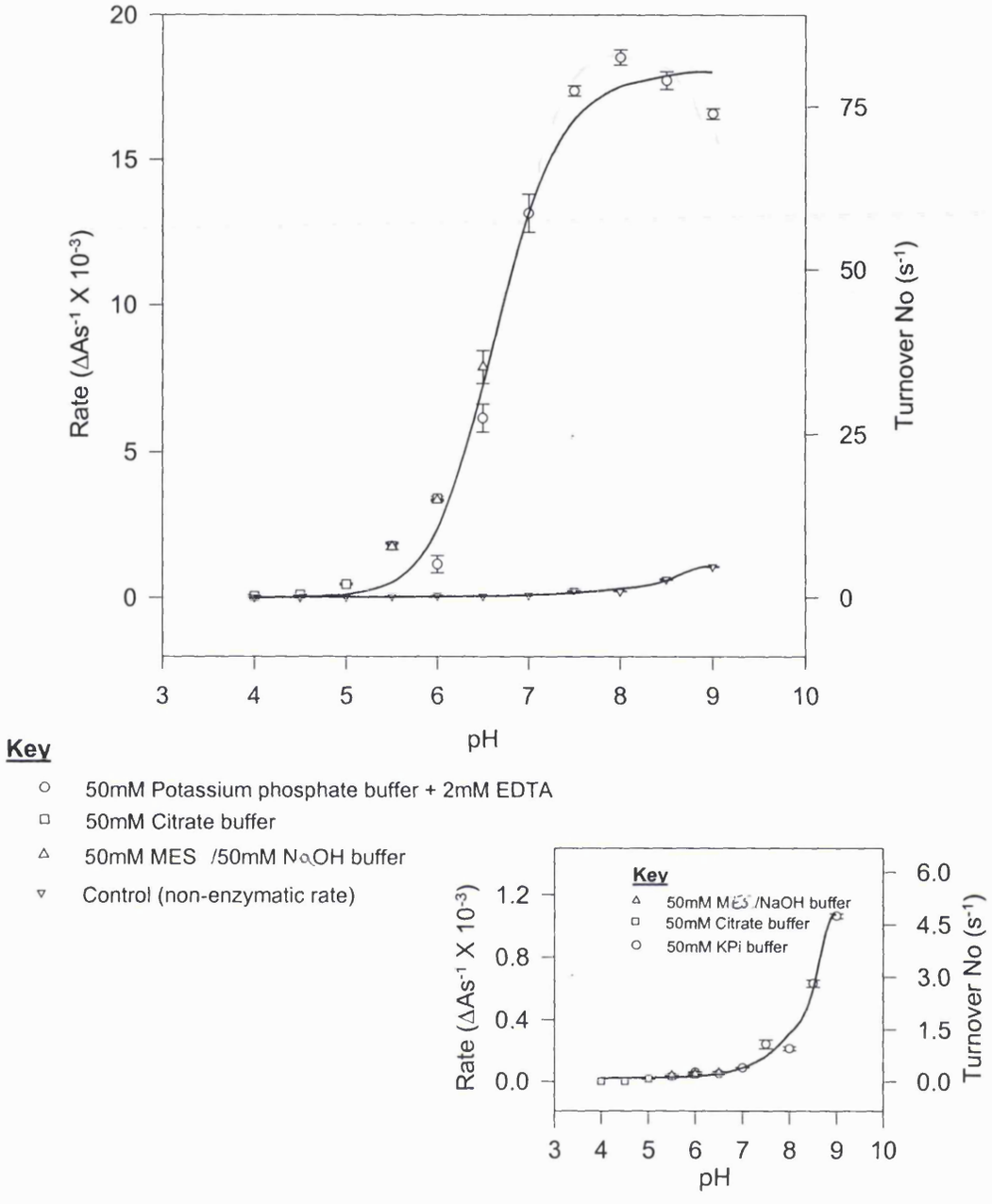

Fig. 3.8. The effect of pH on the steady state kinetics of the bc_1 complex. Experimental conditions as described in Section 3.2.2. The enzyme was incubated in 50mM Potassium phosphate, 2mM EDTA at pH 7. The reaction buffer was 50mM citrate buffer (tri-sodium citrate and citric acid) at pH 4-6, 50mM MES and NaOH buffer at pH 5.5-6.5 and 50mM Potassium phosphate, 2mM EDTA at pH 6-9. The inset shows the non-enzymatic reaction rates.

The non-ionic detergents contain uncharged, hydrophilic head groups that consist of either polyoxyethylene moieties as in Triton X-100, Nonidet P40, Lubrol PX and WX, and Tween 80 or glycosidic groups as in octyl glucoside, dodecyl maltoside, Hecameg and MEGA-9. In general, non-ionic detergents are better suited for breaking lipid-lipid and lipid-protein interaction rather than protein-protein interaction [109]. Hence, they are considered non-denaturant and are widely used in the isolation of membrane proteins in their biologically active form. In addition, the performance of detergents is also dependent on these factors, concentration, ionic strength, length of alkyl chain, pH, presence of organic additives, purity and temperature [109].

Alkyl glycosides such as dodecyl maltoside and octyl glucoside are more popular as non-ionic detergents in the isolation of membrane proteins for several reasons. Firstly, they are homogeneous with respect to their composition and structure. Secondly, several variations of alkyl glycosides containing different combinations of the hydrocarbon (cyclic or straight) and the polar sugar group can be easily synthesise in pure forms. Thirdly, subtle differences in the physicochemical properties of alkyl glycosides bearing various alkyl chains, attached either to a glucose, maltose, or a sucrose head group, can be exploited for selective solubilisation of membrane proteins [109]. A change in their hydrocarbon chain and the polar sugar group from octyl glucoside to dodecyl maltoside results in an increase in the apparent K_M of decylubiquinol for the bc_1 complex and k_{cat} (Fig. 3.9 and Table 3.3). Dodecyl maltoside gave the highest k_{cat} out of all the detergents with more than a two-fold increase (Fig. 3.9B).

The other non-ionic detergents with glycosidic polar head groups are the glucamides, MEGA-9 and Hecameg. They decreased the apparent K_M but had a smaller effect on the k_{cat} (Fig. 3.9 and Table 3.3).

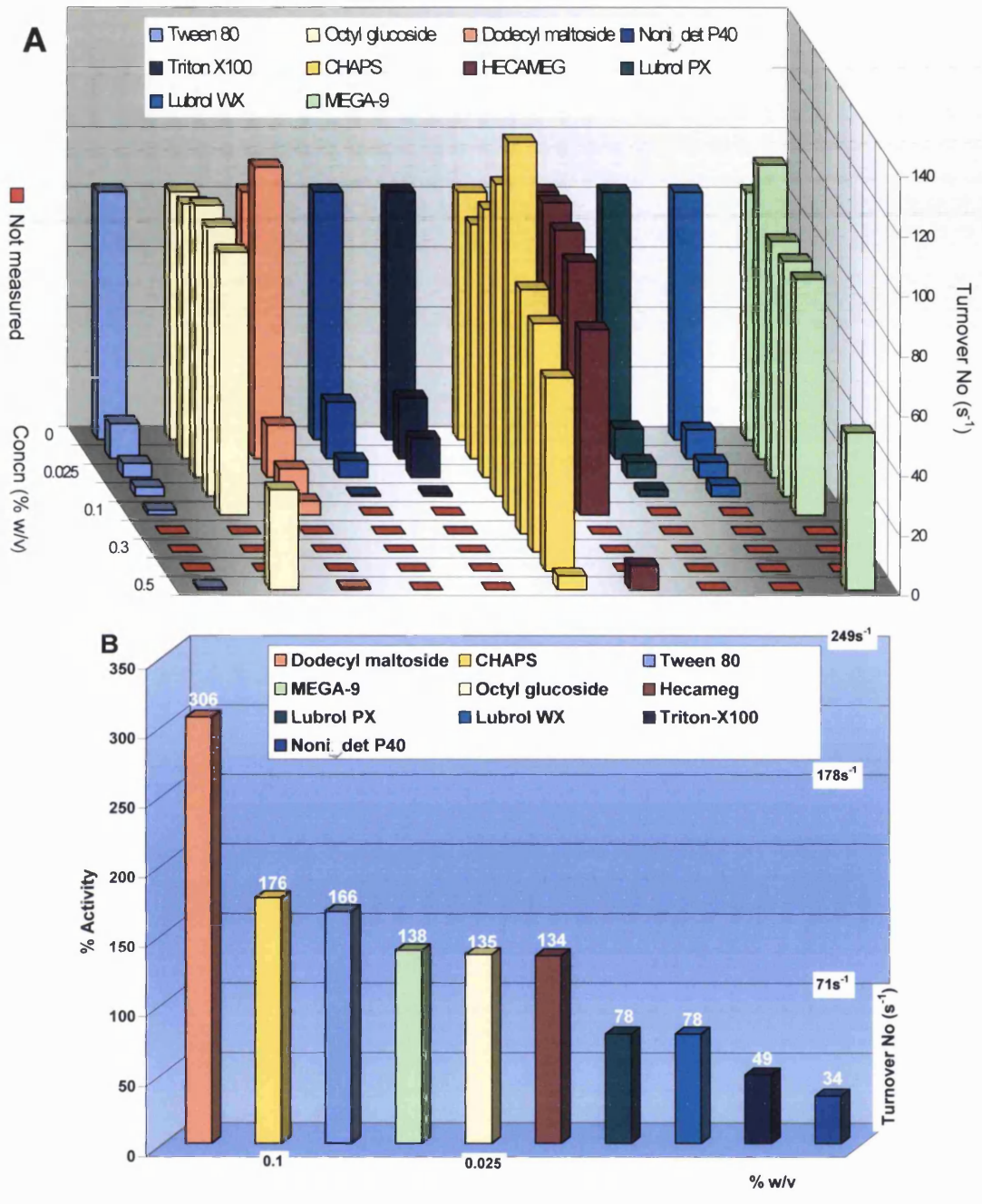

Fig. 3.9. The effect of decylubiquinol on the steady state kinetics of the bc_1 complex in the presence of varying (A) and optimum (B) concentrations of detergents. Experimental conditions as described in Section 3.2.2. The reaction buffer was at pH 8 and detergent was added prior to the addition of KCN. (B) The values of % activity (defined as the ratio of k_{cat} in the presence and absence of detergent expressed as percentage) for each detergent is displayed on top of each bar and unless otherwise stated the optimum detergent concentration was 0.01% w/v for all detergents (bottom of the bar charts).

Detergents with polyoxyethylene head groups, may contain alkylpolyethylene ethers with a general formula $C_nH_{2n+1}(OCH_2CH_2)_XOH$, e.g. Lubrol PX and WX, or a phenyl ring between the alkyl chain and the ether group, e.g. Triton X-100, Noni det P40 and Tween 80 (which has a tetrahydrofuran ring). Noni det P40 is the purified form of Triton X100, which contains peroxides. Lubrol PX and WX have shorter polyoxyethylene chains than the rest and thus form aggregates and viscous solutions in water at room temperature [109]. The polyoxyethylene detergents, with the exception of Tween 80 showed an apparent inhibition with a decrease in k_{cat} and increase in apparent K_M of decylubiquinol for the bc_1 complex (Fig. 3.9 and Table 3.3). Triton X-100 and Noni det P40 exhibits non-competitive type inhibition (results not shown). They have structural similarities to the substrate decylubiquinol. This apparent inhibition of the bc_1 complex activity may be due to one or a combination of the following, denaturing of the enzyme, an increase in the apparent K_M of decylubiquinol for the enzyme or depletion of the bc_1 complex essential lipid.

The zwitterionic detergents, e.g. CHAPS, are unique in that they offer the combined properties of ionic and non-ionic detergents [109]. They are efficient at breaking protein-protein interactions but are less denaturing than the ionic detergents. In this assay, CHAPS increased the k_{cat} and decreased the apparent K_M of decylubiquinol for the bc_1 complex. Therefore CHAPS appears not to be denaturing the protein at the specified concentration (Fig. 3.9 and Table 3.3).

In general detergents with glycosidic head groups are better than those with polyoxyethylene head groups, (an exception is Tween 80) in this assay. The zwitterionic detergent CHAPS is an intermediary between these two groups of non-ionic detergent.

In summary, the optimum conditions for the bc_1 complex assay using SCR at room temperature is a reaction buffer containing 50mM potassium phosphate, 2mM EDTA at pH 8 and 0.01% w/v of dodecyl maltoside.

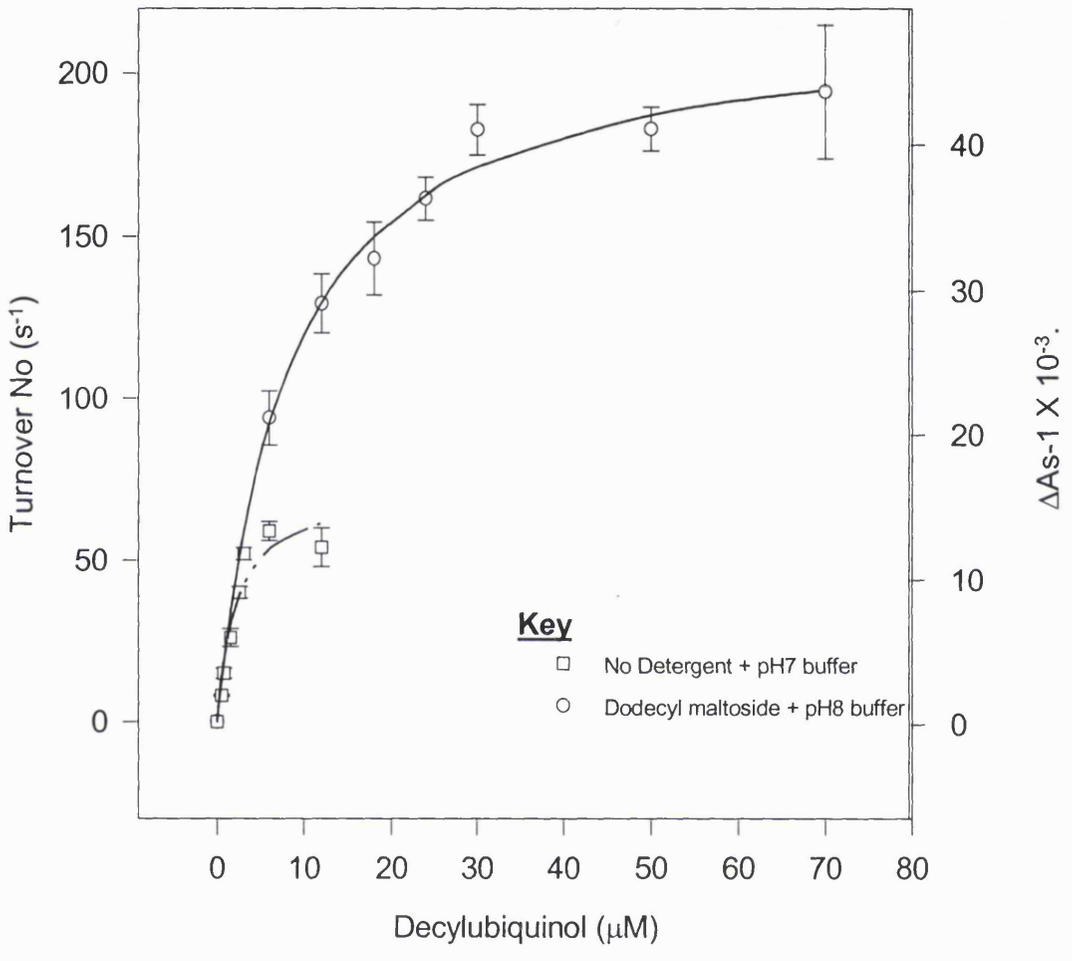

of decylubiquinol

Fig. 3.10. The apparent K_M for the bc_1 complex in the presence of dodecyl maltoside. Experimental conditions as described in Section 3.2.2. The reaction buffer was pH 8 and 0.01% w/v dodecyl maltoside was added prior to the addition of KCN.

Table 3.3. The effect of different detergents on the steady state kinetics of the bc_1 complex

Detergents	% w/v	% Activity	App. V_{max} (μMs^{-1})	App. K_M for DQH_2. (μM)	k_{cat} (s^{-1})
None	-	100	0.9±0.1	2±1	71±9
Dodecyl maltoside	0.01	306	2.6±0.01	8 ±0.9	217±6
CHAPS	0.1	176	1.5±0.1	0.5±0.7	125±8
Tween 80	0.01	166	1.4±0.3	25±13	118±23
MEGA-9	0.01	138	1.2±0.08	0.85±0.8	98±7
Octyl glucoside	0.025	135	1.2±0.3	0.45±3	96±25
Hecameg	0.01	134	1.1±0.4	1±4	95±36
Lubrol PX	0.01	78	0.66±0.13	20±11	55±11
Lubrol WX	0.01	78	0.63±0.16	20±14	52±13
Triton-X100	0.01	49	0.42±0.05	3.5±2	35±4
Noni det P40	0.01	34	0.29±0.04	2.8±2	24±3

The calculated kinetic constants, k_{cat} and K_M were from a Michaelis-Menten (hyperbolic) fitted curve using Sigma plot software (SPSS Science). The standard error (±) is the asymptotic standard errors of the k_{cat} and K_M, and can be used as a gauge of the accuracy of the fitted curve. Experimental conditions as described in Section 3.2.2. % Activity is the ratio between the k_{cat} obtained in the absence and presence of detergent expressed in percentage.

Table 3.4. Steady state kinetic constants of different preparations of the bc_1 complex

bc_1 complex preparation	V_{max} (μMs^{-1})	k_{cat} (s^{-1})	K_M (μM) DQH_2	k_{cat}/K_M ($M^{-1}s^{-1}$) x 10^6 DQH_2
SCR*	0.9±0.1	71±9	2±0.7	36±13
SCR	2.6±0.01	217±6	8±0.9	27±3
KHP	7.3±0.8	606±68	32±7	19±4
Purified Triton-prepared enzyme	10±0.1	811±8	35±7	23±4
Purified Triton prepared yeast enzyme	5±0.4	446±32	55±9	8±1

The calculated parameter values, k_{cat} and K_M were from a Michaelis-Menten (hyperbolic) fitted curve using Sigma plot software (SPSS Science). The standard error (±) is the asymptotic standard errors of the k_{cat} and K_M and can be used as a gauge of the accuracy of the fitted curve. *SCR, assay buffer did not contain dodecyl maltoside.

3.3.2 Steady state kinetics of yeast and bovine bc_1 complex in different preparations

The effects of decylubiquinol on the steady state activity of the bc_1 complex in KHP were investigated for comparative purposes (Fig. 3.11). As a result, the kinetic constants for decylubiquinol were determined (Table 3.4). The specificity constant of this preparation is in good agreement with other preparations. Again the rate of cytochrome *c* reduction decreases with increasing ionic strength. As well as possible effect of ions on cytochrome *c* reduction by the bc_1 complex, the ions may also be decreasing the critical micelle concentration (CMC) of the detergent.

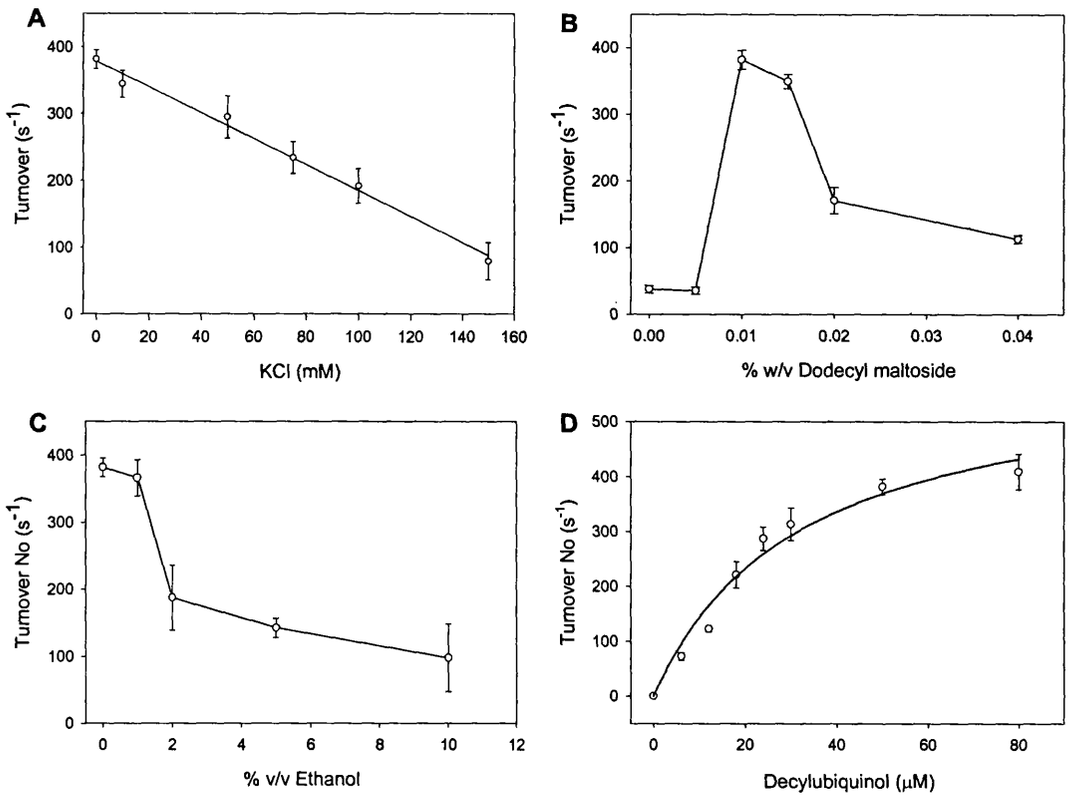

Fig. 3.11. The effect of different conditions on the steady state kinetics of the bc_1 complex in KHP. A) Ionic strength **B)** Dodecyl maltoside **C)** Ethanol **D)** Decylubiquinol. Experimental conditions as described in Section 3.2.2. The reaction buffer was pH 8 and 0.01% w/v detergent was added prior to the addition of KCN (A, C and D). The reaction was started with 60μM decylubiquinol (A-C).

The maximal turnover number was also obtained at 0.01% w/v dodecyl maltoside. At a concentration greater than 2% v/v ethanol (340mM), the rate is severely affected. In addition, a multiphasic reaction was also observed. Ethanol has been reported to interfere with the 'Rieske' ISP, evident by a change in its EPR line shape but not to affect the catalytic rate in *Rb. sphaeroides* [57], in contrast to this result. This may indicate slight differences in the functioning of the bacterial enzyme in comparison to its mammalian counterpart. However, it is important to note that in the former case, single and multiple flash-induced cytochrome bc_1 complex turnover kinetics were investigated using endogenous ubiquinol in chromatophore membranes rather than the

steady state kinetics with the addition of decylubiquinol used in this studies. The diffusion rate of decylubiquinol through a multiphasic system may be affected by the addition of ethanol, which would then affect the catalytic rate. This could provide an explanation for the multiphasic reaction rate observed at high concentrations of ethanol.

The effect of decylubiquinol on the steady state activity of the Triton-prepared purified bovine and yeast bc_1 complexes was investigated (Fig. 3.12A) for comparative purposes and determination of dissociation constants (Chapter 5). The effect of different concentrations of dodecyl maltoside on the steady state kinetics of the bovine enzyme was also investigated (Fig. 3.12A). As a result, the kinetic constants for decylubiquinol were determined (Table 3.4). The specificity constants of both preparations are in good agreement with the other preparations. The maximal turnover number was again obtained at 0.01% w/v dodecyl maltoside for the Triton-prepared bovine bc_1 complex.

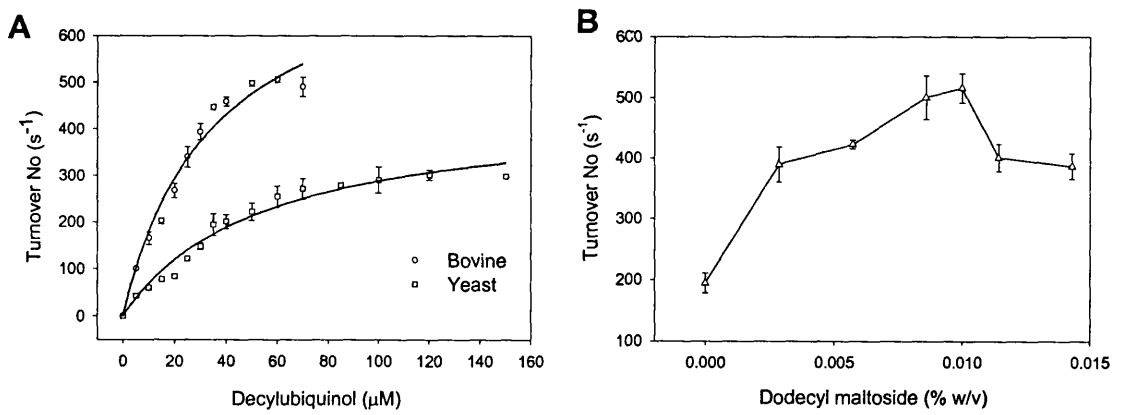

Fig. 3.12. (A) The effect of decylubiquinol on the steady state kinetics of Triton-prepared yeast and bovine bc_1 complexes. (B) The effects of dodecyl maltoside on the steady state kinetics of the bovine enzyme. Experimental conditions as described in Section 3.2.2. The reaction buffer was pH 8 and 0.01% w/v detergent was added prior to the addition of KCN (A). The reaction was started with 30μM decylubiquinol.

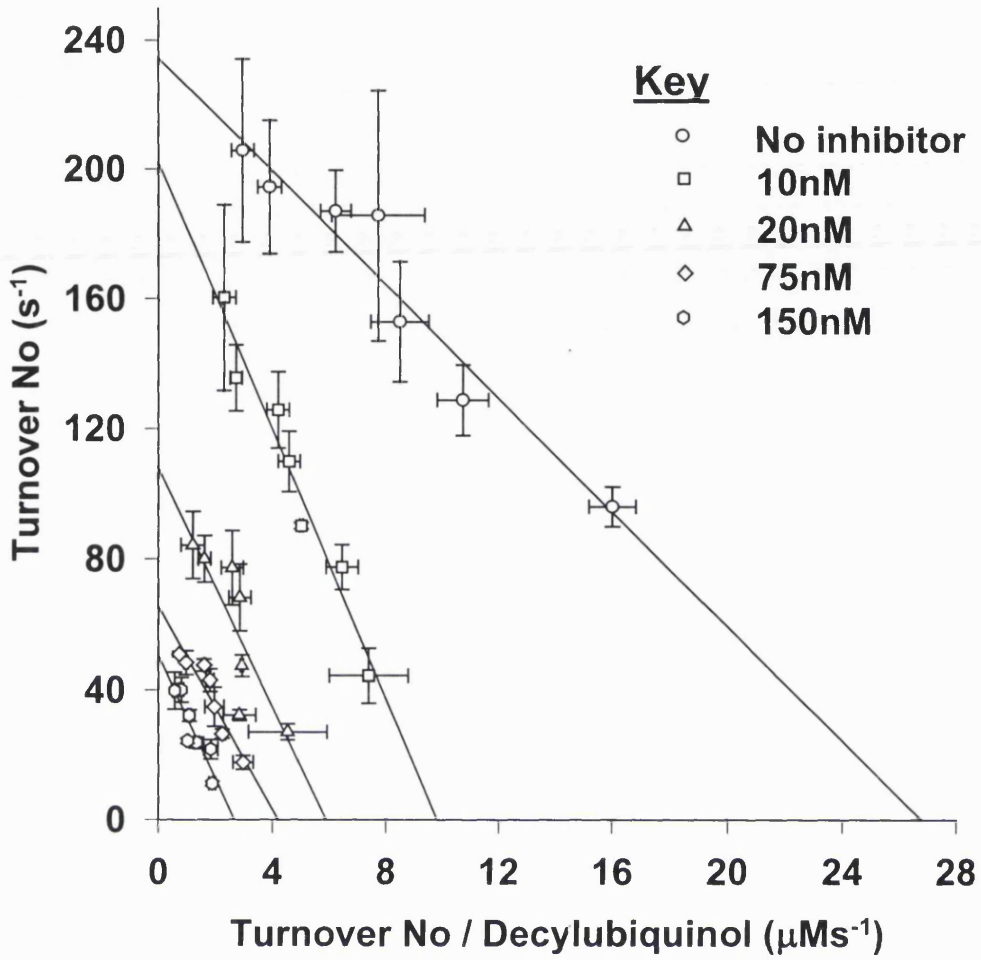

Fig. 3.13. Eadie-Hofstee plot of inhibition kinetics: Characterisation of the binding of MOA-stilbene to the Q_o site. Experimental conditions as described in Section 3.2.2.1.

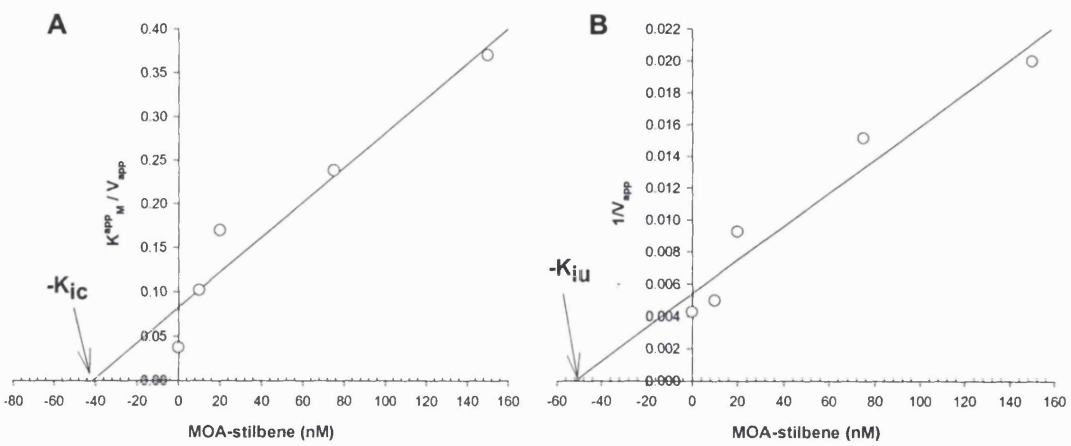

Fig. 3.14. Inhibition of the bc_1 complex by MOA-stilbene: Determination of inhibition constants K_{ic} (A) and K_{iu} (B).

Table 3.5. Kinetic constants and I_{50} values from steady state kinetics of two independent experiments

Results	bc_1 complex preparation	Quinol / K_M (μM)	Kinetic plot / type of inhibition	App. inhibition constants (nM)		
				I_{50}	K_{ic}	K_{iu}
Chapter 3	SCR	DQH_2/ 8±0.9	Eadie-Hofstee / Mixed	13±2	41	52
Brandt *et al.* (1988)	Embedded in proteoliposome	NQH_2/ 1.8±0.7	Eadie-Hofstee / Non-competitive	14±3	14±9	38±23

The inhibition constants K_{ic} and K_{iu} were determined from (Fig. 3.14). The K_{ic} and K_{iu} were also determined using the Dixon and Cornish-Bowden plot respectively (Fig. 3.5). The median value for K_{ic} is 23nM and that for K_{iu} is 85nM (results not shown). Otherwise if an average value of all the intercepting points is taken, K_{ic} = 28±15 and K_{iu} = 108±50.

3.3.3 Characterisation of the mode of binding of MOA-stilbene to the Q_o site

The steady state kinetics of the bc_1 complex were used to characterise the binding modes of MOA-stilbene in respect to the substrate decylubiquinol. This revealed a mixed type inhibition (Fig. 3.13), which suggest overlapping binding sites for the inhibitor and the substrate, i.e. the inhibitor affects both the catalytic (V^{app}) and binding (K_M^{app}) properties of the substrate. In a previous study of inhibitor titrations of steady-state turnover and binding studies (Table 3.5) by Brandt and colleagues, a non-competitive inhibition was proposed [75]. This means the binding of the substrate is unaffected by the presence of the inhibitor i.e. apparent value of V_{max} is decreased with no corresponding effect on that of K_M. On re-examination of the data, a mixed

type of inhibition best fit the data i.e. K_{iu} is not equal to K_{ic} and Eadie-Hofstee plots of inhibition kinetics are more reminiscent of mixed inhibition. In any case, as indicated in the introduction non-competitive inhibition is a special case of mixed inhibition. The values for K_{ic} and K_{iu} obtained for both studies cannot be identical due to the different hydrophobic phases and substrates (Table 3.5).

The data requires careful interpretation for the following reasons. Firstly, it is based on the classical treatment of enzymatic data, which was developed for a soluble enzyme, water-soluble ligands and three-dimensional diffusion in a monophasic system. In contrast to the membrane bound enzyme, the hydrophobic inhibitor (MOA-stilbene) and substrate (decylubiquinol), which will partition almost completely in the hydrophobic phases of a multiphasic system, a partition coefficient and a quasi-two-dimensional instead of a three dimensional diffusion behaviour will have to be assumed. Secondly, due to their amphiphilic properties, decylubiquinol and MOA-stilbene tend to accumulate in the small hydrophobic membrane phases so that the actual target site concentrations are very difficult to determine [75].

Crofts et al. (2000) [34] have also challenged the use of classical non-competitive scheme by *Brandt et al.* (1988) [75] in which the inhibitor could bind to both enzyme ($E + I \leftrightarrow EI$) and enzyme-substrate complex ($ES + I \leftrightarrow ESI$) to explain their data. They argued that such a scheme is only appropriate under conditions in which all equilibria determining the concentration of ES are rapid compared with the dissociation of ES to product (P). This would be the case only with a weak binding inhibitor, with on and off rates rapid compared to turnover. Inhibitor titrations of the single turnover of the Q_o site assayed by flash activation of *Rb. sphaeroides* chromatophores showed unambiguously that myxothiazol and MOA-type inhibitors bind tightly from the membrane phase. In addition, dissociation of the inhibitors was

several orders of magnitude slower than the turnover of the reaction, i.e. the condition of a weak binding inhibitor is not met. Therefore, it was suggested that the use of such a scheme was inappropriate and the conclusion derived by *Brandt et al.* (1988) [75] was not justified. They further suggested that the inhibitors show non-competitive effects because they remove the enzyme from reaction mixture by binding tightly to E, not because they bind to ES [34].

However, the kinetic analysis results presented here clearly shows that the binding site for decylubiquinol is not identical to that for MOA-stilbene. It supports overlapping binding sites, which is consistent with previous competition experiments with two classes of Q_o site inhibitor [58-60, 62, 63, 68, 75].

3.4 Summary

The optimum condition for the bc_1 complex assay using the SCR preparation of the enzyme at room temperature is a reaction buffer containing 50mM potassium phosphate, 2mM EDTA at pH 8 and 0.01% w/v of dodecyl maltoside. The specificity constants of all preparations are in good agreement (Table 3.4).

The steady state kinetics of the bc_1 complex was used to characterise the binding mode of MOA-stilbene with respect to the substrate decylubiquinol. This revealed a mixed type inhibition (Fig. 3.13), which shows that the previous conclusion of separate binding sites for MOA-stilbene and ubiquinone is open to question. It supports a model of overlapping binding sites consistent with previous competition experiments with two classes of Q_o site inhibitor [58-60, 62, 63, 68, 75].

CHAPTER 4

Single or double occupancy of the Q_o reaction site studied by molecular modelling, and optical and EPR spectroscopy

4.1 Background

The steady state kinetic results presented in chapter 3 are fully consistent with previous inhibitor studies [58-60, 62, 63, 68, 75] in supporting a model of overlapping binding sites for occupants of the Q_o site and questioning the notion of separate binding sites for MOA-stilbene and ubiquinone. To complement this study, further studies were carried out using more direct methods. To address the question of whether two inhibitors can be accommodated within the Q_o site, competition between two classes of Q_o site inhibitors was investigated. In addition, computer modelling studies with the available crystal structure co-ordinates and data from mutagenesis studies [32, 33, 110] to identify residues conferring resistance to inhibitors were also used to address this question. The question of whether two ubiquinone molecules can bind simultaneously was assessed by trying to model their binding into the Q_o site. Finally, electron paramagnetic resonance (EPR) spectroscopy was used to investigate whether the Q_o site can bind one or two compounds simultaneously. The information obtained was combined with molecular modelling studies to assess whether rational design of new pesticides to have radically altered activity at the site might be feasible.

EPR spectroscopy, also known as electron spin resonance (ESR) spectroscopy, utilises the resonant absorbtion of microwave radiation by paramagnetic ions or molecules with at least one unpaired electron spin whose energy has been split by a static magnetic field. EPR spectroscopy was first developed by Zavoisky in 1944 and for technical reasons it is normally performed with a fixed microwave frequency and a variable magnetic field. The 'Rieske' ISP has an ill-defined visible spectrum but has very characteristic EPR spectra in the paramagnetic reduced form [1]. The environment of the unpaired electron, e.g. hydrogen bonding, influences the features of this EPR signal. The 'Rieske' ISP is useful for probing the occupancy state of the

Q_o reaction site because it docks firmly at the interface with cytochrome *b*, moving its ligand (H161) within H-bonding contact of the occupants of the Q_o site bound at the distal end to haem b_L. The line shape and position of the 'Rieske' [2Fe2S] cluster g_x band in particular has provided an essential part of the progress into the Q_o site character. It has proved to be highly sensitive to the degree and nature of the Q_o site occupants (Q/QH_2 or inhibitors) [70-74], and provides a useful tool in dissecting cytochrome bc_1 complex function [57].

4.1.1 Probing the Q_o site occupancy of bacterial bc_1 complex using EPR spectroscopy

The solvent extraction and re-titration of quinone to a redox poised iron-sulphur cluster of the bc_1 complex [70-74], resulting in changes in the EPR line shape of the reduced cluster, offers good evidence in favour of the double occupancy model. These experiments were carried out on bacterial cytochrome bc_1 complex in *Rb. capsulatus* chromatophore membranes. The results (Fig. 4.1) were interpreted in terms of binding of two ubiquinone molecules within two distinct binding domains, a strongly bound prosthetic species (Q_{os}) located near the iron-sulphur cluster (distal domain) and a weakly bound exchangeable species (Q_{ow}) located near the b_L haem (proximal domain). In native chromatophores with the Q-pool oxidised, the 'Rieske' [2Fe2S] cluster EPR line shape exhibits a prominent g_x resonance centered at 1.800. Partial extraction results in the broadening and an upfield shift of the g_x resonance to 1.783 (Fig. 4.1B). Finally, upon complete quinone extraction, further broadening and an upfield shift of the g_x resonance to 1.765 occur (Fig. 4.1C) [72].

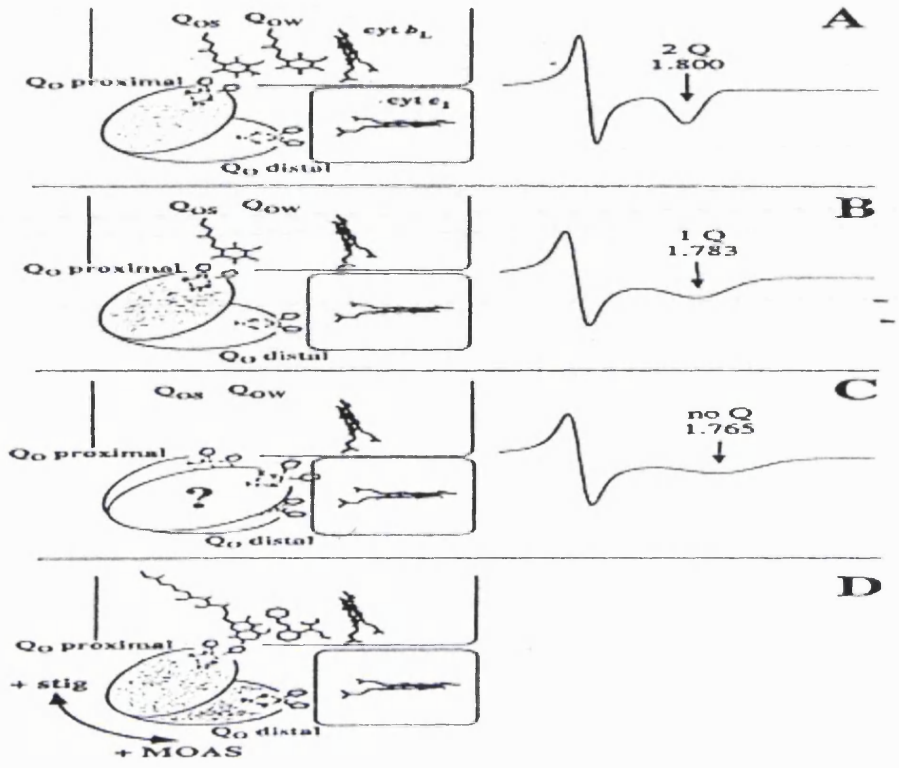

Fig. 4.1. Structural interpretation of the Q_o-site occupancy and correlation with the reduced [2Fe2S]-cluster EPR line shape. (A-C) Panels represent different Q_o site quinone (Q) occupancies. The left-hand side shows schematic representations of the cytochrome bc_1 complex region surrounding the Q_o site, based on the crystal structure data. On the right-hand side the characteristic [2Fe2S] cluster EPR spectral line shapes are depicted, suggested previously to be dependent on the number of Q occupants in the Q_o site [4849, 7971]. **(A)** Two quinones in the Q_o site, the iron-sulphur subunit is positioned so that the [2Fe2S] cluster is close to the strongly bound prosthetic quinol species (Q_{os}), (Q_o proximal), the EPR line shape has a g_x resonance centered at 1.800. **(B)** One quinone in the Q_o site, the iron-sulphur subunit is still Q_o proximal, but the EPR line shape is now indicative of quinone in the Q_{os} site only, g_x at 1.783. **(C)** Q_o site devoid of quinone, the iron-sulphur subunit is in the equilibrium position, i.e. between the proximal and distal positions, g_x at 1.765. **(D)** The iron-sulphur subunit position in the co-crystals of stigmatellin (stig, bound close to [2Fe2S]) and MOA-stilbene (MOAS, bound close to cytochrome b_L). The iron-sulphur subunit is positioned proximal and distal to the Q_o site in the presence of stigmatellin and MOA-stilbene respectively. Q_{ow}, weakly bound exchangeable quinone species. Cyt, cytochrome. The figure was reproduced from *Sharp et al.* (1999) [74].

The quinone extraction studies were further complemented by experiments on the binding of inhibitors [70-74]. The binding of stoichiometric MOA-stilbene and excess diphenylamine (DPA) were interpreted to be competitive with respect to Q_{ow} and non-competitive with respect to Q_{os} [72, 73]. It was concluded that when stoichiometric MOA-stilbene or excess DPA were added to native chromatophores, they displace the Q_{ow} quinone and shift the g_x resonance from 1.800 to 1.783. Also the addition of the inhibitors to partially (g_x = 1.783) or fully Q-extracted (g_x = 1.765) chromatophores had no effect on the [2Fe2S] cluster EPR spectral line shape, resulting in unaltered g_x resonance, i.e. the inhibitor is competing for the Q_{ow} domain alone with no effect on the Q_{os} domain.

In these experiments [73], it was also shown that up to 100μM DPA could inhibit quinol oxidation without influencing the g_x 1.800 or 1.783 species. As the concentration was raised above that giving inhibition of electron transfer, the g_x 1.800 species was lost before the 1.783 species. They interpreted this as showing a triple occupancy of the Q_o site with DPA binding in a non-competitive manner at a site other than Q_{os} and Q_{ow}.

4.2 Methods

4.2.1 Binding spectra

The samples contained 2μM SCR in 0.1M Tricine pH 8.5 buffer and 0.01% w/v dodecyl maltoside (0.5ml final volume). The sample was reduced with 50mM sodium dithionite and incubated for 2-3min. Difference spectra were then recorded in the Soret and visible regions after addition of 1μl 96% ethanol (as control) followed by the addition of 10μM stigmatellin or 48μM AG204 (final concentration). For the Fig. 4.3,

competition experiment, a further 48μM AG204 (final concentration) was added to a sample already containing 10μM stigmatellin and the resulting binding spectrum was recorded. The spectra were recorded using a single beam spectrophotometer. Binding spectra are the difference between the dithionite-reduced enzyme with and without a saturating amount of inhibitor.

4.2.2 Molecular modelling

All visualisation and manual docking were carried out using $Cerius_2$ from Molecular Simulations Inc (MSI, now Accelrys). The representation of the protein surface was generated using MSMS [111] followed by processing of the 'raw' MSMS data files with in-house written scripts to allow display of the relevant parts of the surface within $Cerius_2$.

4.2.3 EPR sample preparation

The EPR experiments were carried out using bovine mitochondrial membranes (KHP) and SCR prepared as described in Chapter 2. The samples contained 20μM KHP or 10-30μM SCR in 0.1M sodium phosphate pH 8.0 buffer (0.35ml final volume) and the 'Rieske' [2Fe2S] cluster was reduced with 10-20mM sodium ascorbate. The incubation time with the reductant before freezing the KHP sample and lowering the pH of the buffer from 8 to 7 had no effect on the EPR line shape of the 'Rieske' [2Fe2S] cluster (results not shown). 10mM fumarate and/or 1mM succinate were added to KHP samples to modulate the redox-state of the Q-pool. 20mM Ethanol (96%) or 5mM DMSO were added as control. Compounds were added to the samples as specified in the figure legends. The concentration of bc_1 complex in the preparation was estimated from the dithionite-reduced *minus*

ferricyanide-oxidised difference spectrum using an extinction coefficient at 562 *minus* 575nm of $\Delta\varepsilon = 28.5 mM^{-1}cm^{-1}$ in a single beam spectrophotometer built in house and linked to a personal computer (PC).

4.2.4 EPR measurements

The EPR samples were immediately frozen in liquid nitrogen and continuous wave EPR spectra were recorded on a Jeol RE1X spectrometer fitted with an Oxford instruments cryostat. The microwave power saturation characteristics of the 'Rieske' ISP in SCR were performed (Fig. 4.2), to reveal the safe working limits of microwave power that should be used when recording its EPR spectra at a defined condition. If a sample becomes microwave power saturated, it can lead to a reduction in the peak intensity and an increase in its effective linewidth. A power saturation profile involves recording EPR spectra over a range of microwave power while monitoring the effect on signal size. The data obtained can then be plotted using the following expression (Eq. 4.1):

$$I(P) = k\sqrt{P[1 + P / P_{1/2}]^{-0.5B}} \qquad \textbf{(Eq. 4.1)}$$

In this expression I(P) is the intensity of the EPR signal as a function of the microwave power P. $P_{1/2}$ the microwave power at half saturation, and *k* and *b* are constants. Plotting log $(I/\sqrt{P})$ against log P results in two straight lines with an intersection point at $P = P_{1/2}$, if the readings are taking over a wide range of microwave powers. At this point the microwave power saturation limit can be read off the graph [112]. Microwave power of 10mW was used to record the spectra of SCR preparations. This is within the safe working limits of microwave power, i.e. where the power used is unsaturating and below the saturation limit (Fig. 4.2). The safe working limits of microwave power (10mW) for the 'Rieske' [2Fe2S] cluster in KHP

was obtained from *Ding et al.* (1992) [71].

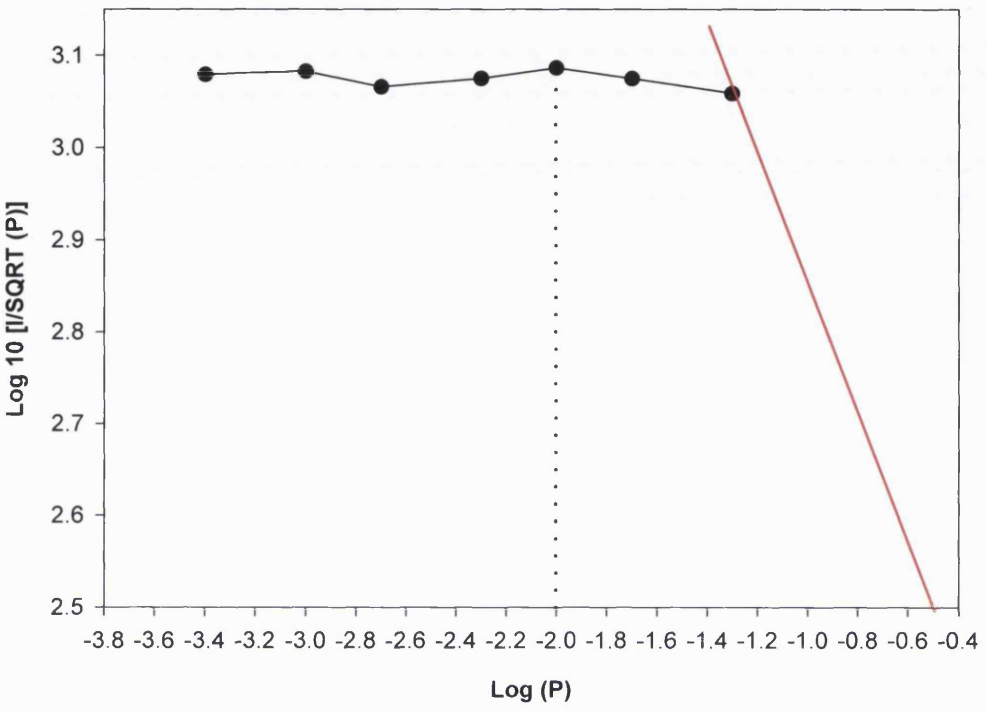

Fig. 4.2. Microwave Power saturation curve of the 'Rieske' ISP of bovine cytochrome bc_1 complex in succinate cytochrome c reductase (SCR). Dotted line represents the microwave power (10mW) used to record the spectra of 'Rieske' [2Fe2S] cluster of bovine cytochrome bc_1 complex in succinate cytochrome *c* reductase. This is within the safe working limits of microwave power, i.e. where the power used is unsaturating and below the saturation limit. The red line represents imaginary data points where the power is saturating. This was drawn to illustrate the type of graph obtained when log ($I/\sqrt{P}$) is plotted against log P, if the readings were taken over a wide range of microwave powers.

Conditions of measurement were as follows: temperature, 25K; modulation amplitude, 20G; microwave power, 10mW. Each spectrum is the average of at least four successive scans. The g_x values were calculated using the equation $h\nu = g\beta H$, where h is Planck's constant, ν is the frequency of the radiation (GHz), β a constant, the Bohr magneton, H the applied magnetic field (mT) and g the spectroscopic constant [1].

4.3 Results and discussion

4.3.1 Inhibitor studies

To address the question of whether two inhibitors can be accommodated within the Q_o site, competition between two classes of Q_o site inhibitors was investigated. The studies clearly show that the class II inhibitor AG204 partially reverses the effect of stigmatellin (Fig. 4.3) on the EPR line shape of the 'Rieske' [2Fe2S] cluster (Fig. 4.4A). It also reverses the stigmatellin effect on the red-shift spectrum of haem b_L (Fig. 4.4B), showing that these compounds cannot bind simultaneously. This is consistent with the kinetic studies (Chapter 3) and the finding that binding of the two classes of Q_o site inhibitors are mutually exclusive [58-60, 62, 63, 68, 75].

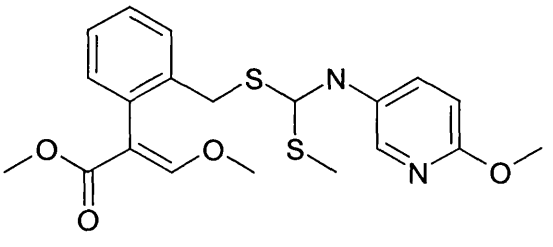

AG204 (AE C608292)

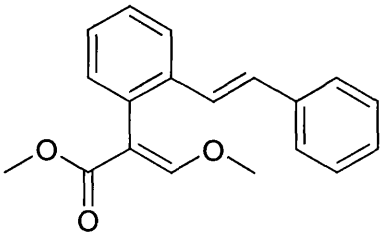

MOA-stilbene

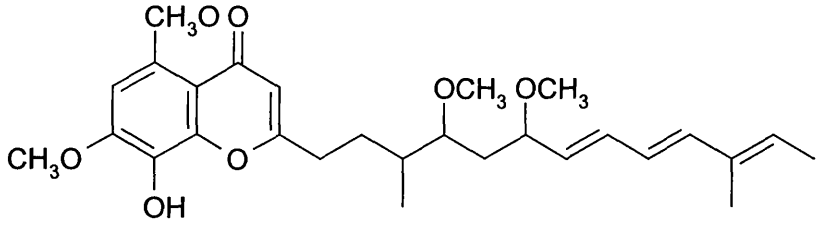

Stigmatellin A

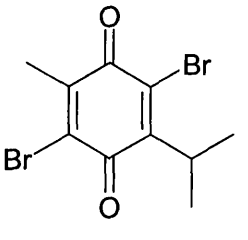

DBMIB

Fig. 4.3. Structures of Q_o site inhibitors. DBMIB (2,5-dibromo-3-methyl-6-isopropyl-p-benzoquinone)

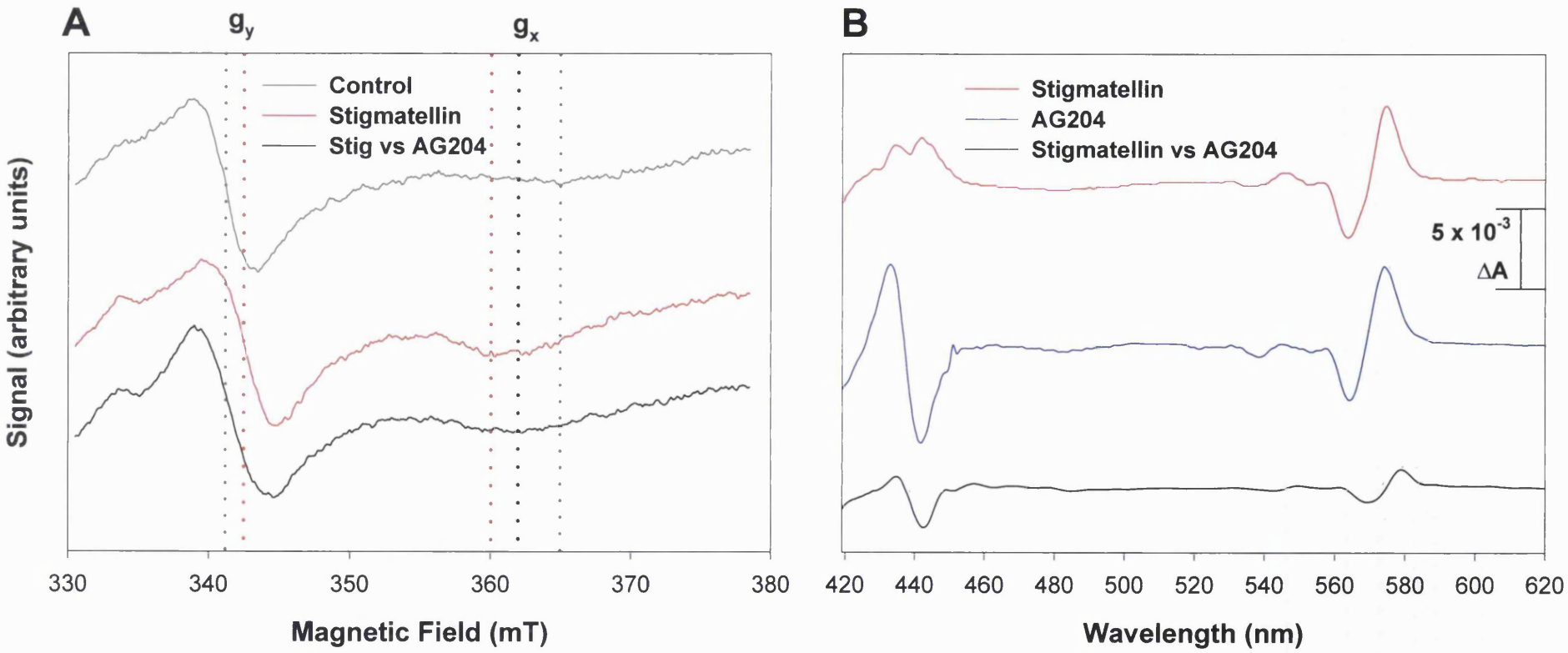

Fig. 4.4. Competition between classes I and II Q_o site inhibitors: A) Effects on the EPR line shape of the 'Rieske' [2Fe2S] cluster. AG204 (class II inhibitor) partially reverses the effect of stigmatellin (Stig, class I inhibitor) on the EPR line shape of the 'Rieske' [2Fe2S] cluster. The sample contained 10μM SCR in 0.1M sodium phosphate pH 8.0 buffer (0.35ml final volume) and the 'Rieske' [2Fe2S] cluster was reduced with 10mM sodium dithionite. 20mM ethanol or 20μM stigmatellin or 50μM AG204 was added accordingly. The EPR conditions were as described in Section 4.2.3-4) **B) Effects on the optical absorbtion spectrum of haem b_L.** AG204 reverses the effect of stigmatellin on the red shift spectrum of haem b_L.

4.3.2 Positions of mutations conferring resistant to inhibitors

Molecular modelling studies with the available crystal structure co-ordinates and data from mutagenesis studies to identify residues conferring resistance to inhibitors were also used to address the question of whether two inhibitors can be accommodated within the Q_o site. *Brasseur et al.* (1996) [33] have reviewed mutations in the bc_1 complex which confer resistance to inhibitors. The mutations conferring resistance to Q_o site inhibitors are listed in Table 4.1 and their positions in the Q_o site are shown in Fig. 4.5. The figure shows that changes conferring resistance to stigmatellin tend to be located in the domain close to the 'Rieske' ISP, where the pharmacophore of the inhibitor binds. It also shows that changes in the proximal domain close to haem b_L, where the pharmacophore of myxothiazol and MOA-type inhibitors bind, confer resistance to these inhibitors. Furthermore, changes in residues located in the entrance tunnel (which connects the site to the membrane phase), where any occupant with a 'tail' would bind, confer resistance to both stigmatellin and myxothiazol, and loss of activity, e.g. M125 [34]. Several residues, e.g. F129, in the middle of the pocket can also affect binding of both inhibitor types, consistent with a model of overlapping binding sites of the inhibitors from the inhibitor studies. Crofts, Berry and colleagues came to similar conclusions after analysing the relation between functional effects, location of the mutations in the structures and effects on the g_x 1.800 signal of the bacterial complex [31, 34, 68].

The positions of the mutations clearly show differential effects on the binding of the two classes of inhibitors. However, it is important to note that inhibitor resistance has not been systematically studied at all sites and where resistance to one inhibitor has been demonstrated, this does not necessarily mean that other inhibitors

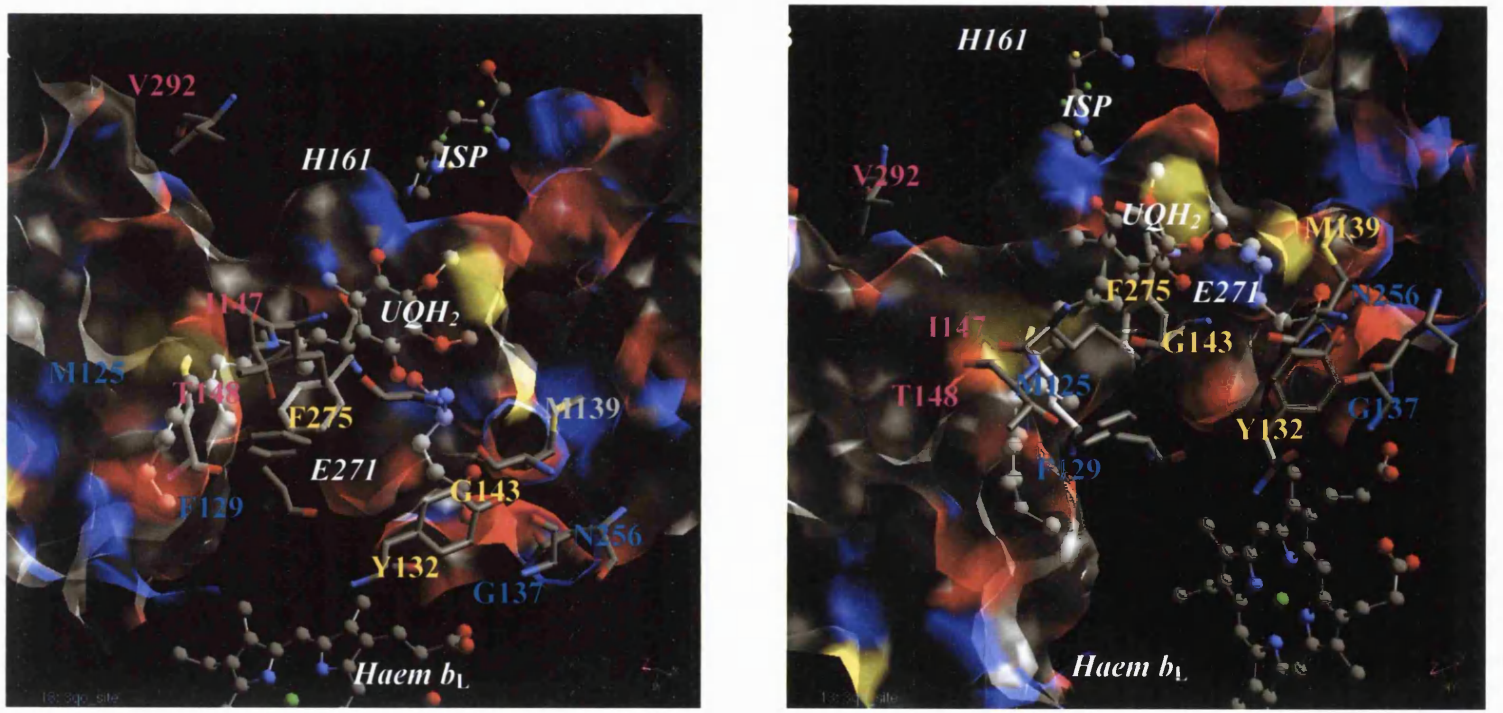

Fig. 4.5. Positions of mutations in the Q_o site that confer resistance to inhibitors. A) Side view. B) Top view. The figures were produced using co-ordinates from *Zhang et al.* datafile 3BCC [35]. A change in residues highlighted in pink confers resistance to stigmatellin, those in yellow to MOA-type inhibitors and those in cyan to both classes of inhibitor. Ubiquinone (UQH_2), E271, 'Rieske' ISP ligand H161 and haem b_L are shown as ball-and-stick models and the rest of the molecules are shown as stick models. 'Rieske' ISP cluster atoms are shown as small green (iron) and yellow (sulphur) spheres. The cloud represents the solvent accessible surfaces. The different colours represent the different atoms making up the access tunnel, yellow, sulphur; red, oxygen; blue, nitrogen; silver, carbon atoms (non-polar groups). The visualisation and manual docking were carried out as described in Section 4.2.2.

Table 4.1. Mutations conferring resistance to Q_o site inhibitors

Prokaryote *Rb. capsulatus*	Eukaryotes Yeast (Chicken)	Effects (Inhibitor resistance)	
		(*Rb. capsulatus*)	Yeast
L106P	M(I)91	My^R, Mu^R, Str^R	nd
M140-I,V,W	I(M)125	My^R, St^R	
-S		My^R	nd
-L,N,D		St^{HS}	
F144-A,H	F129	My^R	
-Y,W		St^R	nd
-C		My^R, St^R	
-I,G,L	-L	My^R, St^R, empty Q_o site, slow QH_2 oxidation	My^R, St^R, Mu^R, modified b_L
Y147	*Y132C	nd	My^R, Mu^R
G152-T,D,E,H,R	G137R,E	My^R	*My^R, Mu^R, Str^R
-K,CY,I,F,L,V,N		St^R, My^R	nd
-S	G137V	My^R, Muc^R	Mu^R
M154V	M139	My^R	nd
G158A,P,S	G143A	My^R	My^R, Mu^R
I162-G,A,L,F	I147F	*no effect*	St^R
T163-A,C	T148M	St^R	St^R
-V,L,I		My^{HS}	
N279Y	N256Y	St^R, My^R	St^R, My^R, Mu^R, affects FeS stability
	-K	nd	St^R, My^R,
	-I	nd	St^R, My^R, Mu^R, affects stability
F298	L(F)275F	nd	My^R
	-S,T	nd	My^R, Mu^R
V333A,M	V292	St^R	nd
M336	L295F		My^R, St^R

The column on the left shows the numerical positions of the amino acids in the *Rb. capsulatus* sequence; the second column shows the numerical positions of the equivalent or homologous amino acids in the yeast sequence in parenthesis; the second column also shows in parenthesis the amino acids present at the equivalent position in the chicken. My, Myxothiazol; St, Stigmatellin; Mu, Mucidin; Str, Strobilurin; R, Resistant; HS, Hypersensitive; n.d, not determined; b_L, haem b_L; FeS – iron-sulphur protein; QH_2, quinol, *The mutant was from *Chlamydamonas reinhardtii* sequence. The mutagenesis data were obtained from *Brasseur et al.* (1996) [33] and *Brandt et al.* (1994) [32].

- have been tested. The distribution of sites affecting inhibitor binding was, with few exceptions, consistent with the binding domains of the inhibitors since they impinge directly on the inhibitor-binding interface. Most of the exceptions could be rationalised in terms of structural dislocation due to disruption to packing and hydrogen bonding close to the sites affected.

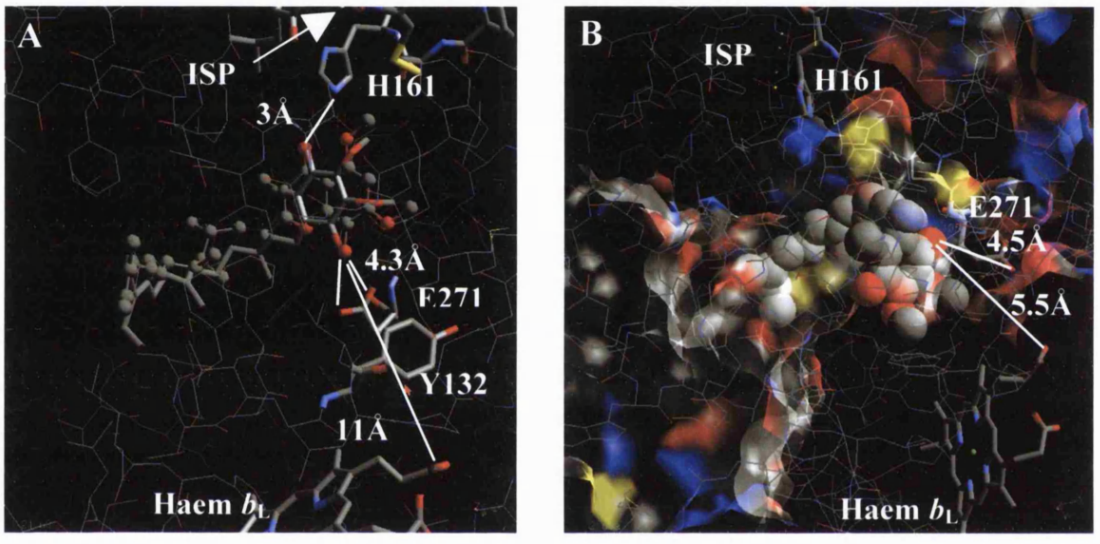

Fig. 4.6. Comparison between the Q_o site binding modes of A) Stigmatellin. Molecular modelling of the Q_o site with ubiquinone modelled onto bound stigmatellin using co-ordinates from *Zhang et al.* datafile 3BCC [35]. Stigmatellin is shown as ball-and-stick model, selected residues as stick models and the rest of the protein as wireframe. **B) MOA-stilbene.** Molecular modelling of ubiquinone into the MOA-stilbene binding site using co-ordinates from *Zhang et al.* datafile 3BCC [35]. Ubiquinone is shown as a space-filling model, selected residues as stick model and the rest of the protein as wireframe. 'Rieske' ISP cluster atoms are shown as small (iron) green and yellow (sulphur) spheres. The cloud represents the solvent accessible surfaces. The different colours represent the different atoms making up the access tunnel, yellow, sulphur; red, oxygen; blue, nitrogen; silver, carbon atoms (non-polar groups). The visualisation and manual docking were carried out as described in Section 4.2.2.

4.3.3 Molecular modelling studies using co-crystals

In available crystal structures of cytochrome bc_1 complexes from mammalian sources [35-40] no electron density ascribed to ubiquinone has so far been identified, presumably because of weak binding of ubiquinone [31]. Therefore, conclusions about the exact location of quinone/quinol binding sites within the structure remain speculative. However, structures obtained with Q_o site-specific inhibitors have revealed the location of the Q_o site and inhibitors occupying different domains (Fig. 4.6). The crystal structures also revealed that binding of different occupants leads to changes in the configuration and a substantial expansion of the site [34, 86]. This has led to the claim that there may be sufficient space to accommodate two ubiquinone molecules [73, 74], a view consistent with the report that two MOA-stilbene inhibitors bind to the fully reduced enzyme Q_o site [78]. However, the expansion suggests that the inhibitors do not displace an existing occupant, as was the case for the Q_i site upon binding of antimycin A [34].

To test whether two ubiquinone molecules can bind at the same time to the Q_o site, they were modelled into the site simultaneously, approximately into the stigmatellin and MOA-stilbene binding domains (Fig. 4.7). The models were built from published structures 3BCC [35] using Cerius2 from MSI. Energy minimised structures of ubiquinones were used as a starting point for manual 'tweaking' to fit them into the solvent accessible surfaces in the site. The best model in terms of the available volume has the headgroups overlapping as proposed by *Brandt et al.* (1996) [69, 85] instead of the edge-to-edge conformation favoured by *Ding et al.* (1992) [70, 71]. However, only one tail could be accommodated within the access tunnel and the adjacent volume. The structure with one tail has little unfilled space and substantial expansion would have to occur for the site to be able to accommodate another tail in

the access tunnel and also in the adjacent volume. Moreover, it is hard to envisage how the quinone bound at Q_{ow} domain could get in and out of the structure (Q_o site) in reasonable physiological timescale. To allow for proper functioning of the bc_1 complex, as proposed by the double Q variant model for the bifurcation reaction at the Q_o site [69, 70]. However, the molecular modelling study presented in this work is consistent with mechanistic models such as the 'mobile' ubisemiquinone model [34, 45, 84, 86] and the 'thermodynamic' explanation [44] (Section 1.9.6.2), involving a single ubiquinone occupant of the Q_o site. The large domain of the Q_o site, which can almost be occupied by two ubiquinone headgroups, may be part of the in-built control to ensure efficient bifurcation of the two electrons from ubiquinol between the high- and low-potential chains.

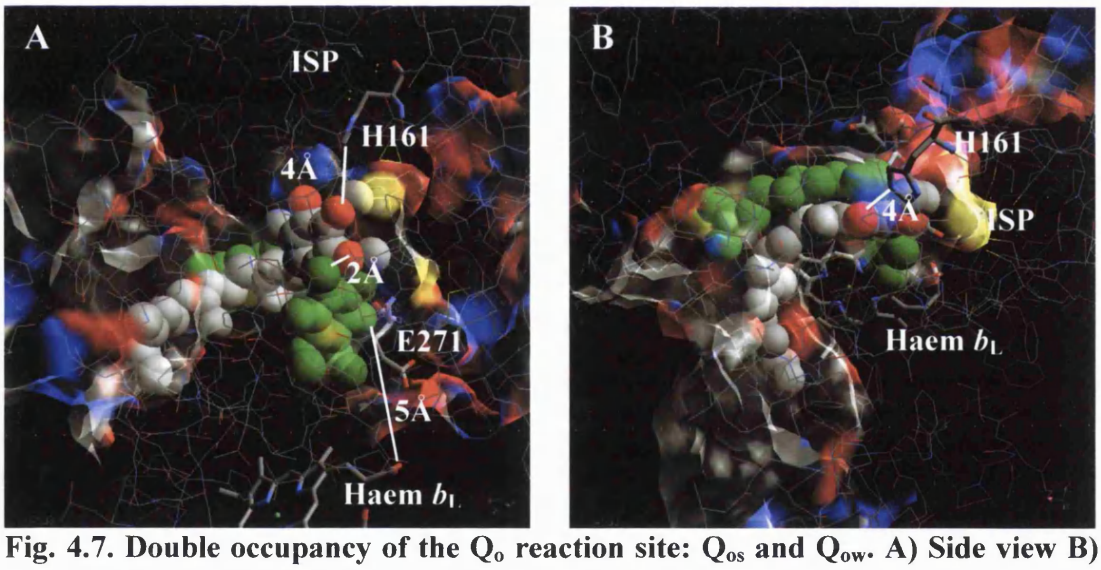

Fig. 4.7. Double occupancy of the Q_o reaction site: Q_{os} and Q_{ow}. A) Side view B) Top view. Molecular modelling of ubiquinones into the Q_o site based on the stigmatellin and MOA-stilbene bound structures using co-ordinates from *Zhang et al.* datafile 3BCC [35]. The ubiquinone molecules are shown as space filling models (Q_{ow}, green and Q_{os}, grey). Selected residues are shown as sticks and the rest of the protein as wireframe. 'Rieske' ISP cluster atoms are shown as small (iron) green and yellow (sulphur) spheres. The cloud and its different colours are the same as previously described in Fig 4.6B. They represent the solvent accessible surfaces. The visualisation and manual docking were carried out as described in Section 4.2.2.

Other recent modelling studies have suggested that changes of the order of only 1.5Å in the atomic positions of a few neighbouring amino acid residues is required for binding of two ubiquinone molecules (*Bartoschek et al.* personal communication, 2001). Movements on this scale are only slightly larger than those, which have been observed experimentally after removal of ubiquinone from the reaction centre from *Rb. viridis* [13]. In this model, two ubiquinone molecules were modelled into the stigmatellin site, in contrast to the model presented here, where the ubiquinone molecules were modelled into the stigmatellin and MOA-stilbene binding domains respectively. The molecular modelling presented here and elsewhere is based on the structures in native crystal, which may not necessarily represent the flexibility of physiological structure. Therefore, it will clearly be of importance in the future to determine the occupancy under physiological conditions.

In summary, the molecular modelling study presented here show that only a single ubiquinone headgroup can be adequately accommodated within the Q_o site and there is a degree of overlap when a second ubiquinone molecule is modelled into the site. Furthermore, only one 'tail' could be accommodated within the access tunnel and adjacent volume. This is fully consistent with a model of overlapping binding sites of two classes of Q_o site inhibitors from the inhibitor competition and mutagenesis studies, and of MOA-stilbene and decylubiquinol from the kinetic studies (Chapter 3).

4.3.3.1 Rational design of inhibitors

Development of fungicide resistance in the field can be a major problem. This could be overcome by applying two compounds, if they bind to the same active site in a dissimilar way, e.g. myxothiazol and stigmatellin. The target is then less likely to develop resistance to both compounds. However, in the case of bc_1 complex Q_o site,

as evident from the studies of mutants resistant to inhibitors, it is certainly possible for resistance to both compounds to be developed by a single mutation. Apart from resistance in the field, there is a need for competing companies to circumvent existing patents (a process termed 'patent busting') and to develop more potent inhibitors. The availability of a great deal of information from molecular, biochemistry and biophysical studies coupled with crystal structures of the bc_1 complex in the native and inhibited states makes it possible for rational design of new inhibitors. The kinetics, inhibitor and mutagenesis studies have indicated that the Q_o site has two binding but overlapping domains, a feature some have interpreted as favouring doubly occupancy [73, 75]. Taking this into consideration, it is feasible that a single compound or two compounds could be designed to fit adequately into the two domains. This compound(s) would have all the favourable contacts exhibited by the two inhibitors.

The co-crystals with stigmatellin and MOA-stilbene bound indicate that E271 (chicken numbering) is a ligand (hydrogen bond) to both of these inhibitors [31, 34]. The backbone NH is modelled as forming an H-bond to MOA-stilbene and mutations at this residue lead to stigmatellin resistance but not resistance to myxothiazol [34]. The side chain presumably plays no role in binding of class II inhibitors. The side chain of E271 is also found in different configurations in the two co-crystals (Fig. 4.6) [34]. It projects into the Q_o pocket in the stigmatellin structures, close enough to H-bond with the OH group of the second ring of the inhibitor. However, in the myxothiazol and MOA-stilbene structures, the side chain is rotated away from the pocket (Fig. 4.6). This residue form part of the well conserved -PEWY-sequence and any substitution of this residue leads to significant loss of activity [31-34].

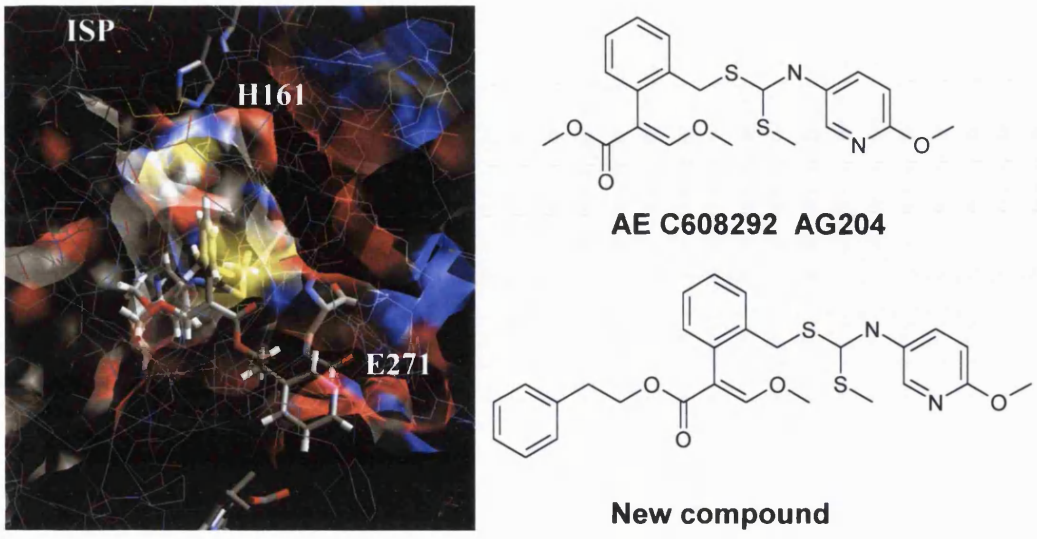

Fig. 4.8. Rational design of new compound based on AG204 (a tight inhibitor of the bc_1 complex). A) New compound modelled into the Q_o site using co-ordinates from *Zhang et al.* datafile 3BCC [35]. The new compound, haem b_L, E271 and 'Rieske' ISP cluster ligand H161 are shown as stick models. The rest of the protein are shown as wireframes. 'Rieske' ISP cluster atoms are shown as small (iron) green and yellow (iron) spheres. The cloud represents the solvent accessible surfaces. The different colours represent the different atoms making up the access tunnel, yellow, sulphur; red, oxygen; blue, nitrogen; silver, carbon atoms (non-polar groups). The visualisation and manual docking were carried out as described in Section 4.2.2. **B) Structure of AG204 and the new compound.**

Using an existing tight inhibitor AG204 (Fig. 4.8), we have proposed a new compound with an extra substituent that should form a strong hydrogen bond to this residue and form a hydrophobic contact with the nearby P270. The latter residue has been proposed to form hydrophobic contact with the pharmacophore of MOA-stibene. The extra substituent on the new compound is strongly electron donating and therefore facilitates stronger hydrogen bonding between its essential carbonyl and backbone NH of E271 of the –PEWY-loop. Future experiments could include chemical synthesis of this compound at Aventis Cropscience Ltd and tests to establish its activity.

4.3.4 Probing the Q_o site occupancy of bovine bc_1 complex using EPR spectroscopy

The EPR line shape of the 'Rieske' [2Fe2S] cluster, in particular the g_x band has proved to be highly sensitive to the degree and nature of Q_o site occupants (Q/QH_2 or inhibitors) and to provide a useful tool in dissecting cytochrome bc_1 complex function [57, 70-74]. Therefore, EPR spectroscopy was used to investigate whether the Q_o site can bind one or two compounds simultaneously. The EPR spectra of the bovine 'Rieske' ISP have been studied previously, in particular the studies of the ubisemiquinone located in the Q sites of bc_1 complex [81, 82, 113]. While there is little dispute on the g_y (1.89) and the g_z (2.03) signals, the g_x has been a subject of discussion. The shape of the g_x signal and the g value varies slightly with the preparation and measuring conditions used [114].

4.3.4.1 Cytochrome bc_1 complex in succinate cytochrome *c* reductase (SCR) preparation

The EPR spectra obtained from SCR preparations are very broad with relatively low S/N ratio (Fig. 4.9), presumably due to low occupancy of the Q_o site with the remaining ubiquinones associated with the preparation and low affinity for added ubiquinones due to the detergent. In addition, perturbation of the interactions of the 'Rieske' ISP with the Q_o site may have occurred as a consequence of the exchange of detergents for lipids. As a result, changes induced by substrates (decylubiquinone and decylubiquinol) and inhibitors were less obvious than in native bacterial chromatophores [57, 70-74]. In addition, the g_x signal is shifted upfield towards a lower g_x value (g_x = 1.792) than those reported for 'Rieske' ISP in the native bovine

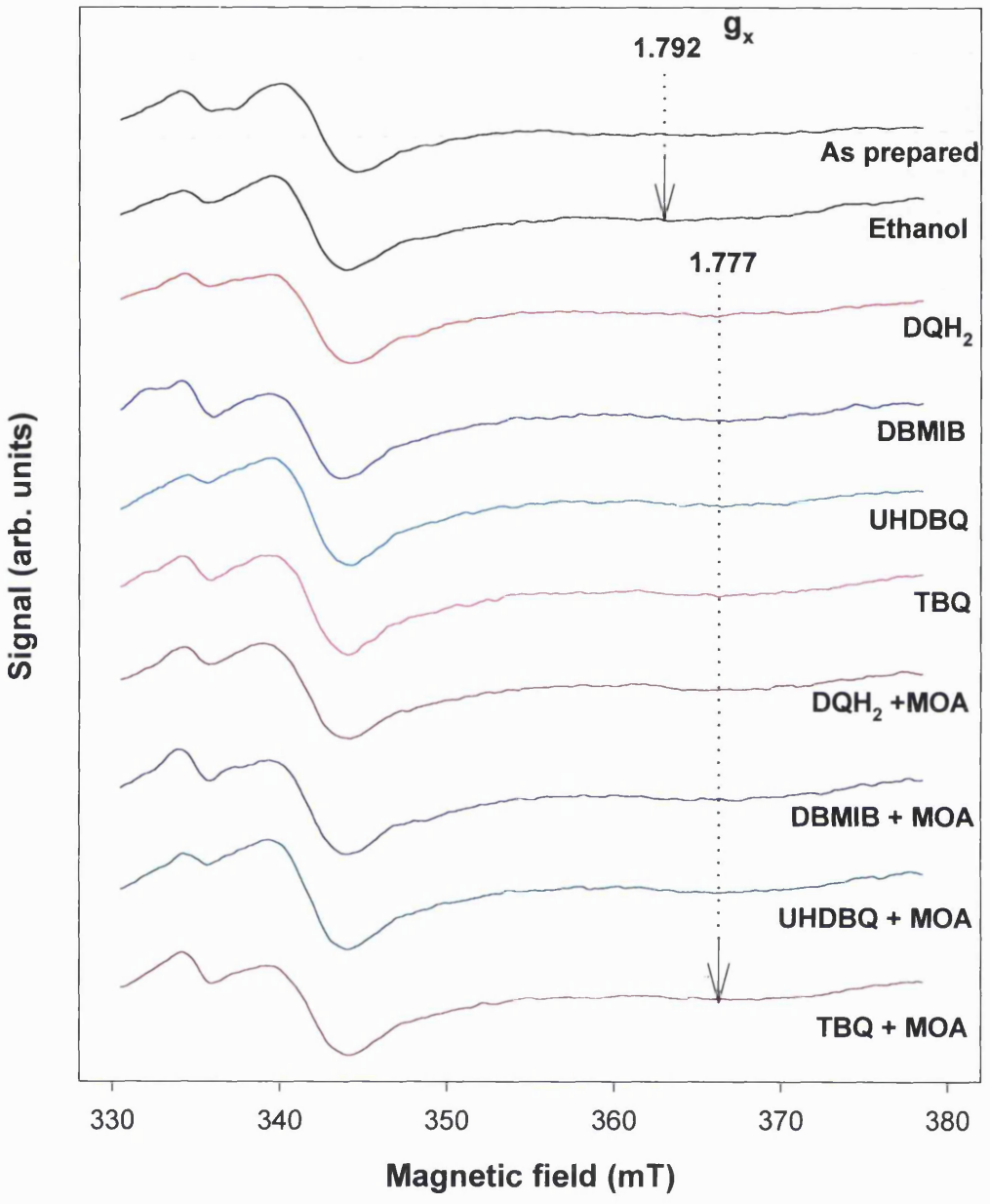

Fig. 4.9. The effects of ethanol, quinone analogues and MOA-stilbene on the EPR line shape of the 'Rieske' [2Fe2S] cluster in succinate *c* reductase (SCR). Sample preparation and EPR conditions as described in Section 4.2.3-4. The samples contained 10μM SCR in 0.1M sodium phosphate pH 8.0 buffer (0.35ml final volume) and the 'Rieske' [2Fe2S] cluster was reduced with 10mM sodium ascorbate. 30μM of quinone analogues and/or MOA-stilbene were added to the sample with the exception of 70μM decylubiquinol (DQH_2). DBMIB, 2,5-dibromo-3-methyl-6-isopropyl-p-benzoquinone; UHDBQ, 5-n-undecyl-6-hydroxy-1,4-benzoquinone; TBQ, tetrabromoquinone. MOA, MOA-stilbene; Ethanol, 20mM Ethanol. All compounds were dissolved in 96% Ethanol.

-membrane (g_x = 1.810) [80]. This same upfield shift to a lower g_x value (from g_x = 1.78 to 1.76) upon ubiquinone and phospholipid depletion of purified bovine heart bc_1 complex was reported by *Gwak et al.* (1986) [114].

However, some conclusions could still be drawn from the SCR experiments. For instance, ethanol had no effect on the EPR line shape of the 'Rieske [2Fe2S] cluster (Fig. 4.9) despite report in the literature to the contrary using bacterial chromatophore membrane [57]. The addition of seven-fold molar excess of decylubiquinol resulted in an upfield shift of the g_x resonance from 1.792 to 1.777. The same upfield shifts were achieved with a variety of quinone analogues, DBMIB (2,5-dibromo-3-methyl-6-isopropyl-p-benzoquinone), UHDBQ (5-n-undecyl-6-hydroxy-1,4-benzoquinone) and tetrabromoquinone. The addition of MOA-stilbene in combination with these quinone analogues made no difference to the shifts observed. This could be interpreted in two ways, either the compounds were displaced by MOA-stilbene or it had no effects on their binding. Since MOA-stilbene has a stronger affinity for the site it can reasonably be assumed that MOA-stilbene displaces the compounds but has a similar effect on the EPR line shape.

In order to increase S/N ratio the final concentration of SCR was increased from 10 to 30μM and the experiment was repeated with decylubiquinol and MOA-stilbene (Fig. 4.10). The addition of a three-fold molar excess of decylubiquinol resulted in the g_x resonance shifted from 1.792 to 1.785, much less than before (Fig. 4.9). The addition of decylubiquinol in combination with MOA-stilbene again resulted in an upfield shift of the g_x resonance from 1.792 to 1.777. This shift was also evident for MOA-stilbene alone, supporting previous assertions that MOA-stilbene may be displacing the compounds from the Q_o site.

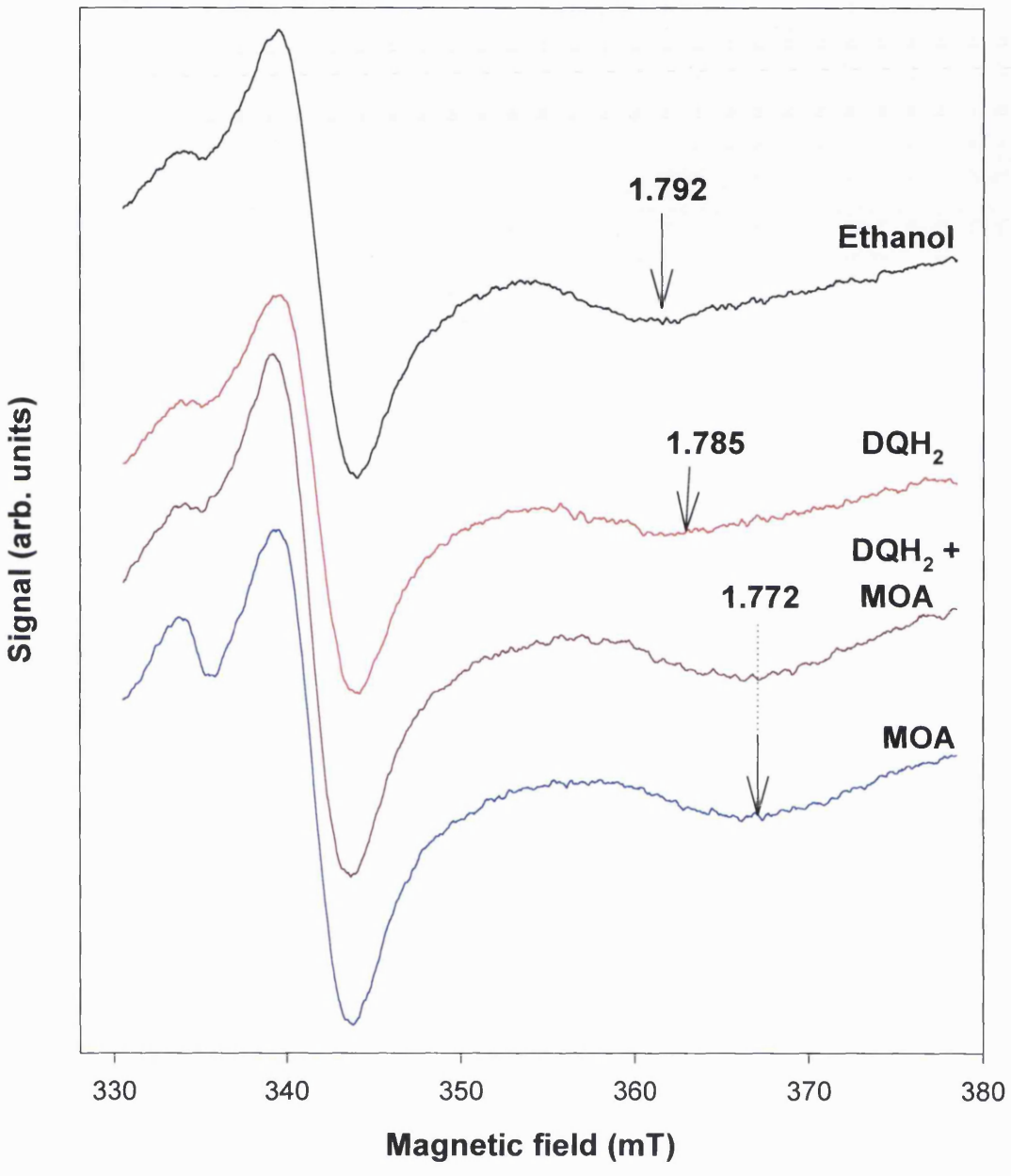

Fig. 4.10. The effects of decylubiquinol and MOA-stilbene on the EPR line shape of the 'Rieske' [2Fe2S] cluster of cytochrome bc_1 complex in succinate *c* reductase (SCR). Sample preparation and EPR conditions as described in Section 4.2.3-4. The samples contained 30μM SCR in 0.1M sodium phosphate pH 8.0 buffer (0.35ml final volume) and the [2Fe2S] cluster was reduced with 10mM sodium ascorbate. 20mM Ethanol or 50μM MOA-stilbene (MOA) and/or 100μM decylubiquinol (DQH_2) were added to the sample. All compounds were dissolved in 96% Ethanol. arb, arbitrary.

Increasing the concentration of decylubiquinol to five-fold molar excess from previous experiment (Fig. 4.10) had no effect on the g_x signal of the control [ethanol (Fig. 4.11)]. This is in contrast to previous experiments with three and seven-fold molar excess of decylubiquinol resulting in upfield shifts of g_x 1.785 (Fig. 4.10) and 1.777 (Fig. 4.9) respectively. This may reflect variation in the amount of detergents present in the sample, which affects the affinity of the site for decylubiquinol. The same variation was also evident for MOA-stilbene exhibiting a g_x of 1.780 in this experiment instead of the 1.777 from the previous experiment (Fig. 4.10) The addition of decylubiquinone to an already oxidised Q-pool also made no difference. This is consistent with other studies, namely differential effects of ubiquinone and ubiquinol. Ubiquinone occupancy generally results in high g-values, whereas ubiquinol occupancy results in low g-values. The addition of decylubiquinone in combination with MOA-stilbene resulted in an upfield shift of the g_x resonance from 1.792 to 1.780. This shift was less than that for decylubiquinol in combination with MOA-stilbene.

In summary, variation in the effects of decylubiquinol is probably due to its low affinity for the site, a problem made worse by the necessary presence of detergents. The addition of decylubiquinol or MOA-stilbene resulted in low g_x values 1.777, whereas the addition of decylubiquinone resulted in a high g_x value of 1.792, consistent with other studies. Overall, the addition of two compounds resulted in the same shift reported for the addition of a single compound. The simplest explanation for this is that only a single compound can occupy the site at one time, consistent with a single occupancy model of the Q_o site.

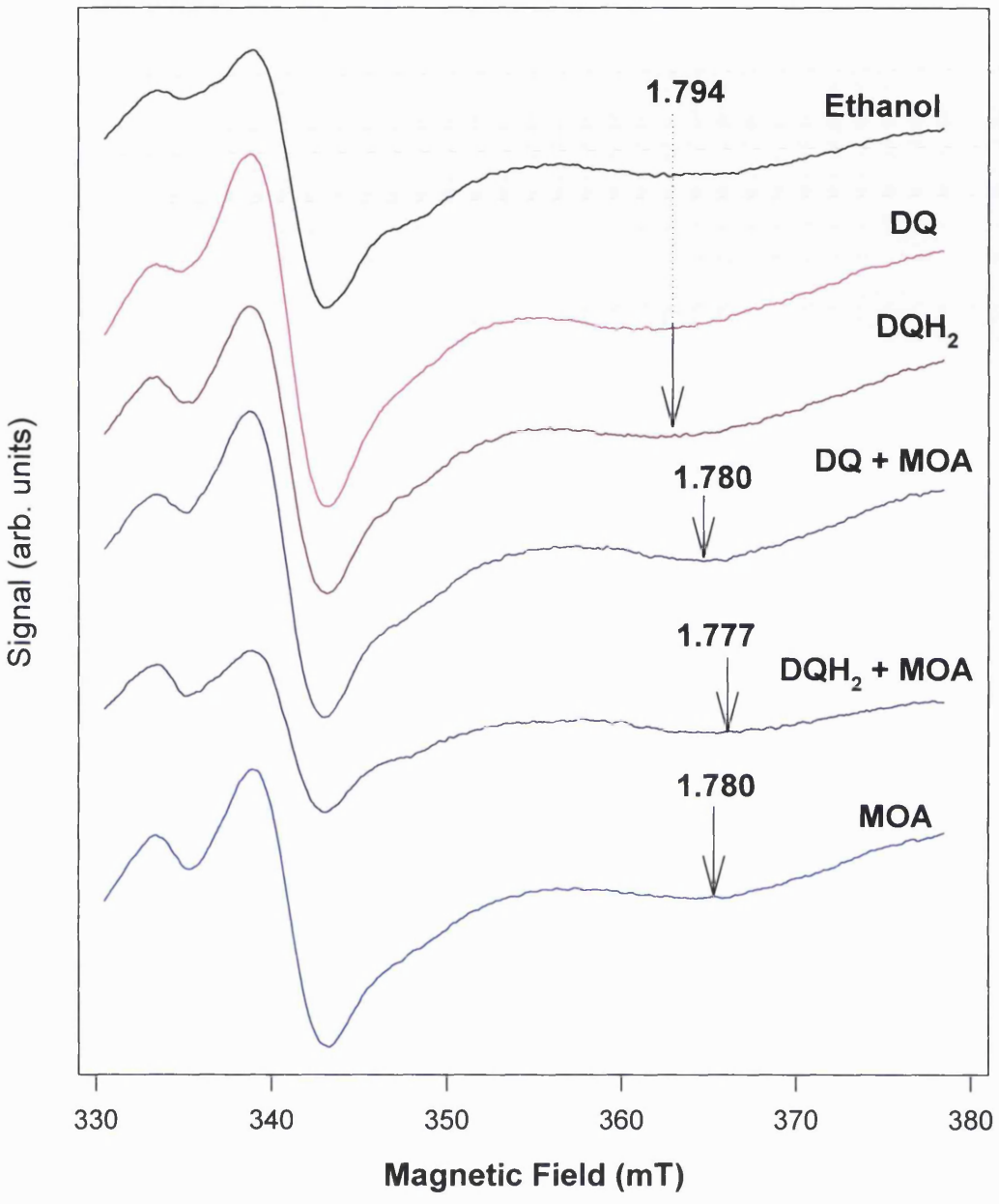

Fig. 4.11. The effects of decylubiquinone, decylubiquinol and MOA-stilbene on the EPR line shape of the 'Rieske' [2Fe2S] cluster of cytochrome bc_1 complex in succinate *c* reductase (SCR). Sample preparation and EPR conditions as described in Section 4.2.3-4. The samples contained 20μM SCR in 0.1M sodium phosphate pH 8.0 buffer (0.35ml final volume) and the [2Fe2S] cluster was reduced with 10mM sodium ascorbate. 20mM Ethanol or 50μM MOA-stilbene (MOA) and/or 100μM decylubiquinone (DQ) or decylubiquinol (DQH_2) were added to the sample. All compounds were dissolved in 96% Ethanol. arb, arbitrary.

4.3.4.2 Cytochrome bc_1 complex in Keilin Hartree particles (KHP) preparation

Due to the broadness and relatively low S/N ratio of the spectra obtained with SCR preparations, KHP were used instead to test the conclusions obtained so far. In contrast to the former preparation, KHP gave a much better resolution and sharper signals (Fig. 4.12). The broadness of SCR samples was due to low occupancy of the Q_o site with the remaining ubiquinones associated with the preparation and low affinity for added ubiquinones due to the detergent. In addition, perturbation of the interactions of the 'Rieske' ISP with the Q_o site may have occurred as a consequence of the exchange of detergents for lipids.

In the 'as prepared' state, two g_x signals at 1.814 and 1.785 were evident (Fig. 4.12). These signals may represent different occupancies of the Q_o site, i.e. binding of endogenous ubiquinol/ubiquinone or an empty site. The Q-pool is fully oxidised in this state and therefore the Q_o site would be expected to bind endogenous ubiquinone, reporting a g_x resonance of 1.814. Previous studies with bovine and bacterial enzyme [31, 70, 71, 115] have attributed the signal at high g_x value (1.814 in bovine and 1.800 in bacterial enzymes) to the interaction of a weakly binding quinone with the reduced 'Rieske' ISP. They proposed that this signal is associated with a complex formed between quinone bound in the Q_o site at the distal end to haem b_L and the reduced 'Rieske' ISP docked firmly at the interface with cytochrome *b*. The extraction of this quinone from the site results in broadening and an upfield shift of the g_x signal [114, 116]. Therefore, the g_x 1.785 species may represent an empty Q_o site. This is further confirmed by the absence of this species (g_x 1.758) upon binding of a strong inhibitor AG204 (Fig. 4.12).

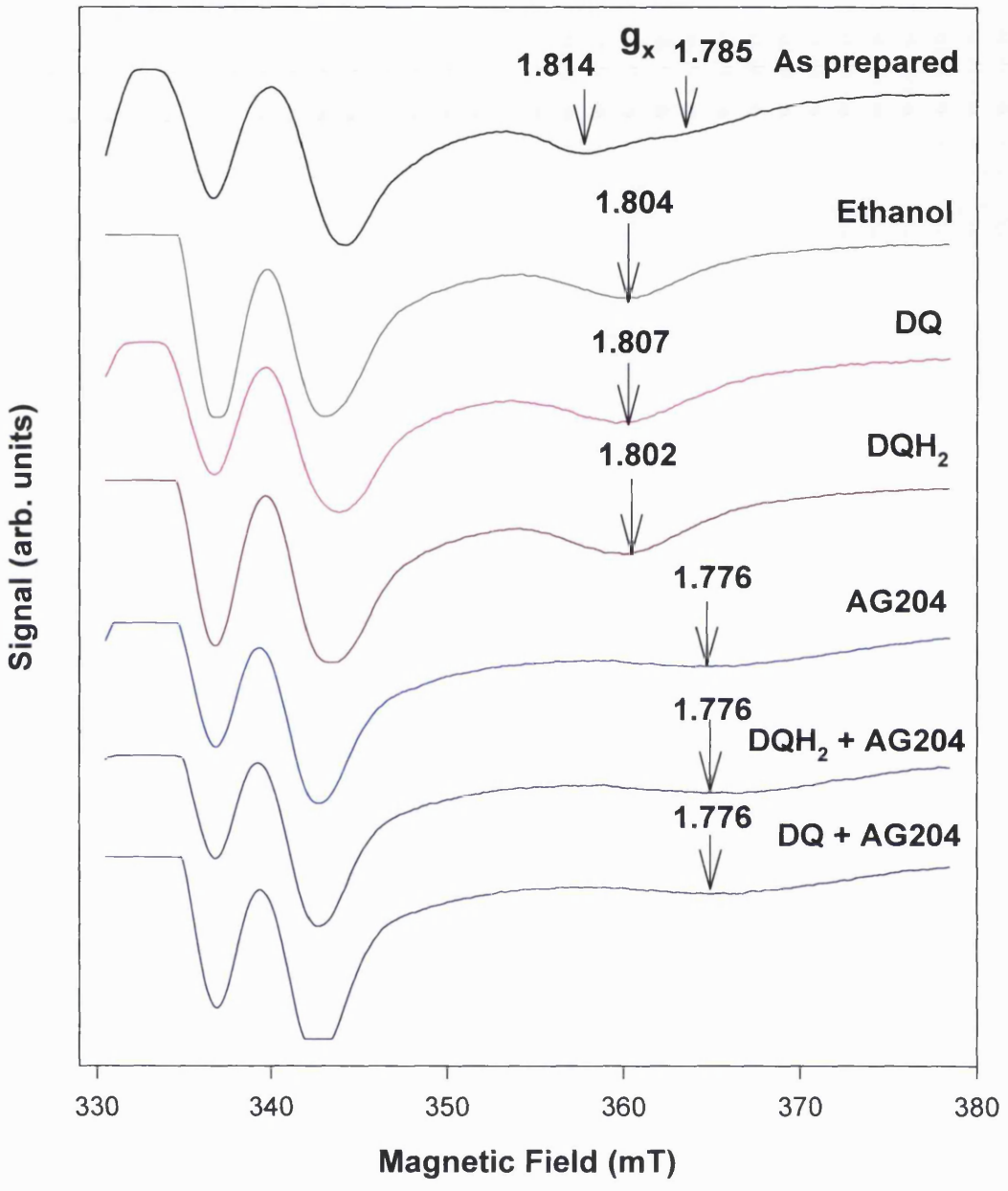

Fig. 4.12. The effects of decylubiquinone, decylubiquinol, ethanol and AG204 on the EPR line shape of the 'Rieske' [2Fe2S] cluster of cytochrome bc_1 complex in Keilin Hartree particles (KHP). Sample preparation and EPR conditions as described in Section 4.2.3-4. 20mM Ethanol or 50μM AG204 and/or 100μM decylubiquinone (DQ) or decylubiquinol (DQH_2) were added to the sample. All compounds were dissolved in 96% Ethanol. arb, arbitrary.

4.3.4.2.1 Effects of decylubiquinone/decylubiquinol

In the presence of ethanol, the two g_x signals present in the "as prepared" state are replaced by a single g_x signal at 1.804 (Fig. 4.12). This is in contrast to the SCR preparation, in which ethanol had no effect on the g_x signal of the 'as prepared' state. In addition, the 'Rieske' [2Fe2S] g_x signal becomes independent of site occupancy by decylubiquinone or decylubiquinol in the presence of ethanol. However, the Q_o site (class II) inhibitor AG204 caused additional effects in the presence of ethanol. The addition of combinations of AG204 and decylubiquinone or decylubiquinol (g_x = 1.776) had the same effects as the addition of AG204 alone (g_x = 1.776). This is consistent with results from the SCR preparation with quinone analogues and MOA-stilbene (class II). The effect of ethanol on the reporting of the binding of decylubiquinol and decylubiquinone complicates the interpretation of this result in terms of whether ubiquinone and AG204 could bind simultaneously to the Q_o site.

The effects of ethanol on the 'Rieske' [2Fe2S] g_x signal and the additional effect of inhibitors in the presence of ethanol is consistent with the results obtained by *Sharp et al.* (1998) [57] using *Rb. capsulatus* chromatophore membranes containing cytochrome bc_1 complex. They described this effect of ethanol as a non-inhibiting perturbation of cytochrome bc_1 complex. Furthermore, they suggested that displacement occur by ethanol acting from the aqueous phase to successfully compete with the Q_o site ubiquinone(s) and water to hydrogen bond the $N_\epsilon H$ atom(s) of the co-ordinating [2Fe2S] cluster histidines.

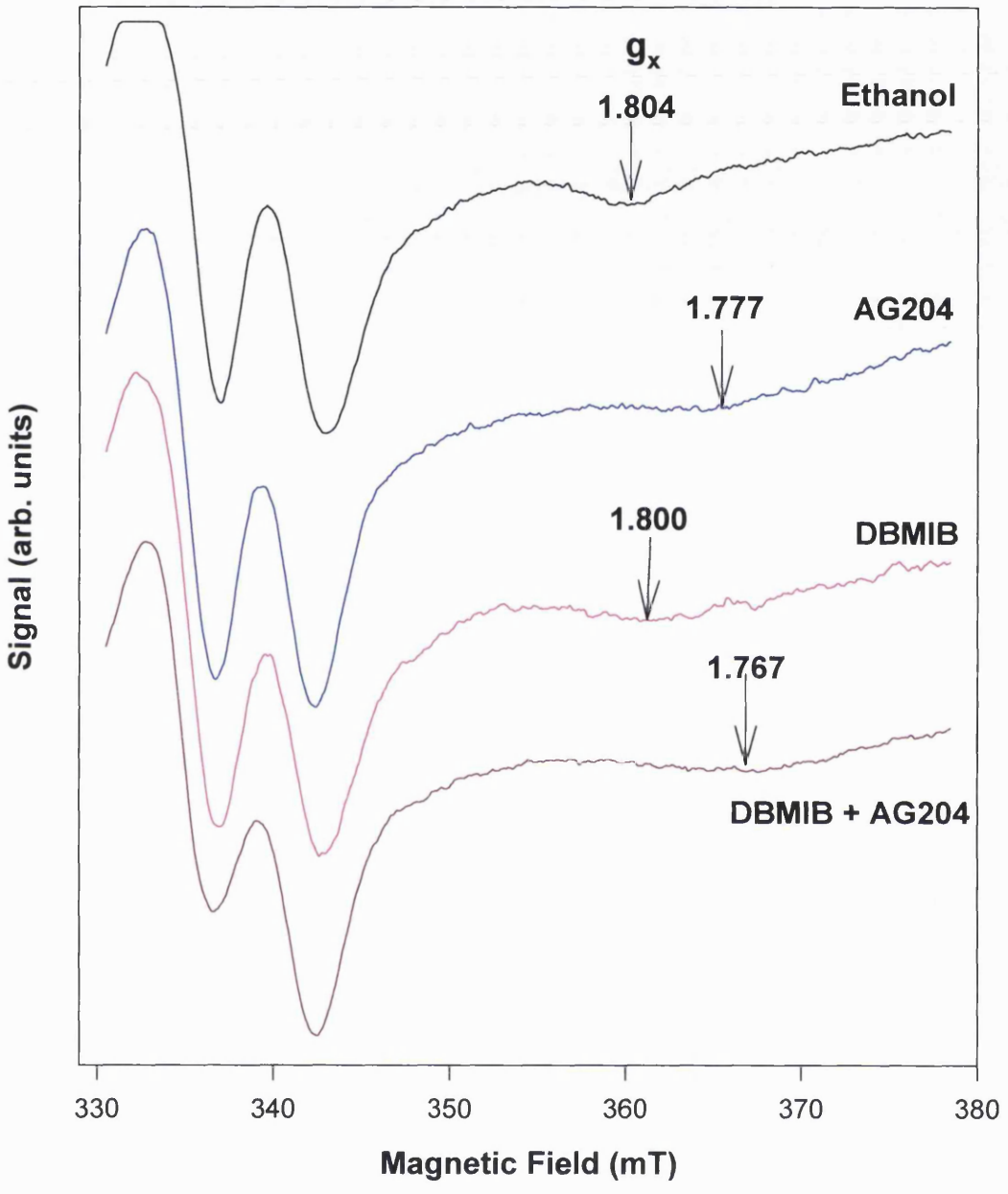

Fig. 4.13. The effects of two classes of Q_o site inhibitors on the EPR line shape of the 'Rieske' [2Fe2S] cluster of cytochrome bc_1 complex in Keilin Hartree particle (KHP). AG204 is a class II inhibitor binding closer to haem b_L, whereas DBMIB (2,5-dibromo-3-methyl-6-isopropyl-p-benzoquinone) is a class I inhibitor binding closer to the 'Rieske' iron sulphur protein. Sample preparation and EPR conditions as described in Section 4.2.3-4. 20mM Ethanol or 50μM AG204 and/or 50μM DBMIB were added to the sample. All compounds were dissolved in ethanol. arb, arbitrary.

4.3.4.2.1.1 Can the Q_o site bind DBMIB and AG204 simultaneously?

Since inhibitors in the presence of ethanol caused additional effects on the 'Rieske' [2Fe2S] g_x signals due to their higher affinity for the Q_o site, the competition experiment described in Section 4.3.1 was repeated with the Q_o site inhibitor DBMIB (class I) [114, 117] using KHP preparations. Its chemical structure is very similar to that of ubiquinone without the 'tail' (Fig. 4.3) and it is also a much smaller compound than stigmatellin. The effects of DBMIB on the EPR line shape of the purified bovine bc_1 complex [114] and chloroplast b_6f 'Rieske' ISP [117] have been characterised. In this study, DBMIB induced an additional broadening of the g_x resonance compared to ethanol (Fig. 4.13). The g_x resonance shift (1.800) is different to that obtained with the SCR preparation (g_x = 1.777). The differential effect of DBMIB in the two preparations may indicate that lipids and detergents influence the effects of this compound on the 'Rieske' [2Fe2S] EPR line shape, consistent with previous studies [114, 117].

The addition of a combination of AG204 (class II) and DBMIB (class I) inhibitors had the same effects (g_x = 1.777) as the addition of AG204 alone (g_x = 1.776). This is consistent with the results obtained with the SCR preparation and decylubiquinol or decylubiquinone (Fig. 4.12). The simplest explanation is AG204 displaces the other compounds from the Q_o site because of its greater affinity for the site. This can be interpreted as favouring a single occupancy model of the Q_o site.

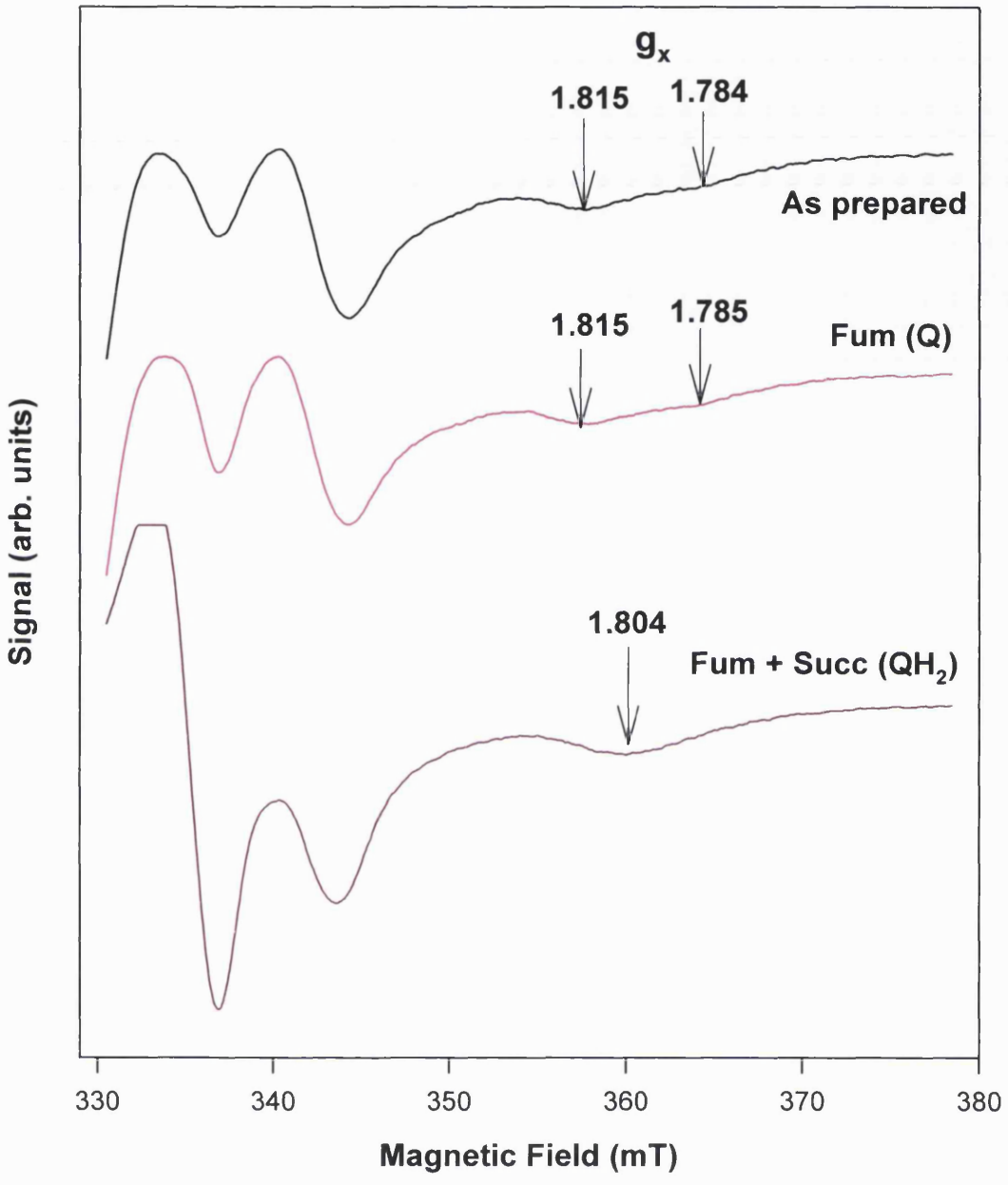

Fig. 4.14. The effects of endogenous substrates on the EPR line shape of 'Rieske' [2Fe2S] cluster of cytochrome bc_1 complex in Keilin Hartree particles (KHP). Sample preparation and EPR conditions as described in Section 4.2.3-4. Fumarate (Fum) was added to the sample to oxidise the Q-pool, ensuring the presence of endogenous ubiquinone (Q) alone. Succinate (Succ)/fumarate couple was added to reduce the Q-pool, ensuring the presence of endogenous ubiquinol (QH_2) alone. arb, arbitrary.

4.3.4.2.3 Effects of endogenous ubiquinone/ubiquinol

In the presence of ethanol, the 'Rieske' [2Fe2S] g_x line shape becomes independent of site occupancy by decylubiquinone or decylubiquinol. However, inhibitors dissolved in ethanol caused additional effect due to their greater affinity for the Q_o site. Since endogenous ubiquinone/ubiquinol also have a greater affinity for the Q_o site than decylubiquinone/decylubiquinol [118], their effects on the 'Rieske' ISP EPR line shape were investigated.

In the 'as prepared' state the Q-pool is oxidised and the Q_o site is occupied by ubiquinone with a g_x resonance value of 1.815 (Fig. 4.14). The g_x resonance at 1.784 was also evident further ruling out the possibility of it being an artefact. In the absence of ethanol, further oxidation of the Q-pool with fumarate, i.e. only ubiquinone present in the sample, made no difference to the spectra and two g_x signals were evident. With the Q-pool fully reduced with a succinate/fumarate couple, i.e. the Q_o site is occupied by quinol, the two signals present in the 'as prepared' state are replaced by a single signal at 1.805. This further supports the assignment of the g_x signal at 1.785 to an empty Q_o site. Ubiquinol has a stronger affinity for the site than ubiquinone therefore it can be expected that most if not all of the site would be occupied when ubiquinol is present. The general direction of the shifts observed with ubiquinone and ubiquinol was fully consistent with results from the SCR samples and other studies [70-74].

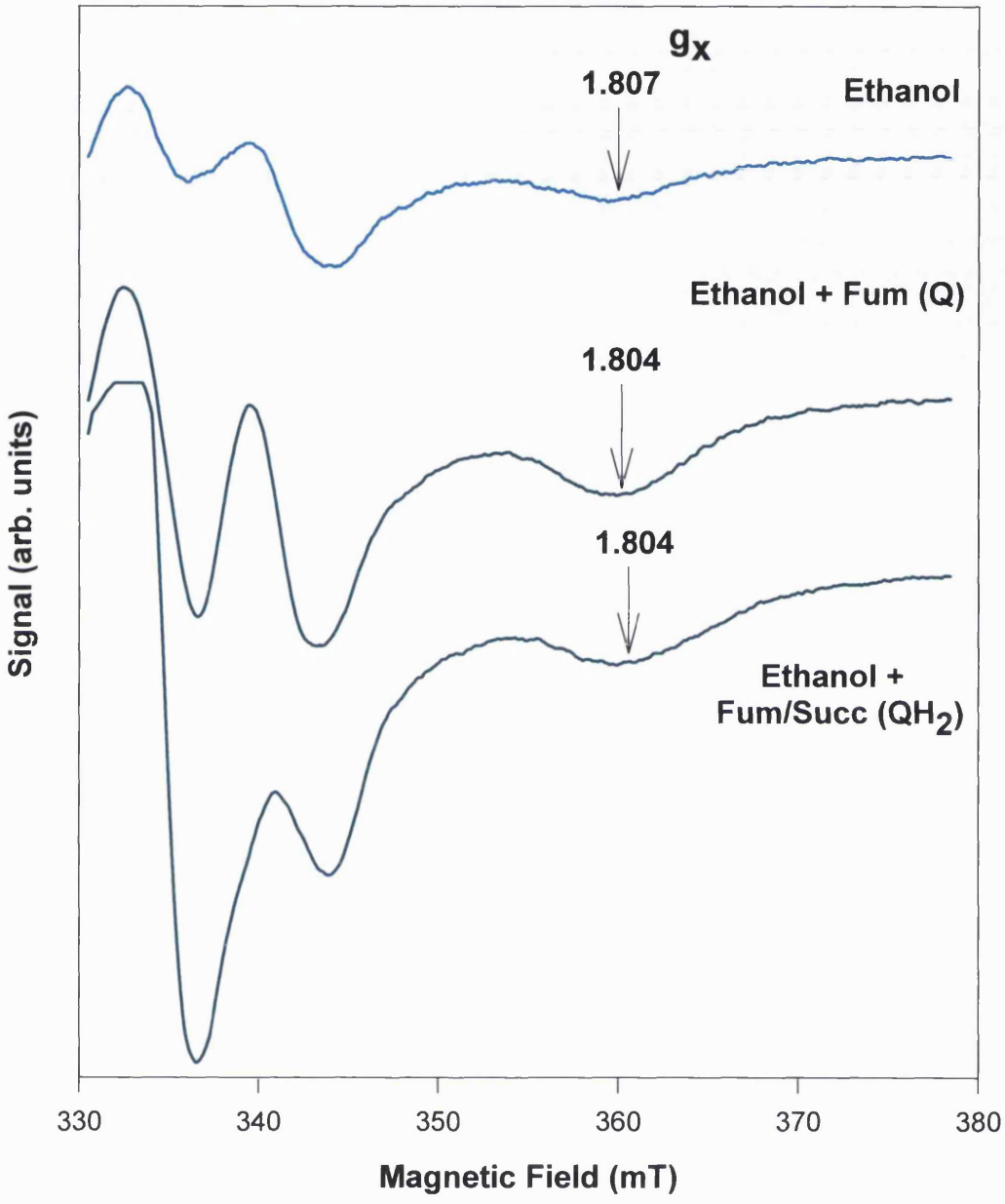

Fig. 4.15. The effects of ethanol and endogenous substrates on the EPR line shape of 'Rieske' [2Fe2S] cluster of cytochrome bc_1 complex in Keilin Hartree particles (KHP). Sample preparation and EPR conditions as described in Section 4.2.3-4. Fumarate (Fum) was added to the sample to oxidise the Q-pool, ensuring the presence of endogenous ubiquinone (Q) alone. Succinate (Succ)/fumarate couple was added to reduce the Q-pool, ensuring the presence of endogenous ubiquinol (QH_2) alone. 20mM Ethanol was also added to the samples. arb, arbitrary.

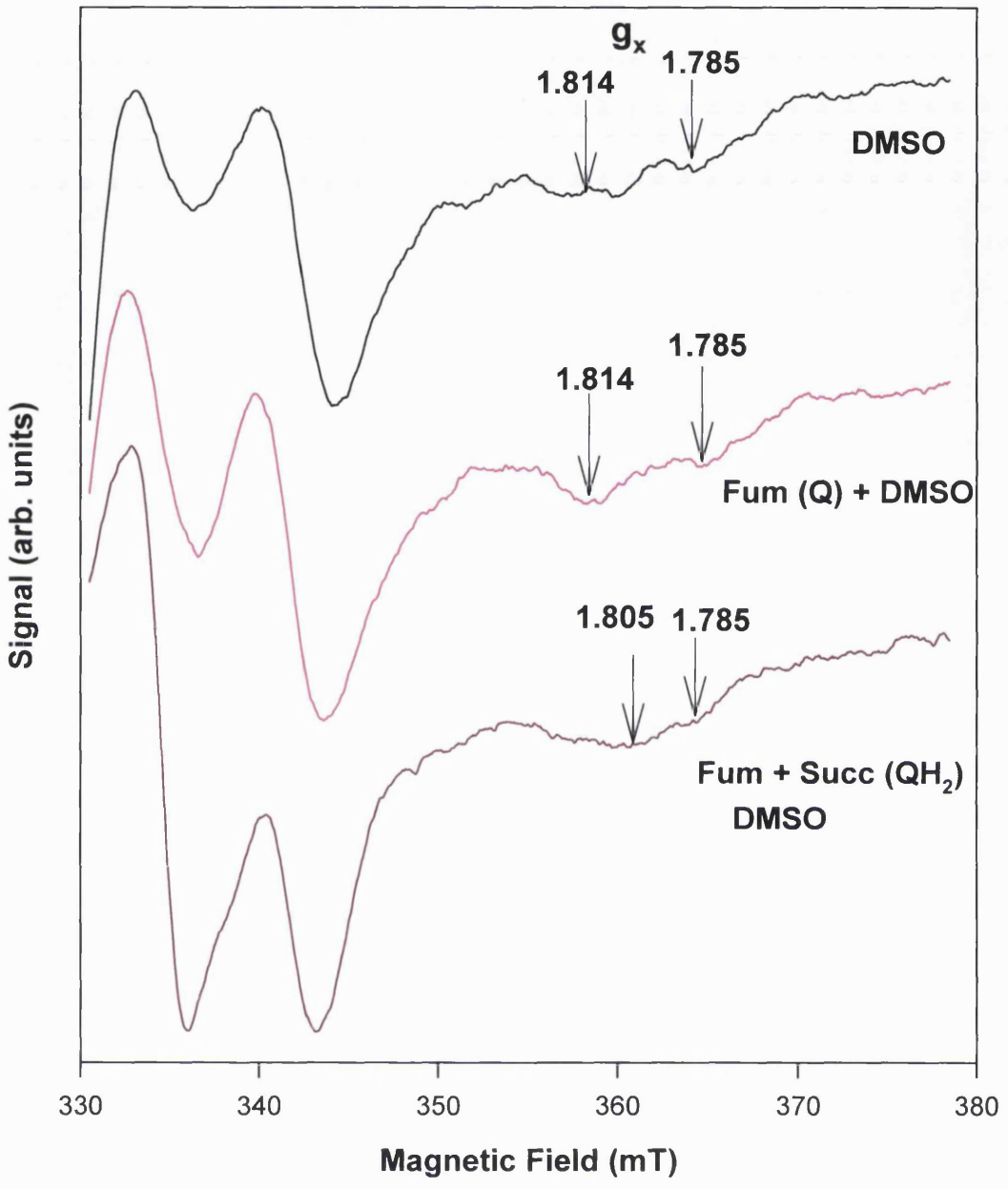

Fig. 4.16. The effects of DMSO and endogenous substrates on the EPR line shape of 'Rieske' [2Fe2S] cluster of cytochrome bc_1 complex in Keilin Hartree particles (KHP). Sample preparation and EPR conditions as described in Section 4.2. Fumarate (Fum) was added to the sample to oxidise the Q-pool, ensuring the presence of endogenous ubiquinone (Q) alone. Succinate (Succ)/fumarate couple was added to reduce the Q-pool, ensuring the presence of endogenous ubiquinol (QH_2) alone. 5mM DMSO (dimethylsulphoxide) was also added to the samples. arb, arbitrary.

In the presence of ethanol, again the 'Rieske' [2Fe2S] g_x signal becomes independent of site occupancy by endogenous ubiquinone or ubiquinol (Fig. 4.15). In contrast, DMSO (dimethylsulphoxide) in agreement with other EPR studies [70] (Fig. 4.16) did not interfere with the EPR spectra of the 'Rieske' [2Fe2S] cluster. Although the S/N ratio was lower than in previous experiments, two major g_x values at 1.814 and 1.785 are clearly evident, the same as the 'as prepared' state. The Q_o site occupancy is dependent on site occupancy by endogenous ubiquinone or ubiquinol. In the ubiquinol spectrum (Fum + Succ (QH_2) DMSO), the g_x 1.785 attributed to an empty Q_o site is evident. However, this signal is much diminished in comparison to the ubiquinone and the 'as prepared' spectra. This shows that in the presence of ubiquinol more of the Q_o site is occupied, again confirming the assignment of the g_x 1.785 signal to an empty site.

4.3.4.2.3.1 Can the Q_o site bind AG204 and ubiquinone or ubiquinol simultaneously?

In this experiment (Fig. 4.17) AG204 was dissolved in DMSO to avoid the effect of ethanol, which obscures any effects of ubiquinone/ubiquinol binding. The presence of AG204 in the Q_o site results in a 'Rieske' [2Fe2S] cluster g_x value of 1.778 and prevents ubiquinone or ubiquinol from binding in the site, since the g_x value remained unchanged when the redox state of the Q-pool was varied by the addition of fumarate (ubiquinone) or fumarate/succinate (ubiquinol) couple. The additional g_x value of 1.785 (corresponding to an empty Q_o site) present in the 'as prepared' and DMSO spectra, diminished in the presence of ubiquinol, is absent in the presence of AG204 (Fig. 4.17). As previously explained, ubiquinol and the inhibitors have stronger affinity for the site.

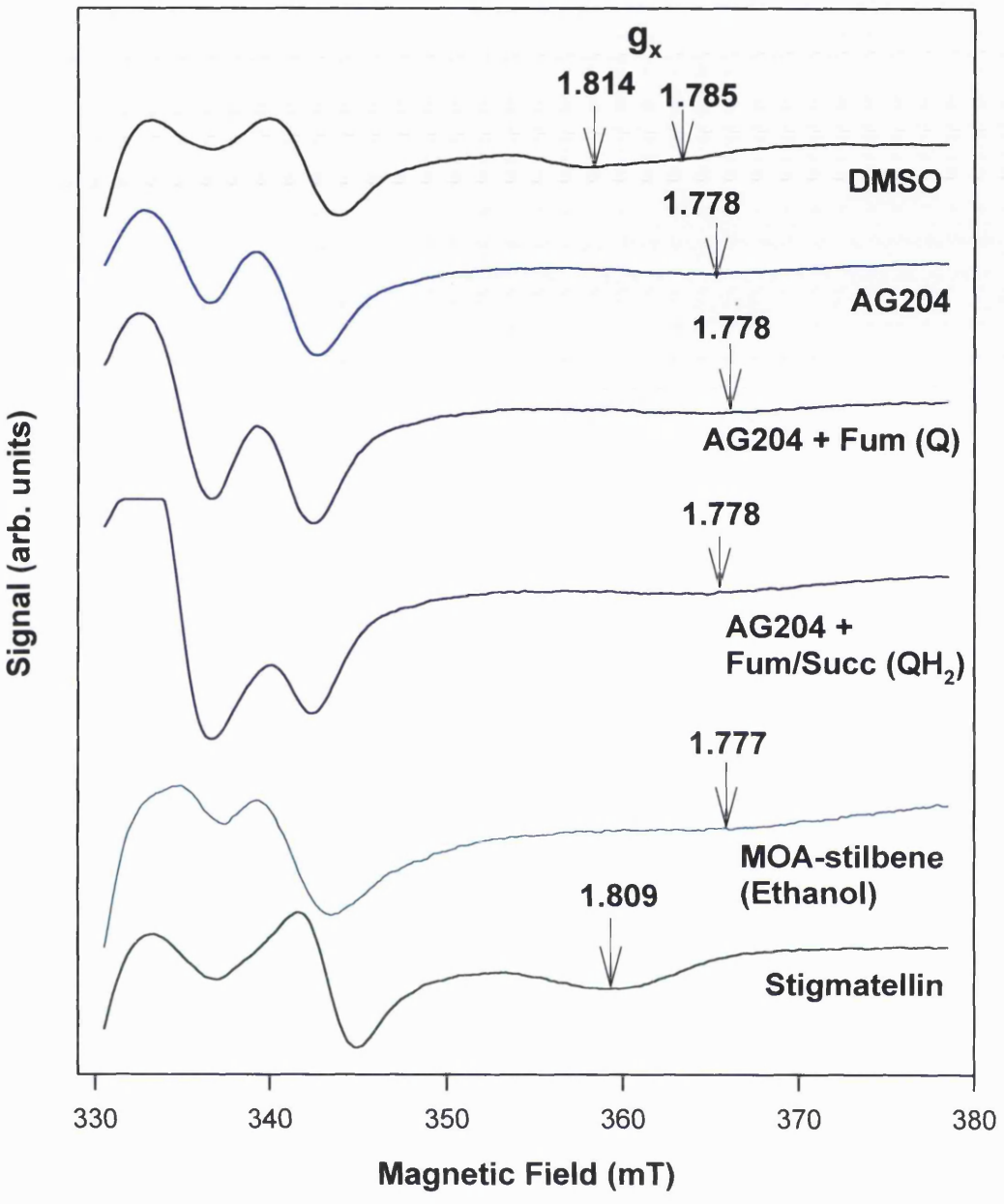

Fig. 4.17. The effects of endogenous substrates, DMSO and Q_o site inhibitors on the EPR line shape of 'Rieske' [2Fe2S] cluster of cytochrome bc_1 complex in Keilin Hartree particles (KHP). Sample preparation and EPR conditions as described in Section 4.2.3-4. Fumarate (Fum) was added to the sample to oxidise the Q-pool, ensuring the presence of endogenous ubiquinone (Q) alone. Succinate (Succ)/fumarate couple was added to reduce the Q-pool, ensuring the presence of endogenous ubiquinol (QH_2) alone. 5mM DMSO or 50μM inhibitor dissolved in DMSO with the exception of MOA-stilbene (dissolved in 96% ethanol) were also added to the sample. arb, arbitrary.

The simplest explanation for the EPR data presented here is that only a single compound can occupy the Q_o site at one time, which is fully consistent with the model of overlapping binding sites of species. The EPR spectra show only a single g_x signal that can be attributed to an occupant of the Q_o site and the other signal present in the ubiquinone or ubiquinol spectra (from KHP samples) report an empty site. Furthermore, AG204 or MOA-stilbene (class II inhibitors) appears to bind and displace DBMIB (class I) or ubiquinone analogues from the site due to its stronger affinity.

4.3.4.3 Comparison of the bovine and bacterial studies

The conclusion of single occupancy model proposed for the bovine enzyme is in contrast, to the double occupancy model proposed for the bacterial enzyme by Ding and colleagues [57, 70-74]. Although the AG204 result is consistent with results from *Ding et al.* (1992) [70, 71] with inhibitors such as stigmatellin and myxothiazol, the MOA-stilbene result differs. In this study, MOA-stilbene (Fig. 4.17) behaves in a similar way to stigmatellin and AG204 in displacing ubiquinone or ubiquinol from the site. Sharp and colleagues have reported [72, 74] that stoichiometric MOA-stilbene and excess DPA displaces the weakly bound Q_{ow}, while the stronger binding species Q_{os} remains bound at the site. The interpretation of the effects of DPA as described in Section 4.1.1 is subject to an alternative explanation by *Berry et al.* (2000) [31], which favours single occupancy model. They proposed that DPA, having no tail, can bind in the proximal domain (equivalent to Q_{ow}) without causing displacement of quinone bound in Q_{os} and could inhibit electron transfer by competing for occupancy of the proximal domain. This is consistent with data (M. Guergova-Kuras & AR. Crofts, unpublished information), which shows that DPA at concentrations in the

100μM range increased the titre for mucidin (a class II inhibitor), as would be expected if both compete for occupancy of the proximal domain.

An equivalent intermediate state reported by a g_x resonance of 1.783 in the bacterial system is not evident in the present study using the bovine system. The additional g_x value of 1.785 present in the 'as prepared' and endogenous ubiquinone spectra corresponds to an empty Q_o site. An alternative explanation of the intermediate state reported for the bacterial enzyme, which favoured single occupancy, was given by *Crofts et al.* (1999) [34]. They suggested that the intermediate states, i.e. with a g_x resonance of 1.783 representing a quinone bound at Q_{os} (Fig. 4.1B), is a mixture of populations of the two extreme states represented by g_x resonances of 1.800 (Fig. 4.1A) and 1.765 (Fig. 4.1C). Alternatively, it may be caused by the different positions of the ubiquinone headgroup or different binding modes of ubiquinone [34]. Furthermore, although it is clear from co-crystals of the mammalian enzymes that the Q_i site is occupied by ubiquinone, the strongly binding Q_{os} species predicted by Ding and colleague's double occupancy model is not seen. This species according to the quinone extraction studies with a g_x resonance of 1.783 was more resistant to extraction than the Q_i site signal, leading to the prediction that the Q_{os} species would bind more tightly than the quinone at the Q_i site [31]. However, Dutton and co-workers [72] carried out linear combinations of the g_x resonances at 1.800 (native Q-pool levels) and 1.765 (fully extracted), which illustrated that the spectral line shape at a g_x value of 1.783 cannot be the average of the 1.800 and 1.765 signals but instead represents a distinct state. They concluded that the three unique [2Fe2S] cluster EPR spectral line shapes must reflect a genuine three-state transition, consistent with a binding site that accommodates two ubiquinone ligands with different binding affinities. To explain the observed EPR changes, their model

incorporated hydrogen bonding interactions between the [2Fe2S] cluster histidine ligands and both proposed Q_o site ubiquinone(s). The absence of the Q_{os} species in the crystal structures of the mammalian enzymes may be explained by differences between it and the bacterial enzyme used for the quinone extraction studies.

However, this absence of the Q_{os} species in the crystal structures of the mammalian enzymes is fully consistent with the EPR data presented here. The EPR spectra show only a single g_x signal that can be attributed to an occupant of the Q_o site and the other signal evident in the KHP experiments is due to an empty site. In addition, all the inhibitors used appeared to displace exogenous or endogenous substrates from the Q_o site. The result is fully consistent with a single occupancy model of the Q_o site.

4.3.4.4 Structural interpretation of EPR data

The crystal structures [35-40] show the extrinsic head domain of the 'Rieske' ISP in at least three different conformations, suggesting that the flexibility of the 'Rieske' ISP may be important mechanistically in the electron transfer process. This feature is included in the structural interpretation of the Q_o site occupancy and correlation with reduced [2Fe2S] cluster EPR line shape of bovine bc_1 complex is shown in Fig. 4.18. When the Q_o site is empty (devoid of ubiquinone or ubiquinol), the 'Rieske' ISP extrinsic head domain is positioned (in the equilibrium position) averaged between the Q_o proximal (closer to cytochrome *b*) and distal positions (closer to cytochrome c_1), the EPR line shape has a g_x resonance centered at 1.786. With a ubiquinone or a ubiquinol in the site, the 'Rieske' ISP extrinsic head domain is positioned so that the [2Fe2S] cluster is in the proximal position close to cytochrome *b*. The EPR line shape is shifted from 1.786 to 1.814 for ubiquinone and 1.804 for ubiquinol. Finally, in the

presence of a MOA-type inhibitor the 'Rieske' ISP extrinsic head domain is positioned in the distal position to the Q_o site reported by a g_x resonance of 1.777. In the presence of stigmatellin the iron-sulphur subunit is positioned in the proximal position close to cytochrome *b*, reported by a g_x resonance of 1.809 (Fig. 4.17).

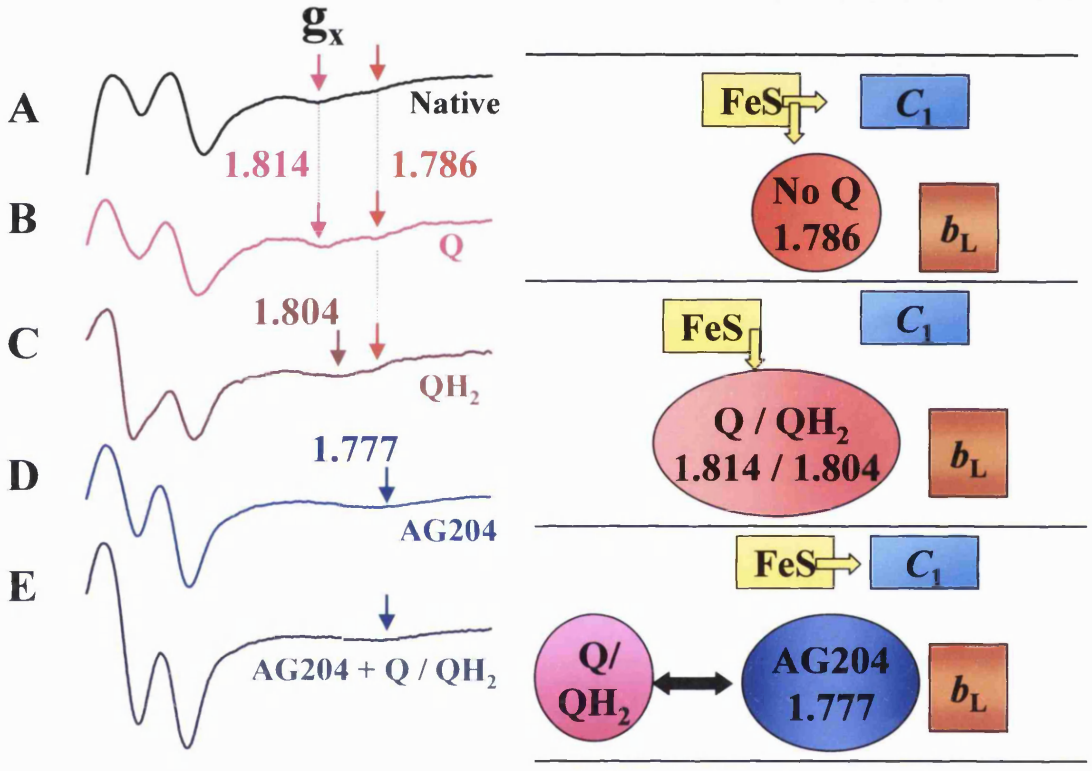

Fig. 4.18. Structural interpretation of the Q_o site occupancy and correlation with the reduced [2Fe2S] cluster EPR line shape of bovine cytochrome bc_1 complex. The (A-E) represent EPR line shapes of different Q_o site ubiquinone (Q) occupancies. The right-hand side shows schematic representations of the cytochrome bc_1 complex region surrounding the Q_o site, based on the crystal structure data. On the left-hand side the characteristic [2Fe2S] cluster EPR-spectral line shapes are depicted. Only a single species can occupy the site at one time. Yellow arrows indicate movement of the 'Rieske' ISP (FeS) extrinsic domain. Black arrow indicates displacement of ubiquinone (Q) or ubiquinol (QH_2). c_1, cytochrome c_1; b_L , haem b_L.

4.4 Summary

The studies presented here have indicated that although the Q_o site reaction site has two binding domains, only a single species can occupy the site at one time and supports the model of overlapping binding sites that arise from the kinetic studies (Chapter 3). The inhibitor studies (Fig. 4.4) showed AG204 (a class II inhibitor) could reverse the effects of stigmatellin (a class I inhibitor) on the redox components of the bc_1 complex, showing that these compounds cannot bind simultaneously. Positions of mutations conferring resistance to inhibitors (Fig. 4.5-6 and Table 4.1) showed that changes in the entrance tunnel and middle of the pocket affect both classes of inhibitors. Molecular modelling (Fig. 4.7) showed that structures with two ubiquinone molecules bound are highly constrained and only one 'tail' could be accommodated within the access tunnel and adjacent volume. Furthermore, exchange of ubiquinone bound at the Q_{ow} domain in reasonable physiological timescale with the Q-pool is hard to envisage. This further reinforces the view that only a single ubiquinone molecule is required for proper functioning of the Q_o reaction site. The EPR spectra (Fig. 4.9-17) showed only one signal that can be attributed to an occupant of the Q_o site. The other signal evident in the ubiquinone or ubiquinol spectra (from KHP samples) reports an empty site. Furthermore, AG204 or MOA-stilbene (class II inhibitors) appear to bind and displace DBMIB (class I) or ubiquinone analogues from the site due to their stronger affinity. Therefore, only one species can occupy the Q_o site at any one time. The difference between the EPR data on the bovine enzyme presented here and those of Ding and colleagues may reflect differences between the bacterial and bovine enzymes, especially the effects of MOA-stilbene, the presence of an intermediate state reported by a g_x resonance of 1.783 in the bacterial system and

the stronger affinity of quinone for the bacterial site. Elucidation of crystal structure for bacterial enzymes may shed light on some of these differences.

The results presented here clearly agree with the simplest model that only a single species can occupy the Q_o site and add support to any bifurcation mechanism involving a single occupant of the Q_o site.

Furthermore, this feature of the Q_o site having two binding but overlapping domains, has been used to propose a new compound based on an existing tight inhibitor AG204. This compound was designed to fit adequately into the two domains, with all the favourable contacts exhibited by the two classes of Q_o site inhibitors. Future experiments could include chemical synthesis of this new compound at Aventis Cropscience Ltd and tests to establish its activity.

CHAPTER 5

Characterisation of new inhibitors for mode of binding to Q-sites of cytochrome bc_1 complex using a combination of spectroscopic methods: Q_o or Q_i-site?

5.1 Background

Inhibitors of the bc_1 complex have been an important tool in the development of mechanistic concepts and evolutionary aspects related to this multi-protein complex. Of particular significance was the observation that these inhibitors can be divided into three classes, the first two binding to the Q_o site and the third to the Q_i site. Specific inhibitors of the two sites were a key prerequisite for demonstrating that cytochrome *b* can be reduced by ubiquinol from two different reaction sites, which are specifically blocked by inhibitors from one of these classes [75]. This was shown in the so-called 'double kill' experiment where cytochrome *b* reduction is blocked only when both a Q_i site inhibitor, e.g. antimycin A, and a methoxyacrylate (MOA) inhibitor, e.g. myxothiazol, are present [75]. The independent binding of antimycin A and the MOA inhibitors could also be demonstrated by the fact that the bathochromic shift of the spectrum of the reduced cytochrome *b* induced by either agent is additive [58, 62, 68]. These studies in combination with other kinetic evidence, e.g. the influence of inhibitors on the oxidant-induced reduction, finally led to the conclusion that antimycin A specifically inhibits the Q_i site of the Q-cycle reaction mechanism, whereas the MOA inhibitors act on the Q_o site [75].

Cytochrome bc_1 complex inhibitors affect mostly the characteristics of the redox centres closest to their binding site. Different properties of the redox centres have been shown to be modulated by inhibitors, e.g. optical absorption spectra and midpoint potential of cytochrome *b*, and the EPR line shape of the 'Rieske' ISP (Fig. 5.1). These effects provide the basis for characterisation of the binding site of new inhibitors. This chapter details the characterisation of the binding modes of a range of new inhibitors of the bc_1 complex (Fig. 5.2) using the following techniques: inhibitor titrations of the steady state kinetics of the bovine and yeast enzyme; absorbtion

spectra (binding spectra); oxidant induced reduction of cytochrome *b*; redox potentiometry and EPR line shape of the 'Rieske' ISP. These compounds were supplied by Aventis Cropscience Ltd and were initially screened in a photometric assay based on a crude preparation from rat liver mitochondria.

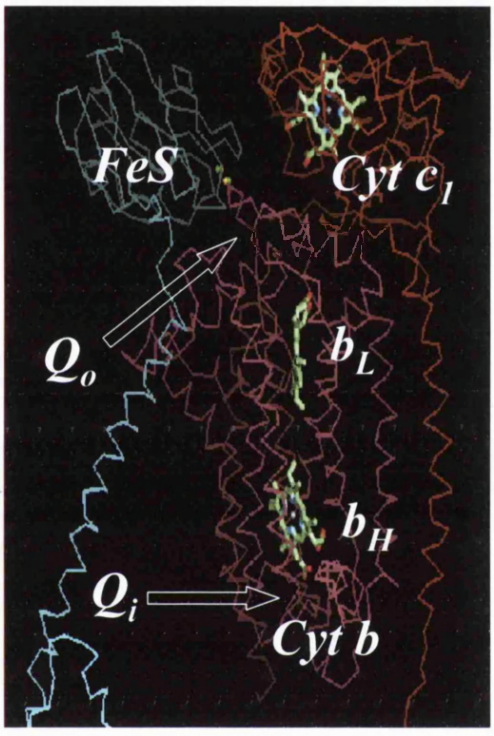

Fig. 5.1. The redox centres of the bc_1 complex. The EPR line shape of the 'Rieske' iron-sulphur protein and its midpoint potential is sensitive to its environment and affected by inhibitors binding close-by, e.g. stigmatellin. The midpoint potentials and the optical absorbtion spectra of cytochrome *b* are affected by Q_o and Q_i inhibitors e.g. myxothiazol and funiculosin. The arrows indicate the ubiquinol oxidation (Q_o) and reduction (Q_i) sites. The figure was produced using co-ordinates from *Zhang et al.* (1998) [35] datafile 3BCC in the molecular simulation software Quanta' 97 protein design (MSI, molecular simulations). Heams are shown in green as stick models. 'Rieske' ISP cluster atoms are shown as small green (iron) and yellow (sulphur) spheres. Cytochrome *b*, magenta, Cytochrome c_1, red; 'Rieske' iron-sulphur protein, blue.

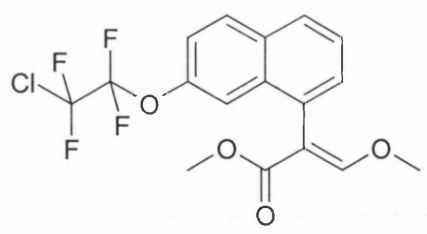

AE C630236 AG201

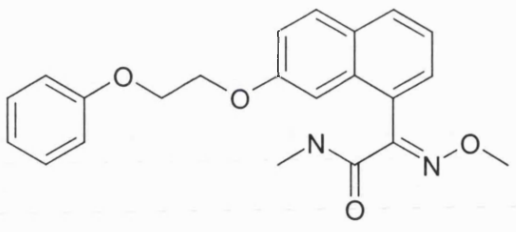

AE C629886 AG202

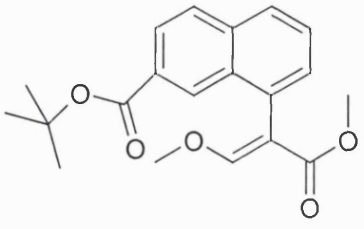

AE F128732 AG203

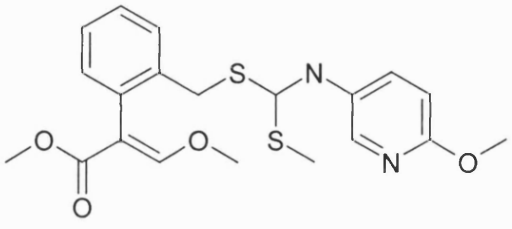

AE C608292 AG204

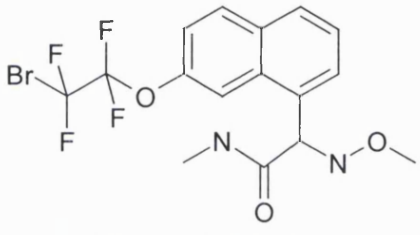

AE C631305 AG205

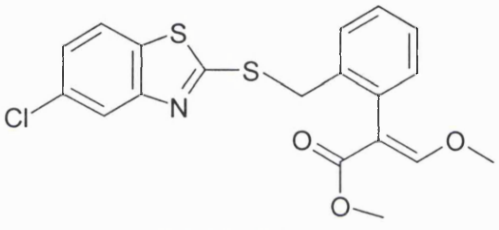

AE C602574 AG206

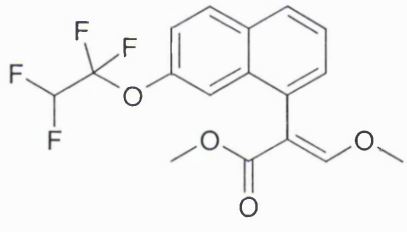

AE C630662 AG207

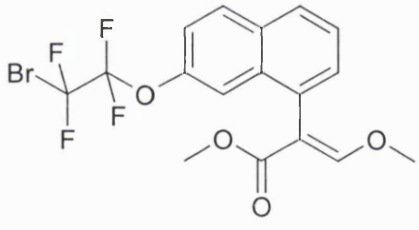

AE C632306 AG208

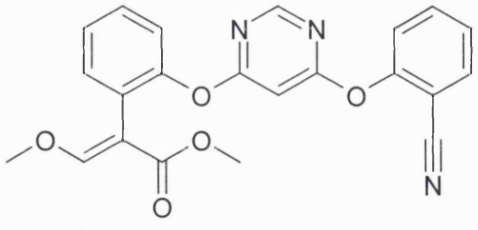

Azoxystrobin

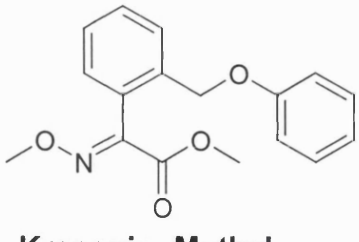

Kresoxim-Methyl

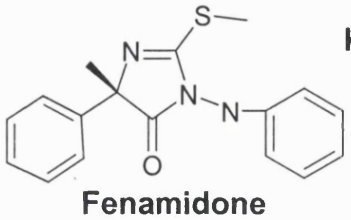

Fenamidone

Fig. 5.2. New and commercial (fungicide) inhibitors of the bc_1 complex supplied by Aventis Cropscience Ltd. The compounds are referred to by their AG codes. The structures of AG209 and AG210 are not shown because they are commercially sensitive compounds.

5.1.1 Inhibitor titrations of the steady state kinetics (Test 1)

Preliminary characterisation of the new inhibitors of the bc_1 complex was carried out by determining the apparent I_{50} values (the concentration for half inhibition of turnover number) and the dissociation constants (K_D) for the yeast and bovine bc_1 complexes. Inhibitor titrations of the steady state kinetics, recorded as the rate of cytochrome *c* reduction by the yeast and bovine bc_1 complexes were used for this purpose.

The inhibitors were titrated to both the bovine and yeast complexes because the latter is a good model for fungal pathogens, which are of great commercial interest. In addition, with the availability of structures of the bovine enzyme [36, 37] and the recently published yeast structure [41], any structural factors that lead to differences in inhibitor effects between the two forms of the enzyme can be investigated using computer methods.

5.1.2 The effects of inhibitors on the optical absorbtion spectra of cytochromes *b* (Test 2)

Earlier studies have shown inhibitors to bring about specific and well defined spectral changes in the α-, β- and γ-absorbtion bands of reduced cytochrome *b* in the isolated complex from beef heart mitochondria [58, 60, 62, 68]. Antimycin A induces a discernible difference spectrum of the oxidised cytochrome *b* and these spectral changes are generally of a smaller size. However, in the Soret region spectral changes in both redox states of the enzyme are significant [58].

The difference spectra induced by the inhibitors are associated with the cytochrome *b* closest to their binding site and hence can be used to determine which site is affected. The spectral changes can also be used to study competition between

inhibitors for binding to the Q-sites [58, 59, 62]. The binding spectra of Q_i and Q_o site inhibitors are additive, indicating that the binding of the two inhibitors occurs independently [59, 62]. Such experiments further confirm the presence of two independent quinone binding site. The analysis of binding spectra formed the basis of the first test carried out here to characterise the binding site of the new inhibitors.

The Q-site compounds fall into four categories of binding effects. These effects vary somewhat between different types of preparation of bc_1 complex, probably dependent at least partly on the occupancy of the Q-site by quinone or detergent before the inhibitor binds. However, effects for a given type of preparation are consistent [58, 62]. The effects of inhibitors on the Soret and α-bands of the reduced *b*- cytochrome under the conditions specified in Methods are summarised in Table 5.1 [58-60, 62].

Table 5.1. Effects of classical inhibitors of the bc_1 complex on the optical spectra of cytochrome *b*

Binding type	Effects
i) Q_i-binding, Antimycin A-like:	large red shift of 562nm band large red shift of Soret band
ii) Q_i-binding, Funiculosin-like:	large blue shift of 562nm band large blue shift of Soret band
iii) Q_o-binding, Stigmatellin-like:	large red shift of 566nm band (with the addition of detergent) small red shift of Soret band
iv) Q_o-binding, MOA-stilbene-like:	large red shift of 566nm band variable shift of Soret band

5.1.3 Oxidant induced reduction of cytochrome *b* (Test 3)

Oxidant induced reduction of cytochrome *b* is a phenomenon whereby the addition of an oxidant, e.g. oxygen, to mitochondria in which cytochrome c_1 is reduced and the *b* cytochromes are oxidised results in transient reduction of the *b* cytochromes and oxidation of cytochrome c_1 [119]. It requires a source of reducing equivalents e.g. succinate, NADH or ubiquinol and depends on the presence of ubiquinone and involves both *b* cytochromes. Although the reduction of cytochrome *b* is most readily demonstrated in the presence of antimycin A, a comparable oxidant-induced reduction can be observed at low temperature, which indicates this reaction is intrinsic to the mechanism of electron transfer in the cytochrome bc_1 complex and not an aberrant response elicited by this inhibitor [119].

The oxidant-induced reduction of cytochrome *b* was used to confirm the position and involvement of the 'Rieske' ISP in the electron transfer pathway [53]. This reaction was also shown to be inhibited by Q_o site inhibitors, e.g. UHDBT. It was the inability to explain the oxidant induced reduction of cytochrome *b* by a classical linear mechanism of electron transfer that ultimately led to the proposal of the protonmotive Q-cycle mechanism to explain the electron transfer and proton translocation properties of the bc_1 complex [119].

The effects of Q-site compounds on the oxidant-induced reduction of cytochrome *b* and the accompanying increased oxidation of cytochromes *c* and c_1 form the basis of the next test used to characterise the binding site of the new inhibitors of the bc_1 complex (Fig.5.3). In this study, oxidant-induced reduction of cytochrome *b* is seen when a pulse of oxygen is added to KHP respiring slowly because of oxygen limitation, and involves both *b* haems and is increased by the addition of Q_i site compounds, e.g. antimycin A.

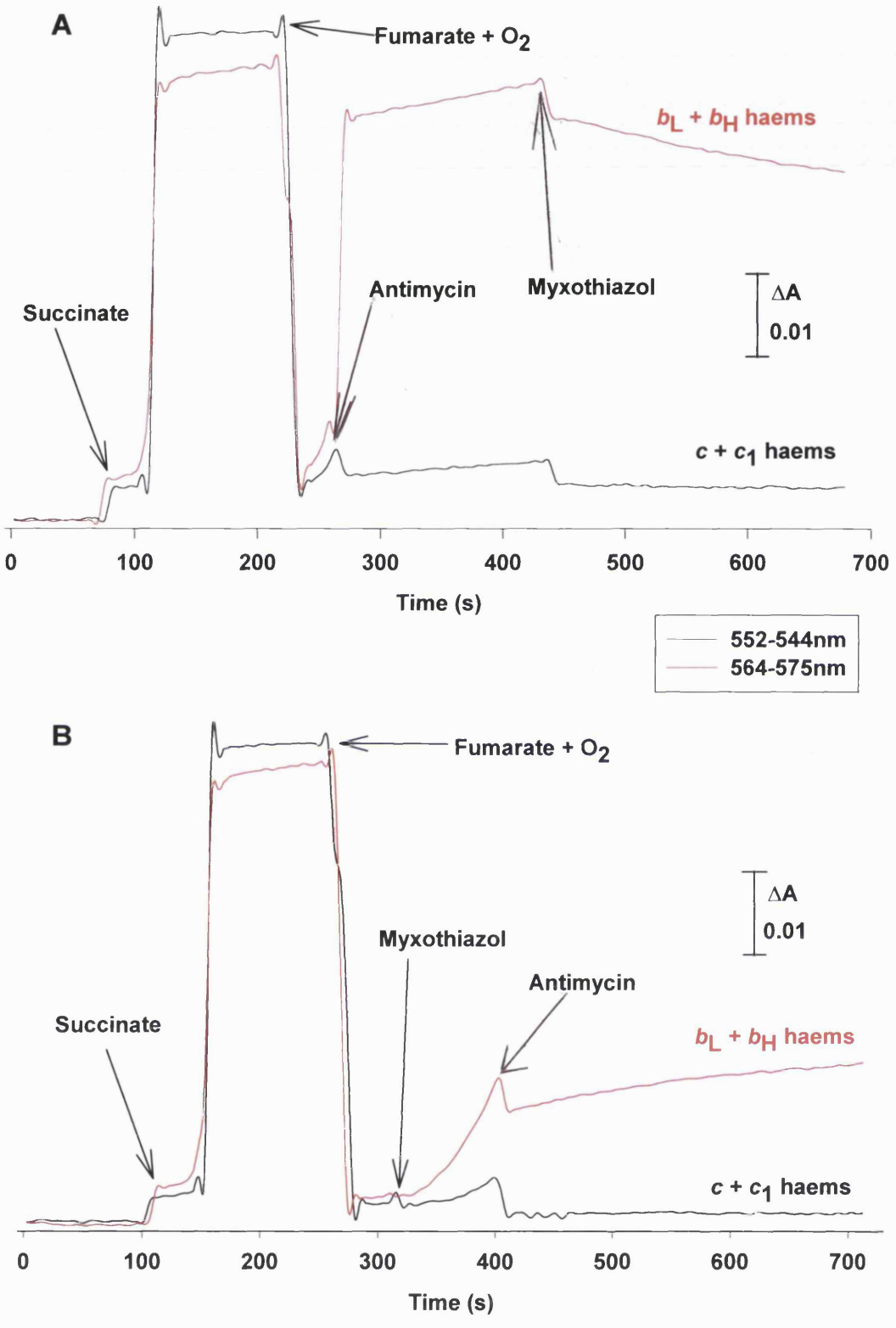

Fig. 5.3. The effects of classical inhibitors of the bc_1 complex on the oxidant-induced reduction of cytochrome *b*. Experimental conditions as described in Section 5.2.3.

Subsequent addition of Q_o site inhibitors leads to re-oxidation of the *b* haems. An enhancement of the oxidant-induced reduction of cytochrome *b* is not seen with the addition of Q_o site compounds, e.g. myxothiazol (Fig. 5.3b). Subsequent addition of Q_i site inhibitor antimycin A leads to re-reduction of the *b* haems [62]. These effects are summarised in Table 5.2.

Table 5.2. Effects of classical inhibitors on the oxidant-induced reduction of cytochrome *b*

Test	Addition	Compounds	$b_L + b_H$ (564-575nm)	$c + c_1$ (552-544nm)	Site of Action
Control	Prior	Fumarate + O_2	O	O	Antimycin A binds to the Q_i site
	1st	Antimycin A	R	O	
	2nd	Myxothiazol	O	O	
Control	Prior	Fumarate + O_2	O	O	Myxothiazol binds to the Q_o site
	1st	Myxothiazol	R	R	
	2nd	Antimycin A	R	O	

R - Reduction O – Oxidation

5.1.4 Redox potentiometry

Midpoint potentials (E_m) can be determined by a combination of redox potentiometry and spectrophotometry. The practical determination of the E_m of a respiratory chain component involves incubating mitochondria anaerobically in the presence of mediators. The state of reduction of the relevant component is monitored by dual wavelength spectrophotometry, while ambient redox potential is usually monitored by a platinum electrode. The mediators allow the respiratory chain components to equilibrate to the same E_m and the potential to be accurately reported

by the electrode. This potential can be made more electronegative by the addition of reductants such as ascorbate, NADH, or dithionite or more electropositive by the addition of oxidants such as ferricyanide, and E_m and the degree of reduction of the component are monitored simultaneously. In this way a redox titration curve for the component can be established [1].

Considerable information can be gathered from such titration. Besides E_m itself, the slope of $\log_{10}$ ([ox]/[red]) establishes whether the component is a one-electron carrier (60mV per decade) or a two-electron carrier (30mV per decade). By repeating the titration at different pH values it can be determined whether the midpoint potential is pH dependent, implying that the component is a ($H^+ + e^-$) carrier [1]. The technique allows the resolution of a single spectral peak into two or more components based on differences in E_m. In this case the Nernst plot is distorted, being the sum of two plots with differing E_m values which can then be resolved, e.g. cytochrome *b* in bc_1 complex. Redox potentiometry in combination with EPR spectroscopy can also be used to determine the E_m of the 'Rieske' ISP [1].

5.1.4.1 Redox titration curves of the *b* cytochromes and inhibitor effects

The Nernst plot of cytochrome *b* of the bc_1 complex is distorted, being the sum of two plots (cytochrome b_L and b_H) with differing E_m values. At pH values above 7, cytochrome b_H becomes heterogeneous in its redox behaviour with a high and low potential form separated by approximately 80mV [120]. This heterogeneity is caused by interaction between a bound ubiquinone at the Q_i site and cytochrome b_H. Not surprisingly it can be removed by the Q_i site inhibitors antimycin A, funiculosin and HQNO but not by the Q_o site inhibitors, myxothiazol or stigmatellin [120]. As

evident from the loss of the high potential form of cytochrome b_H, so that it reverts back to a single n = 1 species with a E_m close to that of the low potential wave of the control cytochrome b_H (at pH below 7) [120, 121]. This property of cytochrome b_H is utilised in this study to confirm the assignment of Q_i site inhibitors.

5.1.4.2 The effect of inhibitors on the E_m of the *b* cytochromes (Test 4)

Most inhibitors have a rather small effect on the haem *b* potentials. In those cases where the effect can be measured, the haem, which is closest to the site of the inhibitor binding is most affected [120]. Antimycin A has been reported to cause a small downshift ($\approx$20mV) of the E_m of cytochrome b_H at low pH [64, 120, 122]. In contrast, HQNO was found to shift the E_m of cytochrome b_H by 20-30mV to the positive [64, 120]. However, the most dramatic effect is by funiculosin, which increases the E_m of cytochrome b_H by >100mV at all pH values [64, 120].

Significant shift (>40mV) of the E_m of cytochrome b_L by any inhibitor has yet to be reported. Myxothiazol is reported to increase the E_m of cytochrome b_L and b_H by 15-30mV only [64] but caused no detectable change in the heterogeneous redox titration behaviour of haem b_H at any pH value. Stigmatellin increases the E_m of the 'Rieske' ISP to the positive from 290mV to 540mV but it has very little effect on the E_m of cytochrome b_L [59, 60].

The shifts of the E_m of *b* cytochromes by inhibitors may contribute in some cases to their mode of inhibition. If so, this property could be exploited in the design of new inhibitors and hence knowledge of such effects may have commercial interest.

5.1.5 The effects of inhibitors on the EPR line shape of the 'Rieske' ISP: Stigmatellin or MOA-like (Test 5)

The EPR spectral line shape of the 'Rieske' ISP, especially the g_x band of the reduced paramagnetic [2Fe2S] cluster, is highly sensitive to the degree and nature of the Q_o site occupants (Q/QH_2 or inhibitors) [57]. Using this technique, it is also possible to distinguish between the two classes of Q_o site inhibitors, since they induce markedly different shifts in the g_y and g_x features of the 'Rieske' ISP EPR line shape (Table 5.3). This technique was therefore used to classify new Q_o-site inhibitors into the two subclasses of Q_o site inhibitors, stigmatellin or MOA-like. The shift due to binding of stigmatellin also differs significantly from that induced by ethanol or DMSO. The g_y and g_x resonances in the presence of the two classes of inhibitors and solvents are summarised in Table 5.3 [59, 60, 62, 70, 71, 123].

Table 5.3. The effects of classical inhibitors and solvents on the EPR line shape of reduced 'Rieske' ISP

Q_o-site content	g_y	g_x
X-[2Fe2S]	1.897	1.815 / 1.788
DMSO	1.899	1.814 / 1.782
Ethanol	1.902	1.807
Stigmatellin	1.892	1.809
MOA-stilbene	1.903	1.777

DMSO, dimethyl sulphoxide.

5.1.6 Alternative methods for studying inhibitor binding

As described previously, some inhibitors induce a spectral shift of the *b* haems. These red shifts are proportional to the amount of bound inhibitor. The dissociation constants of the inhibitors can be determined by titrating the reduced enzyme in a dual wavelength mode [68]. Using a standard binding equation, *Brandt et al.* (1988) [75] calculated the values for bound and free inhibitor by means of computer fit to the titration curve. A similar technique to this is florescence quench titration of inhibitors such as MOA-stilbene and antimycin A, which monitors the inhibitor rather than the enzyme. This technique is suited to the study of different redox states of the enzyme, whereas the red shift titration is limited to the reduced enzyme [68].

Single turnover reduction kinetics is another method that could be used to determine the site of inhibition. The reduction of cytochrome c_1 is blocked by Q_o site inhibitors, whereas Q_i site inhibitors do not inhibit this reaction. The reduction of cytochrome *b* could only be blocked if both types of inhibitors were added together, the "double kill" phenomenon [68].

5.2 Methods

5.2.1 Inhibitor titrations

The method used was essentially as described in Chapter 3 (Section 3.2.2-3.2.2.1). The reaction buffer was 50mM potassium phosphate, 2mM EDTA at pH 8.0 and 25°C (2.5ml final volume). The order of addition of components was (final concentration): (a) 1mM KCN; (b) 24nM purified bovine or 33nM yeast bc_1 complex; (c) 30μM horse heart cytochrome *c* (Sigma); d) new inhibitors. The protein was

incubated with the inhibitor for at least 1min before the reaction was started by the addition of 30μM decylubiquinol. Cuvettes, Hamilton syringes and glass vessels containing inhibitor solutions were washed with ethanol before and after use to avoid adsorption of inhibitor onto glass surfaces. The concentration of serial dilutions of inhibitor was determined by taking the UV spectra of the inhibitor.

5.2.1.1 Simulations of AG compounds inhibition curves

For a weak binding AG inhibitor, Eq. 5.1 was simulated by a PC using software written in-house by Prof. Rich to determine dissociation constants. The best fit of an equation for a tight binding inhibitor for the new AG compounds inhibition data were determined by least squares analyses [124]. The equation was derived from:

$$E + I \xleftrightarrow{K} EI \qquad \text{(Eq. 5.1)}$$

Since K= [EI]/[E][I], $AG_{added} = I + EI$ and $bc_1 = E + EI$, it follows that

$$EI^2 - EI(1/K + AG_{added} + bc_1) + AG_{added}bc_1 \qquad \text{(Eq. 5.2)}$$

This simultaneous equation was conventionally solved to produce curves of EI (i.e., fractional inhibition) vs AG_{added} at a specific concentration of bc_1 complex [124, 125].

5.2.2 Binding spectra

The samples were prepared essentially the same as described in Chapter 4 (Section 4.2.1). Difference spectra were recorded in the Soret and visible regions after addition of 1μl 96% ethanol (as control) followed by the addition of final concentration of 2.5μM test compound in ethanol or 20μM of classical inhibitors. For competition experiments, a further 20μM MOA-stilbene or 10μM antimycin A was added to each sample and the resulting binding spectrum was recorded.

5.2.3 Oxidant-induced reduction of cytochrome *b*

The samples contained 25-40μl KHP (10μM bc_1 complex) in 50mM potassium phosphate pH 7.0 (0.5ml final volume) reaction buffer at 25°C. The order of addition of components as indicated in the figures was i) 3.2μl of 1M succinate pH 7.0 (6.4mM final concentration) ii) 32μl of 1M fumarate pH 7.0 (64mM final concentration) and oxygen (by stirring in air) iii) 10μM antimycin A or 4μM myxothiazol or 50μM of test compound (final concentration). Spectra were recorded in a single beam spectrophotometer at 552-544nm (c + c_1 haems) and at 564-575nm (b_L + b_H haems).

5.2.4 E_m of *b* cytochromes studied by redox potentiometry

The method employed is essentially the same as those described in *Rich et al.* (1990) [120]. KHP were prepared according to the method described in Chapter 2.

5.2.4.1 Redox potentiometry with redox mediators

Conventional anaerobic redox titrations were carried out under argon gas in a buffer of 50mM potassium phosphate pH 7 containing KHP at a final bc_1 complex concentration of around 2.5μM (2.5ml final volume). 1μg/ml gramicidin and 1μg/ml valinomycin were added to ensure the KHP were fully uncoupled. Redox mediators (all kept in the dark) are listed in Table 5.4. They were added to the sample at a final concentration of 20-100μM. The potential was varied with additions of 125mM potassium ferricyanide and 125mM sodium dithionite, 4min were usually allowed for equilibration after each addition and the data represents points taken in both oxidative and reductive directions. For measurement of ambient redox potential, a 3mm

diameter glassy carbon rod (Sigradur K, Sigri), sealed into PTFE sleeve (Goodfellows, Cambridge) with epoxy resin or with vaseline was used. The glassy carbon was cleaned before use with 0.05μm alumina polishing powder. The reference electrode was a chloride-coated silver wire in 3M KCl, connected to the test solution by a 3M KCl salt bridge. The glassy carbon reference system was calibrated against quinhydrone in anaerobic 50mM potassium phosphate at pH 7 both before and after the experiment. The midpoint potential of quinhydrone in this medium was taken to be +296mV [126] vs. SHE (standard hydrogen electrode).

Table 5.4. Mediator mixture for redox potentiometry experiments

Redox mediators	Midpoint potential (E_m) (mV)	Soluble in
#Anthraquinone 2-sulphonate	-225	water
Anthraquinone 2,6-disulphonate	-184	water
*1,4-Naphthoquinone-2-sulphonate	+120	Water
2,6-Dimethyl-1,4-benzoquinone	+180	ethanol
*2-Methyl-1,4-benzoquinone	+230	ethanol
Trimethyl-1,4-benzoquinone	+115	ethanol
Duroquinone	+50	ethanol
5-Hydroxy-1,4-naphthoquinone	+33	water
#2-Hydroxy-1,4-naphthoquinone	-125	water
Phenazine methosulphate (PMS)	+80	water
Phenazine ethosulphate (PES)	+120	water
#Benzyl viologen	-352	water
Methyl viologen	-450	water
#Hexamine-ruthenium chloride	+200	water
Diaminodurene	+275	Ethanol

Midpoint potential values from *Clark et al.* (1960) [126], #*Baymann et al* (1999) [127] and **Trumpower et al.* (1982) [105].

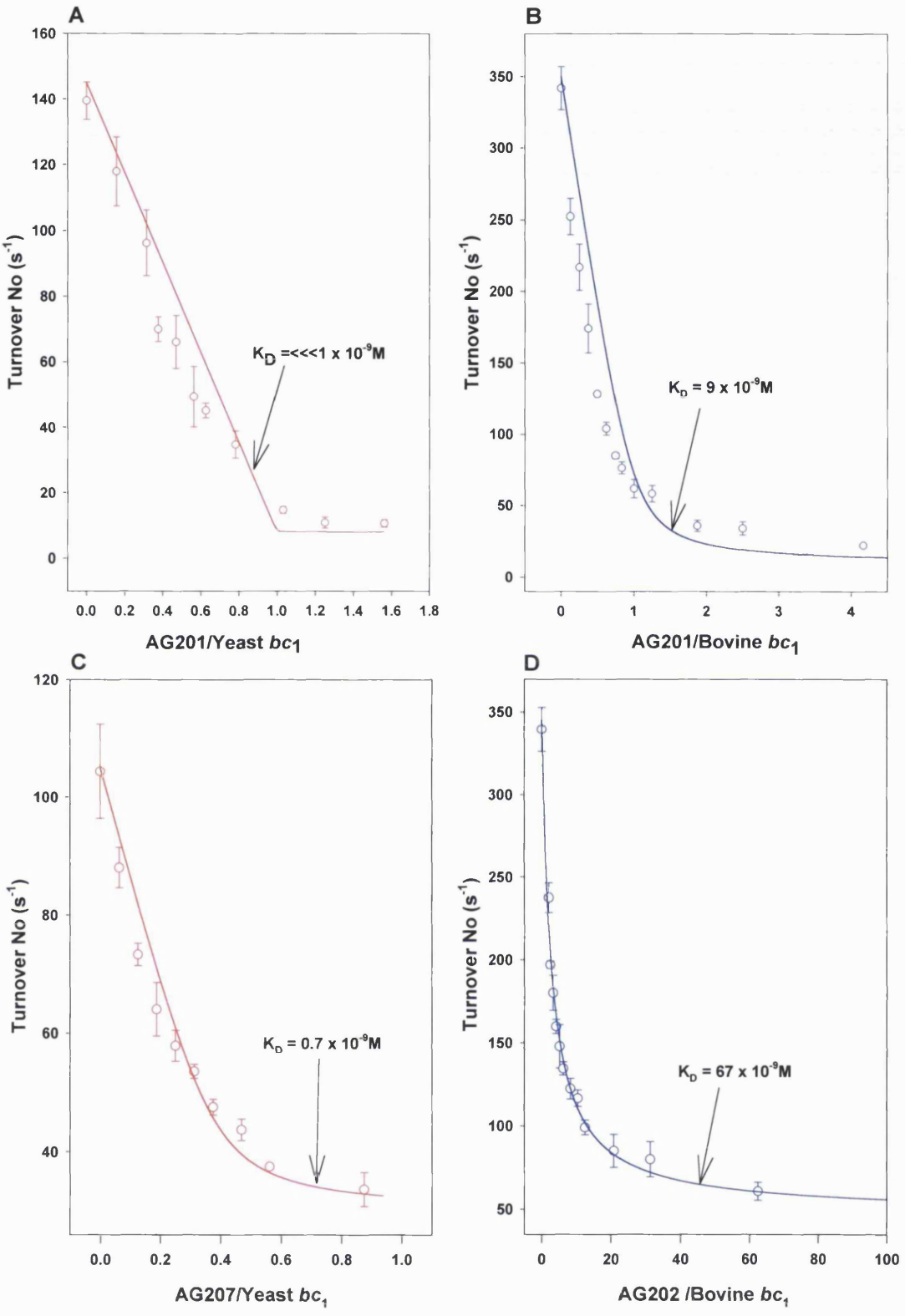

Fig. 5.4. Determination of the dissociation constant (K_D) of new inhibitors of the yeast and bovine bc_1 complexes. Experimental conditions as described in Section 5.2.1. Best fit curves were computer-produced by least square analyses with the constraint that 1AG compound/monomer was required for inhibition.

5.2.4.2 Data collection

At each ambient potential, spectra were recorded at approximately 1nm intervals from 400 to 600nm. Normally three spectra were recorded and averaged before storage. Ambient potential was recorded at the start and end of scans. A programme accessed these accumulated scans to produce the appropriate plots of absorbance change versus averaged potential during data collection. In this way, there was no user subjectivity in data derivation. Nernstian curves that approximated to two n = 1 components of roughly 0.7:0.3 contributions were overlaid on these plots to produce a best fit [120].

5.2.5 'Rieske' ISP studied by EPR spectroscopy

The samples were prepared essentially as described in Chapter 4 (Section 4.2.3) using KHP. 50μM test compound dissolved in ethanol with the exception of stigmatellin and AG204, which were dissolved in DMSO, were added as required. The EPR measurements were carried out as described in Chapter 4 (Section 4.2.4).

5.3 Results and discussion

5.3.1 Inhibitor titrations of the steady state kinetics of the purified bovine and yeast bc_1 complexes

Compounds AG201-208 are relatively good inhibitors of both the bovine and yeast enzymes (Table 5.5 and Fig. 5.4), binding more tightly to the yeast enzyme. In contrast, AG209-210 are relatively weak inhibitors of both enzymes, binding more strongly to the bovine enzyme. DCMU is a weak inhibitor of the yeast bc_1 complex

with an I_{50} of 8.7μM (Table 5.5), this is consistent with *Šubik et al.* (1981) [128]. Furthermore, it binds more weakly to the bovine enzyme.

Table 5.5. Dissociation constants (K_D) of new inhibitors of the yeast and bovine bc_1 complexes

Compounds	I_{50} (nM)		K_D (nM)	
	Bovine	Yeast	Bovine	Yeast
AG201	9±0.1	13±1	1	0.001 (<1)
AG202	89±7	22±2	67	0.001 (<1)
AG203	44±4	12±1	33	0.001 (<1)
AG204	21±2	*7±1	17	*0.001 (<1)
AG205	42±10	19±3	50	0.7
AG206	*9±1	*7±1	*1	*0.001 (<1)
AG207	14±4	25±2	14	0.7
AG208	11±2	17±2	9	0.1 (<1)
AG209	251±7	5374±418	222	1000
AG210	303±84	6930±113	250	1250
DCMU	98±5μM	14±1μM	83μM	12.5μM

The I_{50} values for the yeast enzyme were normalised for enzyme concentration of 33nM. The concentration of the bovine enzyme used in this assay was 24nM. *K_D per dimer.

AG201 and AG206 are the tightest binding inhibitors of the bovine enzyme. The stoichiometry of inhibition of the latter was surprisingly one AG206 per bc_1 complex dimer (0.5AG206/momomeric bc_1 complex). This is the first report of such co-operative behaviour in the bovine enzyme. The co-operative mechanism of inhibition could be rationalised in terms of perturbation of the structure of the dimer. Specifically, the binding of the inhibitor in one monomer may be sufficient to prevent

any substrate binding in the other monomer or disrupt the other monomer's 'Rieske' ISP, the hydrophobic anchor of which is associated with the opposite cytochrome *b*.

There are correlations between the structure of the compounds and their dissociation constants for the bovine enzyme (Fig. 5.2 and Table 5.5). The replacement of a chlorine atom in the backbone of AG201 for a bromine atom as in AG208 (Fig. 5.2) results in weaker binding (increase in K_D). The absence of an extra halogen atom in this position as in AG207 also results in further increase in K_D. However, the greatest increase in K_D occurs as a result of the introduction of two nitrogen atoms instead of the two oxygen atoms in the toxophore of AG208, as in AG205 (Fig. 5.2). Not surprisingly AG202 also with two nitrogen atoms in its toxophore is the weakest of all the Q_o site inhibitors. As already demonstrated for stigmatellin, alterations in the backbone as well as the toxophore results in changes in the binding affinity of the inhibitor [60].

AG201-8 are very tight binding inhibitors of the yeast enzyme with dissociation constants in some instances well below 1nM (Table 5.5). Two of the inhibitors AG204 and AG206 display a stoichiometry of one inhibitor per yeast bc_1 complex dimer. The same stoichiometry has been reported for stigmatellin (B.Trumpower, personal communication). The two inhibitors differ from the rest of the compounds in possessing a benzene ring rather than a naphthalene ring immediately attached to the toxophore (Fig. 5.2). Replacing a chlorine atom in the backbone of AG201 with a bromine atom as in AG208 results in an increase in the K_D for the yeast enzyme. Furthermore, the introduction of nitrogen atoms into the toxophore of AG208 as in AG205 and a lack of a halogen atom as in AG207 caused an increase in the K_D. The same pattern was found in the bovine enzyme but was less pronounced. The weakening effect of nitrogen on the toxophore may be related to its

lower electronegativity in comparison to oxygen i.e. weakening hydrogen bonds formed by the toxophore. The toxophore of MOA-stilbene is modelled in the bovine structure to form hydrogen bond with E271 (chicken numbering) and its hydroxyl group is within 5.6Å of haem b_L's propionate group (Fig. 5.5).

AG202 is a relatively weak inhibitor of the bovine enzyme but a very tight inhibitor of the yeast enzyme. The same correlation applies to a number of the compounds (Table 5.5) including AG203, 205, 209 and 210. With the availability of structures of the bovine and yeast enzyme, it will be interesting to investigate using computer methods the structural factors that leads to such differences in K_D between the two forms of the enzyme.

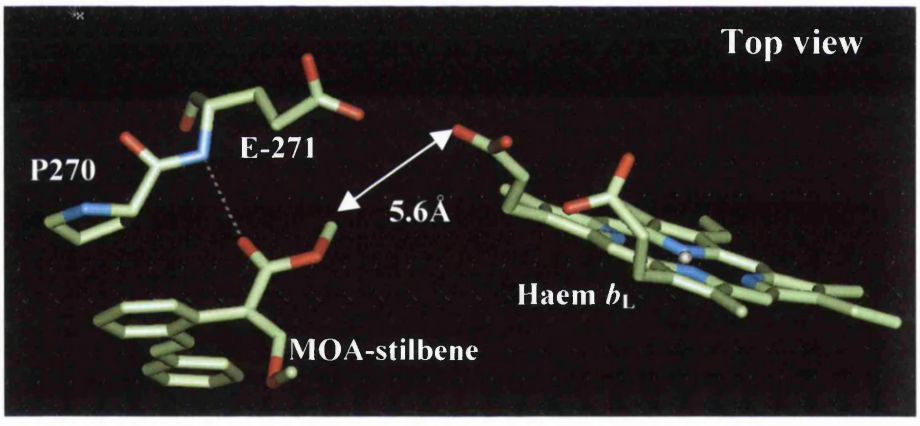

Fig. 5.5. Structure of the Q_o site with MOA-stilbene bound. The figure was produced using co-ordinates from *Zhang et al.* (1998) [35] datafile 3BCC in the molecular simulation software Quanta' 97 protein design (MSI, molecular simulations). All molecules are shown as sticks.

5.3.2 Binding spectra of new and commercial inhibitors

From the visible band data (Fig. 5.6 and Table 5.6), all compounds except AG209 and AG210 caused a significant red shift of the α-band of haem b_L, consistent with their MOA-like binding to the Q_o site. In Cholate prepared SCR (with added dodecyl maltoside), stigmatellin caused a significant red shift of the α-band. Therefore, the possibility of some of the compounds such as AG201, 203, 206, 207 and 208 binding like stigmatellin cannot be completely ruled out. These compounds caused a similar red shift of the α-band as stigmatellin (Table 5.6).

According to the dissociation constant, AG203 is weaker binding than a number of the other compounds but yet induced the greatest red shift of the α-band. It is the only compound with a carbonyl in its backbone structure (Fig. 5.2). The opposite could be said about AG204, which is one of the stronger binding compounds but yet induced the weakest red shift of the α-band. However, AG206 is the tightest binding compound and accordingly induced a significant red shift of the α-band. This suggests that there is no correlation between the size of the shift and potency of the inhibitors, which is consistent with previous study [60]. The introduction of nitrogen atoms into the toxophore as in AG202, AG205 and kresoxim-methyl (Table 5.6 and Fig. 5.2) reduces the size of the red shift of the α-band, consistent with the K_D data.

Of the commercial inhibitors of the bc_1 complex, fenamidone with an odd structure for a Q_o site inhibitor causes the greatest red shift of the α-band (Table 5.6). Azoxystrobin and kresoxim-methyl bind in a MOA-like way to the Q_o site (Fig. 5.5), as expected since they have structural similarity to MOA-stilbene.

The shift caused by AG209 was too small in extent for an assignment to be made. AG210 caused a small red shift of the α-band of the b_H haem, consistent with its antimycin A-like binding to Q_i site. Not surprising for a derivative of antimycin A.

In the cases of AG201-208 (Table 5.7 and Fig. 5.7A), subsequent addition of antimycin A induced a full antimycin A-induced shift of haem b_H, showing that none of the compounds interfered with binding of antimycin A to the Q_i site. In contrast, the subsequent addition of MOA-stilbene did not induce a shift of haem b_L, showing that all the compounds bind at the Q_o site. The same result was obtained for the commercial (fungicide) bc_1 complex inhibitors (data not shown).

In the case of AG209 and AG210 (Fig. 5.7B and Table 5.8), subsequent addition of MOA-stilbene induced a full MOA-induced shift to haem b_L, showing that none of the compounds interfered with binding of MOA-stilbene to the Q_o site and so, are likely to be Q_i site inhibitors. The subsequent addition of antimycin A (Fig. 5.7B and Table 5.8) in the case of both AG209 and AG210 induced a full antimycin A-induced shift of haem b_H showing that both compounds were likely to be displaced by antimycin A from the Q_i site. In contrast, subsequent addition of AG210 to a sample with antimycin A already bound resulted in lack of red shift of the α band. This suggests that AG210 is weaker binding than antimycin A to the Q_i site. Soret band changes are unreliable for distinguishing between different modes of binding to the Q-sites of the complex (data not shown)

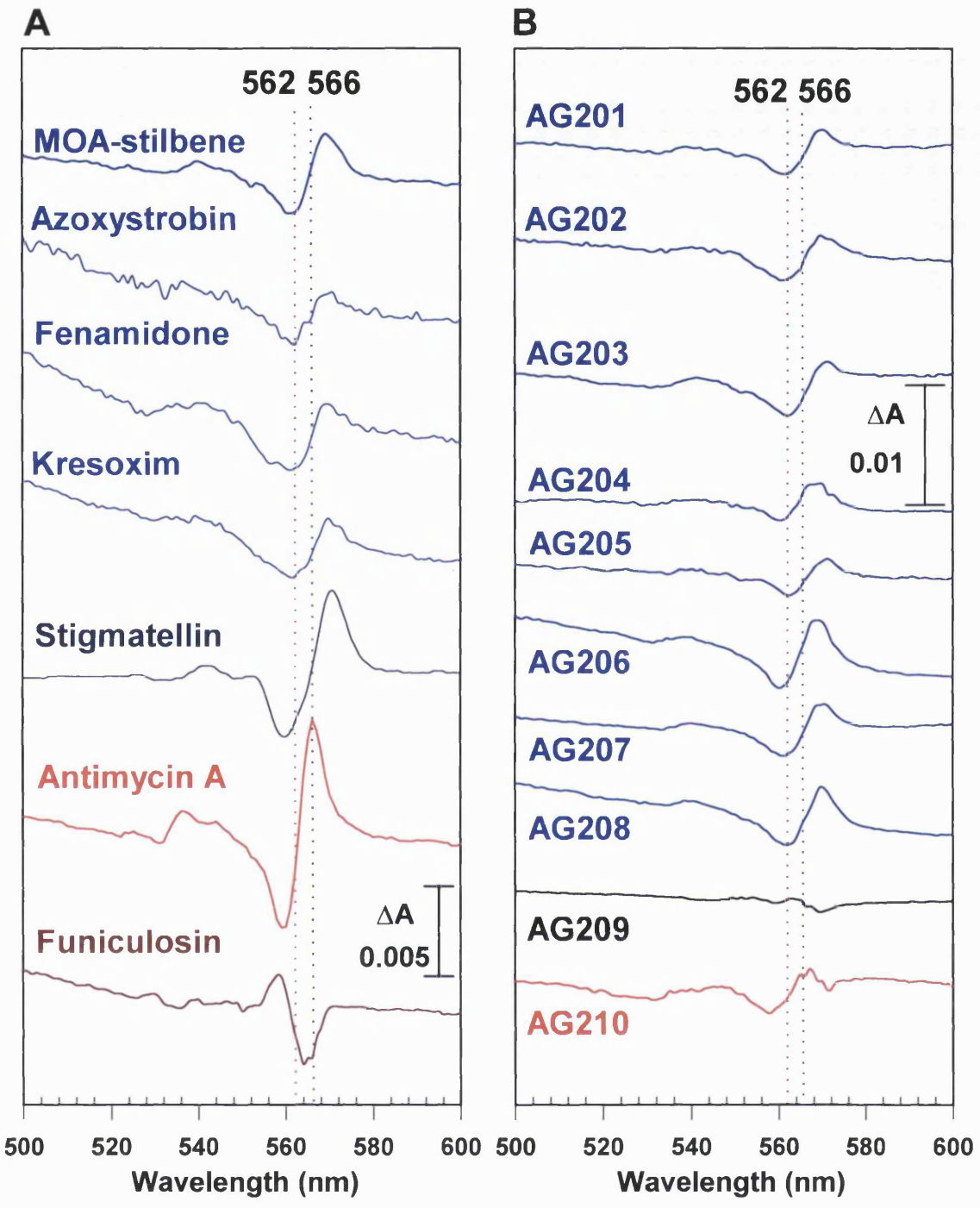

Fig. 5.6. Characterisation of the binding site of inhibitors of the bc_1 complex studied by difference optical spectroscopy (Reduced + inhibitor *minus* Reduced + Ethanol). **A)** Binding spectra of classical and commercial (fungicides) inhibitors. **B)** Binding spectra of new inhibitors. Experimental conditions as described in Section. 5.2.2.

Table 5.6. The effect of new compounds on the reduced bc_1 complex (Binding spectra)

Compd	Crossing point (±1nm)	Peak (±1nm)	Trough (±1nm)	Peak-Trough ($\Delta A \times 10^{-3}$)	Ratio $\Delta A_{P-T}/\Delta A_{562-575} \times 10^{-3}$	Site of Action
AG201	566	570	561	3.77	56.81	Q_o
AG202	566	569	561	3.74	43.07	Q_o
AG203	566	570	562	6.28	61.42	Q_o
AG204	564	569	560	3.14	30.70	Q_o
AG205	566	569	562	3.95	41.35	Q_o
AG206	564-565	568	560	5.8	60.61	Q_o
AG207	566	570	560	4.41	56.64	Q_o
AG208	566	569	561	4.93	49.17	Q_o
AG209	-	-	-	-	-	?
AG210	561-562	564	560	1.2	21.49	Q_i
Azoxy	565	569	561	2.99	45.77	Q_o
Fen	565	568	560	3.68	46.12	Q_o
Kres	565	569	561	3.24	39.92	Q_o
MOA	565	568	561	2.79	45.09	Q_o
Stig	566	571	559	5.3	50.46	Q_o
Funi.	562-563	559	565	5.48	55.70	Q_i
Ant.	562	565	559	7.58	102.77	Q_i

Compd, compound. Azoxy, Azoxystrobin; Fen, Fenamidone; Kres, Kresoxim-Methyl; MOA, MOA-stilbene; Stig, Stigmatellin; Funi, Funiculosin; Ant, Antimycin A. ΔA_{P-T}, absorbance change of red shift spectra of reduced α band from peak-trough. $\Delta A_{562-575} \times 10^{-3}$, absorbance change of the reduced absolute spectra from 562-575nm.

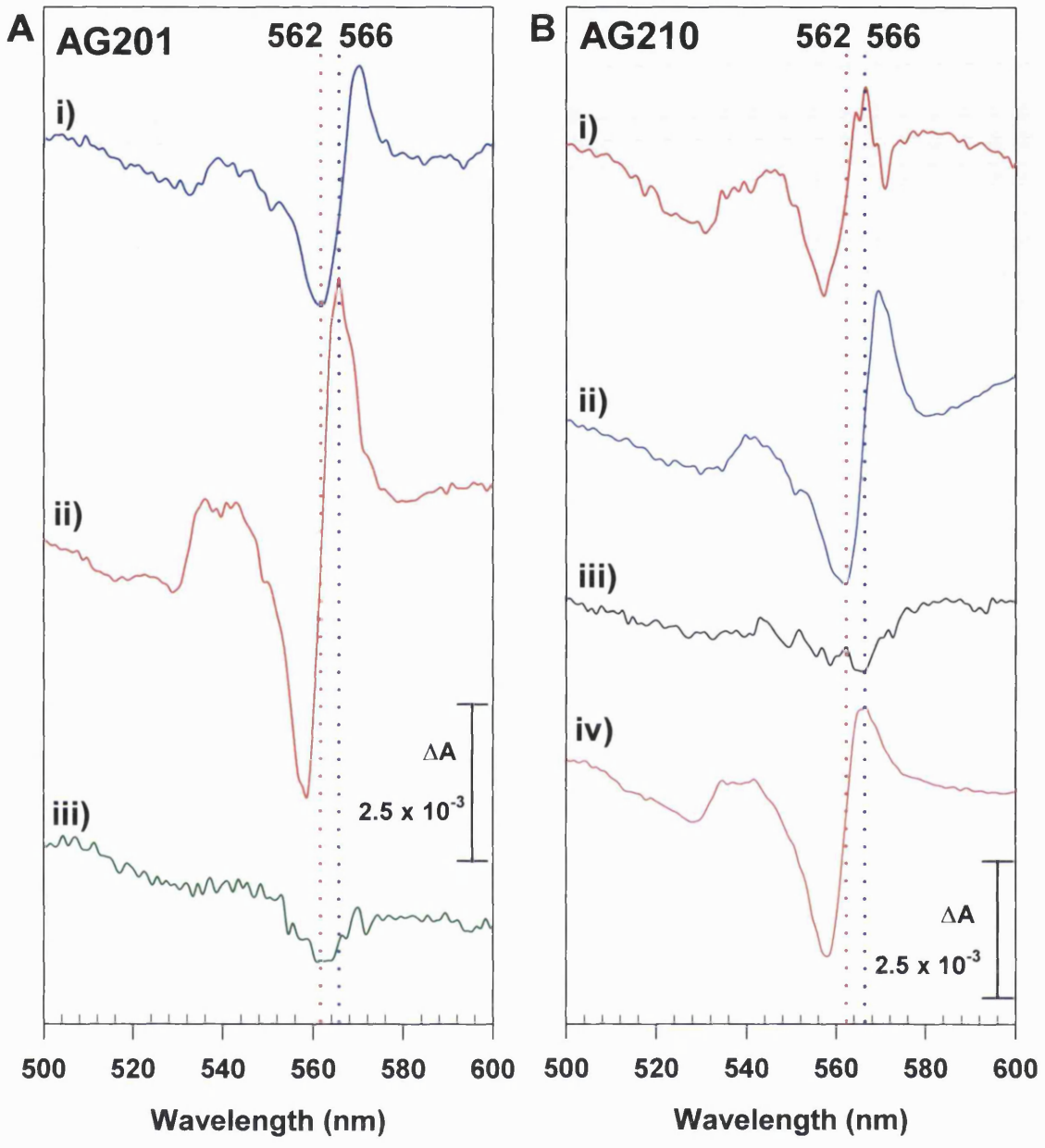

Fig. 5.7. Competition experiments between AG compounds and classical inhibitors of the bc_1 complex. Experimental conditions as described in Section. 5.2.2. **A)** AG201 **i)** Reduced + AG201 *minus* Reduced + Ethanol. **ii)** Reduced + AG201 + Antimycin A *minus* Reduced + AG201 + Ethanol. **iii)** Reduced + AG201 + MOA-stilbene *minus* Reduced + AG201 + Ethanol. **B)** AG210, **i)** Reduced + AG210 *minus* Reduced + Ethanol. **ii)** Reduced + AG210 + MOA-stilbene *minus* Reduced + AG210 + Ethanol. **iii)** Reduced + Antimycin A + AG210 *minus* Reduced + Antimycin A + Ethanol. **iv)** Reduced + AG210 + Antimycin A *minus* Reduced + AG210 + Ethanol.

Table 5.7. Competition experiments between new Q_o site compounds and classical inhibitors of the bc_1 complex (Binding Spectra)

Expt	Cross Pt (±1nm)	Peak (±1nm)	Trough (±1nm)	Peak-Trough ($\Delta A \times 10^{-3}$)	Ratio (ΔA_{P-T} / $\Delta A_{562-575} \times 10^{-3}$)	Site of Action
AG201 Vs Ant	563	567	560	8.17	89.63	Q_o site
Vs MOA	-	-	-	-	22.41	
AG202 Vs Ant	563	567	559	7.08	81.47	Q_o site
Vs MOA	-	-	-	-	9.73	
AG203 Vs Ant	562-563	566	559	10.23	99.14	Q_o site
AG204 Vs Ant	562	566	559	10.92	104.5	Q_o site
Vs MOA	-	-	-	-	13.53	
AG205 Vs Ant	562	566	559	11.78	123.3	Q_o site
Vs MOA	-	-	-	-	12.92	
AG206 Vs Ant	562-563	566	559	6.44	90.32	Q_o site
Vs MOA	-	-	-	-	7.79	
AG207 Vs Ant	562-563	566	559	6.96	88.5	Q_o site
Vs MOA	-	-	-	-	12.91	
AG208 Vs Ant	562	566	559	11.04	109.2	Q_o site.
Vs MOA	-	-	-	-	13.37	

Expt, experiment; Cross Pt, Crossing point; Ant, Antimycin A; MOA, MOA-stilbene. ΔA_{P-T}, absorbance change of red shift spectra of the α-band from peak-trough. $\Delta A_{562-575} \times 10^{-3}$, absorbance change of the reduced absolute spectra from 562-575nm.

Table 5.8. Competition experiments between new Q_i site compounds and classical inhibitors of the bc_1 complex (Binding Spectra)

Expt	Cross Pt (±1nm)	Peak (±1nm)	Trough (±1nm)	Peak-Trough ($\Delta Ax10^{-3}$)	Ratio (ΔA_{P-T} / $\Delta A_{562-575}$ x 10^{-3})	Site of Action
AG209 Vs Ant	563	566	559	5.22	76.65	Antimycin A displaces AG209 from Q_i site
Vs MOA	565	569	561	3.82	58.04	Q_i site
AG210 Vs Ant.	563	567	559	4.53	100	Antimycin A displaces AG210 from the Q_i site
Ant. Vs AG210	-	-	-	-	18.81	AG210 cannot displace Antimycin A from the Q_i site
Vs MOA	566	569	562	4.85	57.36	Q_i site

Expt, experiment; Cross Pt, Crossing point; Ant, Antimycin A; MOA, MOA-stilbene. ΔA_{P-T}, absorbance change of red shift spectra of the α band from peak-trough. $\Delta A_{562-575} \times 10^{-3}$, absorbance change of the reduced absolute spectra from 562-575nm.

5.3.3 Effects of new inhibitors on the oxidant-induced reduction of cytochrome *b*

In oxidant induced reduction experiments, AG201-AG208 like myxothiazol (Table 5.9, Fig. 5.3B and Fig. 5.8-9), when added to slowly respiring KHP after an oxygen pulse do not enhance the transient reduction of cytochrome *b* seen with the addition of antimycin A (Fig. 5.3A). This is consistent with their action at the Q_o site. Subsequent addition of myxothiazol had no additional effects, showing that AG201-208 binds at the Q_o site. The additions of AG201-AG208 like myxothiazol (Table 5.9, Fig. 5.3A and Fig. 5.8-9) after the transient reduction of cytochrome *b* (caused by the

addition of antimycin A) resulted in re-oxidation of the haems. This is also consistent with their action as Q_o site inhibitors. The oxidant-induced profile of AG201 suggests that it increases the E_m of haem b_L and may have possible secondary inhibitory effects on Complex II (Fig. 5.8).

An indication of the binding strength of the inhibitor can be tentatively gauged from the rate of re-oxidation of the *b* haems after the addition of the compounds. From these qualitative analyses AG201 (Fig. 5.8B), 206, 208 and 202 (Table 5.9) are stronger inhibitors than AG203, 204 (Fig. 5.9A), 205 and 207, in contradiction of the K_D data. This discrepancy may be explained by a combination of subtle effect of the inhibitors on the E_m of the *b* haems, inhibitor 'on' and 'off' rates, the presence of different amounts of endogenous oxidants in the KHP and contamination by oxygen during mixing.

The addition of AG209 (Fig. 5.10A) or AG210 (data not shown) to slowly respiring KHP after an oxygen pulse resulted in an enhancement of the transient reduction of cytochrome *b*. This is consistent with antimycin A like binding to the Q_i site (Fig. 5.3A). AG209 and AG210 also appeared to lower the E_m of haem b_H, as seen by the fast re-oxidation of the *b* haems after subsequent addition of myxothiazol (Fig. 5.10A) compared to that seen with antimycin A (Fig. 5.3A). The addition of antimycin A after the transient reduction of cytochrome *b* [caused by the addition of AG209 or AG210 (data not shown)] had no effect on the haems (Fig. 5.10B). This showed that these compounds have no effect on the Q_o site. The addition of AG209 and AG210 after the addition of myxothiazol caused differing effect on the *b* haems (Fig 5.11). AG209 caused a slow re-reduction of the *b* haems, (Fig. 5.11A) whereas AG210 resulted in the fast oxidation of the *b* haems (Fig. 5.11B). This suggests that the binding of the two compounds to the Q_i site may be different.

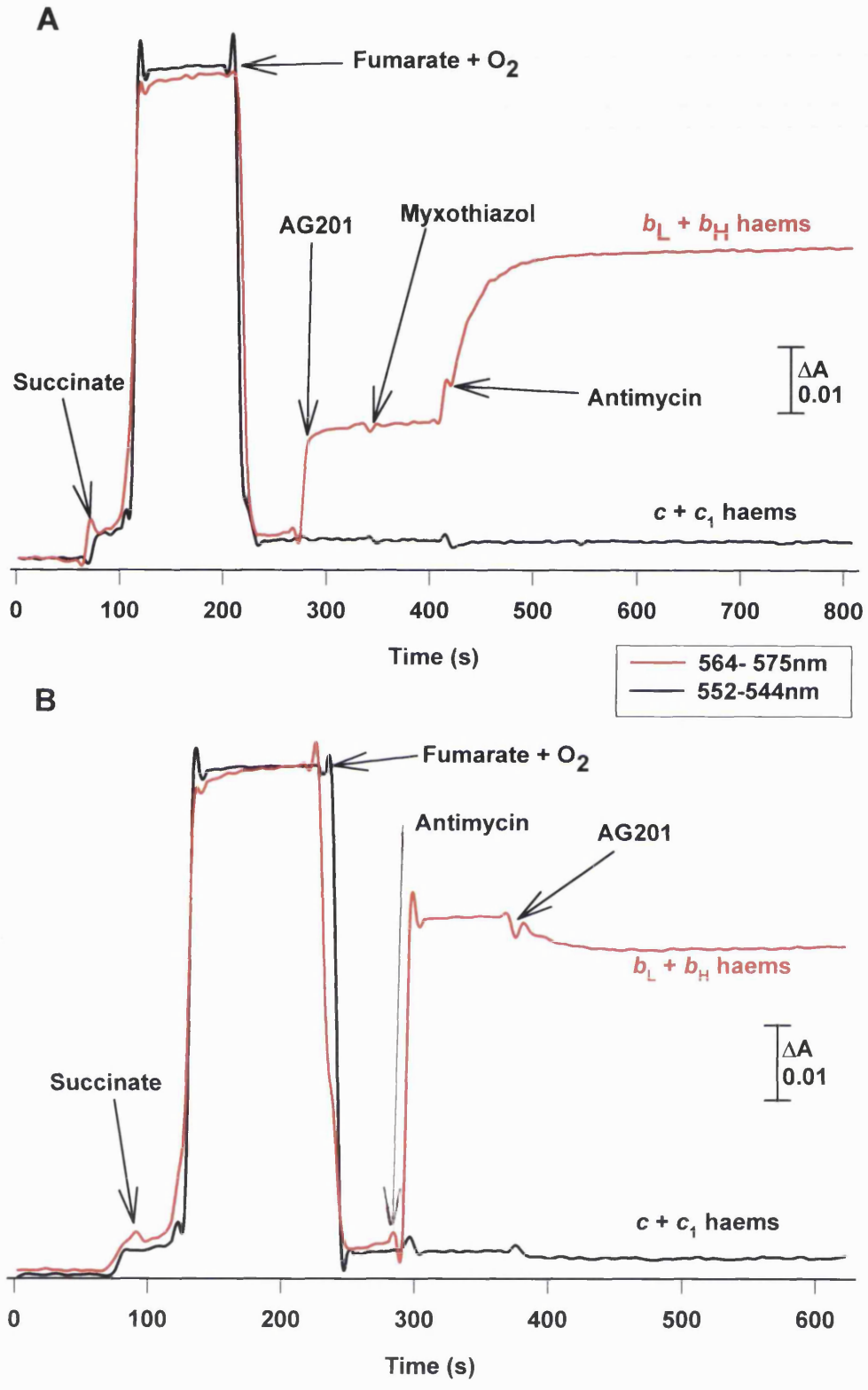

Fig. 5.8. The effects of AG201 on the oxidant induced reduction of cytochrome *b*.
Experimental conditions as described in Section 5.2.3.

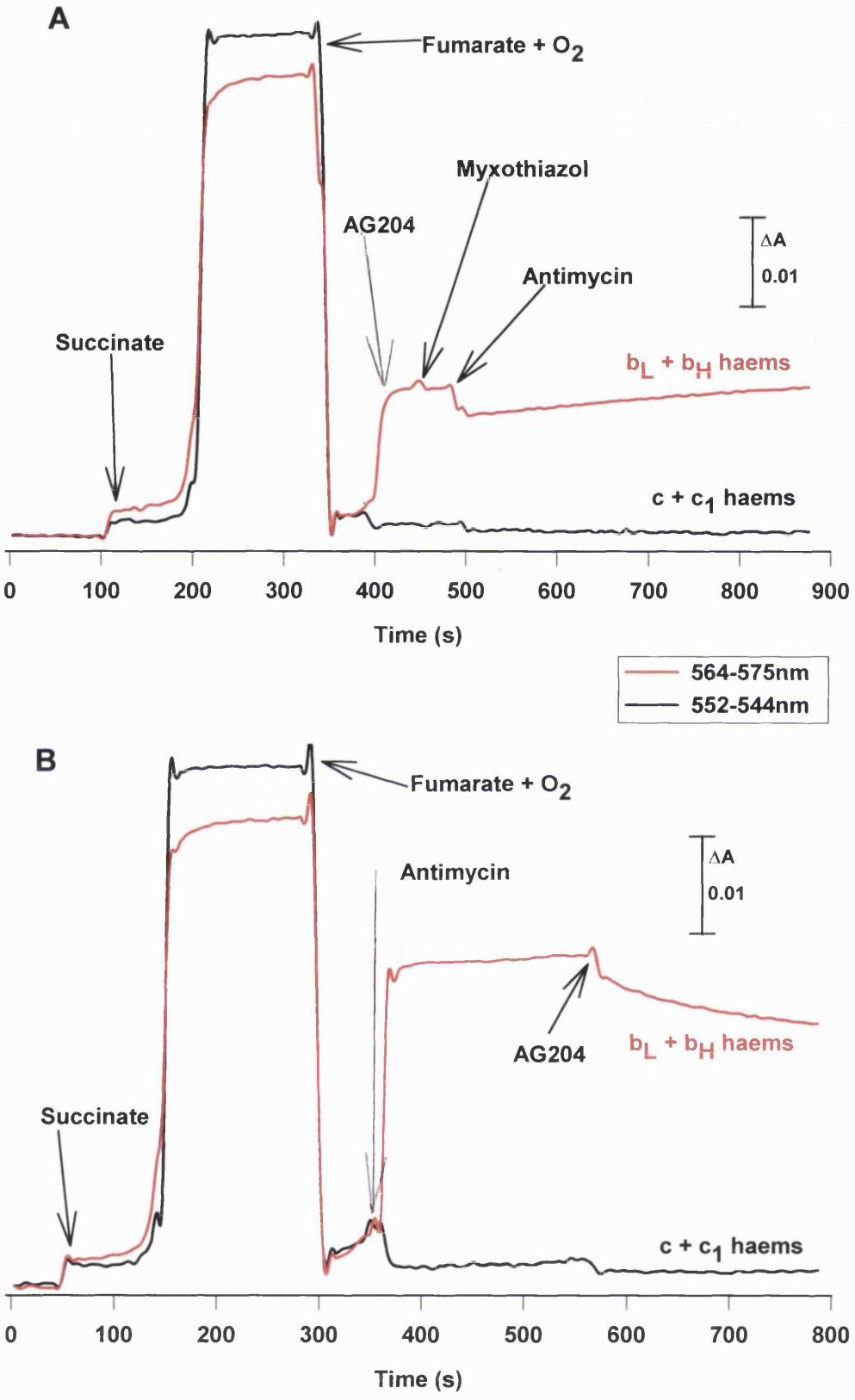

Fig. 5.9. The effects of AG204 on the oxidant induced reduction of cytochrome *b*.

Experimental conditions as described in Section 5.2.3.

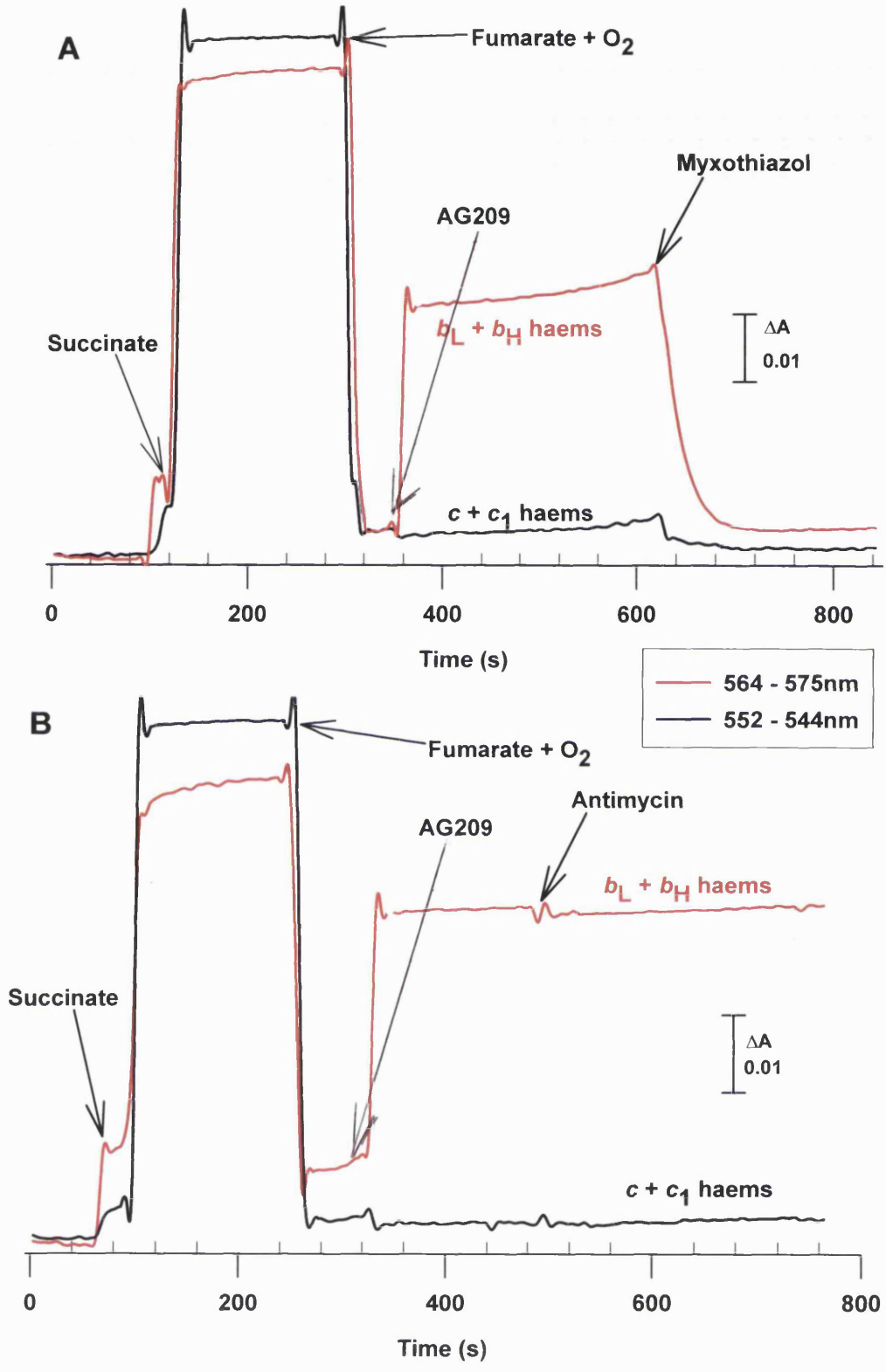

Fig. 5.10. The effects of AG209 on the oxidant induced reduction of cytochrome *b*. Experimental conditions as described in Section 5.2.3.

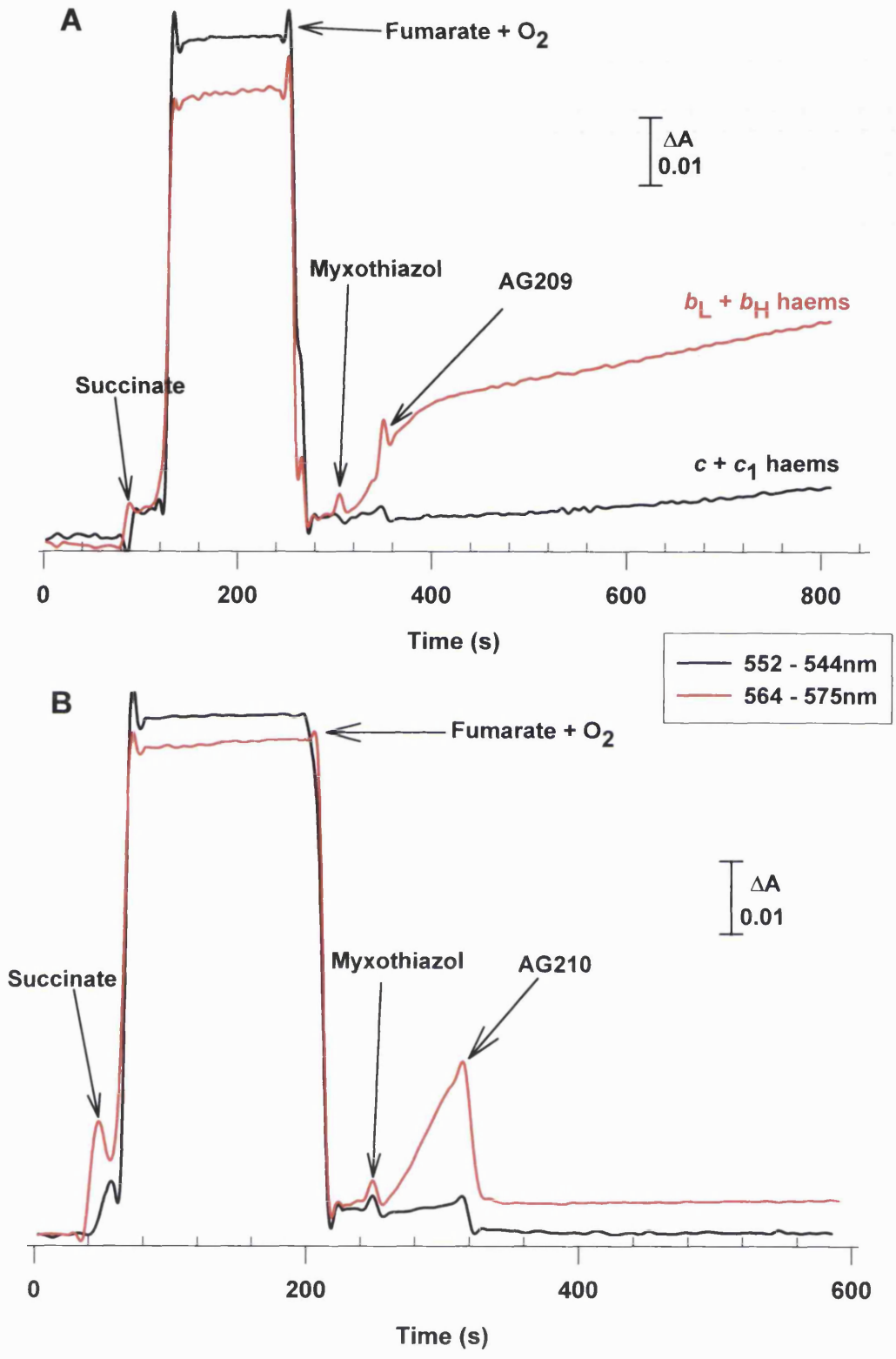

Fig. 5.11. The effects of AG209 (A) or AG210 (B) on the oxidant induced reduction of cytochrome *b*. Experimental conditions as described in Section 5.2.3.

Table 5.9. Summary of the different effects of new Q-site inhibitors on the oxidant-induced reduction of cytochrome *b*

Test	Addition	Compounds	$b_L + b_H$ (564-575nm)	$c + c_1$ (552-544nm)	Site of Action
AG202, 206 & 208	Prior 1st 2nd	Fumarate + O_2 Antimycin A AG Cmpd	O R Slow O	O O O	Q_o site
AG203, 205 & 207	Same order as above		O R Faster O than AG202	O O O	Q_o site
AG209-210	Same order as above		O R No additional effect	O O O	Q_i site
AG202	Prior 1st 2nd 3rd	Fumarate + O_2 AG Cmpd Myxothiazol Antimycin A	O Slow R No additional effect Fast R	O O O O	Q_o site
AG203 & AG206	Same order as above		O Faster R than AG202 No additional effect Slow R	O O O O	Q_o site
AG205 & AG207-208	Same order as above		O Faster R than AG202 No additional effect Fast R	O O O O	Q_o site
AG210	Prior 1st 2nd	Fumarate + O_2 AG210 Antimycin A	O R No additional effects	O R O	Q_i site

R – Reduction, O – Oxidation, The oxidant-induced reduction of cytochrome *b* profiles shown in the figures are not summarised in this table.

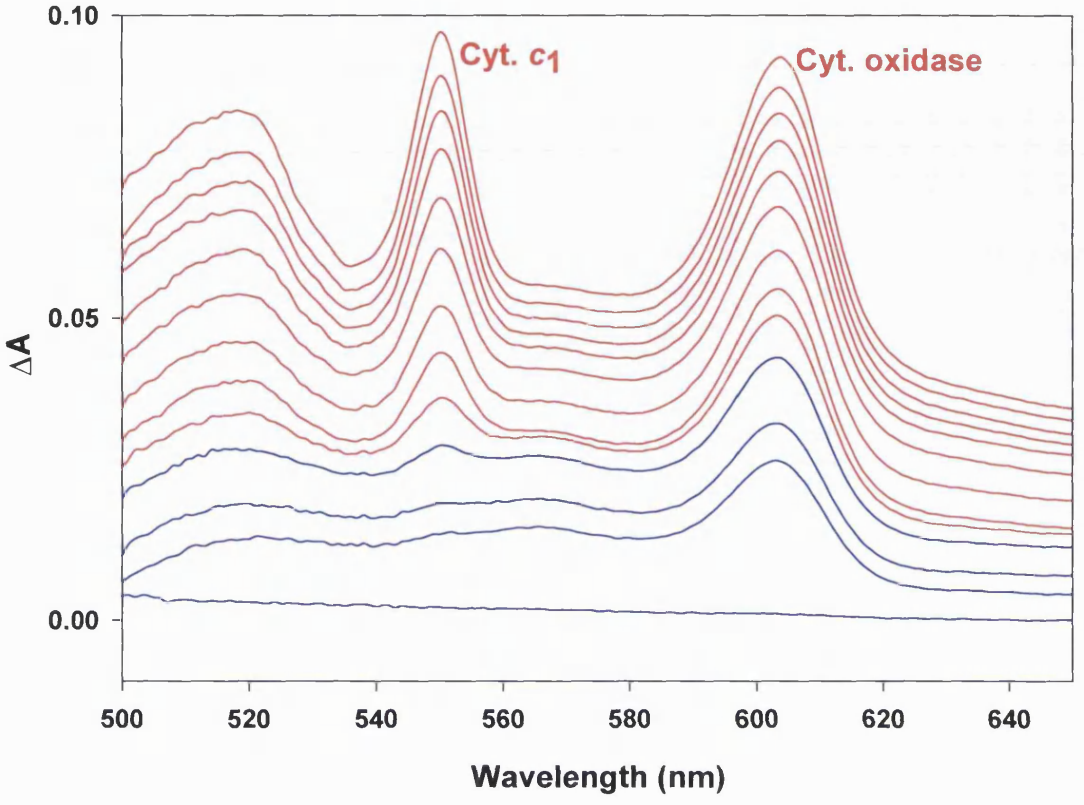

Fig. 5.12. Redox titration of cytochrome c_1 of the bovine cytochrome bc_1 complex studied by optical spectroscopy. Anaerobic titrations in the presence of redox mediators at pH 7.33 were carried out as described in Section 5.2.4. Absorption spectra were recorded in both oxidative and reductive directions.

5.3.4 Redox potentiometry

Redox potential data points were taken in both oxidative and reductive directions (Fig. 5.12). The redox titrations of the *b* haems produced a characteristic curve (Fig. 5.13) which approximated to two n = 1 components of roughly 0.7:0.3 contributions. None of the compounds tested were found to have significant effect (>30mV) on the E_m of the haem closest to their binding site (Fig. 5.13), as indicated by their effect on the qualitative oxidant induced reduction of cytochrome *b*. AG210 lowers the E_m of haem b_H by ~30mV. In contrast, AG201 had no effect on the E_m of haem b_L. The removal of the heterogeneous redox behaviour of cytochrome b_H by

AG210, confirms the assignment of the inhibitor as a Q_i site inhibitor.

Similar experiments were carried out using *Rb. capsulatus* chromatophores, this confirmed that none of the Q_o site compounds (AG201-208) altered the midpoint potential of either *b*-type haem by any significant amount (< ±20mV, A. Osyczka, personal communication). Furthermore, AG201 and 206 were found to slightly lower the E_m of the [2Fe2S] cluster of the 'Rieske' ISP by about -30mV, which is comparable to the effect of MOA-stilbene.

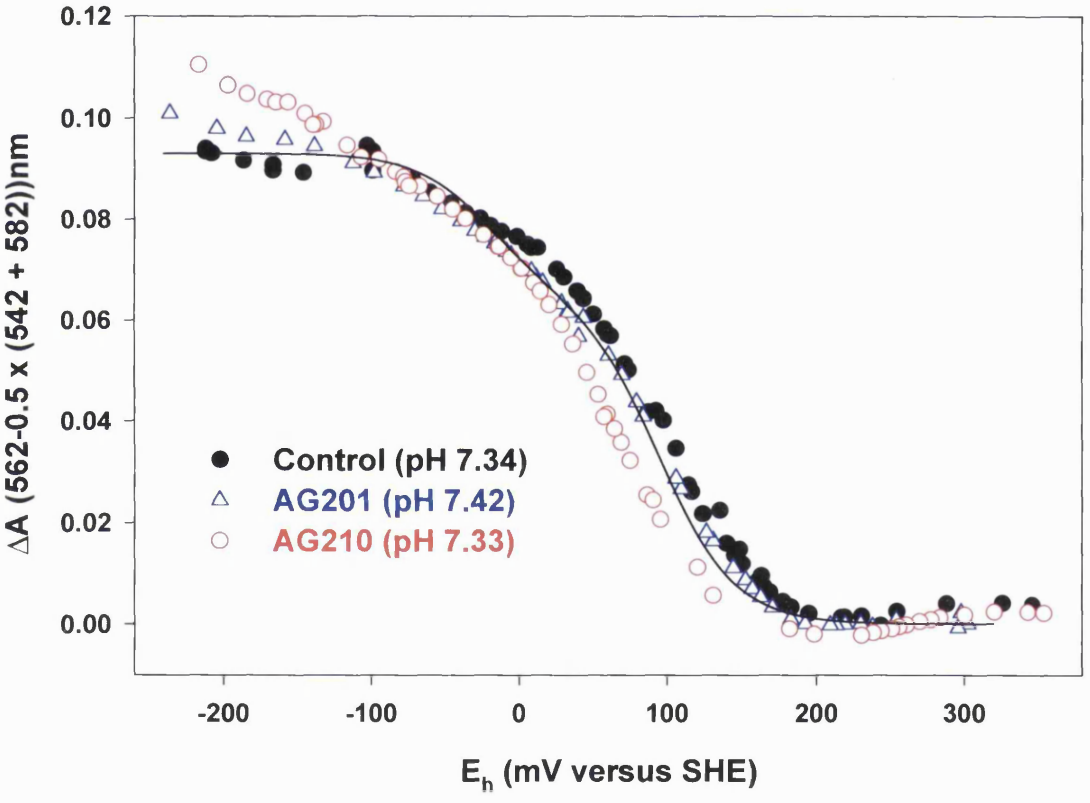

Fig. 5.13. The inhibitor dependence of the redox titration curves of haems *b*. Anaerobic titrations in the presence of redox mediators were carried out at indicated pH as described in Section 5.2.4. Data points were taken in both oxidative and reductive directions. Only deconvolutions of b_H plus b_L at 562-(542 + 582)nm are shown. Simulations are an 0.7:0.3 ratio of two n = 1 components of midpoints at pH 7, +95 and –20mV [120]. At the low-potential end (<-50mV) of the titration, interference from cytochrome *b*-560 of succinate dehydrogenase (Complex II) can be seen in all the deconvolutions [120]. SHE, standard hydrogen electrode.

5.3.5 EPR line shape: Stigmatellin or MOA-like

All the inhibitors were dissolved in ethanol with the exception of AG204 and stigmatellin, which were dissolved in DMSO. Ethanol has an effect on the 'Rieske' [2Fe2S] EPR line shape, in contrast to DMSO. However, inhibitors caused additional effect in the presence of ethanol (Fig. 5.14A). Five of the new Q_o site inhibitors were examined and all showed a MOA-stilbene-like EPR spectrum of the reduced [2Fe2S] cluster of the 'Rieske' ISP (Fig. 5.14B), a clear downshift of the g_x resonance value from 1.814 (native) to 1.806-1.777. AG202 and AG206 behave slightly differently from the rest of the compounds. The downshift is less pronounced than the others (1.814 to 1.806), but the spectra are still reminiscent of class II inhibitors (MOA-like) of the Q_o site. This confirms earlier observations from the binding spectra. There is no reason to suggest the rest of the compounds are different, since the compounds are similar in structure (Fig 5.2).

Similar experiments carried out using *Rb. capsulatus* chromatophores confirmed that all the compounds, AG201-208 showed a myxothiazol-type, i.e. class II, EPR spectra of reduced [2Fe2S] cluster of the 'Rieske' ISP (A. Osyczka, personal communication).

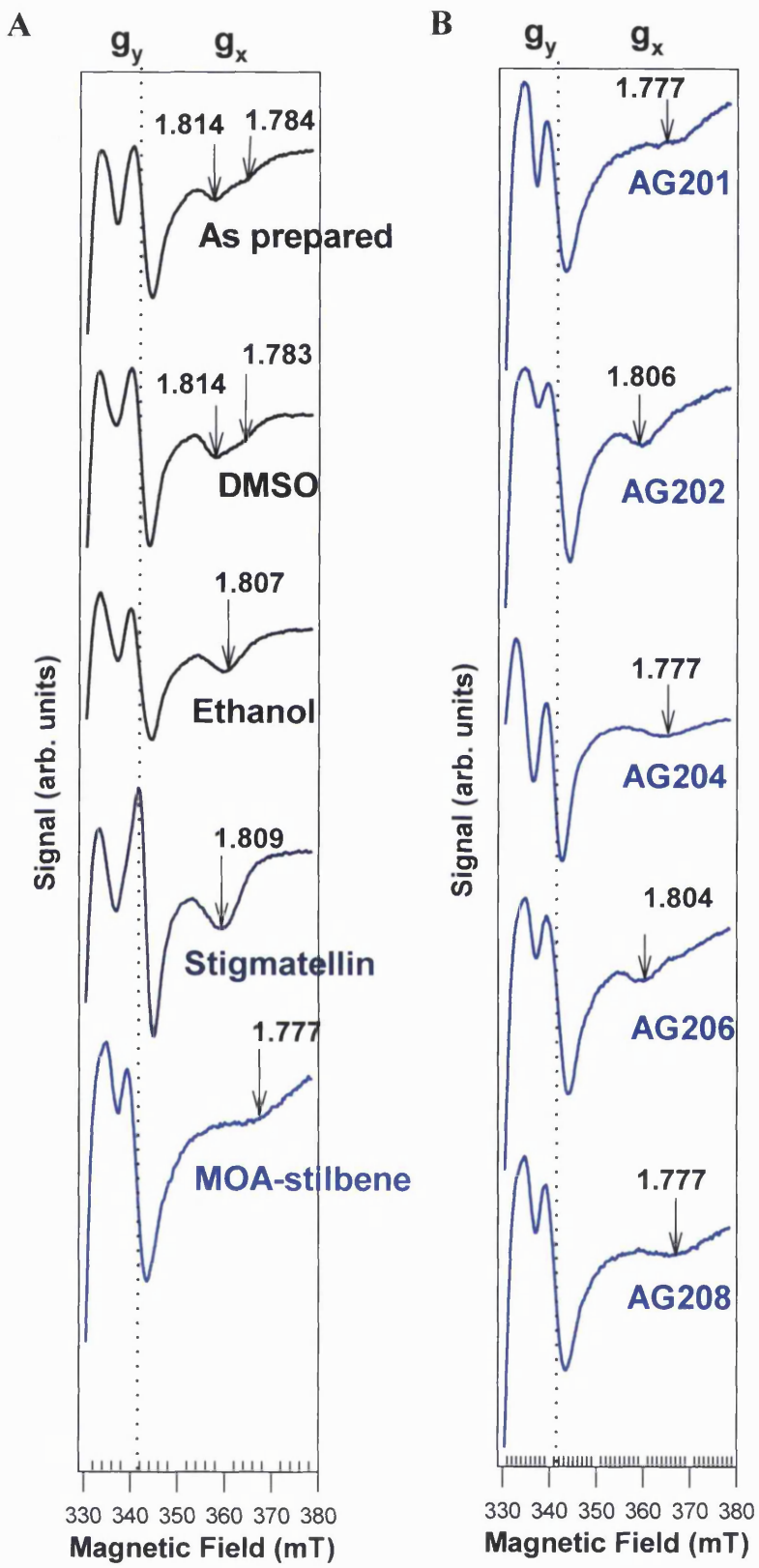

Fig. 5.14. The effects of solvents, new and classical Q_o site inhibitors on the reduced 'Rieske' ISP EPR line shape. Experimental conditions as described in Section 5.2.5. arb, arbitrary.

5.4 Summary

The new Q_o site compounds AG201-208 are relatively good inhibitors of both bovine and yeast enzymes (Table 5.5), binding more tightly to the yeast enzyme. The two Q_i site inhibitors AG209-210 are relatively weak inhibitors of both forms of the enzyme, binding more tightly to the bovine enzyme. AG206 binds to both forms of the enzyme with a stoichiometry of 0.5 AG206/monomeric bc_1 complex. AG204 mimics this behaviour but only in the yeast enzyme. This is the first report of such co-operative behaviour in the bovine enzyme.

From all the tests, AG201-AG208 are MOA-stilbene-like Q_o site inhibitors. An assignment cannot be made from the visible band data of AG209. However, the competition and the oxidant-induced experiments confirmed AG209 to be a Q_i site inhibitor. AG210 from all the tests is an antimycin A-like Q_i site inhibitor.

From the oxidant-induced experiments, additional secondary effects on the haems were evident. AG201 appeared to increase the E_m of haem b_L and had possible secondary inhibitory effects on complex II. AG209 and AG210 lowered the E_m of haem b_H and there was also evidence to suggest that the binding of the two compounds to the Q_i site may be different.

The redox potentiometry results showed that neither of the two compounds tested had any significant effect (>30mV) on the haem closest to their binding site. The result confirmed the assignment of AG210 as a Q_i site inhibitor.

CHAPTER 6

Photochemical reduction of the bc_1 complex studied by optical and Fourier transform infrared (FTIR) difference spectroscopy

6.1 Background

FTIR difference spectroscopy is a powerful technique for studying changes in protein and prosthetic group conformations upon photochemical reduction. This chapter describes its application to the bovine heart cytochrome bc_1 complex to determine redox-induced IR difference spectra of each redox component in native and inhibitor-bound states. These difference spectra can indicate conformational changes of the polypeptide backbone and the side chains, protonation and deprotonation reactions of amino acid residues, hydrogen bonding changes, and the interactions between inhibitors, substrates, prosthetic groups and the protein [127]. This technique is also potentially suitable for investigating possible conformational changes associated with the mobile head domain of 'Rieske' ISP [86, 129]. Kinetically resolved vibrational FTIR spectroscopy could eventually be used to resolve the detail mechanism of the Q_o site oxidation reaction by allowing kinetic resolution of reaction intermediates and providing local and specific structural information on each of the states [54]. For comparative purposes, FTIR redox difference spectra of horse heart cytochrome *c*, turnip cytochrome *f*, and cytochrome *f* and 'Rieske' ISP of lettuce cytochrome b_6f complex were also determined.

6.1.1 Infrared spectroscopy

Infrared spectroscopy is a key analytical method to measure vibrational spectra of small molecules. A spectrum is obtained by passing infrared radiation through a sample and determining what fraction of the incident radiation is absorbed as a function of frequency. The peaks in an absorbtion spectrum correspond to the frequencies of vibrational modes of the sample molecule. The absolute spectrum obtained thus provides a fingerprint of the entire molecular structure [130, 131].

Significant advances in infrared measurement came with the introduction of Fourier transform infrared spectrometers. This instrument generates an interferogram from which an absorbance versus frequency spectrum is obtained by the well-established mathematical process of Fourier transformation. The method has led to an improvement in the quality of infrared spectra (i.e. the signal to noise ratio, S/N) and the time required to obtain data. Liquids, solutions, pastes, powders, films, fibres, gases and surfaces can all be examined by a judicious choice of sampling technique. Biological systems such as proteins, peptides, lipids, biomembranes, carbohydrates, pharmaceuticals, foods and both plant and animal tissues have also been successfully characterised by using infrared spectroscopy [131].

FTIR spectroscopy is based on the interference of radiation between two beams of offset pathlength to yield an interferogram. The two domains of distance and frequency are interconvertible by the mathematical method of Fourier transformation. The basic components of an FTIR spectrometer are shown in (Fig. 6.1). The radiation emerging from a source is passed through an interferometer before passing through the sample to a detector. After amplification of the signal, in which high-frequency contributions have been eliminated by a filter, the data are digitised and then Fourier transformed [131].

Due to the large number of atoms in a protein and its solvent there is a large overlap of signals resulting in a (absolute) spectrum consisting of only a few broad bands. Such a spectrum yields valuable information at the level of secondary structure but interpretation at the level of individual bonds is usually not feasible. A useful strategy to overcome this problem is difference spectroscopy. Where a spectrum is obtain by subtraction of the spectra of a protein in two different states. The resulting

difference spectrum shows signals only due to the structural changes associated with the state change since the bulk of the protein signals are unchanged.

Reduced *minus* oxidised FTIR difference spectra of redox-active proteins can be obtained either photochemically or electrochemically. In this study the technique of photochemically induced FTIR redox difference spectroscopy was used, which has also been applied to cytochrome *c* oxidase [132]. The equivalent technique of electrochemically-induced FTIR redox difference spectroscopy has been applied to the bc_1 complex from *Rb. capsulatus* [127], cytochrome bo_3 [133], cytochrome *b*559 [134], myoglobin and haemoglobin [135], and cytochrome *c* oxidase [136]. These techniques are comparable to light *minus* dark FTIR difference spectroscopy, which has been applied to photosystem I and II [137], bacteriorhodopsin [138], rhodopsin [139], cytochrome *b*559 [134], the bacterial reaction center [140-145], and proteins with photolysable ligands, e.g. cytochrome *c* oxidase [146].

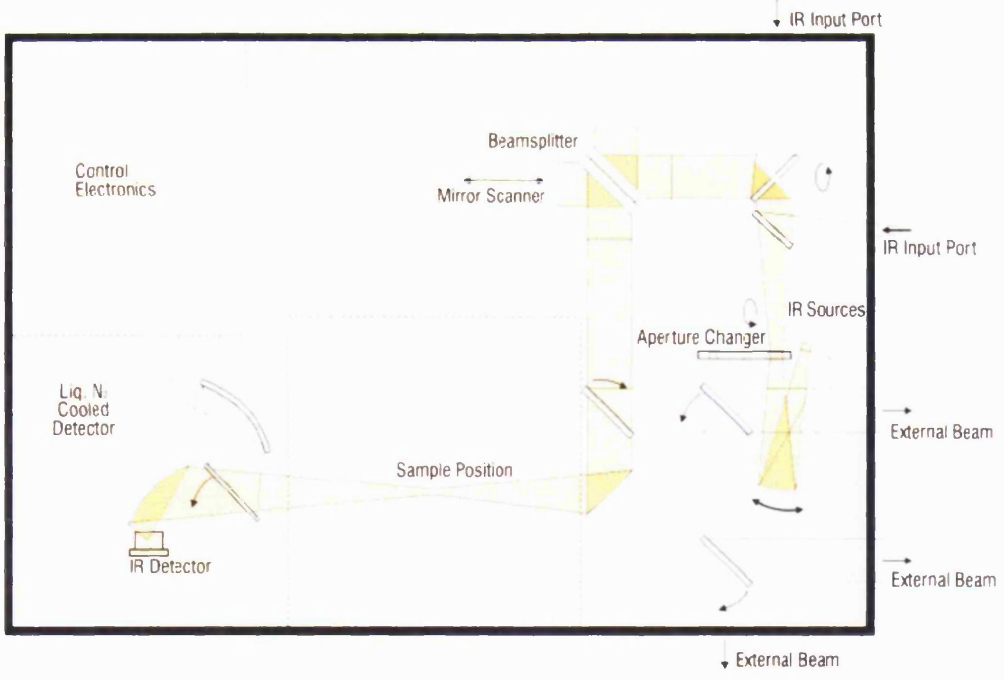

Fig. 6.1. The Brüker IFS 66/S FTIR spectrometer optical layout. The figure was reproduced from the Brüker manual.

6.1.2 Interpretation of FTIR spectra

The infrared spectrum can be divided into three regions: the far-infrared (<400cm^{-1}), the mid-infrared (4000-400cm^{-1}) and the near-infrared (15000-4000cm^{-1}). Proteins have absorbances mainly in the mid-infrared region. Generally, there are few bands in the region between 4000 and 1800cm^{-1} but many bands below 1800cm^{-1}.

The assignment of protein bands in FTIR difference spectroscopy is a laborious task. However, there are a number of approaches, which have aided the process such as H/D exchange, global isotopic substitution with ^{13}C or ^{2}H and genetic engineering, which has enabled researchers to assign single amino acid vibrations. In a promising approach, individual amino acids are isotope labelled in a site-specific way [147].

6.1.2.1 Amide I and II

The amide I (between 1700-1600cm^{-1}) and amide II (1570-1549cm^{-1}) bands are the most prominent features of the absolute and difference spectra of proteins. The amide I band represents 80% of the C=O stretching vibration of the amide group (coupled to the in-phase bending of the N-H bond and the stretching of the C-N bond). The amide II band represents mainly N-H bending (60%), with some C-N bond stretching (40%). It is generally accepted that the shape of the bands reflects the composition of secondary structure elements [130, 131, 148-150]. Deconvolution of the amide I band (absolute spectrum) is the most useful for the analysis of the secondary structure of proteins in aqueous media [148, 149]. The position of the amide II band is sensitive to deuteration, shifting from around 1550cm^{-1} to a frequency of 1450cm^{-1} when deuterated [127, 130, 131]. In addition, it is also sensitive to temperature and pH [151]. Water absorbs strongly in the amide I region,

distorting the ratio of amide I to II (in the absolute spectrum). By using a concentrated sample, the interference from water can be minimised. Changes in the amide signals in difference spectra indicate changes in the geometry of the protein backbone due to localised conformational changes [127].

6.1.2.2 Amino acid side chains

Some characteristic side-chain infrared frequencies of amino acids are summarised in Table 6.1. A more comprehensive list has recently been published by *Barth* (2001) [152].

Table 6.1. Overview of amino acid side chain infrared bands

Amino acid	Wavenumber (cm^{-1})	Assignment
Alanine	1465	CH_2 bending
Valine	1450	CH_3 asymmetric bending
Leucine	1375	CH_3 asymmetric bending
Serine	1350-1250	O-H deformation
Aspartic acid	1716-1788 (COOH)	C=O stretching
	1574-1579	CO_2^- asymmetric stretching
	1402	CO_2^- symmetrical stretching
Glutamic acid	1712-1788 (COOH)	C=O stretching
	1556-1560	CO_2^- asymmetric stretching
	1404	CO_2^- symmetrical stretching
Asparagine	1650	C=O stretching
Glutamine	1615	NH_2 bending
Lysine	1640-1610, 1550-1485	NH_3^+ deformation
	1160,1100	NH_3^+ rocking
Phenylalanine	1602, 1450, 760, 700	Ring vibrations
Tyrosine	1600, 1450 (protonated)	Ring vibrations
	1516-1518	CC vibrations, CH bending

The assignments were obtained from *Stuart* (1997) [131] and *Barth* (2001) [152].

6.2 Methods

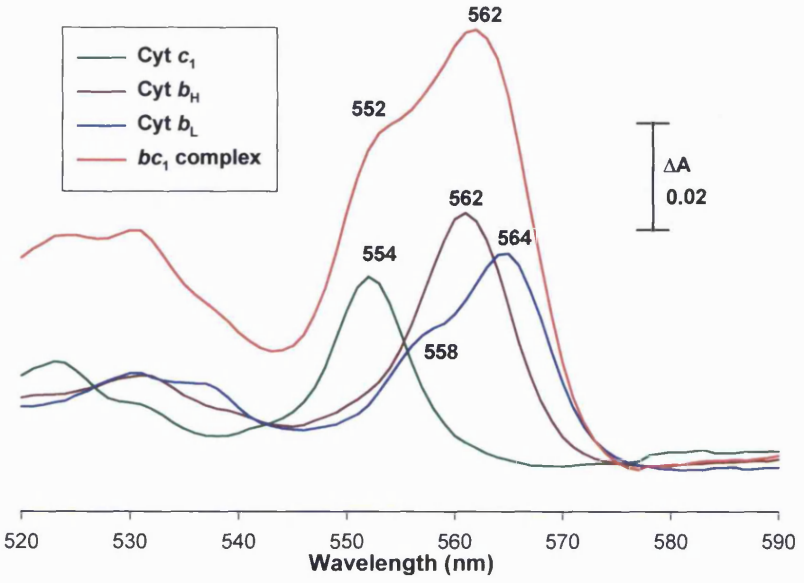

Fig. 6.2. Reduced *minus* oxidised difference spectra of bovine bc_1 complex cytochromes. Experimental conditions are as described in Section 6.2.1. The optical spectra of FTIR samples were recorded before and after FTIR measurements using a single beam spectrophotometer adapted for use with samples in CaF_2 windows. This allowed for direct comparison of FTIR and visible difference spectra in the same sample and for quantitation of the level of reduction of individual species.

6.2.1 Optical difference spectroscopy of the redox components of the bc_1 complex

Optical spectra of the redox components of purified Triton-prepared bc_1 complex are shown in Fig. 6.2. The spectra were taken using a single beam spectrophotometer built in-house. The final concentration of the bc_1 complex was 2.8μM. A grain of sodium ascorbate was added to obtain the difference spectrum of cytochrome c_1, the addition of 100μM duroquinol (final concentration) to the same sample resulted in cytochrome b_H difference spectrum and subsequent addition of a grain of sodium dithionite gave the cytochrome b_L difference spectrum. The full bc_1 complex spectrum is the difference of sodium dithionite reduced *minus* oxidised

spectrum. The optical spectra of FTIR samples were recorded before and after FTIR measurements using a single beam spectrophotometer adapted for use with samples in CaF_2 windows. This allowed for direct comparison of FTIR and visible difference spectra in the same sample and quantitation of the level of reduction of individual species.

6.2.2 Sample preparation

The FTIR study was carried out using Cholate and Triton-prepared bc_1 complex. The enzymes were prepared according to the methods described in Chapter 2. An aliquot of the enzyme was thawed and concentrated for 2hrs at 4°C in a 2 or 6ml Vivaspin concentrator to a final optically determined concentration typically around 400-470μM for bc_1 complex and 130-200μM for the cytochrome c_1 sub-complex. Horse heart cytochrome *c* and turnip cytochrome *f* were obtained from Sigma. Crude lettuce cytochrome b_6f complex was prepared as described in *Hurt et al.* (1981) [153].

The optimal conditions for obtaining photochemical redox spectra of the different proteins are listed in Table 6.2. An aliquot of the concentrated enzyme solution and FMN were placed on a CaF_2 window, together with reagents shown in Fig. 6.3. The mixture was partially dried under argon and then re-hydrated with 1-2μl 0.1M Tricine NaOH buffer pH 8.5 or 0.2M HEPES buffer pH 8.5. A second CaF_2 window was placed on top and the windows were squeezed until the sample had spread to an optimal absorbance of around 1.0 at the $1650cm^{-1}$ peak (absolute spectrum). The rim between the two windows was then sealed with silicon grease. Control samples of reagents in the absence of protein were made in a similar manner to allow their FTIR changes to be distinguished from those of the protein.

Table 6.2. Characterisation of optimal conditions for obtaining photochemical redox spectra of specific redox centres

Protein	Prot:FMN (nmol: nmol)	Illum. (s)	Reagents (nmol)	Comments
Cyt *c*	38:40*	30	-	*PMS used as the photoreductant in HEPES buffer
Cyt *c*	1:8	120	-	3min illumination in total
Cyt *f*	1.2:1	10	Ferricyanide (3)	-
Cyt *f* + ISP	3:10	10	Ferricyanide (3)	Crude preparation
SCR Cyt c_1 + ISP	2:2	20	Ferricyanide (6) 5µl of 10% w/v dodecyl maltoside	Illumination time adjusted depending on the state of ferricyanide reduction. HEPES buffer used.
Cyt c_1 + ISP	4:1	20	Ferricyanide (6)	Again illumination time adjusted depending on the state of ferricyanide reduction
Cyt c_1 sub-complex	1.3:1	10	Ferricyanide (2)	Glycerol removed with G25 column
Cyt c_1 + Stigmatellin	4:1	20	Ferricyanide (6) and stigmatellin (5)	Again illumination time adjusted depending on the state of ferricyanide reduction
Cyt b_H	4:1	15	Ferrocyanide (6-7)	Cyt b_H unusually reduced by sodium ascorbate in this system
Cyt b_L	4:2.5	5	Sodium ascorbate (10)	Protein resolubilised in 10% w/v dodecyl maltoside. Sodium ascorbate added to pre- reduce all other components
bc_1 complex	4:0.2	25	Ferricyanide (8) and 2µl of 10% w/v dodecyl maltoside	Protein resolubilised in 10% w/v dodecyl maltoside solution. Spectra of all redox components obtained with successive 25s illumination of the same sample

Prot:FMN refers to the ratio of protein to FMN added to the CaF_2 window. The amount of reagents added to the sample is given in the brackets. Tricine buffer and Triton-prepared purified bc_1 complex used unless specified otherwise; Illum. illumination time; Prot, Protein; SCR, succinate cytochrome *c* reductase; Cyt, cytochrome; ISP, 'Rieske' iron-sulphur protein.

The conditions for selective reduction of specific components are depicted in Fig. 6.3. Illumination of samples containing ferricyanide alone resulted in both cytochrome c_1 and 'Rieske' ISP reduction; those containing stigmatellin and ferricyanide resulted in cytochrome c_1 only reduction; those containing ferrocyanide resulted in cytochrome b_H reduction; those containing sodium ascorbate resulted in cytochrome b_L reduction. For enzyme-inhibitor samples, 5nmol of antimycin A or 5nmol of AG204 were added to the concentrated enzyme solution. Successive controlled illumination of samples containing ferricyanide alone can also be used to successively reduce different components of the bc_1 complex.

6.2.3 FTIR difference spectroscopy

Infrared spectra were recorded on a Brüker IFS 66/S FTIR spectrometer (Fig. 6.1) equipped with a liquid nitrogen cooled MCT-A detector selected for high sensitivity and purged with dry CO_2 free air. The samples were illuminated with a 100W quartz lamp via a light pipe. The FTIR cell was water-thermostatted at 288K. Typically, 300 interferograms at $4cm^{-1}$ resolution were averaged over 20s to provide an initial baseline in the dark and after a 5s wait the recording was repeated in order to provide an indication of sample baseline drift. The light was then switched on for typically 15s and after the light has been switched off, the recording was repeated. After a 5s dark relaxation the recording was again repeated to provide an indication of sample stability and relaxation rate. Finally, the state of reduction of the complex was determined by visible spectroscopy to establish which components had reduced.

6.3 Results and discussion

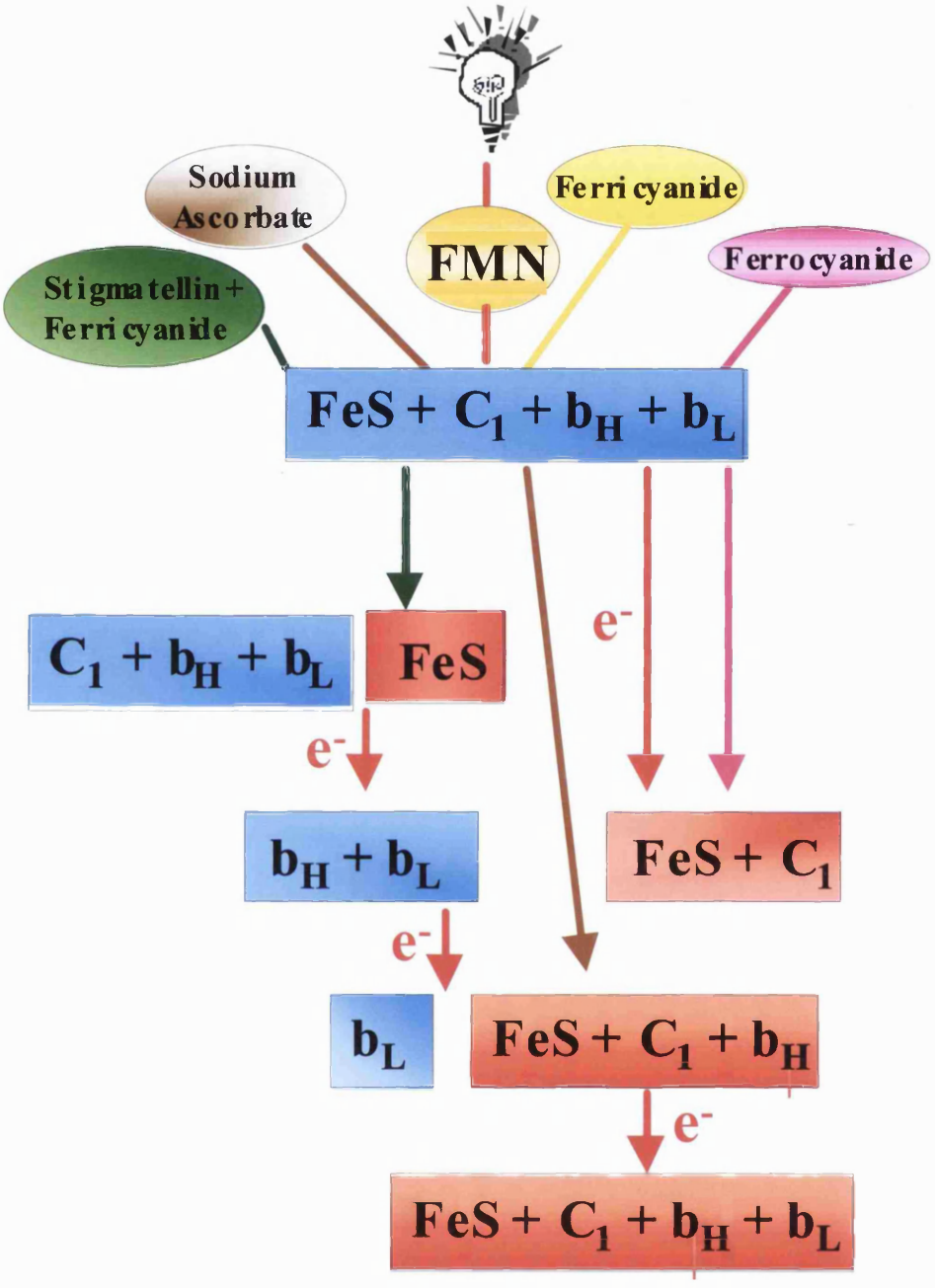

Fig. 6.3. Isolation of FTIR redox difference spectra of the redox components of bc_1 complex flowchart. The light bulb represents a light source. Blue boxes indicate an oxidised state. Red boxes indicate a reduced state. Brown, pink, and green arrows indicate the effect of respective compounds on the fully oxidised bc_1 complex: ferricyanide to keep the 'Rieske' protein and cytochrome c_1 oxidised; stigmatellin to pre-reduce and immobilise the 'Rieske' protein; ferrocyanide to pre-reduce the 'Rieske' protein, and cytochrome c_1 and sodium ascorbate to leave only the b_L haem oxidised. Red arrows and electrons indicate illumination of sample.

6.3.1 Optimisation of conditions

Only the prosthetic groups and a small number of amino acids residues out of a total of about 4000 undergo IR detectable changes upon photochemical reduction of the bc_1 complex. The amplitude of the changes in the reduced *minus* oxidised difference spectrum are less than 1% of that of the absolute spectrum (Fig. 6.4 compared to Fig. 6.8). For this reason and the fact that water has a strong absorbance in the amide I and II regions, FTIR requires a small volume (5-10μl) of highly concentrated (400-470 μM) protein sample to achieve a high signal to noise ratio. The sample has to be dried down carefully, so that biological activity is retained and background water interference is kept to a minimum. However, the detergent Triton X-100 and glycerol, which are present in the purified bc_1 complex, also interfere as they have IR absorbances and also prevent adequate concentration of the protein. Hence, the amounts of both glycerol and Triton X-100 were reduced whilst concentrating the protein using a 'Vivaspin' concentrator. As a result, the contribution of both substances to the absolute spectrum was reduced and so was background water interference (Fig. 6.4). The SCR preparation contained Cholate, which has IR absorbtion in the protein region. The bands in the amide I and II regions of the Cholate absolute spectrum are largely due to background water interference. Cholate at low concentrations does not present any problems in drying the sample down and causes little distortion of the ratio of protein absorbtions in the amide I and II regions (of the absolute spectrum).

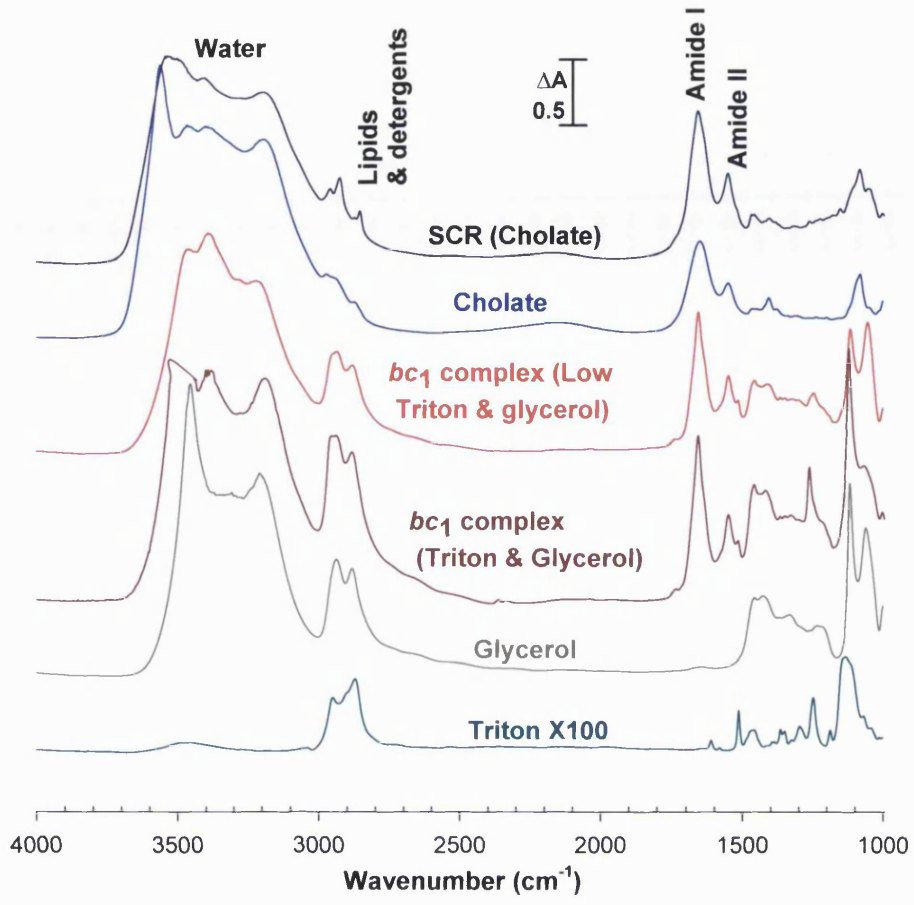

Fig. 6.4. The effects of detergents and glycerol on the absolute FTIR spectra of bc_1 complex at 288K and pH 8.5. Cholate at low concentration causes a slight distortion of the ratio of protein absorptions in the amide I and II regions. The bands in these regions of the Cholate absolute spectrum are largely due to background water interference. Glycerol (grey) and Triton X-100 (cyan) have IR absorbances and also prevent adequate concentration of the protein. Therefore, in the bc_1 complex (Triton & glycerol) absolute spectrum shown in dark red, background water interference distorts the ratio of protein absorptions in the amide I and II regions. This is evident from the signal amplitude of the redox difference spectra. Upon removal of a large amount of both substances using a 'Vivaspin' concentrator, background water interference is reduced and so is the contribution of both substances to the absolute spectrum shown in red. The SCR sample contained 2nmol protein and 2nmol FMN in 0.2M HEPES buffer. The Triton-prepared purified bc_1 complex sample contained 4nmol protein and 2nmol FMN in 0.1M Tricine/NaOH buffer. 100% glycerol or 100% Triton X-100 with no other additions were used to obtain their respective absolute spectra. 1M Cholic acid dissolved in distilled water was used to obtain the Cholate absolute spectrum. Refer to Methods for experimental conditions.

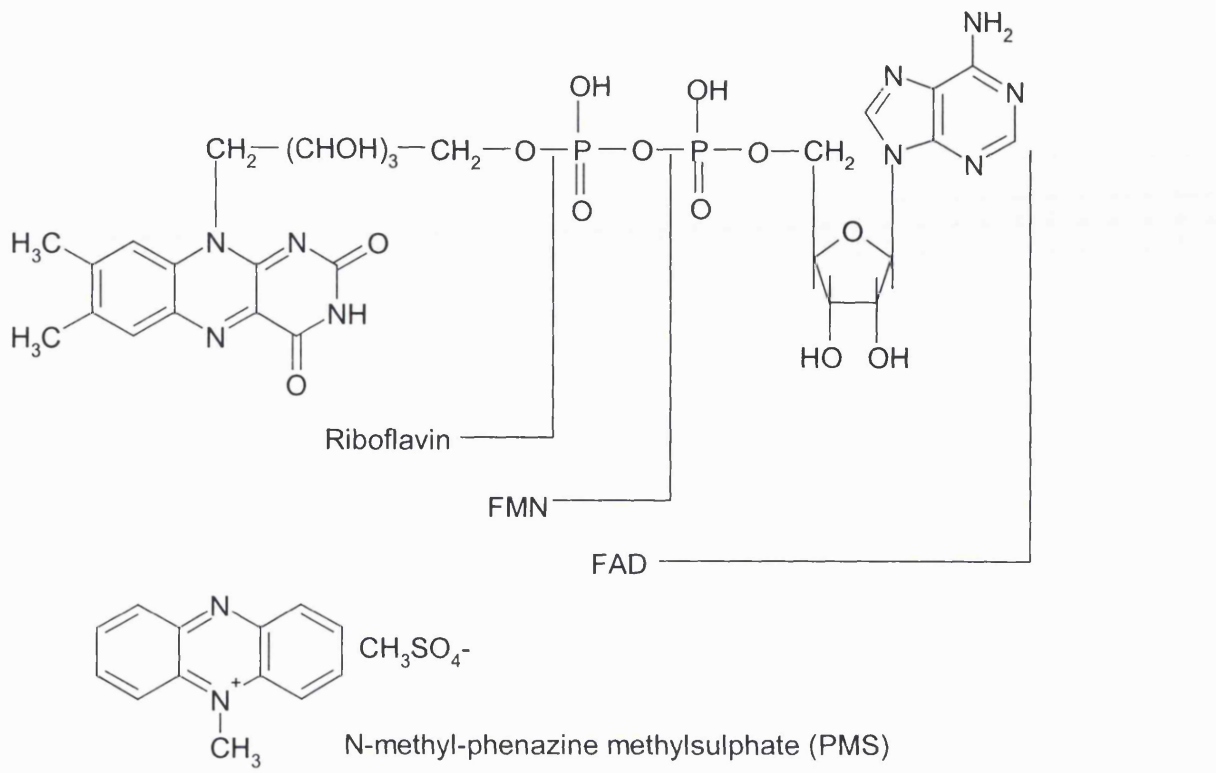

N-methyl-phenazine methylsulphate (PMS)

Fig. 6.5. Structures of flavins and phenazine methylsulphate (PMS). FMN, flavin mononucleotide; FAD, flavin adenine dinucleotide.

6.3.1.1 Photochemicals

Since the FTIR sample is sealed, quantitative reproducibility is hard to achieve between different samples. Other factors that require optimisation include choice of a suitable photoreductant (Fig. 6.5, Phenazine methosulphate (PMS), flavin mononucleotide (FMN), flavin adenine dinucleotide (FAD), or hexamine ruthenium chloride), with respect to, its ability to reduce all components with short illumination times, limited or no dark reduction 'leak' rate and lack of IR interference in the region of interest. Due to the baseline drift associated with FTIR measurements the illumination time was kept below 30s whilst varying the amount of photoreductant added. After illumination with different amounts of photoreductant for specific periods of time, the state of reduction of the complex was monitored by visible spectroscopy to establish which components had reduced. Since photoreductants could also absorb IR

and have IR redox difference spectra in the region of interest, the photoreductant was kept to a minimum to avoid interference in the difference spectrum.

Five photochemicals were tested (Table 6.3), Hexamine ruthenium chloride was incapable of reducing any of the proteins used in this study. PMS and phenazine ethosulphate (PES) were effective in photoreducing cytochrome *c* prepared in Tricine buffer (Table 6.2) but required long illumination time in order to reduce the high-potential components and were incapable of reducing the low-potential components. Deazoflavin behaved similarly but was not tested with cytochrome *c*.

Table 6.3. The effectiveness of photochemicals at reducing redox components

Photochemicals	Result
PMS PES	Only the high-potential components were reduced with long illumination times, typically 1min
Hexamine ruthenium chloride	Incapable of reducing any of the redox components
Deazoflavin	Only the high-potential components were reduced and gave spectral interference
FMN	Reduced all components but gave spectral interference. Only reduced cytochrome *c* in Tricine buffer
FAD	Reduced all components but gave increased spectral interference compared to FMN

FMN and FAD were effective at reducing all redox components but could interfere in the region of interest. FAD was less effective at reducing the high-potential components and caused greater spectral interference in the reduced *minus* oxidised difference spectra than equivalent concentrations of FMN (results not shown). The mechanism of protein reduction by the flavins is similar to that discussed in detail by

Tollin et al. (1995) [154] and *Lübben et al.* (1996) [132] for cytochrome *c* oxidase reduction by riboflavin using EDTA as the electron donor (Fig. 6.6). The spectral interference by flavins is due to accumulation of the half or fully reduced states of flavin. The increased spectral interference with FAD may be due to its hydrophobicity in comparison to FMN, preventing it from reacting efficiently with its substrate resulting in accumulation of the half- or fully-reduced states of FAD.

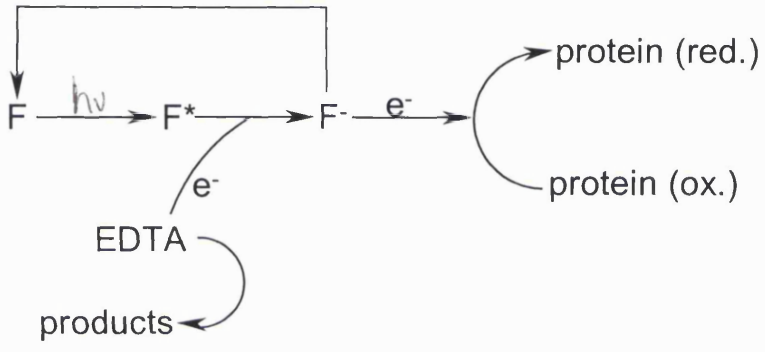

Fig. 6.6. Reaction scheme of the photoreduction mechanism with the caged electron compound riboflavin (F), simplified for the sake of clarity. The asterisk (*) represents the photoactivated state and the (-) sign indicates the uptake of an electron without further specification of the half or fully reduced states of riboflavin. More details about the reaction mechanism of flavin are given in [154, 155]. Light absorbtion leads to the formation of an activated state F* with a redox potential sufficient for extraction of electrons from the 'sacrificial' electron donor EDTA. The reduced form (for simplification symbolised as F⁻) could donate electrons directly to the protein. As long as EDTA is present in excess, the reduced form of riboflavin is continuously regenerated [132]. The scheme was reproduced from *Lübben et al.* (1996) [132].

FMN was the best photoreductant in terms of its ability to reduce all redox components with short illumination times. However, its own redox difference spectrum (Fig. 6.7) has strong features in the protein region of the bc_1 complex redox difference spectra (Fig. 6.8). The signal in the amide II region is particularly strong

due to its *v*NH bending modes. Major features in the redox difference spectra are around 1583, 1571, 1549 and 1517cm^{-1} (Fig. 6.7). In order to avoid FMN interference in the redox difference spectra, illumination time was increased and FMN ratio decreased to the amounts listed in Table 6.2.

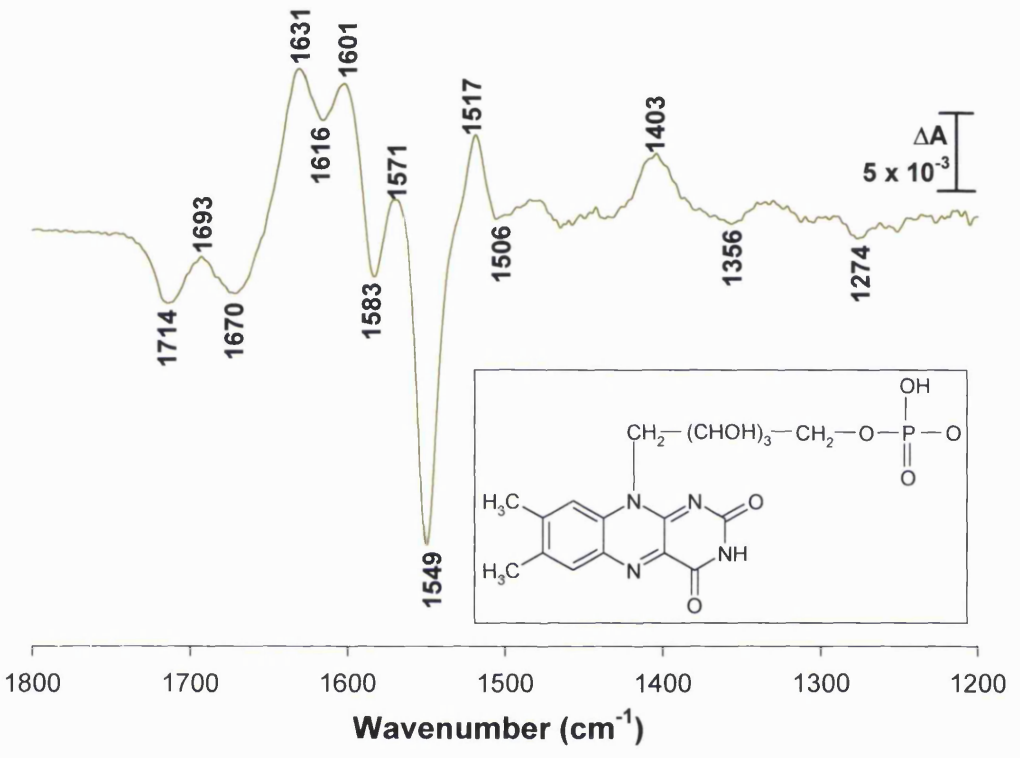

Fig. 6.7. Reduced *minus* oxidised FTIR difference spectrum of FMN at 288K and pH 8.5. Difference spectrum was obtained from a 1M FMN solution prepared in 0.2M HEPES buffer and recorded at 2cm^{-1} resolution. Inset shows the structure of FMN. Refer to Section 6.2.2 for experimental conditions.

Samples in Tricine/NaOH buffer were found to undergo better photoreduction and reduced FMN interference in the difference spectra in comparison to those in HEPES buffer. Previous studies have shown that in the presence of light Tricine efficiently reduces flavin photoactivated state to the half or fully reduced states of flavin [156].

For the high-potential components, reducing FMN concentration and increasing illumination times eliminated FMN interference. However, for the low-potential components this was not the case. In order to obtain adequate reduction of

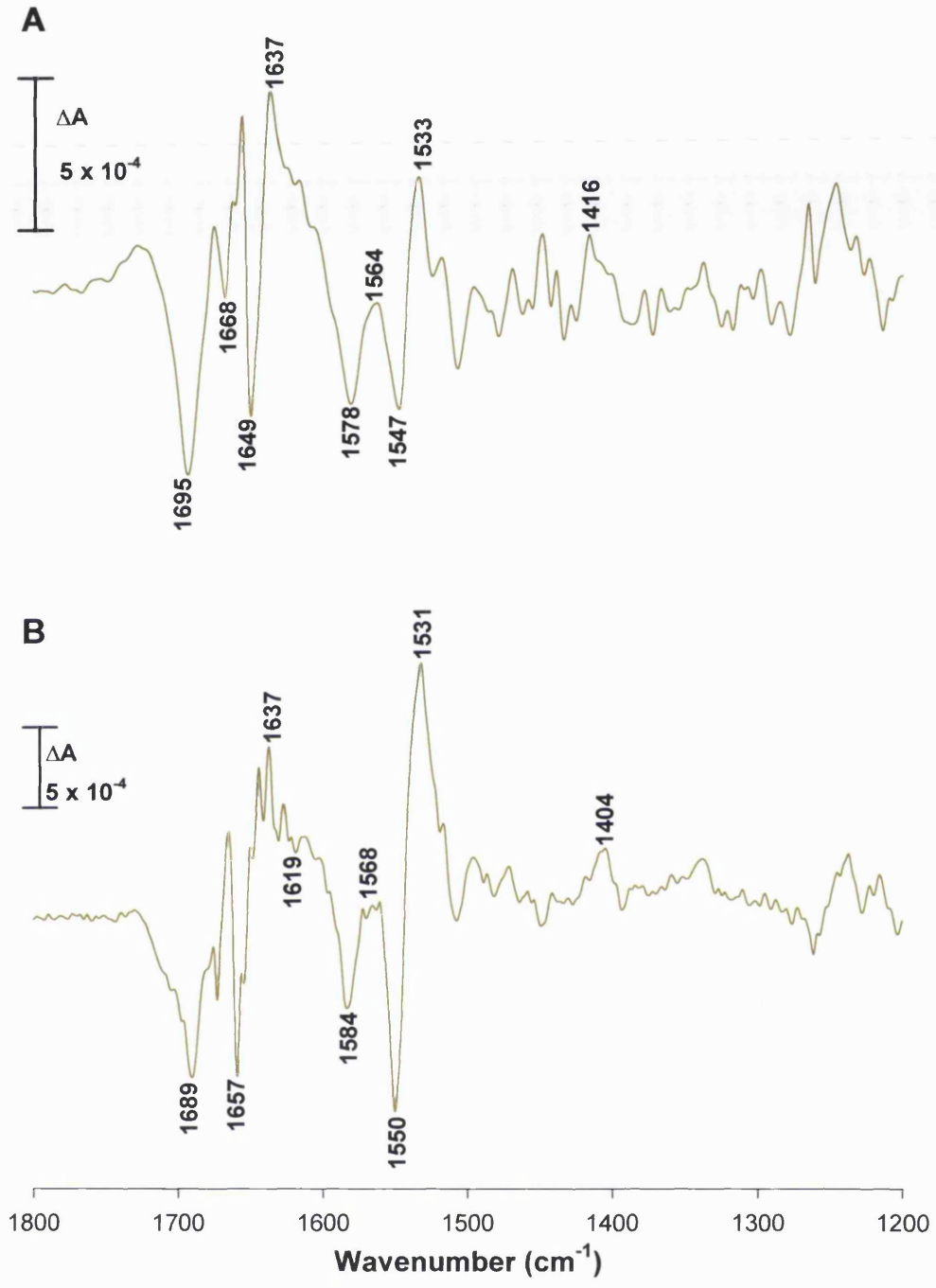

Fig. 6.8. Reduced *minus* oxidised FTIR difference spectra of cytochrome c_1 and 'Rieske' iron-sulphur protein at 288K and pH 8.5 with varying degree of FMN interference. A) Spectrum was obtained from Triton-prepared purified bc_1 complex. The sample contained 1nmol FMN and 1nmol protein in 0.2M HEPES buffer, and was illuminated for 10s. The spectrum was recorded at $4cm^{-1}$ resolution. **B)** Spectrum was obtained from SCR. The sample contained 10nmol FMN and 1nmol protein in 0.2M HEPES buffer, and was illuminated for 10s. The spectrum was recorded at $2cm^{-1}$ resolution. Refer to Section 6.2.2 for experimental conditions.

-cytochromes b_H and b_L at least 2nmol of FMN and 30s illumination were required. The addition of a redox mediator such as methyl viologen made no difference (result not shown). Resolubilising Triton-prepared bc_1 complex in 10% w/v dodecyl maltoside solution or the addition of up to 5µl of 10% w/v detergent solution to the sample was found to eliminate FMN interference. This presumably broke up the Triton X100 micelles, hence allowing cytochrome *b* reduction without accumulation of significant amounts of half or fully reduced states of FMN.

6.3.1.2 Dark reduction

Ferricyanide was added to prevent pre-reduction of the high-potential components in the dark. This was due to a combination of chemical reaction between the photochemical and the protein, endogenous reductants, and contamination by light during preparation, and optical and infrared measurements. IR absolute spectra of ferricyanide and ferrocyanide are at 2115 and 2039cm^{-1} respectively (Fig. 6.9), and could be used to monitor the level of ferricyanide reduction, hence allowing for control of the state of reduction of the high-potential components before illumination.

In order to achieve optimal cytochrome c_1 and 'Rieske' ISP redox spectra, a ratio of 2nmol of FMN to 2nmol SCR was used with illumination for typically 20s (Table 6.2). Under this condition without ferricyanide, up to 50% of cytochrome c_1 and 'Rieske' ISP undergoes reduction in the dark (results not shown). At least 6nmol of ferricyanide were required to keep the sample oxidised for an hour.

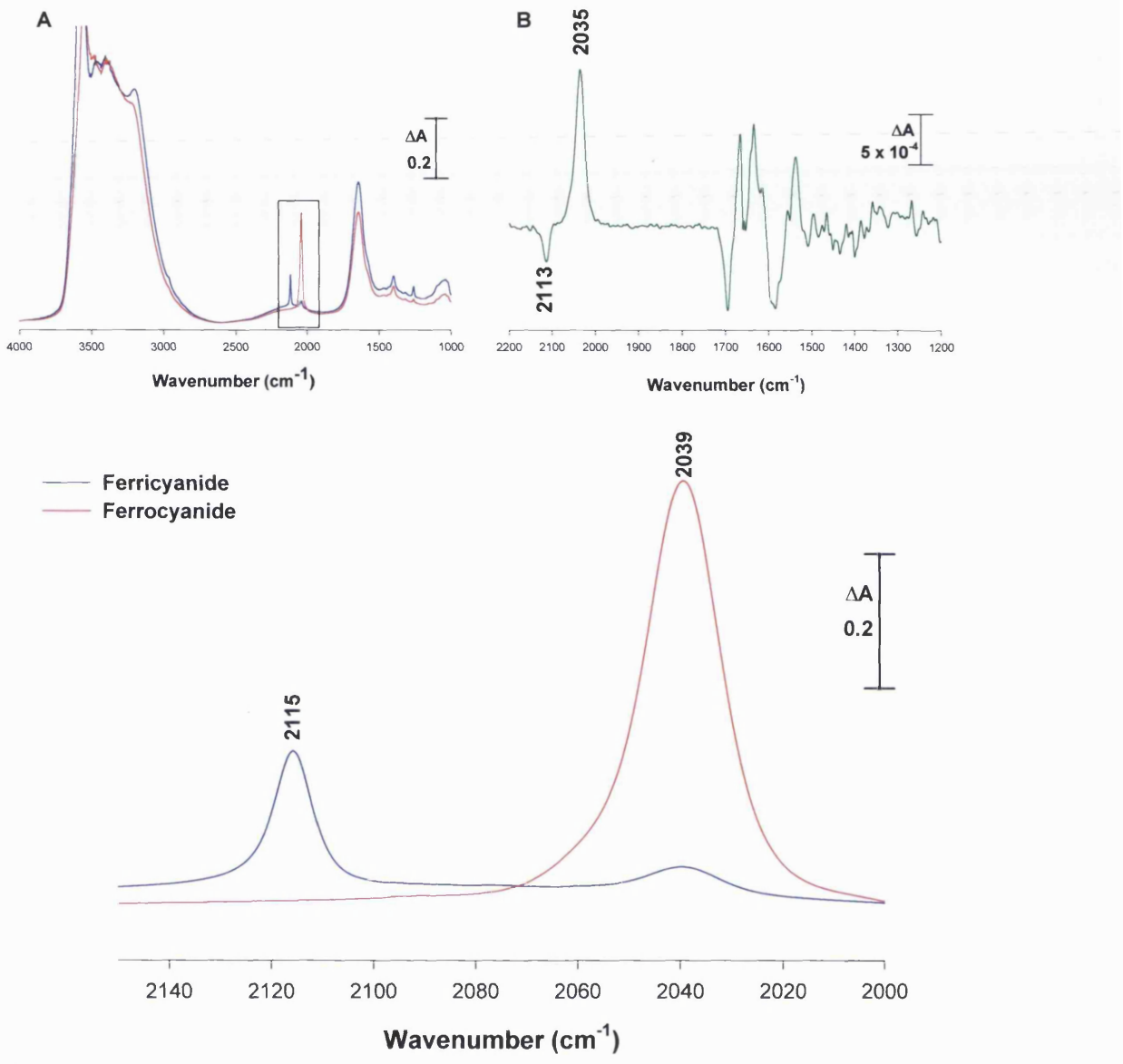

Fig. 6.9. Preventing the pre-reduction of the high-potential components in the dark: Absolute FTIR spectra of ferricyanide and ferrocyanide at 288K and pH 8.5. Ferricyanide was added to prevent pre-reduction of the high-potential components in the dark. IR absolute spectra of ferricyanide (blue) and ferrocyanide (red) were used to monitor the level of ferricyanide reduction by recording dark *minus* dark difference spectra of the sample during the 1hr equilibration period. Left inset shows the absolute spectra of ferri- and ferrocyanide from 4000-1000cm^{-1}. Right inset shows reduced *minus* oxidised difference spectrum of cytochrome c_1 and the 'Rieske' iron-sulphur protein in Triton-prepared purified cytochrome bc_1 complex, showing negative ferricyanide signal at 2113cm^{-1} and positive ferrocyanide signal at 2035cm^{-1}. The sample contained 1M ferri- or ferrocyanide in 0.1M Tricine buffer. Refer to Section 6.2.2 and Table 6.2 for experimental conditions.

6.3.2 Cytochrome *c* as a model system

Redox FTIR difference spectra of cytochrome *c* have been studied and the majority of the bands assigned (Fig. 6.10) [130, 151]. In these studies, redox changes were induced electrochemically, in contrast to the present work, in which the changes were induced photochemically. The photochemical technique was evaluated by comparison of spectra obtained by both methods.

Horse heart cytochrome *c* was photochemically reduced with PMS or FMN. Redox difference spectra obtained were comparable to each other (Fig. 6.11) and to those obtained by the electrochemical method (Fig. 6.10). The positions of most of the signals in the two photochemical spectra were the same. However, large differences in their relative amplitude were observed, leading in some cases to the masking and/or disappearance of some IR signals. These differences was also noted by *Schlereth et al.* (1993) [151], upon investigating the influence of temperature, pH and electrode surfaces on reduced *minus* oxidised FTIR difference spectra of horse heart cytochrome *c*. Cytochrome *c* is known to exist in two conformational states, a native and an alkaline state [151, 157]. Schlereth et al. (1993) concluded that the thermal and pH induced dependence of the redox difference spectra reflect transition of ferricytochrome *c* from the native to the alkaline states. They further proposed that the influence of the electrode surface on the redox difference spectra arise from the different nature of the interaction between the protein and the promoter molecules adsorbed on the electrode surface [151]. The differences evident in the redox difference spectra presented here (Fig. 6.11) are likely to arise from the different nature of the interaction between the protein and the photoreductants, FMN and PMS.

A comprehensive assignment of horse heart cytochrome *c* redox difference spectra have been described by *Moss et al.* (1990) [130] and *Schlereth et al.* (1993)

[151]. The most prominent features of the spectra are the amide I (1700-1664cm^{-1}) and amide II (1570-1549cm^{-1}) bands [130]. The broad negative signal at 1581cm^{-1} is more prominent in the FMN spectrum than the PMS spectrum. Its amplitude is very sensitive to temperature, pH and electrode surfaces, often absent at low temperature/acidic pH and emerging at high temperature/alkaline pH [151]. Its position and amplitude is also influenced by the electrode surface used in the electrochemical cell [151]. As noted previously, FMN spectral interference can occur in this region and is indicated by very sharp negative signals around 1583 and 1549cm^{-1} (Fig. 6.7-8). However, the lack of such signals in the FMN reduced cytochrome *c* spectrum shows that no half- or fully-reduced states of FMN are accumulating and precludes the assignment of the negative band at 1581cm^{-1} to FMN. Another characteristic feature of the cytochrome *c* spectrum is the sharp apparent differential at 1518cm^{-1}, due to tyrosine ring C=C stretching [130]. Other features include the haem propionates (1693cm^{-1} and 1550-1610cm^{-1}) stretching, and lysine NH_3^+ deformations (1542cm^{-1}).

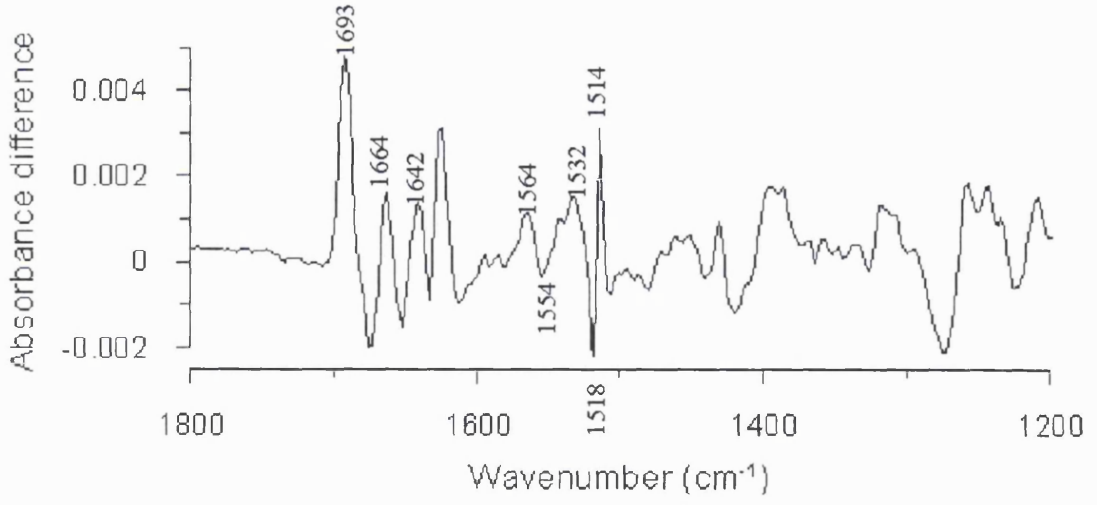

Fig. 6.10. Electrochemically induced reduced *minus* oxidised FTIR difference spectrum of horse heart cytochrome *c*. Cytochrome *c* was prepared in 50mM potassium phosphate pH 7 buffer. For detail experimental conditions refer to *Moss et al.* (1989) [130]. The figure was reproduced from *Moss et al.* (1989) [130].

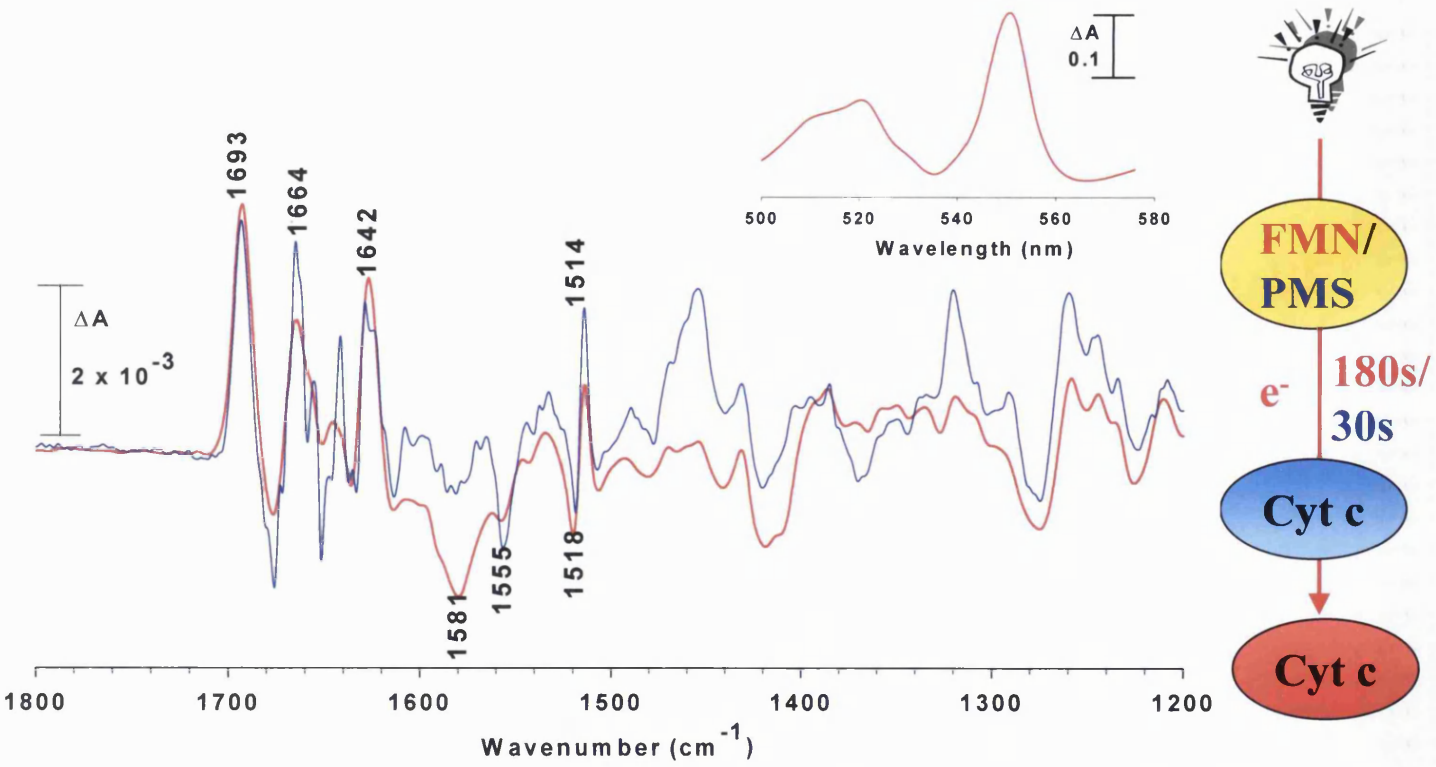

Fig. 6.11. Reduced *minus* oxidised FTIR difference spectra of horse heart cytochrome *c* photochemically reduced by FMN (red) or PMS (blue) at 288K and pH 8.5. FMN (8nmol) reduced cytochrome *c* (1nmol, in 0.1M Tricine buffer) spectrum (red), was recorded at 4cm^{-1} resolution and the PMS (40nmol)-reduced protein (38nmol, in 0.2M HEPES buffer) at 2cm^{-1} resolution (blue spectrum). Only a fraction of the cytochrome *c* present was reduced by PMS. Inset shows the optical spectrum of reduced cytochrome *c* and a scheme of the reduction of cytochrome *c* using either FMN or PMS and indicating the illumination time. Red oval indicates reduced state. Blue oval indicates oxidised state. Red arrow indicates flow of electrons. Light bulb represents a light source. Refer to Section 6.2.2 and Table 6.2 for experimental conditions.

6.3.3 General features of the bc_1 complex IR difference spectra

Spectra of individual redox components of the bc_1 complex were generally recorded from different samples as shown in Fig. 6.3. However, under some conditions (Table 6.2), high S/N spectra can be obtained from the same sample by successive 25s illumination as shown in Fig. 6.12. The first 25s illumination resulted in the reduction of cytochrome c_1 and 'Rieske' ISP, the second in the reduction of cytochrome b_H and the third in the reduction of cytochrome b_L. These spectra, as expected, are the same as the spectra of individual redox components obtained from different samples. In addition, these spectra are also similar to the spectra obtained with the *Rb. capsulatus* bc_1 complex [127]. The differences between the spectra of the bovine (presented here) and that of the bacterial enzyme are most likely due to differences in the structure and sequences of the two enzymes.

6.3.3.1 Amide I and II

The difference spectra of redox components of the bc_1 complex (Fig. 6.12) show large signals in the 1700-1610cm^{-1} and in the 1575-1480cm^{-1}, amide I and II spectral regions. The amide I bands arises from C=O stretch vibrations of the protein backbone (notably 1690cm^{-1} turns and bends, and 1660-1650cm^{-1} for α-helical structures [131, 134, 149]). The signals in this region are narrow in the redox spectra of all cofactors. In addition, at a maximum ΔA (peak to trough) of around 0.003 they are several orders of magnitude smaller than the absolute spectrum, which has an absorbance of around 1.0 at the 1656cm^{-1} amide I/water peak in these samples (of which 50% is attributable to protein absorbance) [146]. This is in agreement with a previous FTIR study of the *Rb. capsulatus* bc_1 complex [127]. The smallness and

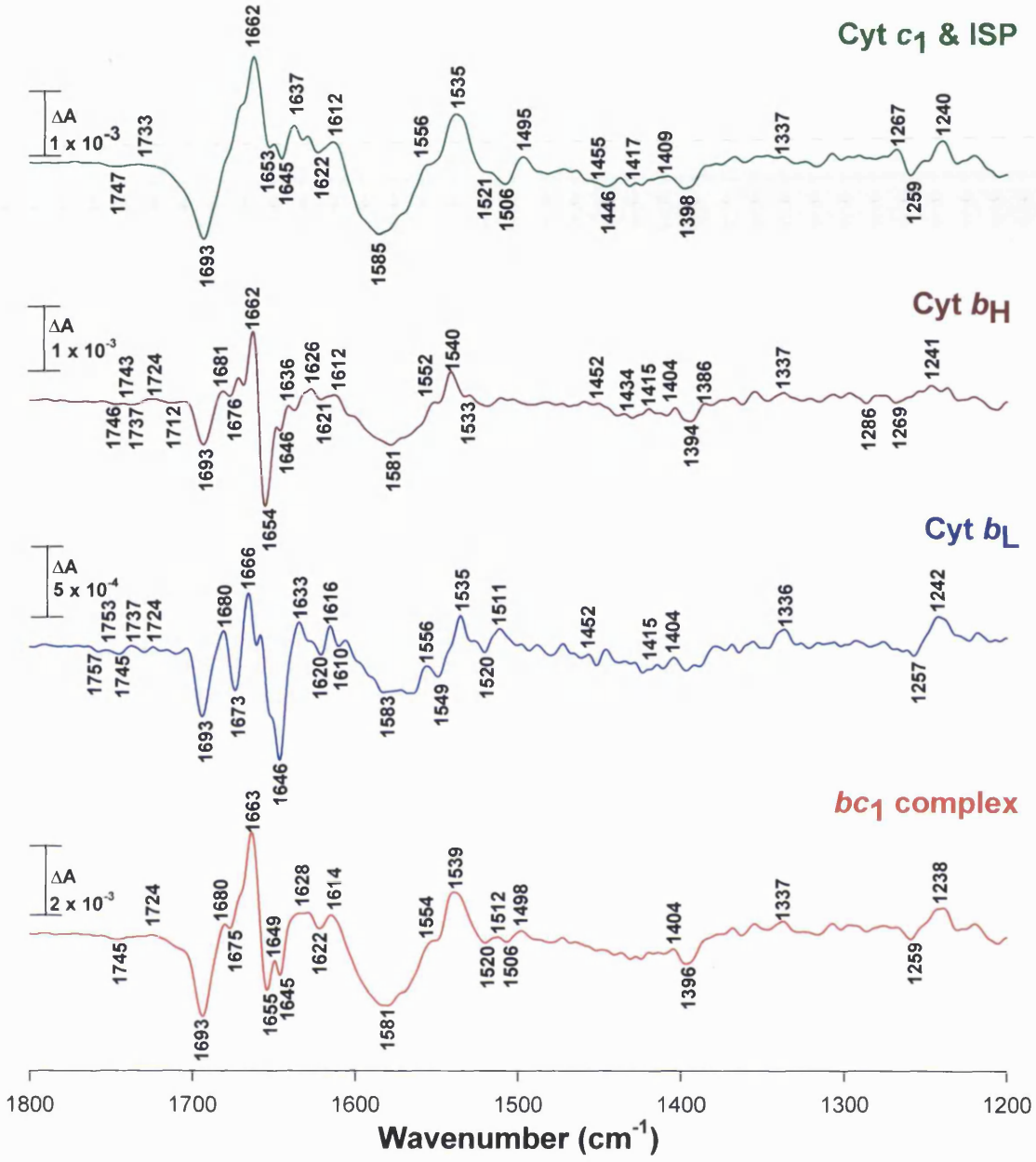

Fig. 6.12. Time course reduced *minus* oxidised FTIR difference spectra of bc_1 complex and its redox components at 288K and pH 8.5. The spectra were generated from successive 25s illumination of the same sample. The first 25s illumination resulted in the reduction of cytochrome c_1 and 'Rieske' ISP, the second in the reduction of cytochrome b_H and the third in the reduction of cytochrome b_L. The bc_1 complex spectrum is the sum of the three redox component spectra and it's the same as the spectrum obtained from a full reduction of the enzyme (result not shown). Sample contained 4nmol protein (resolubilised in 10% w/v dodecyl maltoside), 0.2nmol FMN, 8nmol ferricyanide and 2μl of 10% w/v dodecyl maltoside in 0.1M Tricine buffer. Refer to Section 6.2.2 for experimental conditions.

-sharpness of the amide I (1700-1610cm^{-1} region) bands indicates that changes in the conformation of the protein backbone are small, localised and redox linked [127]. Besides amide I and II signals, haem and ubiquinone modes can absorb in this spectral region.

In the cytochrome *c* difference spectra (Fig. 6.10-11) the maximum at 1693cm^{-1} was tentatively assigned to the vibrations of a protonated haem propionate in reduced cytochrome *c* [130]. In all the difference spectra (Fig. 6.12) a negative signal at 1693cm^{-1} is present. If this signal were a haem propionate it would mean that protonation of the propionate occurs during the oxidation of the haem. This, however, is highly improbable for reasons of electrostatic interaction energy. Therefore, this signal is most probably not due to protonation of propionates, but rather to amide I vibrations [127].

The 1575-1480cm^{-1} region arises from amide II, a coupled mode of the C-N stretch and N-H bending vibration of the protein backbone. However, haem C=C modes from the porphyrin (at 1540cm^{-1}), ubiquinone modes and aromatic amino acid vibrations also occur in this region [133]. Antisymmetric COO- modes from deprotonated haem propionates and aspartic or glutamic acid side chains, caused by protonation/deprotonation of COOH groups, may also contribute here. FMN interference could also occur in this region. However, the lack of the characteristic sharp negative signals at around 1583 and 1549cm^{-1} (Fig. 6.7-8) in any of the difference spectra precludes such an FMN contribution. The broad 1581-87cm^{-1} vibration mode found in the difference spectra (Fig. 6.12) likely represents amide II signal. The amide II signals arising from different secondary structures appear in the same range of frequencies, in contrast to amide I signals, leading to extensive overlapping of the signals [149].

6.3.3.2 Haem signals

The difference spectra of each haem and its protein environment show positive signals at about 1554-58cm^{-1} and 1535-40cm^{-1} (Fig. 6.12). They can be assigned to the C_aC_m and C_bC_b haem stretch vibrations by comparison with redox difference spectra of model compounds [127, 134]. The former signal at 1554-58cm^{-1} is overlapped by the broad amide II band at 1581-87cm^{-1}. The CαN haem stretch vibrations are present at 1404-09cm^{-1} in all the difference spectra (Fig. 6.12). Contributions of haem vinyl vibrations of the *b*- and *c*-type haems could tentatively be assigned to the positive signal at 1637-28cm^{-1} (vinyl $C_\alpha C_\beta$), 1612-16cm^{-1} ($C_\alpha C_\beta$ vinyl) and negative signal at 1140cm^{-1} (data not shown). The 1612-16cm^{-1} signals are slightly overlapped by amide II vibration centered at 1581-89cm^{-1}. In addition, contributions from amino acid side chains like glutamine, asparagine, histidine, tyrosine and arginine potentially overlap the haem vinyl vibration, provided that the extinction coefficients are strong enough, which makes histidine the less probable candidate [127]. There are other bands assigned to porphyrin skeletal and vinyl vibrational modes in the redox spectra of model compound [134], these include signals at 1455, 1415 and 1337cm^{-1}. There are equivalent bands in all the redox spectra (Fig. 6.12), which can be tentatively assigned to these vibrational modes. Contributions from C=O mode of propionic groups and haem formyl are usually found between 1700 and 1620cm^{-1} [146]. These signals are difficult to assign in these spectra (Fig. 6.12) because of the presence of amide I vibrations in this region.

6.3.3.3 Amino acid side chain signals

The absorption of amino acids side chains such as tyrosine, aspartic and glutamic acid, asparagine, glutamine and arginine are intense enough to be detectable in FTIR difference spectra [152, 158]. Histidine, lysine, tryptophan and proline show smaller extinction coefficients but they might be detected in some cases as well [127, 152, 158]. Vibrations of other amino acids side chains are not supposed to contribute to FTIR signals in the spectral range investigated here [127, 152, 158]. In most spectral regions side-chain signals are overlapped by signals of the protein backbone or the cofactors, making assignment difficult.

An exception is the C=O stretch vibration of protonated aspartic and glutamic acid side chains, absorbing above 1700cm^{-1}, where no other protein modes are expected [127]. Such signals are present in the redox difference spectra shown in Fig. 6.12. However, due to the S/N ratio in this region it is hard to distinguish whether these signals are symmetrical peak/trough signals or negative/positive signals, particularly in the cytochrome c_1 and 'Rieske' ISP spectra (Fig. 6.12). The most likely candidates for the C=O stretching vibrations absorbing above 1700cm^{-1} in all the difference spectra (Fig. 6.12) are conserved glutamic and aspartic acids present in the vicinity of the redox centres. A loss in the band at 1700cm^{-1} upon deprotonation of the side chain normally results in two bands at about 1620 and 1570cm^{-1} (antisymmetric COO^- mode), and about 1420-50cm^{-1} (symmetric COO^- mode). These difference signals are much more difficult to detect due to multiple overlap by other difference signals of the protein, e.g. the ν(CC), ν(CN) and δ(CH) modes from tryptophan [133, 159], amide II and other cofactors. However, there are signals in the redox difference spectra of cytochrome b_H and b_L, which can be tentatively assigned to these groups (Table 6.4). The ν(C=O) vibration of glutamic and aspartic acids are known to be

sensitive to their environment and hydrogen bonding, as a general rule, with shifts of approximately -50cm^{-1} observed upon formation of strong hydrogen bonds above 1740cm^{-1} [152].

Signals at 1740cm^{-1} have previously been observed in the FTIR redox difference spectra of quinone [133]. This signal was attributed to the detergent used to solubilise the quinone, sucrose monolaurate, reflecting the re-organisation of a C=O group of the detergent orientated towards the quinone and affected by the quinone redox transition [133]. In control measurements of the buffer/detergent system lacking the quinone, the signal was not present, nor in the redox difference spectra of the quinone in organic solvents [133]. A difference signal at 1744cm^{-1} has also previously been assigned in a combined IR/mutagenesis study, to the COOH mode of Glu286 residue in cytochrome bo_3 from *E. coli* and Glu278 in cytochrome *c* oxidase from *Paracoccus denitrificans* [133].

Arginine vibrations can tentatively be assigned in all the difference spectra (Fig. 6.12). The symmetric stretching vibration of arginine's guanidine group-$CN_3H_5^+$ is expected at 1635cm^{-1} and the antisymmetric stretching vibration at around 1670cm^{-1} [127, 158]. Arginines have already been postulated to form salt bridges to the propionic acids of cytochromes [127, 160]. The recent crystal structure has shown that the propionate of haem b_H, found in a twisted conformation, forms an ion-pair with the guanidine of Arg101 in the cytochrome bc_1 complex from chicken mitochondria [35, 127].

6.3.4 IR difference spectra of individual components

6.3.4.1 Cytochrome *f*, and cytochrome *f* and 'Rieske' ISP

For comparative purposes, the reduced *minus* oxidised FTIR difference spectra of purified turnip cytochrome *f* (Fig. 6.13A) from cytochrome b_6f complex, and cytochrome *f* and 'Rieske' ISP in cytochrome b_6f complex from crude lettuce preparation (Fig. 6.13B) upon photochemical reduction were resolved. The amide I signal around 1688cm^{-1} is overlapped by a broad signal at 1700cm^{-1} for cytochrome *f* (Fig. 6.13A) in comparison to the other *c*-type cytochromes (Fig. 6.16). In the cytochrome *f* and 'Rieske' ISP redox difference spectra, the equivalent signal is at 1694cm^{-1} and it is also broader than the other *c*-type cytochromes. The broad amide II vibration mode at 1581-87cm^{-1} found in all the redox difference spectra shown in Fig. 6.12 is shifted down to 1572cm^{-1} in the cytochrome *f*, and 1578cm^{-1} in the cytochrome *f* and 'Rieske' ISP redox difference spectra (Fig. 6.13). These differences in the amide regions between cytochrome *f* and the other *c*-type cytochromes may indicate a subtle difference in the conformational changes of the protein backbone of cytochrome *f* compared to the latter proteins. There are also notable differences between the turnip cytochrome *f*, and lettuce cytochrome *f* and 'Rieske' ISP spectra in the amide and other regions. These differences are likely to be due to differences between the structure, sequences and preparation (isolated or whole complex), of the turnip and lettuce enzymes.

The C_aC_m and C_bC_b cytochrome *f* haem stretch vibrations are present as positive signals at 1555 and 1543cm^{-1} (Fig. 6.13A), shifted up in comparison to redox difference spectra of model compounds [134]. The CαN haem stretch vibrations are present at 1408cm^{-1} and the C_mH haem vibrations are at 1240cm^{-1}. These haem vibrations are also present in the cytochrome *f* and 'Rieske' ISP redox difference spectra (Fig. 6.13B). Contributions of cytochrome *f* haem $C_\alpha C_\beta$ vinyl vibrations could

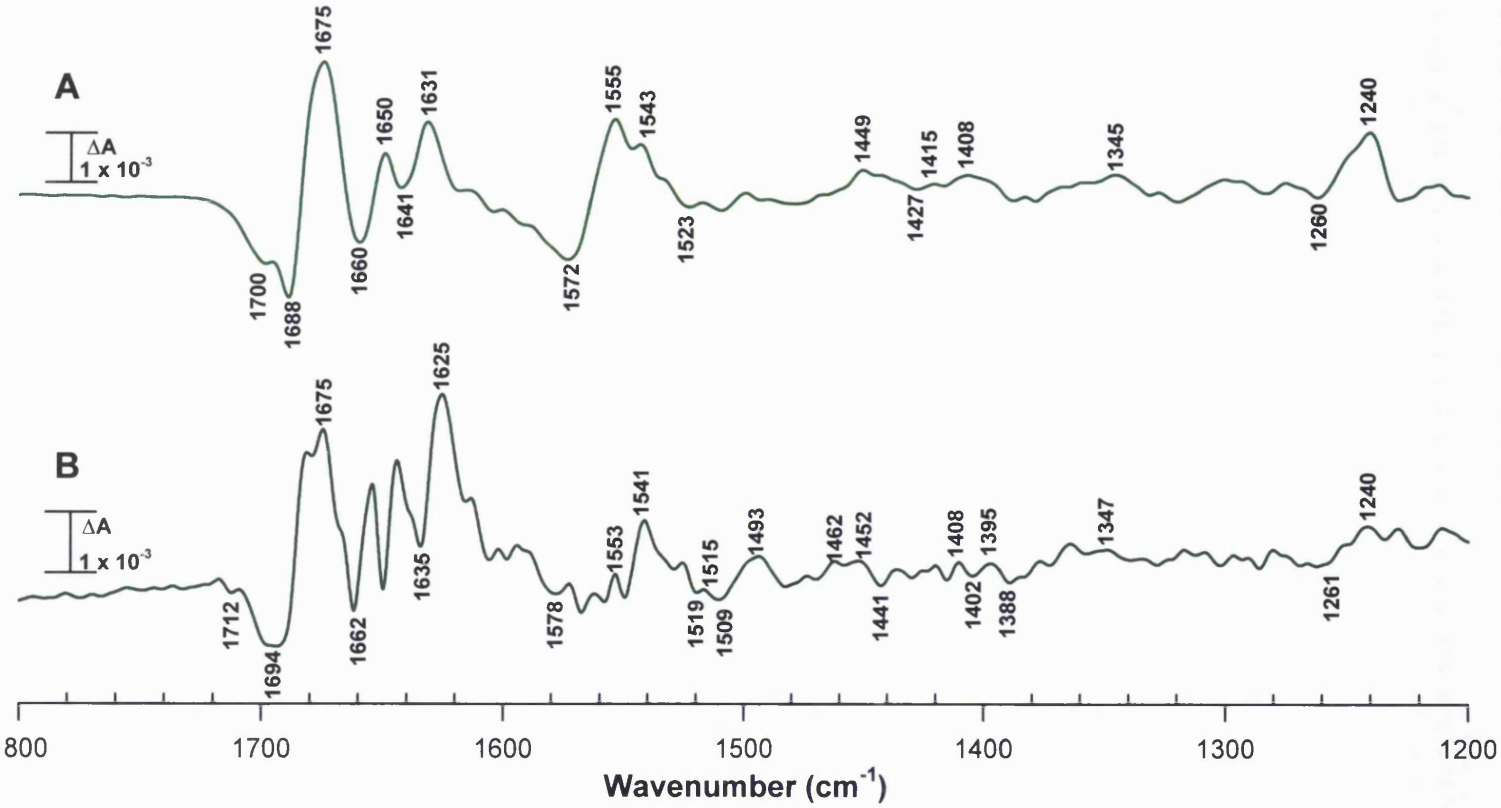

Fig. 6.13. Reduced *minus* oxidised FTIR difference spectra of *c*-type cytochromes at 288K and pH 8.5 A) Purified cytochrome *f* from turnip cytochrome b_6f complex. Sample contained 1.2nmol protein, 1nmol FMN and 3nmol ferricyanide in 0.1M Tricine buffer, and illuminated for 10s. **B)** Cytochrome *f* and the 'Rieske' iron-sulphur protein in cytochrome b_6f complex from crude lettuce preparation. Sample contained 3nmol protein, 10nmol FMN and 3nmol ferricyanide in 0.1M Tricine buffer, and illuminated for 10s. Refer to Section 6.2.2 for experimental conditions.

-be assigned to the positive signal at 1631cm^{-1} for cytochrome *f* and 1625cm^{-1} for cytochrome *f* and 'Rieske' ISP. In contrast, the 1614-19cm^{-1} signal attributed to $C_\alpha C_\beta$ haem vinyl vibrations is completely overlapped by amide II vibration centered at 1572-78cm^{-1}, in both redox difference spectra (Fig. 6.13). Signals at 1455, 1415 and 1337cm^{-1}, which have been assigned to porphyrin skeletal and vinyl vibration modes in the redox difference spectra of model compounds [134] could also be assigned in both spectra (Fig. 6.13).

There are no clear signals above 1700cm^{-1} in the cytochrome *f* redox difference spectra (Fig. 6.13A), which can be attributed to glutamic and aspartic acids present in the vicinity of the redox centre. This is not surprising since cytochrome *f* structure reveal only Glu14 and Asp162 (turnip numbering) are located within 10Å of the haem (Fig. 6.14). The broad signal at 1700cm^{-1} may tentatively be assigned to these groups. In the lettuce cytochrome *f* and 'Rieske' ISP redox difference spectra there is a prominent signal at 1712cm^{-1} and other less clear signals above 1700cm^{-1}. These signals are likely to be due to the same glutamic and aspartic acid groups that are present in the turnip cytochrome *f*. The differences between the two spectra in this region (above 1700cm^{-1}) may reflect differences in the environment of the glutamic and aspartic acid groups in the turnip enzyme compared to those in the lettuce enzyme.

Arginines have already been postulated to form salt bridges to the propionic acids of cytochromes [127, 160]. Cytochrome *f* redox difference spectra show positive signals at 1675 and 1631cm^{-1}, which could be assigned to Arg156 (turnip numbering) located in the vicinity of the cytochrome (Fig. 6.14). Equivalent signals are present in the cytochrome *f* and 'Rieske' ISP spectra at 1675 and 1625cm^{-1}.

In redox difference spectra, tyrosine's ring vibrations show positive signal at 1520cm^{-1} and negative signal at 1509cm^{-1}. This signal is unique for its sharpness [130, 134]. There is a positive signal around 1516cm^{-1} and a negative signal at 1508cm^{-1} in cytochrome *f* redox difference spectra (Fig. 6.13A), which could be assigned to tyrosine's ring vibrations. There is also a negative signal at 1394-6cm^{-1} in the same redox difference spectra, which may be due to in plane bending vibration of threonine CH_3 groups [152]. As before, equivalent signals can be found in the cytochrome *f* and 'Rieske' ISP spectra.

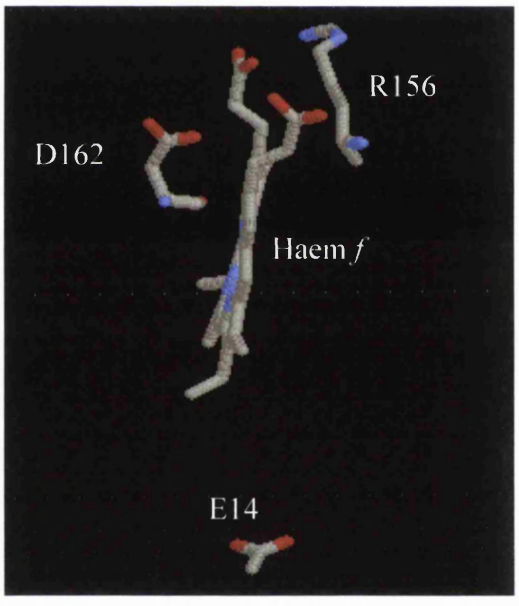

Fig. 6.14. Amino acid residues assigned in the turnip cytochrome *f* FTIR redox difference spectra and located in the vicinity of the haem. The figure was produced using co-ordinates from *Martinez et al.* (1994) [94] datafile 1CTM in the molecular simulation software RasMol (R.Sale). Selected residues and haems are shown as sticks.

6.3.4.2 Cytochrome c_1, and cytochrome c_1 and 'Rieske' ISP

The reduced *minus* oxidised FTIR difference spectra of cytochrome c_1 and 'Rieske' ISP from different preparations (Fig. 6.15A) and in different buffers (Fig. 6.15B) upon photochemical reduction were resolved. In addition, those of cytochrome c_1 sub-complex (Fig. 6.16A), cytochrome c_1 and 'Rieske' ISP (Fig. 6.16B) and cytochrome c_1 [with stigmatellin bound (Fig. 6.16C)] were also resolved. As expected, the redox difference spectra of cytochrome *f* (Fig. 6.13A) and cytochrome c_1 are similar (Fig. 6.16A,C). The same applies to the redox difference spectra of cytochrome c_1 and 'Rieske' ISP (Fig. 6.16B), and cytochrome *f* and 'Rieske' ISP (Fig. 6.13B). Spectra of cytochrome c_1 and 'Rieske' ISP from different preparations (Fig. 6.15A) gave essentially identical spectra with minor shifts in the positions of the signals. However, when the spectra were recorded in different buffers (Fig. 6.15B), there was a greater shift in the positions of some bands and new signals in the 1200-1000cm^{-1} regions (data not shown). This confirms that the signals observed, in particularly, in the 1800-1200 regions are largely due to protein conformational changes.

The amide I signal at 1686cm^{-1} for cytochrome c_1 sub-complex (Fig. 6.16) is shifted slightly up to 1693-94cm^{-1} in the cytochrome c_1 (with stigmatellin bound), and cytochrome c_1 and 'Rieske' ISP redox difference spectra. The amide II vibrations remain largely the same in all the redox difference spectra at 1581-3cm^{-1}. This indicates that the conformational changes of the protein backbone in these proteins are similar in both the isolated and whole complex states. In addition the 'Rieske' [2Fe2S] cluster has little to no spectral changes in the protein region.

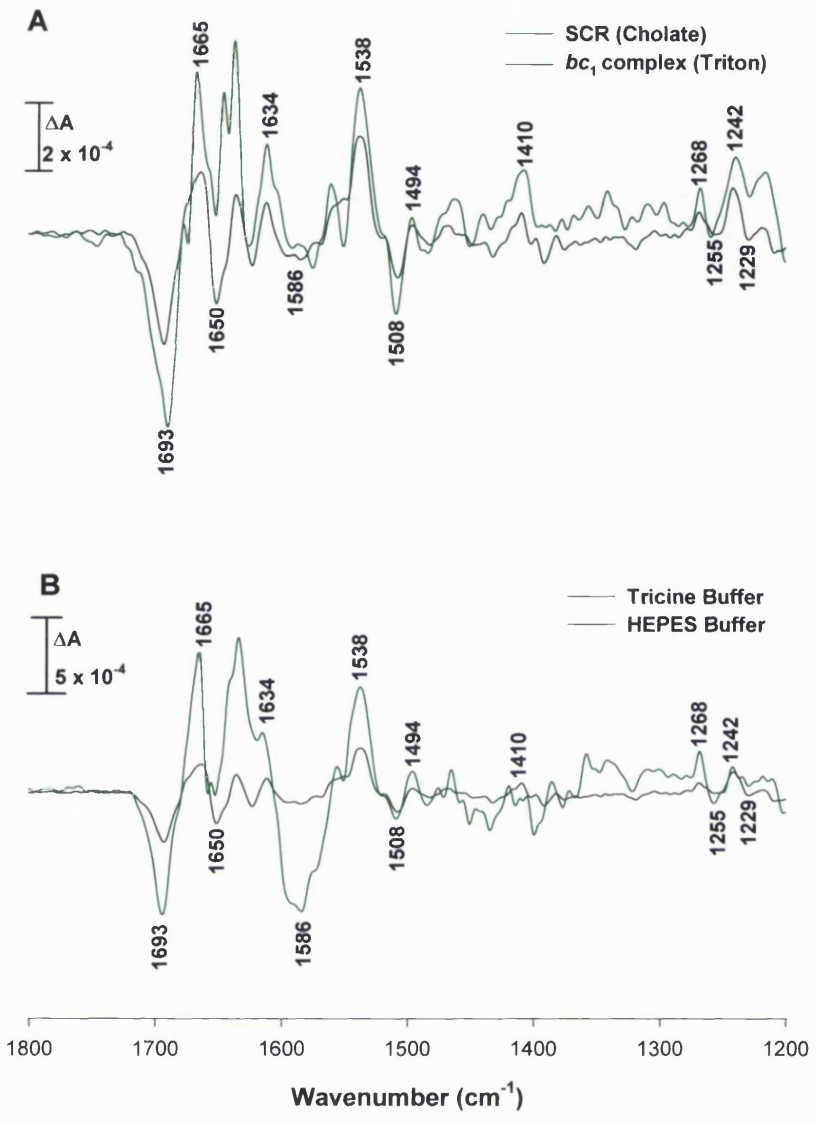

Fig. 6.15. The effects of methods of enzyme preparation (A) and buffer (B) on the reduced *minus* oxidised FTIR difference spectra of cytochrome c_1 and 'Rieske' iron-sulphur protein at 288K and pH8.5. A) SCR sample contained 2nmol protein, 5µl of 10% dodecyl maltoside and 1nmol FMN in 0.2M HEPES, and illuminated for 15s. Triton-prepared purified bc_1 complex sample contained 2nmol protein, 3nmol FMN and 5nmol ferricyanide in 0.2M HEPES, and illuminated for 15s. **B)** Triton-prepared purified bc_1 complex in HEPES (dark green) as described in (A). The other sample contained 4nmol protein, 1nmol FMN and 6nmol ferricyanide in 0.1M Tricine, and illuminated for 20s. Spectra are the signal average of at least two measurements. The difference in signal amplitudes between the spectra is likely to represent differences in the extent of reduction. Refer to Section 6.2.2 for experimental conditions.

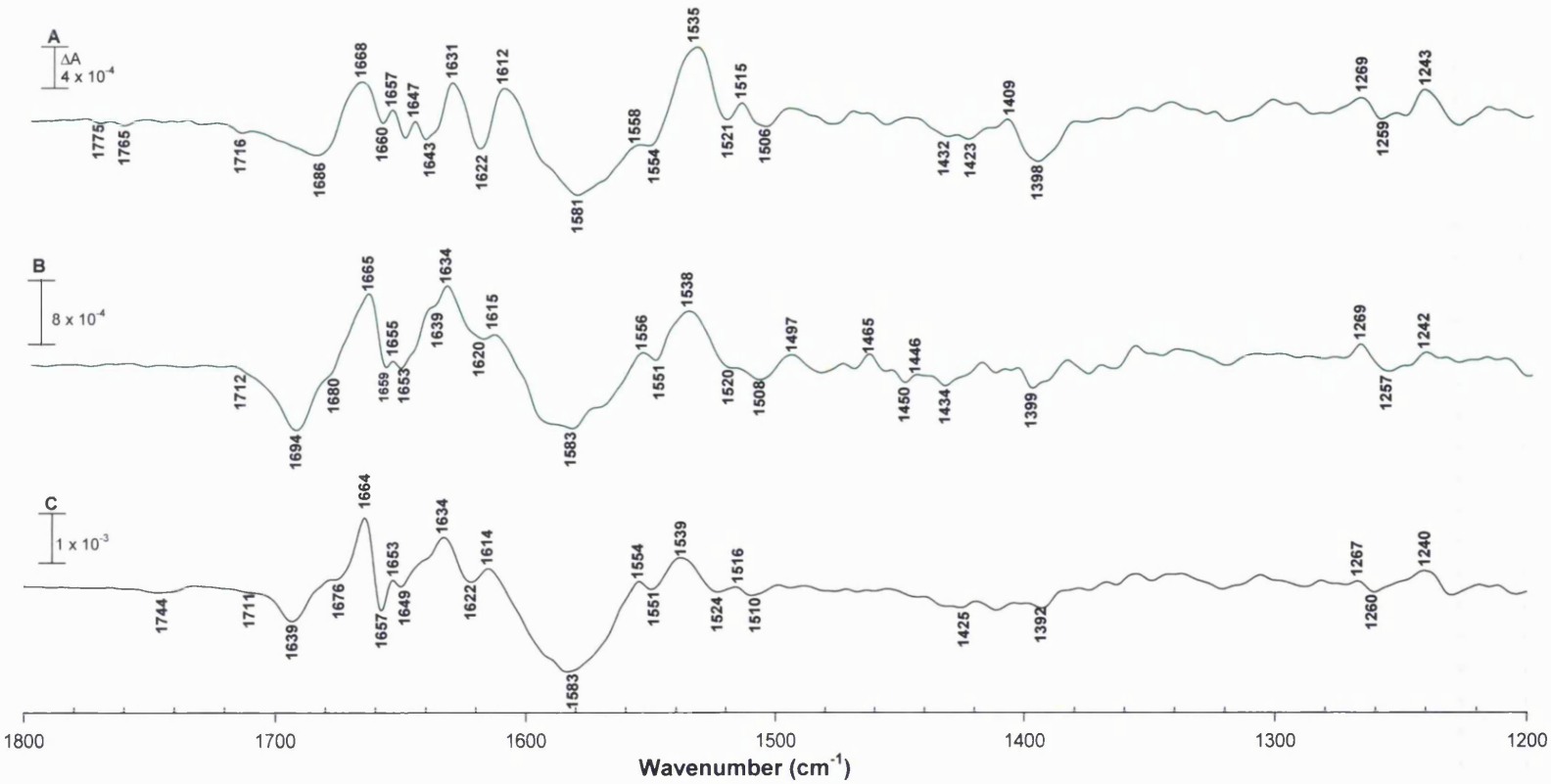

Fig. 6.16. Reduced *minus* oxidised FTIR difference spectra of the high-potential components at 288K and pH 8.5. A) Purified bovine cytochrome c_1 sub-complex. Sample contained 1.3nmol protein, 1nmol FMN and 2nmol ferricyanide in 0.1M Tricine, and illuminated for 10s. **B)** Cytochrome c_1 and 'Rieske' iron-sulphur protein in bovine cytochrome bc_1 complex. Sample contained 4nmol protein, 1nmol FMN and 6nmol ferricyanide in 0.1M Tricine, and illuminated for 20s. **C)** Cytochrome c_1 in the stigmatellin bound bovine cytochrome bc_1 complex. Sample as described previously with 5nmol stigmatellin added. Spectra are signal average of at least two measurements Refer to Section 6.2.2 for experimental conditions.

The C_aC_m and C_bC_b haem stretch vibrations of the *c*-type cytochromes are present as positive signals at 1554-58 and 1535-38cm^{-1}, whereas the CαN haem stretch vibrations are present at 1404-09cm^{-1} (Fig. 6.16). The latter signals are less pronounced in amplitude in the redox difference spectra of cytochrome c_1 and 'Rieske' ISP (Fig. 6.16B), and cytochrome c_1 (with stigmatellin bound (Fig. 6. 16C)) compared to the cytochrome c_1 sub-complex redox difference spectra (Fig. 6.16A). The C_mH haem vibrations are present at 1240-1243cm^{-1} in all the spectra. Contributions of the *c*-type haem vinyl $C_\alpha C_\beta$ vibrations could be tentatively assigned to the positive signal at 1631-34cm^{-1}. The 1614-19cm^{-1} signals attributed to $C_\alpha C_\beta$ haem vinyl vibrations are slightly overlapped by amide II vibration centered at 1583cm^{-1} in the cytochrome c_1 and 'Rieske' ISP, and cytochrome c_1 (with stigmatellin bound) redox difference spectra. Signals at 1455, 1415 and 1337cm^{-1} which have been assigned to porphyrin skeletal and vinyl vibration modes in the redox difference spectra of model compounds [134] could also be tentatively assigned in these spectra (Fig. 6.16).

The *c*-type cytochrome spectra show negative signals at 1711-1716cm^{-1} and above 1744cm^{-1}, which could be attributed to glutamic and aspartic acids present in the vicinity of the redox centre. The cytochrome c_1 structure reveals five such residues that are located within 10Å of the haem (Fig. 6.17). Cytochrome c_1 has a pH independent E_m [127], therefore changes in 1700cm^{-1} region are most likely due to changes in the environments of these groups rather than protonation/deprotonation changes.

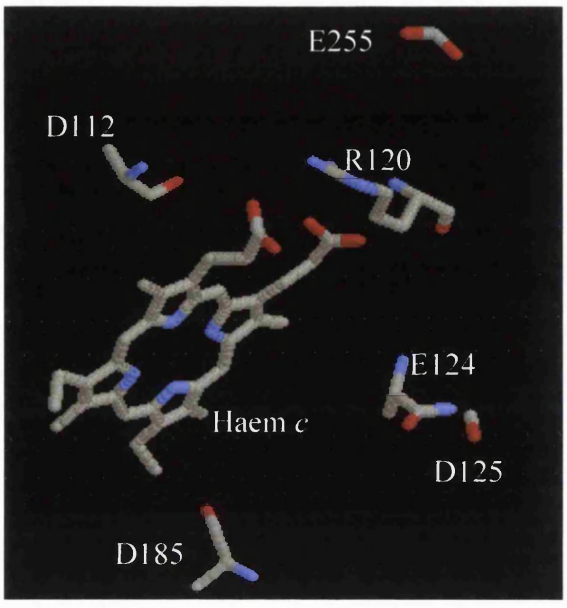

Fig. 6.17. Amino acid residues assigned in the cytochrome c_1 FTIR redox difference spectra and located in the vicinity of the haem *c*. The figure was produced using co-ordinates from *Zhang et al.* (1998) [35] datafile 3BCC in the molecular simulation software RasMol (R. Sale). Selected residues and the haem are shown as sticks.

All the redox difference spectra (Fig. 6.16) show positive signals at 1664-68 and 1631-34cm^{-1}, which can be tentatively assigned to Arg120 (chicken numbering) located in the vicinity of the cytochrome (Fig. 6.17). There is also a positive signal around 1515-6 and negative signal at 1508-10cm^{-1}, which could be assigned to tyrosine's ring vibrations. A negative signal at 1394-6cm^{-1} in these spectra may be due to in plane bending vibration of threonine CH_3 groups [152].

6.3.4.3 'Rieske' ISP

An attempt was made to resolve the FTIR redox difference spectra of Triton-prepared purified 'Rieske' ISP, prepared as described in Chapter 2. However, the inability to remove high concentration of glycerol and in particular Triton X-100

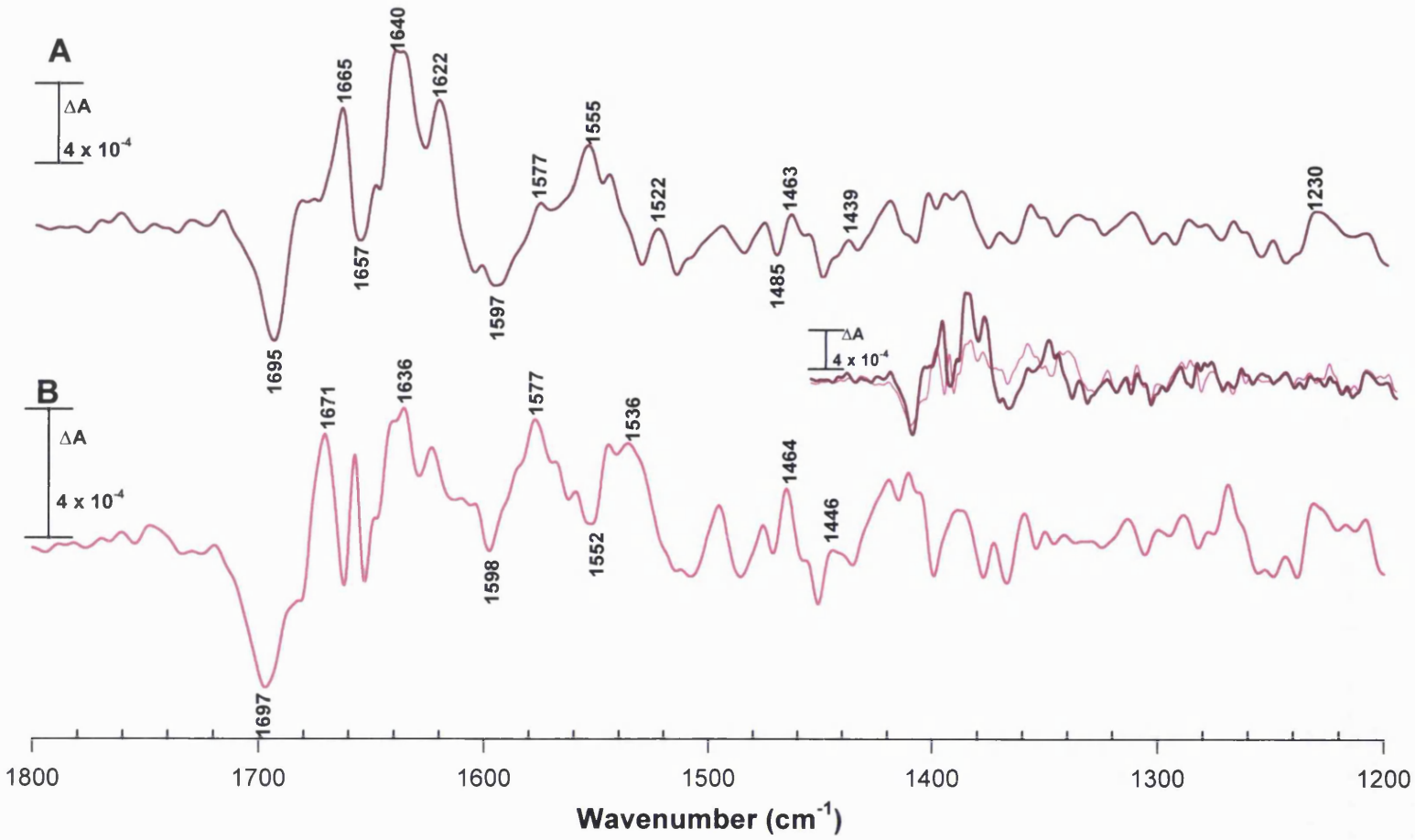

Fig. 6.18. Double difference spectra showing signals attributed to the 'Rieske' iron-sulphur protein. Spectra were calculated by subtraction of the difference spectra of cytochrome c_1 in the stigmatellin bound cytochrome bc_1 complex **(A)** or cytochrome c_1 sub-complex **(B)** from that of cytochrome c_1 and 'Rieske' iron-sulphur protein. Inset shows a superimposition of the two spectra.

-from the enzyme preparation prevented the resolving of the redox difference spectra of the 'Rieske' ISP. These compounds prevent adequate concentration of the protein. The redox difference spectra of the 'Rieske' ISP (Fig. 6.18) was therefore, calculated by subtraction of the difference spectra of cytochrome c_1 in the stigmatellin bound bc_1 complex or cytochrome c_1 sub-complex from that of cytochrome c_1 and 'Rieske' ISP in the bc_1 complex. The resulting double difference spectra from the two calculations were very similar with only minor differences. The spectra show limited structural changes since the '[2Fe2S] cluster has no spectral changes in the protein region. As previously mentioned, the sharpness of the amide I (1690-1610cm^{-1} region) bands in all the redox difference spectra presented in this study indicate that changes in the conformation of the protein backbone are small, localised and redox linked [127]. With regards to the 'Rieske' ISP, the small conformational changes observed are in agreement with the structural data that only the conformation of a few backbone bonds change that are localised in the hinge region between the transmembrane helix and the extramembraneous domain [31, 43, 79].

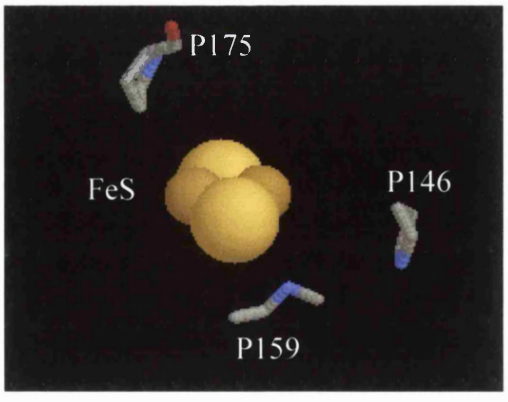

Fig. 6.19. Amino acid residues assigned in the 'Rieske' iron-sulphur protein FTIR double difference spectra and located in the vicinity of the iron-sulphur cluster. The figure was produced using co-ordinates from *Zhang et al.* (1998) [35] datafile 3BCC in the molecular simulation software RasMol (R. Sale). Selected residues are shown as sticks. 'Rieske' ISP cluster atoms are shown as brown spheres.

The spectral region between 1430 and 1480cm^{-1} may include signals arising from CH_2 and CH_3 bending modes of amino acid side chains [151]. The spectra of 'Rieske' ISP (Fig. 6.18), cytochrome *f* and 'Rieske' ISP (Fig. 6.13B), and, cytochrome c_1 and 'Rieske' ISP (Fig. 6.16B) show signals at around 1464 and 1450cm^{-1}, a region where ring vibrations of proline and tryptophan absorb [127]. Three prolines are present in the vicinity of the [2Fe2S] cluster [Pro146, 159 and 175, chicken numbering (Fig. 6.19)]. The conserved Pro159 is proposed to interact with the cluster, since mutation of this residue shifts the midpoint potential of the [2Fe2S] cluster in yeast [127, 161].

6.3.4.4 Cytochrome b_H with ubiquinone or antimycin A bound at the Q_i site

The redox difference spectra of cytochromes b_H with ubiquinone bound at the Q_i site (Fig. 6.20A) and with antimycin A bound (Fig. 6.20B) upon photochemical reduction were resolved. The amide I signals between 1693-1656cm^{-1} in both redox difference spectra (Fig. 6.20) are very similar. This suggests that the effect of ubiquinone or antimycin A on backbone conformational changes may be similar. However, there are differences in the amide I signals between 1656-1620cm^{-1}, which could be attributed to ubiquinone vibrational modes. Ubiquinone contributions are also likely to be present in the 1575-1480cm^{-1} amide II region of cytochrome b_H (with ubiquinone bound) redox difference spectra but are overlapped by the broad amide II band at 1583cm^{-1}.

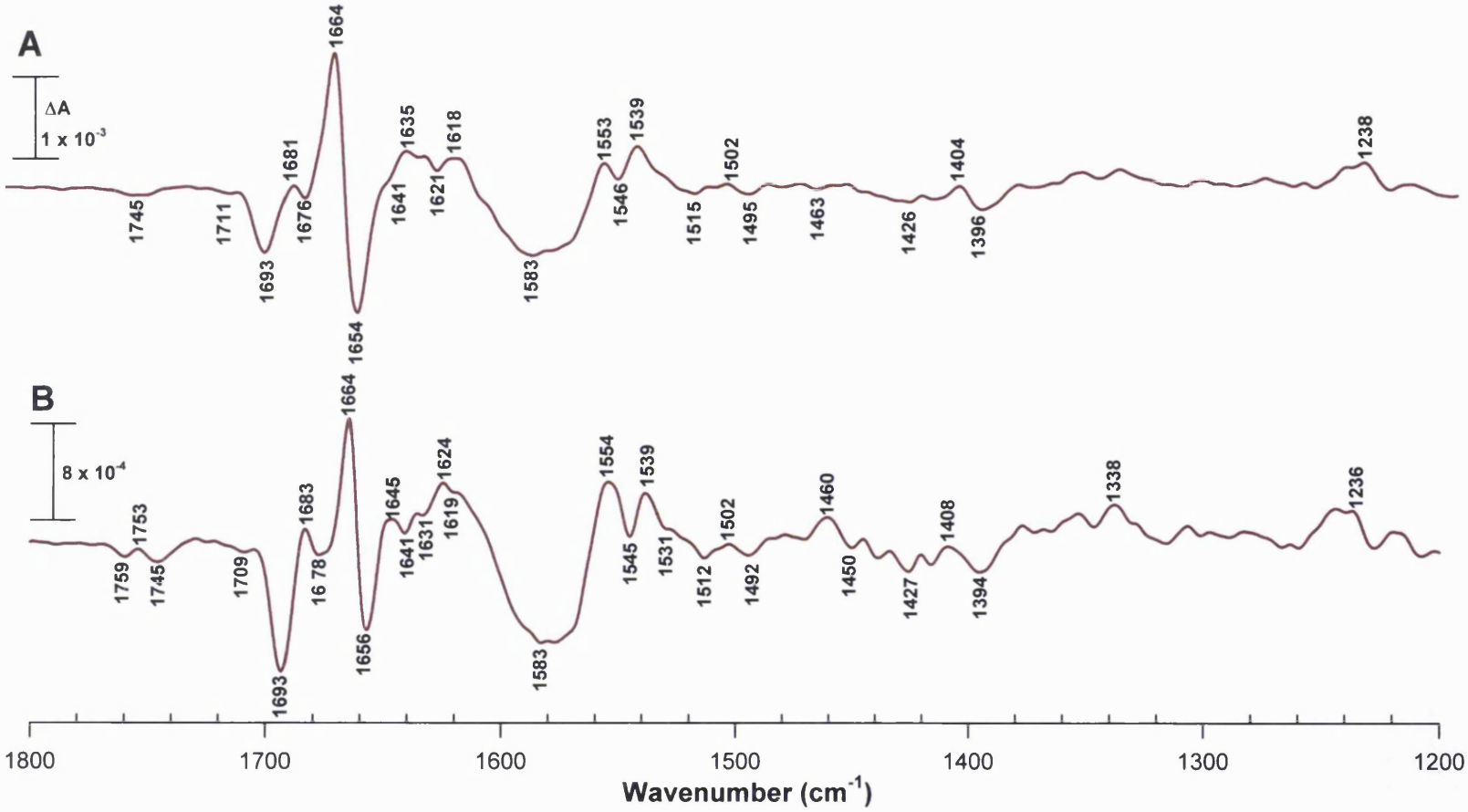

Fig. 6.20. Reduced *minus* oxidised FTIR difference spectra of cytochrome b_H of bovine heart cytochrome bc_1 complex at 288K and pH 8.5. A) Cytochrome b_H from ubiquinone bound enzyme. Samples contained 4nmol protein, 1nmol FMN and 6-7nmol ferrocyanide in 0.1M Tricine, and illuminated for 15s. **B)** Cytochrome b_H from antimycin A bound enzyme. Samples as before but includes 5nmol antimycin A. Spectra are signal average of two measurements. Refer to Section 6.2.2 for experimental conditions.

Cytochrome b_H haem C_aC_m and C_bC_b stretch vibrations are present as positive signals at 1552-54 and 1539cm^{-1}, whereas the C_mH haem vibrations are at 1236-38cm^{-1}. Contributions of cytochrome b_H haem $C_\alpha C_\beta$ vinyl vibrations could be tentatively assigned to the positive signal at 1635cm^{-1} for the ubiquinone bound enzyme and 1645cm^{-1} for the antimycin A bound enzyme. Again, the 1614-1619cm^{-1} signals attributed to $C_\alpha C_\beta$ vinyl haem vibrations are slightly overlapped by the amide II vibration centered at 1583cm^{-1}, in both spectra (Fig. 6.20). Cytochrome b_H haem signals are largely unaffected by binding of ubiquinone or antimycin A. Hence, the binding of either compound does not produce dramatic structural perturbations of cytochrome b_H haem.

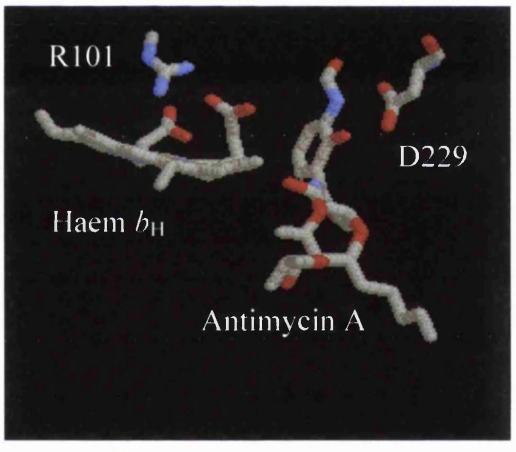

Fig. 6.21. Amino acid residues assigned in cytochrome b_H FTIR redox difference spectra and located in the vicinity of the haem b_H. Antimycin A bound at the Q_i site of cytochrome bc_1 complex. The figure was produced using co-ordinates from *Zhang et al.* (1998) [35] datafile 3BCC in the molecular simulation software RasMol (R. Sale). Selected residues, antimycin A and haem are shown as sticks.

Both cytochrome b_H spectra (Fig. 6.20) show signals at 1710-11 and above 1740cm^{-1}. The addition of inhibitor results in the splitting of the signal at 1745cm^{-1}. This may suggest interactions between the inhibitor and an aspartic or glutamic acid

residue. The ν(C=O) vibrations of these groups above 1740cm^{-1} are known to be sensitive to their environment and hydrogen bonding, and depending on the strength and nature of this interaction the shifts in wavenumbers could be up or down [152]. The most likely candidate for the C=O stretching vibrations absorbing above 1700cm^{-1} in the spectra of the cytochrome b_H is Asp229 (chicken numbering). Co-crystal has shown antimycin A and ubiquinone to be within hydrogen bonding contact of this residue (Fig. 6.21). Indeed Asp229 has been modelled along with His202 and Ser206 as ubiquinone ligands [31, 44]. In addition, it is a conserved residue located in the vicinity of the redox centre and has been shown by mutational studies to play a critical role in the mechanism [44].

Haem b_H has a weak pH dependent E_m, which means there are groups present with varying pK_a [120]. These groups may be in the protonated or deprotonated state. The cytochrome b_H spectra (Fig 6.12) clearly show signals above 1700cm^{-1}, which could tentatively be assigned to protonated (peaks)/deprotonated (troughs) aspartic and glutamic acid side chains. The deprotonation or protonation of these groups results in two bands at about 1620 and 1570cm^{-1}, and about 1420-50cm^{-1}. These difference signals are difficult to detect due to multiple overlap with other difference signals of the protein, e.g. the ν(CC), ν(CN) and δ(CH) modes from tryptophan [133, 159], amide II and other cofactors. However, it was possible to assign symmetric COO^- mode to the negative signals at around 1426-1436cm^{-1}.

The positive signals at 1664 and 1634-5cm^{-1} in both spectra can be tentatively assigned to Arg101 (chicken numbering), which has been shown in the crystal structure to form ion pairs with the propionate of haem b_H (Fig. 6.21) [35, 127]. There is a negative signal at 1394-6cm^{-1} prominent in both spectra, which may be due to in plane bending vibration of threonine CH_3 groups [152].

6.3.4.4.1 Ubiquinone bound at the Q_i site

Purified cytochrome bc_1 complex contains a ubiquinone molecule bound at the Q_i binding site, which would be expected to contribute to the FTIR redox difference spectra of cytochrome b_H. The addition of a tight binding inhibitor such as antimycin A would be expected to displace the ubiquinone and remove its contribution from the redox difference spectra. Vibrational modes from the bound ubiquinone in the photochemically induced FTIR redox difference spectra were separated by double difference spectroscopy from the protein contributions. The double difference spectrum (Fig. 6.22) was calculated by subtraction of the difference spectrum of cytochrome b_H in the ubiquinone bound at the Q_i site enzyme from cytochrome b_H in antimycin A bound at the Q_i site enzyme. The spectrum (Fig. 6.20) show signals, which may tentatively be attributed to ubiquinone by comparison to redox difference spectra of ubiquinones and ubiquinols in solution [133, 162, 163].

The addition of antimycin A resulted in the disappearance of overlapping bands at about 1654cm^{-1} (Fig. 6.20). This broad band is indicated in the double difference spectrum at 1653cm^{-1} (Fig. 6.22) and can be tentatively attributed to the C=O stretching mode of ubiquinone [127, 133]. There is also amide I contribution in this signal. The 1605cm^{-1} signal could be tentatively assigned to C=C vibration of the ubiquinone ring, which is found at 1612cm^{-1} in aqueous solutions [127, 133, 162]. The C-OCH_3 vibration mode from the 2- and 3-methoxy groups of ubiquinone [133] may correspond to the signals at 1282, 1270 and 1201cm^{-1} (the first two appears at 1288 and 1266cm^{-1} in aqueous solutions). These signals were also indicated to correspond to C-C vibration of ubiquinone [127]. However, this vibration has been assigned to the signal at 1452cm^{-1} [133], evident here at 1455cm^{-1}. Difference signals of reduced ubiquinone could tentatively be assigned to the signals at 1471, 1425 and

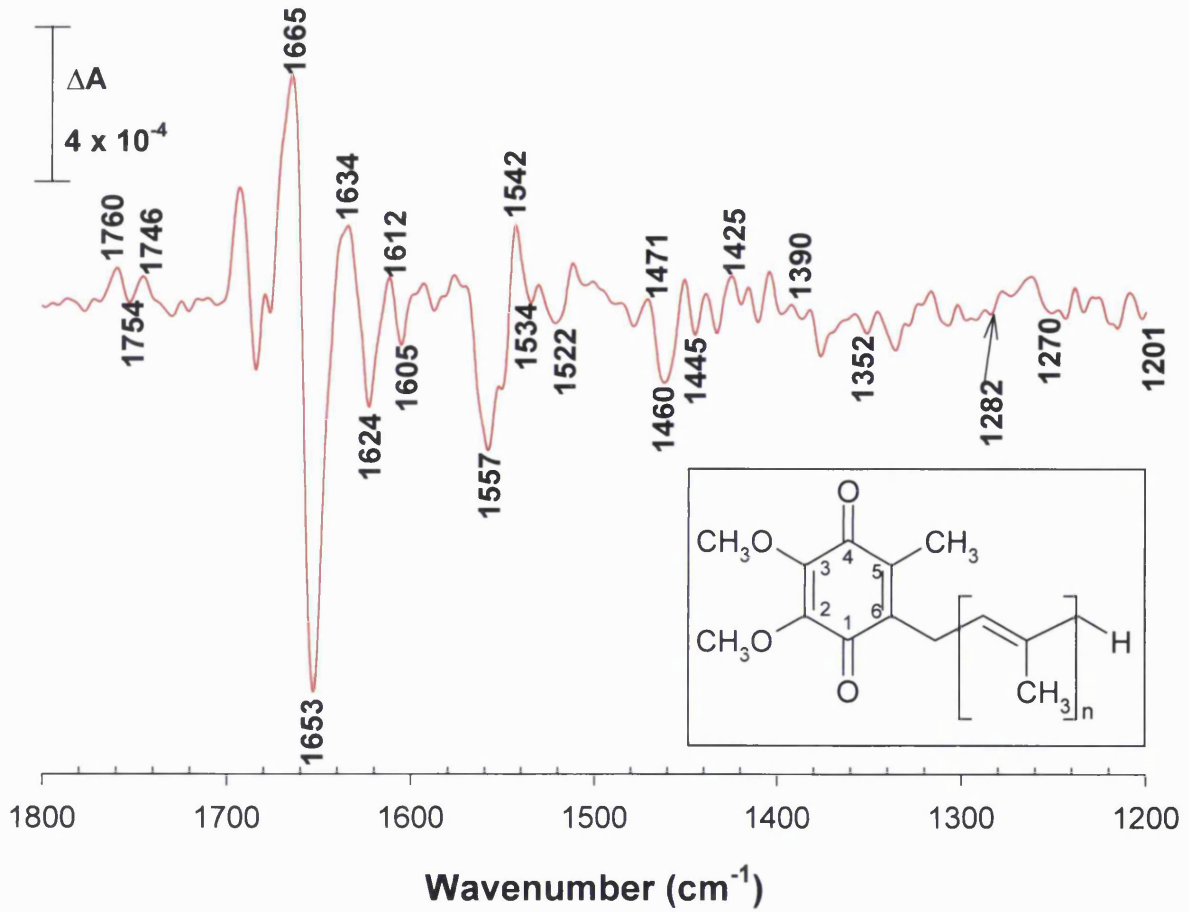

Fig. 6.22. Double difference spectrum showing signals attributed to a ubiquinone molecule bound at the Q_i site. The spectrum was calculated by subtraction of the difference spectra of cytochrome b_H in ubiquinone bound at the Q_i site enzyme from cytochrome b_H in antimycin A bound at the Q_i site enzyme. Inset shows the structure of ubiquinone. 'n' is generally between eight and 10 for ubiquinone [3].

-1390cm^{-1} [127, 133]. Positive signals in the 1500-1350cm^{-1} spectral region are typical for the reduction of ubiquinone [127, 162].

In the double difference spectrum (Fig. 6.22) there are likely to be signals that reflect alterations in the protein structure upon ubiquinone or antimycin A binding. A candidate is the signal at 1539cm^{-1}, which has been tentatively assigned in the difference spectra of cytochrome b_H (Fig. 6.20) as the C=C modes of the porphyrin ring on the basis of model compound studies of haem *b* [134]. Previous resonance Raman study showed that ubiquinone and inhibitor binding affects the porphyrin modes of oxidised low spin haem *b* [133, 164]. In addition, ubiquinone and antimycin A are known to affect the E_m of cytochrome b_H and their co-crystals show these compounds binding within van der Waals contact of the haem. Therefore, the signal observed here may be interpreted in this sense, presuming the compounds interact with the haem. A shift of this signal is seen in the cytochrome b_L redox difference spectra with AG204 bound (Fig. 6.23). This inhibitor binds close to haem b_L since it causes a red shift of its optical spectrum (Chapter 6).

6.3.4.5 Cytochrome b_L with and without AG204 bound at the Q_o site

Cytochrome b_L redox difference spectra without (Fig. 6.23A) and with AG204 bound (Fig. 6.23B) upon photochemical reduction were resolved. Unlike the rest of the redox difference spectra, cytochrome b_L spectra show two large narrow amide I signals at 1693cm^{-1} and 1672cm^{-1} (Fig. 6.23A). The latter signals are reduced in amplitude upon binding of AG204 at the Q_o site (Fig. 6.23B). The binding of AG204 also result in the sharpening of the broad amide I bands at around 1658-1644cm^{-1}.

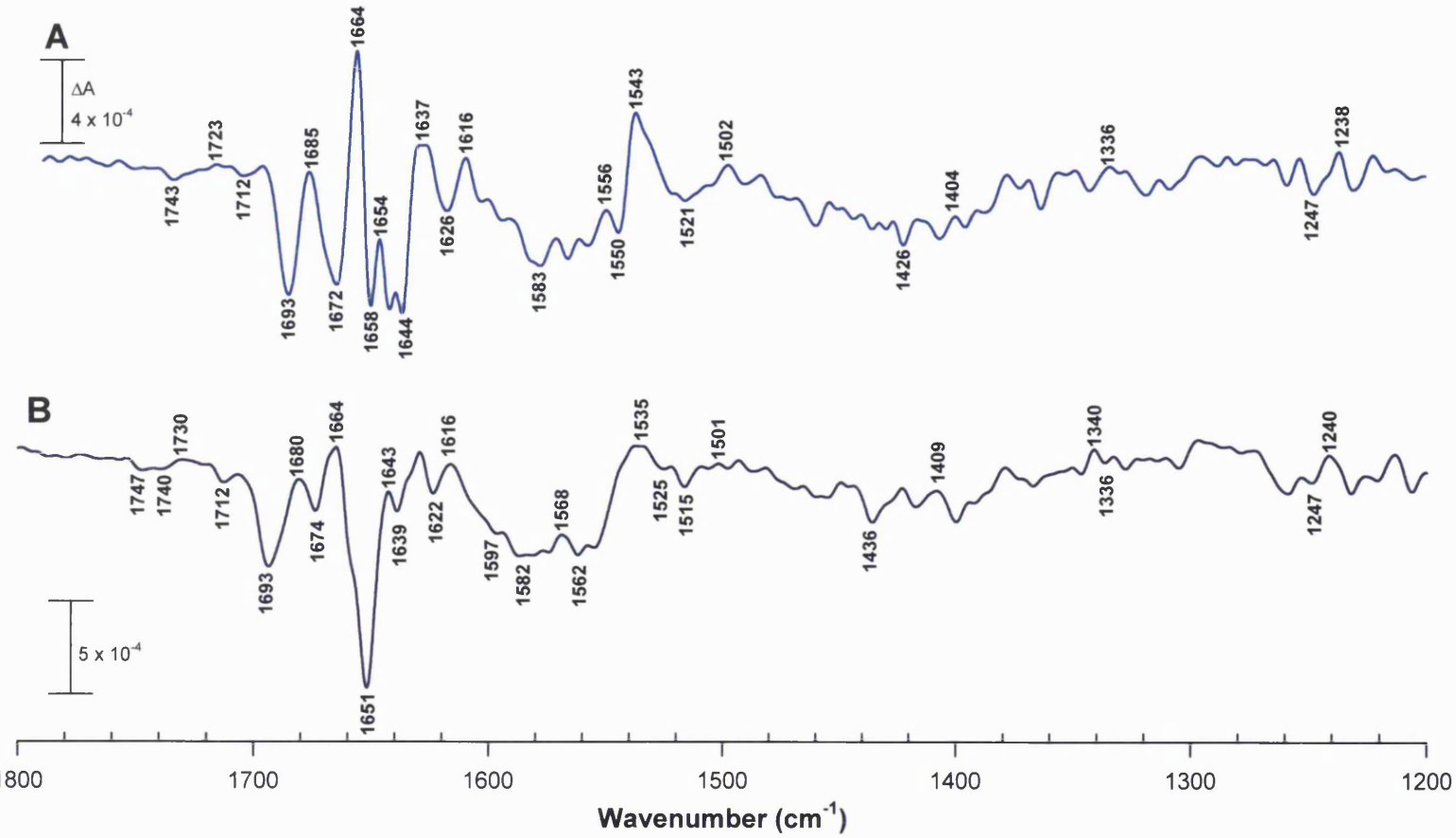

Fig. 6.23. Reduced *minus* oxidised FTIR difference spectra of cytochrome b_L of bovine heart cytochrome bc_1 complex at 288K and pH 8.5. A) Cytochrome b_L. Samples contained 4nmol protein (resolubilised in 10% w/v dodecyl maltoside), 2.5nmol FMN and 10nmol sodium ascorbate in 0.1M Tricine, and illuminated for 5s. **B)** Cytochrome b_L from the AG204 bound enzyme. Sample as before but includes 5nmol AG204. Spectra are signal average of two measurements. Refer to Section 6.2.2 for experimental conditions.

Hence, AG204 appears to be having an affect on the redox-induced backbone conformational changes of the protein. The amide II bands at around 1582cm^{-1} in both spectra are broader than in the other redox difference spectra with the exception of cytochrome *f* and, cytochrome *f* and 'Rieske' ISP spectra (Fig. 6.13). The broadness of the amide II band at 1582cm^{-1}, the two large narrow amide I signals unique to the cytochrome b_L spectra at 1693cm^{-1} and 1672cm^{-1} (Fig. 6.23A), and the effect of the binding of AG204 on these signals, may reflect the large volume of the Q_o site.

A signal at 1554cm^{-1} in cytochrome b_L redox difference spectra (Fig. 6.23A), which might be tentatively assigned to C_aC_m haem stretch vibrations is overlapped by amide II vibration and shifted to 1568cm^{-1} upon binding of AG204 to the Q_o site (Fig. 6.23B). In contrast the signal at 1546cm^{-1}, which might also be tentatively assigned to C_bC_b haem stretch vibrations is shifted down to 1535cm^{-1} upon binding of AG204 to the Q_o site. Cytochrome b_L haem CαN stretch vibrations are present at 1409-1404cm^{-1}. However, they are less pronounced in amplitude in the redox difference spectra of cytochrome b_L (Fig. 6.23) compared to cytochrome b_H (Fig. 6.20). The C_mH haem vibrations are present at 1238-40cm^{-1}. Contributions of cytochrome b_L haem $C_\alpha C_\beta$ vinyl vibrations could be tentatively assigned to the positive signal at 1637cm^{-1} for the uninhibited enzyme and 1643cm^{-1} for the AG204 bound enzyme. Unlike the other redox components, the 1614-1619cm^{-1} signals attributed to $C_\alpha C_\beta$ vinyl haem vibrations are not overlapped by amide II vibration centered at 1583cm^{-1}, in both cytochrome b_L spectra (Fig. 6.23). Cytochrome b_L haem signals are not greatly affected by binding of AG204. Hence, the binding of AG204 does not produce dramatic structural perturbations of cytochrome b_L haem.

Cytochrome b_L with and without AG204 bound redox difference spectra show signals at 1712 and 1743cm^{-1} (Fig. 6.23). Again the addition of inhibitor results in the

splitting of the signal at 1740cm^{-1}, which may suggest interactions such as hydrogen bonding between the inhibitor and an aspartic and/or glutamic acid residue. As previously mentioned, the ν(C=O) vibrations of these groups above 1740cm^{-1} are known to be sensitive to their environment and hydrogen bonding, and depending on the strength and nature of this interaction the shifts in wavenumbers could be up or down [152]. The crystal structure of the bc_1 complex shows that there are several conserved glutamic or aspartic acids in the 20Å environment of cytochrome b_L, which are the most likely candidates for the C=O stretching vibrations absorbing above 1700cm^{-1} in both redox difference spectra (Fig. 6.23). One conserved glutamic acid of the cytochrome c_1 subunit (Glu255, chicken numbering) and an aspartic acid of the transmembrane helix of the 'Rieske' ISP (Asp20), described as the first residue of the tether, are close to the haem b_L [127]. Furthermore, three carboxylic residues of the *b*-subunits (Glu271, Asp173 and Asp253) are in the vicinity of the haem (Fig. 6.24). Glu271 is closest to haem and just beside the conserved Asn256, both of which have been identified by mutagenesis to be part of the Q_o binding site [33, 34]. In addition, co-crystal has shown the Glu271 to be hydrogen bonded to MOA-stilbene (Fig. 6.24). It therefore seems to be the most promising candidate for one of the discussed difference signals.

Haem b_L also has a weak pH dependent E_m [120] and cytochrome b_L spectra (Fig 6.12) clearly show signals above 1700cm^{-1}, which may be assigned to protonated (peaks)/deprotonated (troughs) aspartic and glutamic acid side chains. There are also negative signals at around 1420-50cm^{-1}, which could be tentatively assigned to their symmetric COO^- mode.

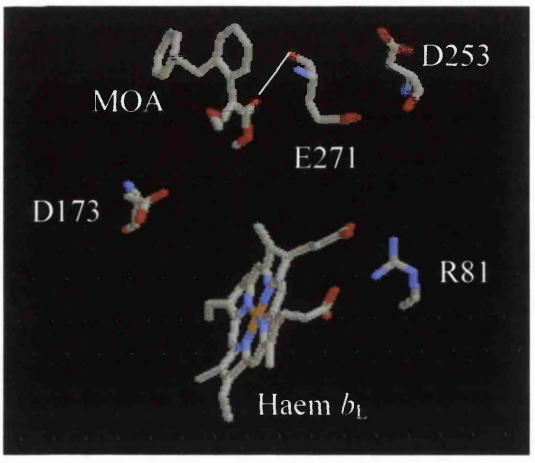

Fig. 6.24. Amino acid residues assigned in cytochrome b_L FTIR redox difference spectra and located in the vicinity of haem b_L. MOA-stilbene bound at the Q_o site. The figure was produced using co-ordinates from *Zhang et al.* (1998) [35] datafile 3BCC in the molecular simulation software RasMol (R. Sale). Selected residues, MOA-stilbene and haem are shown as sticks.

Positive signals at 1664 and 1630-37cm^{-1} in both redox spectra may tentatively be assigned to Arg81 [160] located in the vicinity of haem b_L (Fig. 6.24), which have already been postulated to form salt bridges to the propionic acids of the cytochrome [127].

6.4 Summary

The reduced *minus* oxidised FTIR difference spectra of the bovine cytochrome bc_1 complex in the native and inhibited state upon photochemical reduction were resolved for the first time. Signal assignments (Table 6.4) were aided by comparison to FTIR redox difference spectra of soluble domains of individual redox centres and model compounds. Redox linked conformational changes associated with the mobile head domain of 'Rieske' ISP, protonation and deprotonation reactions of amino acid residues, hydrogen bonding changes to side chains and to the backbone, and the interactions between inhibitors, substrate, prosthetic groups and the protein are all

Table 6.4. Peak positions and band assignment of the reduced *minus* oxidised difference signals in FTIR difference spectra

Cyt c_1 sub-complex	Cyt c_1 (with Stig. bound)	Cyt *f*	Cyt c_1 & ISP	ISP	Cyt b_H Q-Ant	Cyt b_L Native-AG204	Ubiquinone (Q_i)	Assignment
1775, 1765, 1716(-)	1744, 1711(-)	1700(-)	1733(+), 1747, 1712(-),		1753, 1743 (+), 1759, 1746, 1737(-)	1753, 1723-30(+), 1743-40, 1747(-)		-C=O Asp/Glu
1686, 1660, 1651, 1643(-), 1668, 1657, 1647, 1631, 1612 (+)	1693, 1676, 1657, 1649, 1622 (-), 1664, 1653, 1634, 1614(+)	1688, 1660, 1641 (-), 1675, 1650, 1631(+)	1694, 1680, 1659, 1653, 1639, 1620 (-), 1665, 1655, 1634, 1614 (+)	1695, 1657 (-), 1665, 1640, 1622 (+)	1693, 1676-78, 1654-56, 1641, 1621-26 (-), 1681-83, 1664, 1635-45, 1618-24 (+)	1693, 1672-74, 1658-51, 1644-39, 1626-22(-), 1685-80, 1664, 1654-43, 1637-30, 1616(+)		Amide I
1668, 1631(+)	1664, 1634(+)	1675, 1631 (+)	1665, 1634(+)		1664, 1634-35(+)	1664, 1637-30(+)		Arginine
							1653 (-)	C=O ubiquinone
1631, 1612 (+)	1634, 1614 (+)	1631(+)	1634, 1615(+)		1635-45, 1618-24 (+)	1637-31, 1616 (+)		vinyl $C_\alpha C_\beta$
					1621-19, 1426(-) (1450-1420)	1626-22, 1426-36		$COO^{-as,\,s}$ Asp,Glu
							1605 (-)	C=C Q- ring
1581(-)	1583(-)	1572(-)	1583(-)	1597(-)	1583(-)	1583-82(-)	1542(+)	Amide II
1558(+)	1554(+)	1555(+)	1556(+)		1552-54(+)	1556-68		C_aC_m haem
1535(+)	1539(+)	1543(+)	1538(+)		1539(+)	1543-35(+)		C_bC_b haem
1515(+), 1506(-)	1516(+), 1510(-)	1516(+) 1508(-)	1518(+) 1508(-)					Tyrosine
							1471, 1425, 1390(+)	Ubiquinol
			1465, 1446(+)	1463, 1439 (+)				Proline
							1460(-)	C-C Q- ring
1409(+)	1404(+)	1408(+)	1404(+)		1405-08(+)	1404-09(+)		CαN haem
							1282, 1270, 1201(-)	C-$COCH_3$
1243(+)	1240(+)	1240(+)	1242(+)		1238-36(+)	1238-40(+)		C_mH haem

Preliminary band assignments to the absorbtion of protein and cofactor bands are given. (-) negative signal;. (+) positive signal; as, asymmetric, s- symmetric. Q or Ant, refer to cytochrome b_H with ubiquinone or antimycin A bound; AG204 or Native, refer to cytochrome b_L with or without AG204 bound; ISP, 'Rieske' iron-sulphur protein; Stig, stigmatellin; Cyt, cytochrome.

-evident in the spectra. The small conformational changes in the amide I region of the 'Rieske' ISP (Fig. 6.18) are in agreement with structural data that only the conformation of a few backbone bonds localised in the hinge region of the amino acid chain between the transmembrane helix and the extramembraneous domain are changed during the redox cycle of the protein [43, 79].

FTIR difference spectroscopy has proved to be a powerful technique in studying changes in protein and prosthetic group conformations upon photochemical reduction. It is well suited to studies of the relationship between structure and function in proteins, i.e. issues such as ligand or substrate induced conformational changes. Furthermore, FTIR data can be examined from a kinetic perspective [130]. This technique is also complementary to others, in the quest for understanding the detail mechanisms of protein reactions. While X-ray crystallography yields the detailed structure of an essentially static state of the protein, FTIR reveals structural changes associated with protein reactions, in contrast to e.g. resonance Raman or optical spectroscopy that yields information on the interactions of the chromophore only. The studies presented here provide a starting point in the eventual goal of applying this technique to study the detail mechanism of the bc_1 complex and aid the development of pesticide.

CHAPTER 7

Overall summary

7.1 Thesis conclusions

The most critical reaction for energy conservation in the bc_1 complex is the obligatory bifurcation of the electron path linked to the two-electron oxidation of ubiquinol at the Q_o reaction site. The detailed mechanism of this reaction remains controversial for two principle reasons: firstly the presence/lack of an EPR detectable semiquinone at the Q_o site and secondly uncertainty as to whether the required occupancy state of the site for catalytic activity is with one or two bound ubiquinones [31]. Resolving these issues is essential for understanding the chemistry of this unique reaction.

Apart from elucidating the mechanism for ubiquinol oxidation at the Q_o site, the question of single or double occupancy of the Q_o binding site is important in the development of fungicides. If more than one compound can bind at the Q_o site, the simultaneous use of two compounds that can bind at the same time could limit the risk of generation of inhibitor resistant strains since it is very likely that fungus would develop resistance to both compounds.

One of the major aims of this project was to try and resolve the controversy concerning whether the Q_o site has to bind one or two quinones to be catalytically active. A further aim was to try to resolve the related question, with the aid of MOA-derivatives, as to whether two inhibitors can be accommodated within the Q_o site simultaneously, and whether a MOA compound and a ubiquinone can bind at the same time within the site. The information obtained was combined with modelling studies to assess whether rational design of new pesticides to have radically altered activity at the site might be feasible (Chapter 4).

The studies into the occupancy state of the Q_o site clearly showed that, although

the Q_o site reaction site has two binding domains, only a single species can occupy the site at one time and supports the model of overlapping binding sites that arise from previous inhibitor studies [58-60, 62, 63, 68, 75].

The steady state kinetics of the bc_1 complex (Chapter 3) revealed a mixed type of inhibition, which supports a model of overlapping binding sites for MOA-stilbene and decylubiquinol, and shows that the previous conclusion of separate binding sites for MOA-stilbene and quinone is open to question [75, 77].

The inhibitor studies (Chapter 4) showed that AG204 (class II) could reverse the effects of stigmatellin (class I) on the redox components of the bc_1 complex, suggesting that these compounds cannot bind simultaneously. This is fully consistent with the positions of mutations conferring resistance to inhibitors, which showed that changes in the entrance tunnel and middle of the pocket affects both classes of inhibitors, supporting a model of overlapping binding sites for inhibitors.

Molecular modelling studies showed that a structure with two ubiquinone molecules bound is highly constrained and only one 'tail' could be accommodated within the access tunnel and adjacent volume. Furthermore, exchange of ubiquinone bound at the Q_{ow} domain in reasonable physiological timescale with the Q-pool is hard to envisage. This further reinforces the view that only a single ubiquinone molecule is required for proper functioning of the Q_o reaction site.

The EPR spectra showed only one signal that can be attributed to an occupant of the Q_o site. The other signals present in the ubiquinone or ubiquinol spectra (KHP preparations) reports an empty site. Furthermore, AG204 or MOA-stilbene (class II) displaces DBMIB (class I) or ubiquinone analogues from the Q_o site due to its stronger

affinity. Therefore, only one species can occupy the Q_o site at any one time. The EPR data are fully consistent with the mammalian crystal structures data showing the absence of the strongly bound Q_{os} species.

The results presented here clearly agree with the simplest model that only a single species can occupy the Q_o site and add support to bifurcation mechanisms involving a single occupant of the Q_o site.

The feature of the Q_o site having two binding but overlapping domains was used to propose a new compound based on an existing tight inhibitor AG204. This compound was designed to fit adequately into the two domains, with all the favourable contacts exhibited by the two classes of Q_o site inhibitors.

The second aim of this project was to use FTIR difference spectroscopy to study changes in protein and prosthetic group conformations upon photochemical reduction. The reduced *minus* oxidised FTIR redox difference spectra of the components of bovine bc_1 complex in native and inhibitor bound states upon photochemical reduction were resolved. For comparative purposes, FTIR redox difference spectra of horse heart cytochrome *c*, turnip cytochrome *f*, and cytochrome *f* and 'Rieske' ISP of lettuce cytochrome b_6f complex were also determined. This is the first report of the FTIR difference redox spectra of these proteins with the exception of cytochrome *c*. Signal assignments were aided by comparison to FTIR redox difference spectra of soluble domains of individual redox centres and model compounds. Redox-linked conformational changes associated with the mobile head domain of 'Rieske' ISP, protonation and deprotonation reactions of amino acid residues, hydrogen bonding changes to side chains and to the backbone, and the interactions between inhibitors, substrate, prosthetic groups

and the protein are all evident in the spectra. The small conformational changes in the amide I region of the 'Rieske' ISP are in agreement with structural data that only the conformation of a few backbone bonds localised in the hinge region of the amino acid chain between the transmembrane helix and the extramembraneous domain are changed during the redox cycle of the protein [43, 79].

The third aim of this project was to characterise the binding modes of 10 new inhibitors of the bc_1 complex (Chapter 5) using a range of spectroscopic techniques. Inhibitor titration of the steady state kinetics of both the yeast and bovine enzyme revealed that AG201-208 are relatively good inhibitors of both bovine and yeast enzymes, binding more tightly to the yeast enzyme. In contrast, AG209-210 are relatively weak inhibitors of both forms of the enzyme, binding more tightly to the bovine enzyme. AG206 binds to both forms of the enzyme with a stoichiometry of 0.5 AG206/ monomeric bc_1 complex. AG204 mimics this behaviour but only in the yeast enzyme. This is the first report of such co-operative behaviour in the bovine enzyme.

All the tests carried out revealed that AG201-AG208 are MOA-like Q_o site inhibitors. An assignment cannot be made from the visible band data of AG209. However, the competition and the oxidant-induced experiments confirmed AG209 to be a Q_i site inhibitor. These tests confirmed AG210 as an antimycin-like Q_i site inhibitor. The oxidant induced experiments also revealed additional secondary effects on the haems. AG201 appeared to increase the E_m of haem b_L and had possible secondary inhibitory effects on complex II. AG209 and AG210 lowered the E_m of haem b_H and there was also evidence to suggest that the binding of the two compounds to the Q_i site may be different. The redox potentiometry results showed that neither of the two compounds tested AG201

and AG210 had any significant effect (>30mV) on the haem closest to their binding site. The result also confirmed the assignment of AG210 as a Q_i site inhibitor. In conclusion, all the major aims of this project were completed.

7.2 Future directions

The studies presented here are fully consistent with a model of single occupancy of the Q_o site. However, conflicting evidence is still emerging that supports double occupancy of the Q_o site. Therefore, despite the consistent single occupancy data reported here, more studies are required using new and more direct methods such as FTIR spectroscopy to further address this question. Elucidation of crystal structures for the bacterial enzymes may shed light on some of the difference between the EPR data on the bovine enzyme presented here and those of Ding and colleagues [57, 70-74] especially, the effects of MOA-stilbene, the presence of an intermediate state reported by a g_x resonance of 1.783 in the bacterial system and the stronger affinity of quinone for the bacterial site. Further useful studies that might resolve bacterial/mammalian enzyme differences would be solvent extraction and re-titration of ubiquinone to a redox poised iron-sulphur cluster of the bovine bc_1 complex.

FTIR difference spectroscopy has proved to be a powerful technique in investigating possible conformational changes associated with the mobile head domain of the 'Rieske' ISP. Kinetically resolved vibrational FTIR spectroscopy could eventually be used to resolve the detailed mechanism of the Q_o site oxidation reaction by allowing kinetic resolution of reaction intermediates, and providing local and specific structural information on each of the states [54]. Attenuated total reflectance (ATR) spectroscopy

may enable quantitative titration of the bc_1 complex with labelled quinone. In addition, it could also be used to confirm signal assignments of the reduced *minus* oxidised spectra obtained in this study. ATR spectroscopy utilises the phenomenon of total internal reflection [131]. A flow-through ATR cell includes both an inlet and an outlet arrangement in the apparatus. It allows for the continuous flow of solutions through the cell and thus permits spectral changes with time to be measured, e.g. ligand induced conformational changes [131, 165].

Signal assignment of the reduced *minus* oxidised FTIR difference spectra will be further aided by processes such as H/D exchange, global isotopic substitution with ^{13}C or ^{2}H and genetic engineering. A comparison of the difference spectra from different species could also aid signal assignments. Obtaining the redox difference spectra of purified 'Rieske' ISP would further aid the signal assignments of the difference spectra of high potential components of bc_1 complex.

With the availability of crystal structures of the bovine and yeast enzyme, it will be interesting to investigate using computer methods the structural factors that leads to differences in dissociation constants of AG201-10 compounds between the two forms of the enzyme.

Although there are further experiments to be carried out, the studies presented here have added to the understanding of the structure-function of the bc_1 complex. The bovine enzyme is very likely to function with a single ubiquinone molecule at the Q_o reaction site. This feature was further used to design a new compound to fit adequately into the site. Also the technique of FTIR spectroscopy has been used for the first time to successfully study the bovine enzyme. This technique offers the

exciting possibility of completely elucidating the detail mechanism of the bc_1 complex and aiding the development of pesticides.

CHAPTER 8

References

1. Nicholls, D.G. and Ferguson, S.J. (1992) Bioenergetics 2. Academic Press, London

2. von Jagow, G., Geier, B.M. and Link, T.A. (1997) The mammalian mitochondrial respiratory chain. In Bioenergetics (Gräber, P. and Milazzo, G. eds.), pp. 273-309. Birkhauser Verlag, Basel

3. Rich, P.R. (1996) Quinone binding sites of membrane proteins as targets for inhibitors. Pesticide Science 47, 287-296

4. Mitchell, P. (1975) Protonmotive redox mechanism of the cytochrome b-c_1 complex in the respiratory chain: protonmotive ubiquinone cycle. FEBS Lett. 56, 1-6

5. Hollingworth, R.M., Ahammadsahib, K.I., Gadelhak, G. and McLaughlin, J.L. (1994) New inhibitors of Complex I of the mitochondrial electron transport chain with activity as pesticides. Biochem. Soc. Trans. 22, 230-233

6. Esposti, M.D. (1998) Inhibitors of NADH-ubiquinone reductase: an overview. Biochim. Biophys. Acta 1364, 222-235

7. Esposti, M.D., Crimi, M. and Ghelli, A. (1994) Natural variation in the potency and binding sites of mitochondrial quinone-like inhibitors. Biochem. Soc. Trans. 22, 209-213

8. Esposti, M.D., Ghelli, A., Crimi, M., Baracca, A., Solaini, G., Tron, T. and Meyer, A. (1992) Cytochrome *b* of fish mitochondria is strongly resistant to funiculosin, a powerful inhibitor of respiration. Arch. Biochem. Biophys. 295, 198-204

9. Wiggins, T. (1992) The relationship between structure and activity of the methoxyacrylate toxophore. Biochem. Soc. Trans. 21, 1S

10. Clough, J.M. and Godfrey, C.R.A. (1995) Growing hopes. Chemistry in Britain 31, 466-469

11. Lümmen, P. (1998) Complex I inhibitors as insecticides and acaricides. Biochim. Biophys. Acta 1364, 287-296

12. Fisher, N. and Rich, P.R. (2000) A motif for quinone binding sites in respiratory and photosynthetic systems. J. Mol. Biol. 296, 1153-1162

13. Lancaster, C.R.D. and Michel, H. (1997) The coupling of light-induced electron transfer and proton uptake as derived from crystal structures of reaction centres from *Rhodopseudomonas viridis* modified at the binding site of the secondary quinone Q_B. Structure 5, 1339-1359

14. Friedrich, T., Abelmann, A., Brors, B., Guénebaut, V., Kintscher, L., Leonard, K., Rasmussen, T., Scheide, D., Schlitt, A., Schulte, U. and Weiss, H. (1998) Redox components and structure of the respiratory NADH:ubiquinone oxidoreductase (Complex I). Biochim. Biophys. Acta 1365, 215-219

15. Vedel, F., Lalanne, E., Sabar, M., Chétrit, P. and De Paepe, R. (1999) The mitochondrial respiratory chain and ATP synthase complexes: Composition, structure and mutational studies. Plant Physiol. Biochem. 37, 629-643

16. Ohnishi, T., Sled, V.D., Yano, T., Yagi, T., Burbaev, D.S. and Vinogradov, A.D. (1998) Structure-function studies of iron-sulfur clusters and semiquinones in the NADH-Q oxidoreductase segment of the respiratory chain. Biochim. Biophys. Acta 1365, 301-308

17. Ackrell, B.A.C. (2000) Progress in understanding structure-function relationships in respiratory chain Complex II. FEBS Lett. 466, 1-5

18. Hägerhäll, C. (1997) Succinate:quinone oxidoreductases variations on a conserved theme. Biochim. Biophys. Acta 1320, 107-141

19. Rich, P.R. and Moody, A.J. (1997) Cytochrome *c* oxidase. In Bioenergetics (Gräber, P. and Milazzo, G. eds.), pp. 419-456, Birkhäuser Verlag AG, Basel

20. Michel, H., Behr, J., Harrenga, A. and Kannt, A. (1998) Cytochrome *c* oxidase: Structure and spectroscopy. Annu. Rev. Biophys. Biomol. Struct. 27, 329-356

21. Lehninger, A. (2000) Lehninger Principles of biochemistry. Worth, USA

22. Wikström, M., Jasaitis, A., Backgren, C., Puustinen, A. and Verkhovsky, M.I. (2000) The role of the D- and K-pathways of proton transfer in the function of the haem-copper oxidases. Biochim. Biophys. Acta 1459, 514-520

23. Zaslavsky, D. and Gennis, R. (2000) Proton pumping by cytochrome oxidase: progress, problems and postulates. Biochim. Biophys. Acta 1458, 164-179

24. Mills, D.A., Florens, L., Hiser, C., Qian, J. and Ferguson-Miller, S. (2000) Where is 'outside' in cytochrome *c* oxidase and how and when do protons get there? Biochim. Biophys. Acta 1458, 180-187

25. Rich, P.R., Jünemann, S. and Meunier, B. (1998) Protonmotive mechanism of heme-copper oxidases. J. Bioenerg. Biomemb. 30, 131-138

26. Wikström, M. (2000) Mechanism of proton translocation by cytochrome *c* oxidase: A new four-stroke histidine cycle. Biochim. Biophys. Acta 1458, 188-198

27. Noji, H. and Yoshida, M. (2001) The rotary machine in the cell, ATP synthase. J. Biol. Chem. 276, 1665-1668

28. Stock, D., Gibbons, C., Arechaga, I., Leslie, A.G.W. and Walker, J.E. (2000) The rotary mechanism of ATP synthase. Curr. Op. Struct. Biol 10, 672-679

29. Nakamoto, R.K., Ketchum, C.J. and Al-Shawi, M.K. (1999) Rotational coupling in the F_oF_1 ATP synthase. Annu. Rev. Biomol. Struct. 28, 205-234

30. Boyer, P.D. (1997) The ATP synthase-A splendid molecular machine. Annu. Rev. Biochem. 66, 717-749

31. Berry, E.A., Guergova-Kuras, M., Huang, L. and Crofts, A.R. (2000) Structure and function of cytochrome *bc* complexes. Annu. Rev. Biochem. 69, 1005-10075

32. Brandt, U. and Trumpower, B.L. (1994) The protonmotive Q cycle in mitochondria and bacteria. Crit. Rev. Biochem. Mol. Biol. 29, 165-197

33. Brasseur, G., Saribaş, A.S. and Daldal, F. (1996) A compilation of mutations located in the cytochrome *b* subunit of the bacterial and mitochondrial bc_1 complex. Biochim. Biophys. Acta 1275, 61-69

34. Crofts, A.R., Barquera, B., Gennis, R.B., Kuras, R., Guergova-Kuras, M. and Berry, E.A. (1999) Mechanism of ubiquinol oxidation by the bc_1 Complex: Different domains of the quinol binding pocket and their role in the mechanism and binding of inhibitors. Biochemistry 38, 15807-15826

35. Zhang, Z., Huang, L., Shulmeister, V.M., Chi, Y.-I., Kim, K.K., Hung, L.-W., Crofts, A.R., Berry, E.A. and Kim, S.-H. (1998) Electron transfer by domain movement in cytochrome bc_1. Nature 392, 677-684

36. Xia, D., Yu, C.-A., Hoeon, K., Xia, J.Z., Kachurin, A.M., Zhang, L. and Deisenhofer, J. (1997) Crystal structure of the cytochrome bc_1 complex from bovine heart mitochondria. Science 277, 60-66

37. Iwata, S., Lee, J.W., Okada, K., Lee, J.K., Iwata, M., Rasmussen, B., Link, T.A., Ramaswamy, S. and Jap, B.K. (1998) Complete structure of the 11-subunit bovine mitochondrial bc_1 complex. Science 281, 64-71

38. Yu, C., Xia, D., Kim, H., Deisenhofer, J., Zhang, L., Kachurin, A.M. and Yu, L. (1998) Structural basis of functions of the mitochondrial cytochrome *bc*1 complex. Biochim. Biophys. Acta 1365, 151-158

39. Yu, C.A., Xia, J.Z., Kachurin, A.M., Yu, L., Xia, D., Kim, H. and Deisenhofer, J. (1996) Crystallization and preliminary structure of beef heart mitochondrial cytochrome-bc_1 complex. Biochim. Biophys. Acta 1275, 47-53

40. Crofts, A.R., Hong, S.J., Ugulava, N., Barquera, B., Gennis, R., Guergova-Kuras, M. and Berry, E.A. (1999) Pathways for proton release during ubihydroquinone oxidation by the bc_1 complex. Proc. Natl. Acad. Sci. USA 96, 10021-10026

41. Hunte, C., Koepke, J., Lange, C., Rossmanith, T. and Michel, H. (2000) Structure at 2.3Å resolution of the cytochrome *bc*(1) complex from the yeast *Saccharomyces cerevisiae* co-crystallized with an antibody Fv fragment. Structure Fold Des. 8, 669-684

42. Iwata, S., Saynovits, M., Link, T.A. and Michel, H. (1996) Structure of a water soluble fragment of the 'Rieske' iron-sulfur protein of the bovine heart mitochondrial cytochrome bc_1 complex determined by MAD phasing at 1.5 Å resolution. Structure 4, 567-579

43. Nett, J.H., Hunte, C. and Trumpower, B.L. (2000) Changes to the length of the flexible linker region of the 'Rieske' protein impair the interaction of ubiquinol with the cytochrome bc_1 complex. Eur. J. Biochem. 267, 5777-5782

44. Berry, E.A., Zhang, Z., Huang, L. and Kim, S. (1999) Structures of quinone-binding sites in *bc* complexes: functional implications. Biochem. Soc. Trans. 27, 565-572

45. Crofts, A., Guergova-Kuras, M., Kuras, R., Ugulava, N., Li, J. and Hong, S. (2000) Proton-coupled electron transfer at the Q_o site: what type of mechanism can account for the high activation barrier? Biochim. Biophys. Acta 1459, 456-466

46. Glaser, E., Eriksson, A. and Sjöling, S. (1994) Bifunctional role of the bc_1 complex in plants: Mitochondrial bc_1 complex catalyses both electron transport and protein processing. FEBS Lett. 346, 83-87

47. Rieske, J.S., Baum, H., Stoner, C.D. and Lipton, S.H. (1967) On the antimycin-sensitive cleavage of complex III of the mitochondrial respiratory chain. J. Biol. Chem. 242, 4854-4866

48. Rieske, J.S. (1967) Preparation and properties of a respiratory chain iron-protein. Meth. Enzymol. 10, 357-362

49. Trumpower, B.L. (1976) Evidence for a protonmotive Q cycle mechanism of electron transfer through the cytochrome b-c_1 complex. Biochem. Biophys. Res. Commun. 70, 73-80

50. Trumpower, B.L. and Landeen, C.E. (1977) Properties of ubiquinone relevant to its function in cellular respiration. Ealing Review 1, 4-7

51. Trumpower, B.L. and Edwards, C.A. (1979) Purification of a reconstitutively active iron-sulfur protein (oxidation factor) from succinate cytochrome *c* reductase complex of bovine heart mitochondria. J. Biol. Chem. 254, 8697-8706

52. Trumpower, B.L., Edwards, C.A. and Ohnishi, T. (1980) Reconstitution of the iron-sulfur protein responsible for the g = 1.90 electron paramagnetic resonance signal and associated cytochrome *c* reductase activities to depleted succinate-cytochrome *c* reductase complex. J. Biol. Chem. 255, 7487-7493

53. Bowyer, J.R., Edwards, C.A. and Trumpower, B.L. (1981) Involvement of the iron-sulfur protein of the mitochondrial cytochrome *b*-c_1 complex in the oxidant-induced reduction of cytochrome *b*. FEBS Lett. 126, 93-97

54. Link, T.A. (1997) The role of the 'Rieske' iron sulfur protein in the hydroquinone oxidation (Q_P) site of the cytochrome bc_1 complex. The 'proton-gated affinity change'mechanism. FEBS Lett. 412, 257-264

55. Link, T.A. and Iwata, S. (1996) Functional implications of the structure of the 'Rieske' iron-sulfur protein of bovine heart mitochondrial cytochrome bc_1 complex. Biochim. Biophys. Acta 1275, 54-60

56. Musatov, A. and Robinson, N.C. (1994) Detergent-solubilized monomeric and dimeric cytochrome bc_1 isolated from bovine heart. Biochemistry 33, 13005-13012

57. Sharp, R.E., Palmitessa, A., Gibney, B.R., Moser, C.C., Daldal, F. and Dutton, P.L. (1998) Non-inhibiting perturbation of the primary energy conversion site (Q_o site) in *Rhodobacter capsulatus* ubihydroquinone:cytochrome *c* oxidoreductase (cytochrome bc_1 complex). FEBS Lett. 431, 423-426

58. Kamensky, Y., Konstantinov, A.A., Kunz, W.S. and Surkov, S. (1985) Effects of bc_1-site electron transfer inhibitors on the absorption spectra of mitochondrial cytochromes *b*. FEBS Lett. 181, 95-99

59. von Jagow, G. and Ohnishi, T. (1985) The chromone inhibitor stigmatellin-binding to the ubiquinol oxidation center at the C-side of the mitochondrial membrane. FEBS Lett. 185, 311-315

60. Ohnishi, T., Brandt, U. and von Jagow, G. (1988) Studies on the effect of stigmatellin derivatives on cytochrome *b* and the Rieske iron-sulfur cluster of cytochrome *c* reductase from bovine heart mitochondria. Eur. J. Biochem. 176, 385-389

61. Hauska, G., Herold, E., Huber, C., Nitschke, W. and Sofrova, D. (1989) Stigmatellin affects both hemes of cytochrome *b* in cytochrome *b6f*/*bc*1-complexes. Z. Naturforsch. 44c, 462-467

62. von Jagow, G., Ljungdahl, P.O., Graf, P., Ohnishi, T. and Trumpower, B.L. (1984) An inhibitor of mitochondrial respiration which binds to cytochrome *b* and displaces quinone from the iron-sulfur protein of the cytochrome bc_1 complex. J. Biol. Chem. 259, 6318-6326

63. von Jagow, G. and Link, T.A. (1986) Use of specific inhibitors on the mitochondrial bc_1 complex. Meth. Enzymol. 126, 253-271

64. Kunz, W.S. and Konstantinov, A.A. (1983) Effect of *b*-c_1-site inhibitors on the midpoint potentials of mitochondrial cytochromes *b*. FEBS Lett. 155, 237-240

65. Ksenzenko, M., Konstantinov, A.A., Khomutov, G.B., Tikhonov, A.N. and Ruuge, E.K. (1983) Effect of electron transfer inhibitor on superoxide generation in the cytochrome bc_1 of the mitochondrial respiratory chain. FEBS Lett. 155, 19-24

66. Wiggins, T.E. (1992) Interactions of the myxothiazol and mucidin toxophores with cytochrome *b*. Biochem. Soc. Trans. 21, 2S

67. Thierbach, G. and Reichenbach, H. (1981) Myxothiazol, a new inhibitor of the cytochrome *b*-c_1 segment of the respiratory chain. Biochim. Biophys. Acta 638, 282-289

68. Link, T.A., Haase, U., Brandt, U. and von Jagow, G. (1993) What information do inhibitors provide about the structure of the hydroquinone oxidation site of ubihydroquinone:cytochrome *c* oxidoreductase?. J. Bioenerg. Biomemb. 25, 221-232

69. Brandt, U. (1996) Bifurcated ubihydroquinone-oxidation in the cytochrome bc_1 complex by proton-gated charge-transfer. FEBS Lett. 387, 1-6

70. Ding, H., Moser, C.C., Robertson, D.E., Tokito, M.K., Daldal, F. and Dutton, P.L. (1995) Ubiquinone pair in the Q_o site central to the primary energy conversion reactions of cytochrome bc_1 complex. Biochemistry 34, 15979-15996

71. Ding, H., Robertson, D.E., Daldal, F. and Dutton, P.L. (1992) Cytochrome bc_1 complex [2Fe-2S] cluster and its interaction with ubiquinone and ubihydroquinone at the Q_o site: A double-occupancy Q_o site model. Biochemistry 31, 3144-3158

72. Sharp, R.E., Moser, C.C., Gibney, B.R. and Dutton, P.L. (1999) Primary steps in the energy conservation reaction of the cytochrome bc_1 complex Q_o site. J. Bioenerg. Biomemb. 31, 225-233

73. Sharp, R.E., Palmitessa, A., Gibney, B.R., White, J.L., Moser, C.C., Daldal, F. and Dutton, P.L. (1999) Ubiquinone binding capacity of the *Rhodobacter capsulatus* cytochrome bc_1 complex: Effect of diphenylamine, a weak binding Q_o site inhibitor. Biochemistry 38, 3440-3446

74. Sharp, R.E., Palmitessa, A., Gibney, B.R., Moser, C.C. and Dutton, P.L. (1999) Probing the ubihydroquinone primary energy conversion site in the *Rhodobacter capsulatus* cytochrome bc_1 complex. Biochem. Soc. Trans. 27, 572-576

75. Brandt, U., Schägger, H. and von Jagow, G. (1988) Characterisation of binding of the methoxyacrylate inhibitors to mitochondrial cytochrome *c* reductase. Eur. J. Biochem. 173, 499-506

76. Brandt, U., Haase, U., Schägger, H. and von Jagow, G. (1991) Significance of the 'Rieske' iron-sulfur protein for formation and function of the ubiquinol-oxidation pocket of mitochondrial cytochrome *c* reductase (bc_1 complex). J. Biol. Chem. 266, 19958-19964

77. Brandt, U. and von Jagow, G. (1991) Analysis of inhibitor binding to the mitochondrial cytochrome *c* reductase by fluorescence quench titration-Evidence for a 'catalytic switch' at the Q_o center. Eur. J. Biochem. 195, 163-170

78. Brandt, U. and Djafarzadeh-Andabili, R. (1997) Binding of MOA-stilbene to the mitochondrial bc_1 complex is affected by the protonation state of a redox-Bohr group of the 'Rieske' iron-sulphur protein. Biochim. Biophys. Acta 1321, 238-242

79. Kim, H., Xia, D., Yu, C.-A., Xia, J.-Z., Kachurin, A.M., Zhang, L., Yu, L. and Deisenhofer, J. (1998) Inhibitor binding changes domain mobility in the iron-sulphur protein of the mitochondrial *bc*1 complex from bovine heart. Proc. Natl. Acad. Sci. USA 95, 8026-8033

80. de Vries, S., Albracht, S.P.J., Berden, J.A. and Slater, E.C. (1982) The pathway of electrons through QH_2:cytochrome *c* oxidoreductase studied by pre-steady state kinetics. Biochim. Biophys. Acta 681, 41-53

81. de Vries, S., Berden, J.A. and Slater, E.C. (1980) Properties of a semiquinone anion located in the QH_2:cytochrome *c* oxidoreductase segment of the mitochondrial respiratory chain. FEBS Lett. 122, 143-148

82. de Vries, S., Albracht, S.P.J., Berden, J.A. and Slater, E.C. (1981) A new species of bound ubisemiquinone anion in QH_2: cytochrome *c* oxidoreductase. J. Biol. Chem. 256, 11996-11998

83. Jünemann, S., Heathcote, P. and Rich, P.R. (1998) On the mechanism of quinol oxidation in the bc_1 complex. J. Biol. Chem. 273, 21603-21607

84. Crofts, A.R. and Wang, Z. (1989) How rapid are the internal reactions of the ubiquinol:cytochrome c_2 oxidoreductase. Photosynth. Res. 22, 69-87

85. Brandt, U. (1996) Energy conservation by bifurcated electron-transfer in the cytochrome-bc_1 complex. Biochim. Biophys. Acta 1275, 41-46

86. Crofts, A.R., Guergova-Kuras, M., Huang, L., Kuras, R., Zhang, Z. and Berry, E.A. (1999) Mechanism of ubiquinol oxidation by the bc_1 Complex: Role of the iron sulfur protein and its mobility. Biochemistry 38, 15791-15806

87. Brandt, U. and Okun, J.G. (1997) Role of deprotonation events in ubihydroquinone:cytochrome *c* oxidoreductase from bovine heart and yeast mitochondria. Biochemisty 36, 11234-11240

88. Brandt, U. (1998) The chemistry and mechanics of ubihydroquinone oxidation at center P (Q_o) of the cytochrome bc_1 complex. Biochim. Biophys. Acta 1365, 261-268

89. Brandt, U. (1999) Control of ubiquinol oxidation at center P (Q_o) of the cytochrome bc_1 complex. J. Bioenerg. Biomemb. 31, 243-250

90. Moser, C.C., Keske, J.M., Warncke, K., Farid, R.S. and Dutton, P.L. (1992) Nature of biological electron transfer. Nature 355, 796-802

91. Rich, P.R. and Fisher, N. (1999) Generic features of quinone-binding sites. Biochem. Soc. Trans. 27, 561-565

92. Zhang, J.M., Carrell, C.J., Huang, D.R., Sled, V., Ohnishi, T., Smith, J.L. and Cramer, W.A. (1996) Characterization and crystallization of the lumen side domain of the chloroplast Rieske iron-sulfur protein. J. Biol. Chem. 271, 31360-31366

93. Carrell, C.J., Zhang, H., Cramer, W.A. and Smith, J.L. (1997) Biological identity and diversity in photosynthesis and respiration: structure of the lumen-side domain of the chloroplast 'Rieske' protein. Structure 5, 1613-1625

94. Martinez, S.E., Huang, D., Szczepaniak, A., Cramer, W.A. and Smith, J.L. (1994) Crystal structure of chloroplast cytochrome *f* reveals a novel cytochrome fold and unexpected heme ligation. Structure 2, 95-105

95. Breyton, C. (2000) The cytochrome b_6f complex: structural studies and comparison with the bc_1 complex. Biochim. Biophys. Acta 1459, 467-474

96. Yu, C.A., Yu, L. and King, T.E. (1974) Soluble cytochrome b-c_1 complex and the reconstitution of succinate-cytochrome *c* reductase. J. Biol. Chem. 249, 4905-4910

97. Hartzell, C.R., Beinert, H., van Gelder, B.F. and King, T.E. (1978) Preparation of cytochrome oxidase from beef heart. Meth. Enzymol. 53, 54-66

98. Schägger, H. (1994) Isolation of complex III, Subcomplexes, and protein subunits from bovine heart: Triton X-100/Hydroxylapatite. In A practical guide to membrane protein purification (von Jagow, G. and Schägger, H. eds.), pp. 107-124, Academic Press, London

99. Schägger, H., Link, T.A., Engel, W.D. and von Jagow, G. (1986) Isolation of the eleven protein subunits of the bc_1 complex from beef heart. Meth. Enzymol. 126, 224-237

100. Schägger, H. (1994) Denaturing electrophoretic techniques. In A practical guide to membrane protein purification (von Jagow, G. and Schägger, H. eds.), pp. 59-79, Academic Press, London

101. Vanneste, W.H. (1966) Molecular proportion of the fixed cytochrome components of the respiratory chain of Keilin-Hartree particles and beef heart mitochondria. Biochim. Biophys. Acta 113, 175-178

102. Clejan, L. and Beattie, D.S. (1986) Preparation of complex III from yeast mitochondria and related methodology. Meth. Enzymol. 126, 173-179

103. Stryer, L. (1995) Biochemistry. W. H. Freeman & Co, New York

104. Cornish-Bowden, A. (1995) Fundamentals of enzyme kinetics. Portland Press, London

105. Trumpower, B.L. (1982) Function of quinones in energy conserving systems. Academic Press, San Diego

106. Lenaz, G. (1985) Coenzyme Q: Biochemistry, bioenergetics and clinical applications of ubiquinone. John Wiley & Sons, Chichester

107. Zweck, A., Bechmann, G. and Weiss, H. (1989) The pathway of the quinol/quinone transhydrogenation reaction in ubiquinol:cytochrome-*c* reductase of *Neurospora* mitochondria. Eur. J. Biochem. 183, 199-203

108. Rich, P.R. and Clarke, S.D. (1982) Reconstitution of cytochrome bc_1 complex into lipid vesicles and the restoration of uncoupler sensitivity. FEBS Lett. 148, 54-58

109. Bhairi, S.M. (1997) A guide to the properties and uses of detergents in biology and biochemistry. Calbiochem, Carlifornia

110. Saribaş, A.S., Ding, H., Dutton, P.L. and Daldal, F. (1995) Tyrosine 147 of cytochrome *b* is required for efficient electron transfer at the ubihydroquinone oxidase site (Q_o) of the cytochrome bc_1 complex. Biochemistry 34, 16004-16012

111. Sanner, M.F., Spehner, J. and Olson, A.J. (1996) Reduced surface: An efficient way to compute molecular surfaces. Biopolymers 38, 305-320

112. Assenheim, H.M. (1966) Introduction to electron spin resonance. Hilger & Watts Ltd, London

113. Salerno, J.C. and Ohnishi, T. (1980) Studies on the stabilized ubisemiquinone species in the succinate-cytochrome *c* reductase segment of the intact mitochondrial membrane system. Biochem. J. 192, 769-781

114. Gwak, S.H., Yang, F.D., Yu, L. and Yu, C.A. (1987) Phospholipid-dependent interaction between dibromothymoquinone and iron-sulfur protein in mitochondrial ubiquinol-cytochrome *c* reductase. Biochim. Biophys. Acta 890, 319-325

115. de Vries, S., Albracht, S.P.J. and Leeuwerik, F.J. (1979) The multiplicity and stoichiometry of the prosthetic groups in QH_2:cytochrome *c* oxidoreductase as studied by EPR. Biochim. Biophys. Acta 546, 316-333

116. Bowyer, J.R., Edwards, C.A., Ohnishi, T. and Trumpower, B.L. (1982) An analogue of ubiquinone which inhibits respiration by binding to the iron-sulfur protein of the cytochrome *b*-c_1 segment of the mitochondrial respiratory chain. J. Biol. Chem. 257, 8321-8330

117. Schoepp, B., Brugna, M., Riedel, A., Nitschke, W. and Kramer, D.M. (1999) The Q_o-site inhibitor DBMIB favours the proximal position of the chloroplast Rieske protein and induces a pK-shift of the redox-linked proton. FEBS Lett. 450, 245-250

118. Warncke, K., Gunner, M.R., Braun, B.S., Gu, L., Yu, C.-A., Bruce, J.M. and Dutton, P.L. (1994) Influence of hydrocarbon tail structure on quinone binding and electron-transfer performance at the Q_A and Q_B sites of the photosynthetic reaction center protein. Biochemistry 33, 7830-7841

119. Bowyer, J.R. and Trumpower, B.L. (1980) Inhibition of the oxidant-induced reduction of cytochrome *b* by a synthetic analogue of ubiquinone. FEBS Lett. 115, 171-174

120. Rich, P.R., Jeal, A.E., Madgwick, S.A. and Moody, A.J. (1990) Inhibitor effects on the redox-linked protonations of the *b* haems of the mitochondrial bc_1 complex. Biochim. Biophys. Acta 1018, 29-40

121. Rich, P.R. (1990) Redox-linked protonations of haems *b* of the bc_1 complex. In Structure, function and biogenesis of energy transfer systems (Papa, S. ed.), pp. 31-34, Elsevier, Amsterdam

122. West, I.C., Mitchell, P. and Rich, P.R. (1988) Electron conduction between *b* cytochromes of the mitochondrial respiratory chain in the presence of antimycin plus myxothiazol. Biochim. Biophys. Acta 933, 35-41

123. Ding, H., Daldal, F. and Dutton, P.L. (1995) Ion pair formation between basic residues at 144 of the cyt *b* polypeptide and the ubiquinones at the Q_o site of the cyt bc_1 complex. Biochemistry 34, 15997-16003

124. Rich, P.R., Madgwick, S.A. and Moss, D.A. (1991) The interactions of duroquinol, DBMIB and NQNO with the chloroplast cytochrome *bf* complex. Biochim. Biophys. Acta 1058, 312-328

125. Bechmann, G., Weiss, H. and Rich, P.R. (1992) Non-linear inhibition curves for tight-binding inhibitors of dimeric ubiquinol-cytochrome *c* oxidoreductases. Evidence for rapid inhibitor mobility. Eur. J. Biochem. 208, 315-325

126. Clark, W.M. (1960) Oxidation-reduction potentials of organic systems. In Oxidation-reduction potentials of organic systems. Bailliere, Tindall & Cox, Ltd. London

127. Baymann, F., Robertson, D.E., Dutton, P.L. and Mäntele, W. (1999) Electrochemical and spectroscopic investigations of the cytochrome bc_1 complex from *Rhodobacter capsulatus*. Biochemistry 38, 13188-13199

128. Šubik, J., Briquet, M. and Goffeau, A. (1981) Spectral properties of cytochrome *b*-561 and cytochrome *b*-565 in mucidin-resistant mutants of *Saccharomyces cerevisiae*. Eur. J. Biochem. 119, 613-618

129. Crofts, A.R., Hong, S., Zhang, Z. and Berry, E.A. (1999) Physicochemical aspects of the movement of the Rieske iron sulfur protein during quinol oxidation by the bc_1 complex from mitochondria and photosynthetic bacteria. Biochemistry 38, 15827-15839

130. Moss, D., Nabedryk, E., Breton, J. and Mäntele, W. (1990) Redox-linked conformational changes in proteins detected by a combination of infrared spectroscopy and protein electrochemistry. Evaluation of the technique with cytochrome *c*. Eur. J. Biochem. 187, 565-572

131. Stuart, B. (1997) Biological Applications of Infrared Spectroscopy. John Wiley & Sons, Chicester

132. Lübben, M. and Gerwert, K. (1996) Redox FTIR difference spectroscopy using caged electrons reveals contributions of carboxyl groups to the catalytic mechanism of haem-copper oxidases. FEBS Lett. 397, 303-307

133. Hellwig, P., Mogi, T., Tomson, F.L., Gennis, R.B., Iwata, J., Miyoshi, H. and Mäntele, W. (2000) Vibrational modes of ubiquinone in cytochrome bo_3 from *Escherichia coli* identified by Fourier transform infrared difference spectroscopy and specific ^{13}C labeling. Biochemistry 1-7

134. Berthomieu, C., Boussac, A., Mäntele, W., Breton, J. and Nabedryk, E. (1992) Molecular changes following oxidoreduction of cytochrome *b*559 characterized by Fourier transform infrared difference spectroscopy and electron paramagnetic resonance: Photooxidation in photosystem II and electrochemistry of isolated cytochrome *b*559 and iron protoporphyrin IX-bisimidazole model compounds. Biochemistry 31, 11460-11471

135. Schlereth, D.D. and Mäntele, W. (1992) Redox-induced conformational changes in myoglobin and haemoglobin: Electrochemistry and ultraviolet-visible and Fourier transform infrared difference spectroscopy at surface-modified gold electrodes in an ultra-thin-layer spectroelectrochemical cell. Biochemistry 31, 7494-7502

136. Hellwig, P., Grzybek, S., Behr, J., Michel, H. and Mäntele, W. (1999) Electrochemical and ultraviolet/visible/infrared spectroscopic analysis of heme *a* and a_3 redox reactions in the cytochrome *c* oxidase from *Paracoccus denitrificans*: Separation of heme *a* and a_3 contributions and assignment of vibrational modes. Biochemistry 38, 1685-1694

137. Hienerwadel, R., Boussac, A., Breton, J. and Berthomieu, C. (1996) Fourier transform infrared difference study of tyrosine$_D$ oxidation and plastoquinone Q_A reduction in photosystem II. Biochemistry 35, 15447-15460

138. Gerwert, K., Hess, B., Soppa, J. and Oesterhelt, D. (1989) Role of aspartate-96 in proton translocation by bacteriorhodopsin. Proc. Natl. Acad. Sci. USA 86, 4943-4947

139. Fahmy, K., Jäger, F., Beck, M., Zvyaga, T.A., Sakmar, T.P. and Siebert, F. (1993) Protonation states of membrane-embedded carboxylic acid groups in rhodopsin and metarhodopsin II. A Fourier-transform infrared spectroscopic study of site-directed mutants. Proc. Natl. Acad. Sci. USA 90, 10206-10210

140. Breton, J., Berthomieu, C., Thibodeau, D.L. and Nabedryk, E. (1991) Probing the secondary quinone (Q_B) environment in photosynthetic bacterial reaction centers by light-induced FTIR difference spectroscopy. FEBS Lett. 288, 109-113

141. Breton, J. and Nabedryk, E. (1996) Protein-quinone interactions in the bacterial photosynthetic reaction center: light-induced FTIR difference spectroscopy of the quinone vibrations. Biochim. Biophys. Acta 1275, 84-90

142. Breton, J., Nabedryk, E., Allen, J.P. and Williams, J.C. (1997) Electrostatic influence of Q_A reduction on the IR vibrational mode of the 10a-Ester C=O of H_A demonstrated by mutations at residues Glu L104 and Trp L100 in reaction centers from *Rhodobacter sphaeroides*. Biochemistry 36, 4515-4525

143. Bauscher, M., Leonhard, M., Moss, D.A. and Mäntele, W. (1993) Binding and interaction of the primary and the secondary electron acceptor quinones in bacterial photosynthesis. An infrared spectroelectrochemical study of *Rhodobacter sphaeroides* reaction centers. Biochim. Biophys. Acta 1183, 59-71

144. Breton, J., Burie, J.-R., Berthomieu, C., Berger, G. and Nabedryk, E. (1994) The binding sites of quinones in photosynthetic bacterial reaction centers investigated by light-induced FTIR difference spectroscopy: Assignment of the Q_A vibrations in *Rhodobacter sphaeroides* using ^{18}O- or ^{13}C-labeled ubiquinone and vitamin K_1. Biochemistry 33, 4953-4965

145. Nabedryk, E., Bagley, K.A., Thibodeau, D.L., Bauscher, M., Mäntele, W. and Breton, J. (1990) A protein conformational change associated with the photoreduction of the primary and secondary quinones in the bacterial reaction center. FEBS Lett. 266, 59-62

146. Rich, P.R. and Breton, J. (2001) FTIR studies of the CO and cyanide compounds of fully reduced bovine cytochrome *c* oxidase. Biochemistry 40, 6441-6449

147. Herberle, J. and Zscherp, C. (1996) ATR/FT-IR difference spectroscopy of biological matter with microsecond time resolution. Applied Spectroscopy 50, 588-596

148. Kalnin, N.N., Baikalov, I.A. and Venyaminov, S.Y. (1990) Quantitative IR spectrophotometry of peptide compounds in water (H_2O) solutions. II. Estimation of the protein secondary structure. Biopolymers 30, 1273-1280

149. Venyaminov, S.Y. and Kalnin, N.N. (1990) Quantitative IR spectrophotometry of peptide compounds in water (H_2O) solutions. Amide II absorption bands of polypeptides and fibrous proteins in α-, β-, and random coil conformations. Biopolymers 30, 1259-1271

150. Surewicz, W.K., Mantsch, H.H. and Chapman, D. (1993) Determination of protein secondary structure by Fourier transform infrared spectroscopy: A critical assessment. Biochemistry 32, 289-394

151. Schlereth, D.D. and Mäntele, W. (1993) Electrochemically induced conformational changes in cytochrome *c* monitored by Fourier transform infrared difference spectroscopy: Influence of temperature, pH, and electrode surfaces. Biochemistry 32, 1118-1126

152. Barth, A. (2000) The infrared absorption of amino acid side chains. Progress in Biophysics and Molecular Biology 74, 141-173

153. Hurt, E. and Hauska, G. (1981) A cytochrome *f*/b_6 complex of five polypetides with plastoquinol-plastocyanin-oxidoreductase activity from spinach chloroplasts. Eur. J. Biochem. 117, 591-599

154. Tollin, G. (1995) Use of flavin photochemistry to probe intraprotein and interprotein electron transfer mechanisms. J. Bioenerg. Biomemb. 27, 303-310

155. Ksenzhek, O.S. and Petrova, S.A. (1983) Electrochemical properties of flavins in aqueous solutions. Bioelectrochemistry and Bioenergetics 11, 105-127

156. Nelson, N., Nelson, H. and Racker, E. (1972) Photoreaction of FMN-Tricine and its participation in phosphorylation. Photochem. Photobiol. 16, 481-489

157. Moore, G.R. (1983) Control of redox properties of cytochrome *c* by special electrostatic interactions. FEBS Lett. 161, 171-175

158. Venyaminov, S.Y. and Kalnin, N.N. (1990) Quantitative IR spectrophotometry of peptide compounds in water (H_2O) solutions. I. Spectral parameters of amino acid residue absorption bands. Biopolymers 30, 1243-1257

159. Bruel, C., di Rago, J.P., Slonimski, P.P. and Lemesle-Meunier, D. (1995) Role of the evolutionarily conserved cytochrome *b* tryptophan 142 in the ubiquinol oxidation catalyzed by the bc_1 complex in the yeast *Saccharomyces cerevisiae*. J. Biol. Chem. 270, 22321-22328

160. Hacker, B., Barquera, B., Gennis, R.B. and Crofts, A.R. (1994) Site-directed mutagenesis of arginine-114 and tryptophan-129 in the cytochrome *b* subunit of the bc_1 complex of *Rhodobacter sphaeroides*: Two highly conserved residues predicted to be near the cytoplasmic surface of putative transmembrane helices B and C. Biochemistry 33, 13022-13031

161. Denke, E., Merbitz-Zahradnik, T., Hatzfeld, O.M., Snyder, C.H., Link, T.A. and Trumpower, B.L. (1998) Alteration of the midpoint and catalytic activity of the Rieske iron-sulfur protein by changes of amino acids forming hydrogen bonds to the iron-sulfur cluster. J. Biol. Chem. 273, 9085-9093

162. Burie, J.-R., Boussac, A., Boullais, C., Berger, G., Mattioli, T., Mioskowski, C., Nabedryk, E. and Breton, J. (1995) FTIR spectroscopy of UV-generated quinone radicals: Evidence for an intramolecular hydrogen atom transfer in ubiquinone, naphthoquinone, and plastoquinone. J. Phys. Chem. 99, 4059-4070

163. Bauscher, M., Nabedryk, E., Bagley, K., Breton, J. and Mäntele, W. (1990) Investigation of models for photosynthetic electron acceptors: Infrared spectroelectrochemistry of ubiquinone and its anions. FEBS Lett. 261, 191-195

164. Gao, F., Qin, H., Simpson, M.C., Shelnutt, J.A., Knaff, D.B. and Ondrias, M.R. (1996) Isolation and characterization of vibrational spectra of individual heme active sites in cytochrome bc_1 complexes from *Rhodobacter capsulatus*. Biochemistry 35, 12812-12819

165. Goormaghtigh, E., Raussens, V. and Ruysschaert, J.-M. (1999) Attenuated total reflection infrared spectroscopy of proteins and lipids in biological membranes. Biochim. Biophys. Acta 1422, 105-185